10/11/2/88 MEH (1) DR#0595-9

PNL-6686
UC-510

PNL--6686
DE89 001847

# Nuclear Waste Treatment Program Annual Report for FY 1987

Compiled by
R. A. Brouns and J. A. Powell

September 1988

Prepared for the U.S. Department of Energy
under Contract DE-AC06-76RLO 1830

Pacific Northwest Laboratory
Operated for the U.S. Department of Energy
by Battelle Memorial Institute

Battelle

PNL-6686

## DISCLAIMER



PACIFIC NORTHWEST LABORATORY
*operated by*
BATTELLE MEMORIAL INSTITUTE
*for the*
UNITED STATES DEPARTMENT OF ENERGY
*under Contract DE-AC06-76RLO 1830*

Printed in the United States of America
Available from
National Technical Information Service
United States Department of Commerce
5285 Port Royal Road
Springfield, Virginia 22161

NTIS Price Codes
Microfiche A01

Printed Copy

| Pages | Price Codes |
|---|---|
| 001-025 | A02 |
| 026-050 | A03 |
| 051-075 | A04 |
| 076-100 | A05 |
| 101-125 | A06 |
| 126-150 | A07 |
| 151-175 | A08 |
| 176-200 | A09 |
| 201-225 | A10 |
| 226-250 | A11 |
| 251-275 | A12 |
| 276-300 | A13 |

## DISCLAIMER

PNL-6686
UC-510

# NUCLEAR WASTE TREATMENT PROGRAM
# ANNUAL REPORT FOR FY 1987

Compiled by
R. A. Brouns and J. A. Powell

Contributing Task Managers

| | |
|---|---|
| W. L. Kuhn | J. R. Carrell |
| L. K. Holton, Jr. | J. L. Buelt |
| J. E. Minor | W. A. Ross |

Contributing authors are listed at the beginning of sections.

September 1988

Prepared for
the U.S. Department of Energy
under Contract DE-AC06-76RLO 1830



Pacific Northwest Laboratory
Richland, Washington 99352

## EXECUTIVE SUMMARY

Two of the U.S. Department of Energy's (DOE) nuclear waste management-related goals are: 1) to ensure that waste management is not an obstacle to the further deployment of light-water reactors and the closure of the nuclear fuel cycle and 2) to fulfill its institutional responsibility for providing safe storage and disposal of existing and future nuclear wastes. As part of its approach to achieving these goals, the Office of Remedial Action and Waste Technology of DOE established what is now called the Nuclear Waste Treatment Program (NWTP) at the Pacific Northwest Laboratory[a] during the second half of FY 1982. To support DOE's attainment of its goals, the NWTP is to provide 1) technology necessary for the design and operation of nuclear waste treatment facilities by commercial enterprises as part of a licensed waste management system and 2) problem-specific treatment approaches, waste form and treatment process adaptations, equipment designs, and trouble-shooting assistance, as required to treat existing wastes. This annual report describes progress during FY 1987 toward meeting these two objectives.

In addition to this series of annual reports, progress in liquid-fed ceramic melter vitrification technology is reported quarterly (starting with the first quarter of fiscal year 1985).

### NONRADIOACTIVE TESTING

Progress emphasized completing and documenting work started in fiscal year 1986 relating to the development of the liquid-fed ceramic melter process for high-level waste treatment. A total of 22 formal reports and professional meeting presentations were completed as part of this effort. The vitrification process model developed in FY 1986 was modified and the control logic added to simulate the West Valley Demonstration Project vitrification system in order to examine the inherent process stability and establish critical parameters for controlling the product quality. Statistical techniques were identified and used to analyze the large data sets of process measurements generated by the model simulation runs and to correlate the chemical durability of waste glass with composition. Additional testing

---

(a) Operated by Battelle Memorial Institute for the Department of Energy under Contract DE-AC06-76RLO 1830

and refinement of the TEMPEST heat-transfer computer code, which is used in predicting the thermal history of glass-filled canisters, was conducted to validate the code.

## FEDERAL REPUBLIC OF GERMANY ISOTOPIC HEAT AND RADIATION SOURCE FABRICATION

Production of the 32 heat and radiation source canisters for the Federal Republic of Germany (FRG) was completed. These isotopic sources containing strontium-90 and cesium-137 isotopes in a borosilicate glass were produced in the radioactive pilot-scale liquid-fed ceramic melter system. Some melter operational difficulties were encountered, including pluggage of the discharge section with glass. Methods were devised, however, for remotely melting the blockage and allowed normal operations to resume.

Two of the canisters were equipped with special instrumentation to measure the effects of cooling rate on glass-cracking and its subsequent effect on the heat-transfer characteristics of the glass waste form. Controlled heating and cooling tests were conducted with these two canisters.

Test welds made with the canister lid-welding system were examined by the FRG regulatory authorities to qualify the procedures and control parameters that we developed. Cleanout and renovation of the 324 Building A-Cell canister decontamination, characterization and storage facility was completed. Fabrication of all the required A-Cell equipment was completed and functional testing initiated for most systems.

## WEST VALLEY SUPPORT

Criteria and remote designs were prepared for several components of the West Valley Demonstration Project's tank jumper pits, in-cell feed and sampling system, melter, off-gas system, canister-capping and decontamination systems, and cell-maintenance station. Wall nozzle locations within the vitrification cell were finalized so that in-cell jumper designs could begin and so the design and fabrication of the cell walls could be finished. The concentrator feed makeup tank and the remote sampler for collecting samples of the feed concentrate slurry were designed for high-level waste vitrification.

A canister decontamination process was developed that uses the cerium (IV) ion to chemically mill a thin layer from the canister surface. Process streams from the waste tanks to the melter feed tank were simulated on a laboratory scale and were characterized in terms of chemical and rheological properties. Methods were developed for removing excess sulfate from the melter feed and for determining the metal fines concentration in the sludge wastes. Shear vane tests were conducted to measure the shear strength of the sludge on the bottom of the 8D-2 tank at West Valley, and a sludge simulant with the appropriate rheological properties was developed. The RECIPE computer code was developed to aid in producing a final glass product within a target composition region. The MASBAL computer code was developed 1) to infer the glass composition in the canister based on chemical analyses of the slurry in the feed tank, process measurements, and knowledge of the mixing characteristics of the melter and 2) to establish confidence limits about the inferred glass composition based on uncertainties in the compositions and process measurements. A failure modes and effects analysis of the West Valley vitrification system was completed.

The chemical durabilities of the reference glasses were tested for the effects of ferrous/ferric ratio and heat treatment, along with the effects of groundwater source and chemistry. Impact testing was completed for several candidate canister designs to determine their resistance to breaching.

## LOW-LEVEL WASTE COORDINATION

A comprehensive program plan to complete development of sorbent barrier technology for shallow land burial grounds was prepared. Additional information on barrier performance using flow-through column tests was obtained to complete the preliminary economic feasibility study. The clinoptilolite formulation tested appears to have superior sorption properties and is cost-effective.

Under the Special Waste-Form Lysimeters - Arid Program, analysis and documentation of the 3 years of hydrologic and chemical data related to leaching of commercial low-level waste forms was started. Two radionuclides, cobalt-60 and tritium, and several other chemical species in the waste were

found in lysimeter leachates to date. These actual field data should allow more definitive analysis of source terms than can be done with currently available laboratory data.

CONTENTS

## FIGURES

## TABLES

# 1.0 NONRADIOACTIVE TESTING

W. L. Kuhn - Manager

## 1.1 OBJECTIVES

The Nonradioactive Testing Task was established in fiscal year 1985 with the broad objectives to: 1) complete the development of liquid-fed ceramic melter (LFCM) vitrification equipment, 2) provide the nonradioactive portion of the information necessary to establish both nonradioactive-to-radioactive LFCM equipment performance correlations and a vitrification process control-to-glass product quality correlation, and 3) document LFCM design and operations technology for use by the private nuclear industry in future commercialization efforts.

When Congressional funding for the Nuclear Waste Treatment Program (NWTP) ended in fiscal year 1986, DOE guidance was provided to close out the program in a safe, efficient and orderly fashion using available funding reserves. Consequently, the major objective in FY 1987 for the Nonradioactive Testing Task was to advance all ongoing work to a logical break point where documentation could be prepared. The four specific objectives defined for FY 1987 activity were:

- Simulate the West Valley Vitrification System with respect to a mass balance model in order to evaluate stochastic process modeling applied to a real process.
- Develop approximate product models predicting the variation in durability and devitrification in glass with variation in composition, and integrate the product models into an overall process simulation.
- Complete improvements in applying the TEMPEST heat transfer code to predict the glass temperatures during cooling in a canister, including comparison to experimental data, development of a user interface, and an example application of the code.

- Complete documentation of various important advances in or investigations of the LFCM technology provided by the NWTP through the end of FY 1986.

## 1.2 SUMMARY

A simulation model has been developed and tested preliminarily by applying it to approximate operation of the West Valley Demonstration Project (WVDP) vitrification system. A control logic for the WVDP process was approximated and cast in the form of an input file as required by the simulation model. Multivariate statistical techniques have been identified and described that can be applied to analyze large sets of process measurements.

The TEMPEST heat-transfer computer code was used to simulate thermal behavior of nuclear waste glass in canisters of varying dimensions. The experimental data obtained provided a sufficiently accurate basis for validation of this code.

A partial least squares method was applied to correlating the chemical durability of a collection of nuclear waste glasses with some success. The ratio of weight fractions of sodium and boron to aluminum and silicon showed the strongest relationship to chemical durability.

A total of 22 formal topical reports and presentations were completed in FY 1987 under the NWTP.

## 1.3 VITRIFICATION PROCESS SIMULATION - W. L. Kuhn, M. R. Toland, and B. A. Pulsipher

A principal objective of the NWTP is to establish relationships between vitrification process control and glass product quality.

An important goal during testing of a vitrification system is to show that departures significant enough to affect product quality can also be detected in time to prevent an unacceptable canister from being produced, while also showing that departures too insignificant to be detected will not significantly decrease the quality of the product. That both of these hold is a practical definition of a successful strategy for sampling, data

analysis, and process control. Simulation of the process allows this definition to be tested early in the development of a process, based on whatever hypothetical departures from ideal process behavior can be identified and included in the simulation.

The NWTP approach to waste-form qualification thus includes:

- simulating the process
- introducing departures from ideal behavior
- analyzing the data as though it were real data in order to determine:
  - the effectiveness of statistical methods to monitor and control the process when departures from ideal behavior occur
  - what impact detectable departures from ideal behavior have on the quality of the product.

Implementation of the approach is not yet complete; two important steps, however, have been added. First, a simulation model has been developed and tested preliminarily by applying it to approximate the operation of the WVDP vitrification system. A control logic for the WVDP process was approximated and cast in the form of an input file as required by the simulation model. The model includes the capability to simulate random errors in measurement and control, systematic errors, and departures from ideal mixing behavior. This provides for generating large sets of simulated process measurements that reflect the existence or absence of systematic errors or departures from ideality. These sets can be investigated using trial data analysis techniques to determine whether such errors or departures can be detected during operation of a real process.

Secondly, multivariate statistical techniques have been identified and described that can be applied to analyze large sets of process measurements. Their use in controlling a process through process control charting is also described. The techniques involve collecting information on the composition of a number of the chemical components in the feed and glass, for batches in each of the tanks (including the melter), and for each repetition of the

batching cycle of the vitrification system. This information over components, tanks, and time is then combined to create a single statistic through which all the information can be used at once to determine whether the process has departed from normal. Process control charting is used to examine the statistic and to make decisions about the need for changes in the process.

### 1.3.1 Simulation Model

In an ideal process there would be ideal mixing in tanks, and, aside from measurement and control errors, the composition of the feed and glass could be predicted from simple mass balances. Plausible departures from such ideality that could affect the validity of an assumed mass balance model would be sedimentation and resuspension of part of a slurry in tanks. Sedimentation and resuspension of solids in a slurry are addressed in the process simulation. Caking of all the slurry on the sides of tanks and return of cake to the slurry are also included. Other phenomena can be included as desired.

A vitrification process was simulated by defining the following:

- tanks (which might not be process tanks) for which transient mass balances are solved by integration time derivatives of masses in the tanks
- phases within tanks that allow water, dissolved solids, undissolved (suspended) solids, and sediment and caked material to be treated separately in the calculations
- streams connecting tanks to each other
- events described in terms of volumes of liquid in tanks or of elapsed time, which when detected interrupt the normal integration over time and cause various actions that modify the process (for example, streams are turned on or off).

Each tank in the process is described in terms of the distribution of each incoming chemical component among phases 1 through 3 (only water resides in phase 1) and the density of each of the phases in that tank. The tanks have no prescribed volume; the volume is manifest only in control actions,

where the volumes at which liquid transfers begin or end are specified. To allow simulation of the disposition of chemical species upon entering tanks, leaving tanks, and while in tanks, five phases are defined to exist in each tank. They are 1) water, 2) dissolved solids, 3) suspended, undissolved solids, 4) undissolved solids settled on the bottom of a tank, and 5) dissolved and undissolved solids caked on the sides of a tank above the liquid level. Each stream in the process is described by its inlet and outlet tanks, and the simulation continuously determines whether it is flowing at any given time. The distribution of mass from a tank into a stream is described in terms of the fraction of the volumes of each of phases 1 through 3 in the tank that contributes to the volumetric flow rate of the stream.

Control of the process is defined in terms of events; these are either that a volume reaches some specified value or time reaches some specified value. Whenever an event occurs, some predetermined control action is taken. Examples of actions are turning a stream on or off, defining that some condition is true or false (for use in future control decisions), taking a sample from a tank, etc. Once an event occurs, any number of control actions might occur, including secondary reactions to actions. However, the entire series of actions always begins when an event is detected. The process is simulated as being stochastic by introducing uncertainty into the simulation of certain measurements and actions as follows:

- The act of sampling is treated as though collecting suspended solids from the liquid is a random process characterized by a normal distribution centered on equal access to liquid and suspended solids by the sampler (this is discussed further below) with a specified standard deviation.
- Chemical analysis of samples is treated as though the reported individual weight fractions were random, uncorrelated, and described by a normal distribution centered on the true weight fractions with a specified relative standard deviation.

- Detection of events by comparing volumes in tanks to specified values is treated as though measurement of the volume is random and described by a normal distribution centered on the actual volume with a specified relative standard deviation.
- Addition of chemical components is treated as being random and described by a normal distribution centered on the calculated masses to be added and with a specified relative standard deviation.

A process control strategy is implemented in a simulation by defining a set of "cases." Each case is described in terms of a set of tests followed by a set of actions. The tests for a case are evaluated using "and" logic. That is, all tests must be satisfied before the case actions are executed. The tests that are included are for a specified liquid volume occurring in a tank, for a stream flowing or not, and for a flag set true or false.

There are currently seven kinds of actions that might be taken, separately or in combination, if a case's tests are met and the case is executed. They are: change stream flow, set flag, delay, sample, test contents, add chemicals, and reset tank.

To evaluate the ability of the methods described above to simulate a vitrification process, they were applied to the case of a system patterned roughly after the West Valley Demonstration Project at West Valley, New York (see Figure 1.1). The simulation is not of this process exactly, since parts of the West Valley process and control strategy are still being determined. Rather, some of the essential features of the process have been included as well as plausible values for the simulation parameters in order to test the simulation methods.

A strategy for controlling the WVDP vitrification process was constructed that is thought to simulate roughly the actual process. We have not attempted to simulate the WVDP control strategy faithfully; rather, we assume the construction is close enough to reality to provide a realistic test of our simulation model. Probably the most significant departure from our understanding of the WVDP strategy is that we have included an additional sampling step.

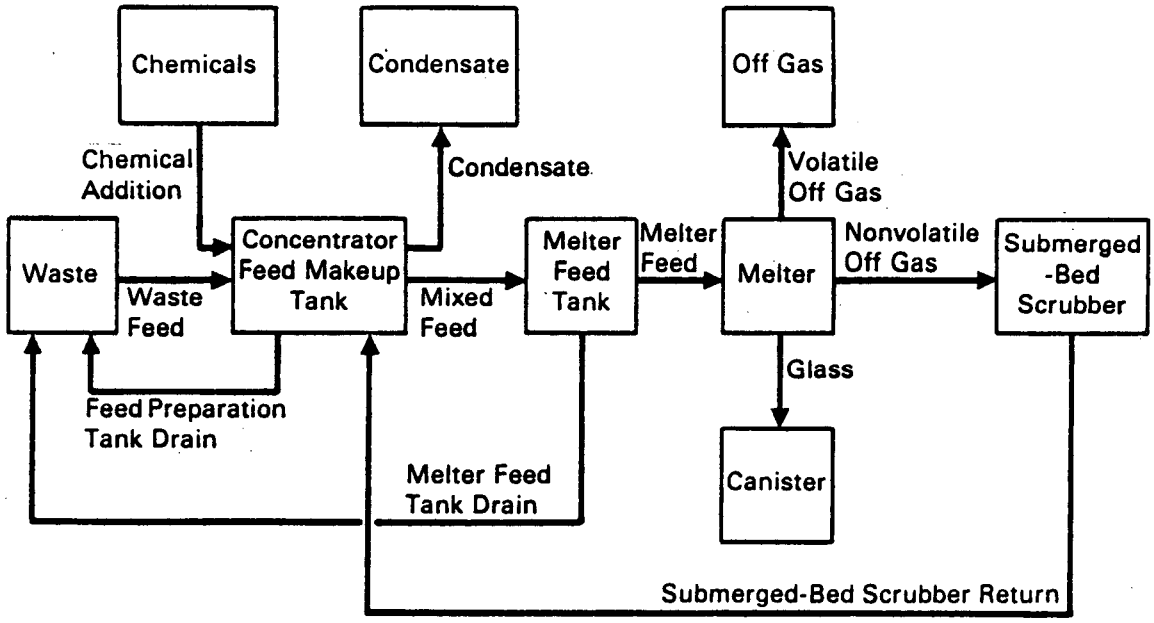


FIGURE 1.1. Schematic of LFCM Vitrification System Patterned Generally After the West Valley System

The salient features of the control strategy simulation are as follows:

1. Liquid is sent from the submerged bed scrubber (SBS) to the concentrator feed makeup tank (CFMT) if the measured liquid volume in the SBS has exceeded a specified level.

2. Waste is transferred from the waste tanks to the CFMT whenever the measured liquid volume in the CFMT is low enough and provided that any need to send liquid from the SBS has been satisfied.

3. After the CFMT receives liquid from the SBS and then is filled from the waste tanks, the contents are sampled, the amount of volume to be removed by evaporation is computed, and evaporation begins.

4. When the evaporation is complete as determined by measuring the volume in the CFMT, chemicals are added to create a feed that will become glass of the target composition, with enough water being added to achieve a desired solids loading in the feed. The chemicals and water are assumed to be added in the form of a slurry; if the solids loading of the slurry

would exceed a specified limit, part of the contents of the tank are sent back to the waste tank, and the chemicals to be added are computed again.

5. After the addition of chemicals is completed, a sample is taken. This is believed to be a departure from current WVDP plans, but was included to simplify (in the simulation) recording the contents of the CFMT after the chemicals are added.

6. The chemical addition cycle in the CFMT is completed and the liquid in the melter feed tank (MFT) is decreased to a specified volume. Then feed is transferred from the CFMT to the MFT until either the liquid in the CFMT has decreased to a specified volume or in the MFT it has increased to a specified volume.

7. The contents of the MFT are sampled. If allowed (see below), feed is sent to the melter. Once the MFT sample results are available, they are checked to see if the contents are acceptable. If not, melter feeding is stopped, the contents are rejected to the waste tank, and the MFT awaits a replacement batch from the next CFMT cycle.

8. Feeding the melter is disallowed if the liquid volume in the SBS exceeds a specified level, if melting is disallowed (see below), or if feed is not available from the MFT.

9. Melting is disallowed if the volume of glass in the melter is too high and a canister is not in place.

10. Glass pours from the melter to the canister by overflow whenever the glass volume exceeds a pouring threshold.

11. When the volume of glass in the canister reaches a specified level, glass is airlifted from the melter to the canister for a specified period. When the airlift is complete, a new canister is installed.

The simulation progressed with an average speed of 200 simulated hours per computer hour using a MicroVax® computer system.

---

® A registered tradename of Digital Equipment Corporation, Maynard, Massachusetts.

### 1.3.2 Multivariate Statistical Process Control

Multivariate statistical methods intended for use as part of waste-form qualification have been developed in four parts as follows.

1. Models have been developed that describe the relationships of the concentrations of chemical components (expressed as oxides in the equivalent glass) in adjacent tanks as batches progress from tank to tank. The models have been formulated in matrix form to facilitate the development and description of a corresponding computational scheme. In the development the vitrification system has been approximated as a feed preparation tank, melter feed tank, and melter; for the WVDP, these would be the CFMT, melter feed tank and melter. All tanks have been assumed to be perfectly mixed. The effect of any accumulation in the cold cap in the melter has been neglected.

2. Multivariate statistical methods have been used to develop equations for estimating the true oxide concentrations in tanks. The methods account for correlation between concentrations (for example, tank to tank and component to component) that would be expected in the data. This is particularly important when trying to sense whether the process is in statistical control or whether it is drifting--that is, fluctuations increasing or changing in character. One needs to evaluate not how a single variable fluctuates, but how several variables fluctuate together. For example, it may be normal--that is, typical of a stable process--for two measured variables to fluctuate independently of each other, but not for them to fluctuate in unison. Multivariate statistical methods have been applied to permit distinguishing between such cases for a large set of measured variables or to discover what relationships <u>are</u> normal among complicated combinations of measured variables.

3. Multivariate process control charts have been described that can be used for monitoring the oxide concentrations of the frit/waste slurry wherever it is sampled in the process. To control the process based on deviations from normal behavior as discerned from many measurements, at several locations, and over weeks of time requires

a method for combining all such data into a single statistic. Data can be combined into a statistic distributed as "Hotelling's $T^2$" statistic; its application to process control charting has been examined.

4. The extent of sampling required and the assumptions that have been made in the statistical analyses have been examined. It is important to determine what sampling is required to build covariance matrices from process measurements one wants to consider when monitoring and controlling the process.

## 1.4 MULTIVARIATE STATISTICAL ANALYSIS OF GLASS DURABILITY - B. A. Pulsipher

In controlling a process it is desirable to limit the number of variables whose values are to be constrained. In the case of a waste vitrification system, one important quality characteristic of the glass to be achieved is adequate chemical durability. Plodinec, Jantzen, and Wicks (1984) and Grambow (1985) have related the durability of nuclear waste glasses to their composition by calculating a free energy of hydration for each glass and correlating it with the chemical durabilities.

It is also possible to reduce such data using purely statistical methods. Data accumulated by Plodinec, Jantzen, and Wicks[(a)] and by Chick et al. (1984) were analyzed to examine the relationship between the logarithm of chemical durability and the composition of the glass. The release of boron into solution after 28 days in a static leach test was taken to be the measure of chemical durability.

The data were analyzed using the partial least squares (PLS) method (Wold 1982). This is an extension of the principal components method for extracting from a covariance matrix a set of variables that are each liner combinations of the original variables used to form the matrix. These new variables, called principal components, more clearly reveal the source of the covariances. Often the majority of the variance over the independent

---

(a) We are indebted to Dr. Carol Jantzen of Savannah River Laboratory for making this data available.

variables is explained by a few principal components; if so, it implies that some of the supposedly independent variables are in fact not statistically independent and should be reduced to a fewer number of variables (viz., principal components) before attempting correlations with a dependent variable.

The PLS method differs from the principal components method in that the principal components are "rotated" (thinking of the principal component in a vector in "space" where the "directions" are the different independent variables, e.g., weight fractions) to line up better with a "vector" representing the dependent variable, e.g., chemical durability. This results in forming a clearer picture of the contribution of the independent variables in predicting the values of the dependent variable. Specifically, the relative importance of the independent variables in predicting the dependent variable is established.

When used in correlating the chemical durability of a collection of nuclear waste glasses to their composition, the PLS method reveals the relative importance of different chemical elements to the correlation. The importance is revealed by examining the contribution of the weight fractions of the elements to the PLS components. These contributions are termed "loadings," and describe how a PLS component is formed as a linear combination of the weight fractions. The magnitude of the loadings is not easily interpreted, but the relative magnitudes of the loadings describe the relative importance of the weight fractions to the chemical durability.

The result of applying a PLS analysis to the data of Plodinec, Jantzen, and Wicks and of Check et al. (1984) is shown in Table 1.1. For the data examined, the "$R^2$" value is 0.75, meaning that 75% of the variance of the dependent variable (chemical durability) can be explained by the nonrandom effect of the independent variables (weight fractions). Practically all of this variance is explained by only the first three of the PLS components. These components are as shown in Table 1.1; the values in the columns are the "loadings" that show how each of the three components depend linearly on the weight fractions of the chemical elements listed.

TABLE 1.1. Results of Applying Partial Least Squares Analysis to Data on Nuclear Waste Glasses

| Element | First PLS Component | Second PLS Component | Third PLS Component |
|---|---|---|---|
| Al | -0.32 | -0.24 | -0.08 |
| Ca | -0.06 | -0.34 | -0.14 |
| Fe | -0.02 | -0.15 | -0.45 |
| Mg | -0.11 | 0.41 | 0.34 |
| Mn | -0.10 | 0.19 | -0.39 |
| Na | 0.53 | 0.04 | 0.06 |
| Li | -0.03 | 0.37 | -0.08 |
| Ni | -0.06 | 0.06 | -0.28 |
| Si | -0.48 | -0.17 | 0.08 |
| Cr | 0.13 | -0.30 | 0.21 |
| B | 0.49 | 0.11 | -0.08 |
| Sr | 0.06 | -0.19 | 0.35 |
| Zr | -0.08 | 0.05 | 0.27 |
| Ti | -0.20 | 0.31 | 0.22 |
| K | -0.14 | 0.26 | 0.10 |
| Cs | -0.04 | -0.20 | 0.14 |
| P | 0.15 | -0.28 | 0.24 |
| Nd | -0.08 | -0.10 | 0.18 |

The first PLS component alone explains about 50% of the variance. A component constructed instead by "loading" in proportion to the free energies of hydration of the chemical elements (which is equivalent to applying the free energy of hydration correlation discussed above) explains about 40% of the variance. From a purely statistical viewpoint, the first PLS component does as well or better than the free energy of hydration in explaining the data. Therefore, it is worth examining the loadings to see what is implied.

The first PLS component depends most strongly on the aluminum, sodium, silicon and boron weight fractions. The signs of the loadings show that, to a rough first approximation, the chemical durability depends on the ratio of the weight fractions of sodium and boron to silicon and aluminum. The implications of this are that in trying to control a waste vitrification process to maintain acceptable chemical durability of the glass, controlling the ratio (for example) of sodium and boron to silicon and aluminum should be emphasized. This implication needs further confirmation, but if confirmed suggests that the fluctuation of some chemical components during processing may need to be closely controlled, while others may not be important enough

to be included in process control criteria. For example, given the above results, it might be desirable to control independently the sodium, boron, silicon and aluminum weight fractions when adding chemicals to form the melter feed from the waste, while it may also be unnecessary to control other chemical species at all.

Details of the work covered here are to be published in a PNL topical report by Kuhn et al., Process Simulation and Statistical Approaches for Validating Waste-Form Qualification Models.

## 1.5 CANISTER THERMAL MODELING - D. W. Faletti, M. J. Budden, and R. K. Farnsworth

The TEMPEST heat-transfer computer code[(a)] was used to simulate thermal behavior of nuclear waste glass after it is poured into canisters for long-term storage. This work was done to determine the accuracy and applicability of the TEMPEST code when used to compute canister thermal histories.

Experimental data were obtained to validate our application of the TEMPEST code. Five canisters were instrumented with appropriately located radial and axial thermocouples. The canisters varied in diameter (12 in., 13 in., and 24 in.), height (45 in., 56 in., and 85 in.), internal insulation thickness (0 to 1/2 in.), and external insulation thickness (0 to 3 in.). The canisters were filled using the pilot-scale ceramic melter at PNL in either a continuous or a batch filling mode. Typical results are shown in Figures 1.2 and 1.3. One of the canisters was also filled within a simulated turntable (a group of cylindrical shells with heat-transfer resistances similar to those of an actual canister in a liquid-fed ceramic melter turntable). This was done to provide a basis for assessing the TEMPEST code's ability to

---

(a) Trent, D. S., L. L. Eyler, and M. J. Budden. 1983. TEMPEST - A Three-Dimensional Time-Dependent Computer Program for Hydrothermal Analysis. Volume I: Numerical Methods and Input Instructions. Pacific Northwest Laboratory, Richland, Washington.

Eyler, L. L., D. S. Trent, and M. J. Budden. 1983. TEMPEST - A Three-Dimensional Time-Dependent Computer Program for Hydrothermal Analysis. Volume II: Assessment and Verification Results. Pacific Northwest Laboratory, Richland, Washington.

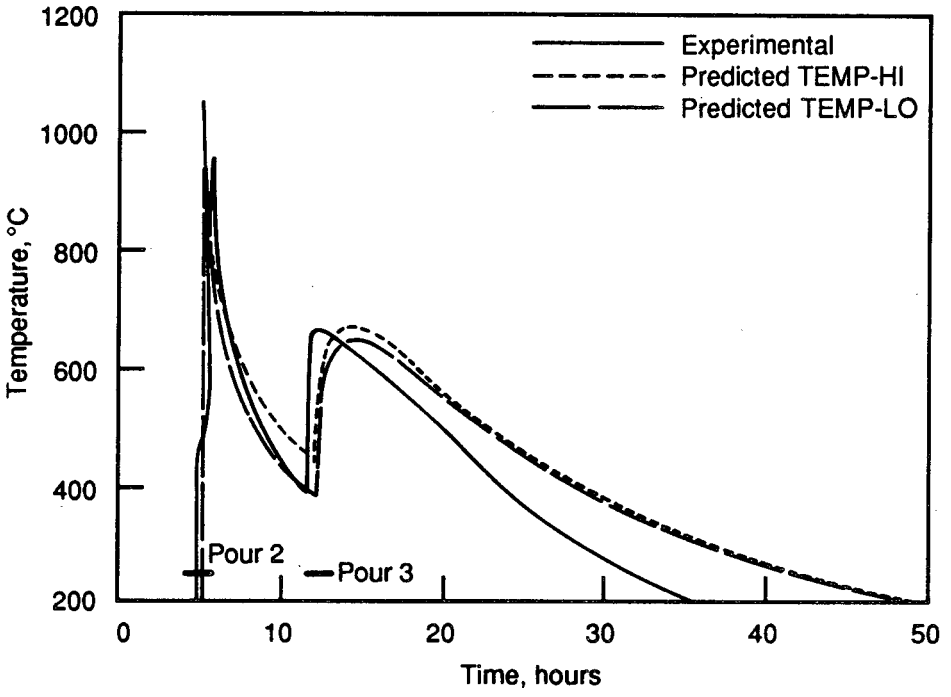


FIGURE 1.2. Typical Experimental and Predicted Temperatures for a 12-in. Canister Filled in Three Batch Pours. The glass level did not reach the thermocouple (located 24.9 in. from the bottom) until the second pour.

also model heat transfer within a structure thermally similar to such a turntable. The turntable as concept-modeled represents a closed tank positioned below the melter discharge region in which canisters are placed to receive the molten glass product and are allowed to cool for some period of time.

After the data were obtained from the pilot-scale ceramic melter runs, two versions of TEMPEST--the batch fill and the continuous fill models--were used to simulate the experimental conditions. The thermal histories predicted by these TEMPEST versions were then compared to the experimentally measured data.

We found that the batch-fill model predicted canister centerline temperatures that agreed closely with experimental temperatures, varying from only 50 to 125°C over most of the canister cooldown period. However, during periods immediately following a glass pour, temperatures were overpredicted by as much as 250°C.

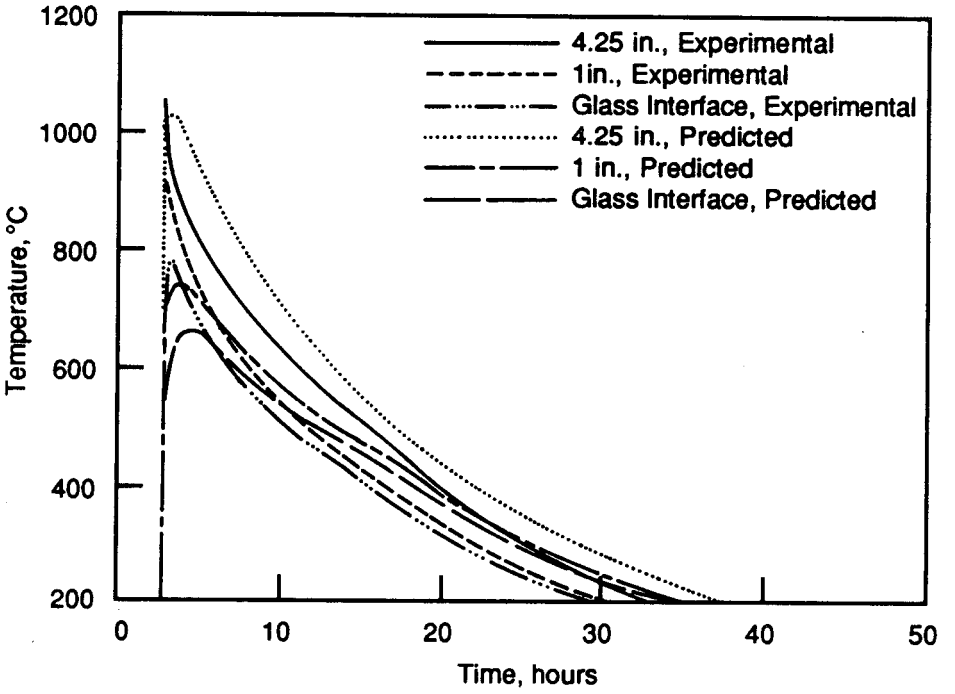


FIGURE 1.3. Typical Experimental and Predicted Temperatures for a 13-in. Canister with Thermocouples Located 26 in. from the Bottom. This canister was filled continuously.

The continuous-fill model was found to predict temperatures with more accuracy. Variation from experimentally measured temperatures was within 50°C or less over most of the cooldown. Close agreement was achieved also for temperatures at other radial positions away from the centerline and for periods long after the glass surface rose above a given elevation.

The experiment using the simulated turntable demonstrated that TEMPEST can adequately model the asymmetric temperature field caused by the turntable geometry. Further, TEMPEST can acceptably predict the temperatures within a turntable, despite code limitations in computing simultaneous radiation and convection heat transfer between shells, along with uncertainty in stainless-steel surface emissivities.

Based on the successful performance of the continuous fill model, development was initiated to incorporate 1) full viscous glass convection, 2) a dynamically adaptive grid that automatically follows the glass/air interface throughout the transient, and 3) a full-enclosure radiation model to allow

radiation heat transfer to non-nearest neighbor cells. At the end of FY 1987, the first feature was fully incorporated and the second feature had been partially accomplished. A more advanced application of TEMPEST was attempted but could not be completed within available time and funding.

Details of the work described here are presented by Farnsworth, Faletti, and Budden (1988).

## 1.6 NWTP TECHNOLOGY DOCUMENTATION

Emphasis was placed on the documentation of NWTP work largely performed in FY 1986 as a key part of the efficient closeout of the program. The complete list of topical reports and presentations prepared in FY 1987 is presented below in reference format.


Bray, L. A., and N. M. Thomas. 1987. "Decontamination of Stainless Steel High-Level Waste Canisters." Presented at American Nuclear Society Winter Meeting, November 15-19, 1987, Los Angeles, California.

Brouns, R. A., C. R. Allen, and J. A. Powell. 1987. LFCM Vitrification Technology Quarterly Progress Report October-December 1986. PNL-6320-1, Pacific Northwest Laboratory, Richland, Washington.

Brouns, R. A., and W. L. Kuhn. 1986. Qualification of Commercial High-Level Waste Forms: Approach and Status. PNL-5929, Pacific Northwest Laboratory, Richland, Washington.

Burkholder, H. C., and C. R. Allen. 1987. LFCM Vitrification Technology Quarterly Progress Report April-June 1986. PNL-5904-3, Pacific Northwest Laboratory, Richland, Washington.

Burkholder, H. C., and C. R. Allen. 1987. LFCM Vitrification Technology Quarterly Progress Report July-September 1986. PNL-5904-4, Pacific Northwest Laboratory, Richland, Washington.

Burkholder, H. C., and R. A. Brouns. 1987. Nuclear Waste Treatment Program Annual Report for FY 1986. PNL-6325, Pacific Northwest Laboratory, Richland, Washington.

Carleson, T. E., et al. 1987. Evaluation of the Transport and Resuspension of a Simulated High-Level Nuclear Waste Melter Feed Slurry. PNL-6302, Pacific Northwest Laboratory, Richland, Washington.

Goles, R. W., et al. 1986. "Remote Canister Level, Turntable Positioning System." Presented at American Nuclear Society 1986 Winter Meeting, November 16-21, 1986, Washington, D.C.

Holton, L. K., Jr., et al. 1987. "Equipment Experience in a Radioactive LFCM Vitrification Facility." Presented at American Nuclear Society National Meeting, November 17, 1986, Washington, D.C.

Koegler, S. S. 1987. Pilot-Scale Ceramic Melter 1985-1986 Rebuild. PNL-6259, Pacific Northwest Laboratory, Richland, Washington.

Larson, D. E., et al. 1987. "Electropolishing Decontamination System for High-Level Waste Canisters." Presented at Waste Management '87, February 28 - March 5, 1987, Tucson, Arizona.

McElroy, J. L., et al. 1987. "Fabrication of Isotopic Heat and Radiation Sources for the Federal Republic of Germany." Presented at the International Conference on Nuclear Fuel Reprocessing and Waste Management RECOD 87, August 23-27, 1987, Paris, France.

Oma, K. H., W. A. Ross, W. L. Smith, and J. R. Adams. 1987. "Innovative HEPA Filter Designs to Reduce Waste Generation and Simplify Waste Treatment." Presented at Waste Management '87, February 28 - March 5, 1987, Tucson, Arizona.

Peterson, M. E., et al. 1987. "Comparison of Rheological Evaluation Techniques and Turbulent Flow Prediction of a Simulated Nuclear Waste Melter Slurry." Presented at the Twelfth International Conference on Slurry Technology, March 31 - April 3, 1987, New Orleans, Louisiana.

Pulsipher, B. A., and W. L. Kuhn. 1987. "Statistical Process Control: An Approach to Quality Assurance in the Production of Vitrified Nuclear Waste." Presented at Waste Management '87, February 28 - March 5, 1987, Tucson, Arizona.

Pulsipher, B. A., and W. L. Kuhn. 1987. Statistical Process Control Applied to the Liquid-Fed Ceramic Melter Process. PNL-6268, Pacific Northwest Laboratory, Richland, Washington.

Reimus, M. A. 1987. "The Use of a Continuously Fed Laboratory-Scale LFCM Mini Melter Nuclear Waste Glass Development." Presented at regional meeting of the American Ceramic Society, Seattle, Washington, October 1986.

Reimus, M. A., S. C. Marschman, and G. L. Graff. 1987. Development of a Continuous Liquid-Fed Laboratory-Scale Mini Melter for Nuclear Waste Glass Development. PNL-6073, Pacific Northwest Laboratory, Richland, Washington.

Ruecker, C. M., and P. A. Scott. 1987. Parameters Influencing the Aerosol Capture Performance of the Submerged-Bed Scrubber. PNL-6035, Pacific Northwest Laboratory, Richland, Washington.

Ruecker, C. M., and P. A. Scott. 1987. Design Procedure for Sizing a Submerged-Bed Scrubber for Airborne Particulate Removal. PNL-6036, Pacific Northwest Laboratory, Richland, Washington.

Westsik, J. H., and B. B. Brenden. 1987. Melter Viewing System for Liquid-Fed Ceramic Melters. PNL-6334, Pacific Northwest Laboratory, Richland, Washington.

Westsik, J. H., Jr. 1986. Temperature Control System for Liquid-Fed Ceramic Melters. PNL-6009, Pacific Northwest Laboratory, Richland, Washington.

About 20 formal reports and papers are being prepared and issued in FY 1988 documenting NWTP work.

## 1.7 CONCLUSIONS

Conclusions from the process and product modeling reported here are as follows:

- For waste-form qualification, a practical definition of a successful system to monitor and control an inherently fluctuating waste vitrification process is the ability to detect departures from assumed ideal process behavior that are great enough to substantially affect product quality.
- The fluctuating behavior of compositions in a waste vitrification process can be simulated in terms of a set of cases, each consisting of a set of tests to be satisfied and a set of actions to then be taken. The tests should include at least tank volume, stream flow, and conditions signified by true/false flags. The actions should include at least: setting a flag, setting a flag after a specified delay, turning a stream on or off, evaporation, sampling tank contents, chemical addition, testing tank contents, and resetting tank masses to zero.
- Mass balances and separation of mass in a process can be simulated sufficiently to address waste-form qualification issues by considering the distribution of chemical components among phases upon entering a tank and in terms of the relative access of the phases to a stream exiting the tank.
- Multivariate statistical methods for analysis of variance and covariance can be combined with simplified mass balance equations cast in matrix

form to estimate compositions and their variance-covariance matrix for a vitrification process, where information from different tanks and different times is used simultaneously.

- The variance-covariance matrix for compositions can be combined into a single statistic approximately distributed as "Hotelling's $T^2$" statistic to provide a reduced variable for process control charting. This will be sensitive simultaneously to composition data over all components, tanks, and previous sample times.
- Given a preliminary multivariate statistical analysis of glass leach data, it might be desirable to independently control the sodium, boron, silicon and aluminum weight fractions when adding chemicals to form the melter feed from the waste, and it may be unnecessary to control other chemical species at all. This approach, however, considers only the chemical durability of the glass.

Conclusions from the work testing TEMPEST code predictions against experimental data are as follows:

- The experimental data provided a sufficiently accurate basis to validate this application of the TEMPEST code and will continue to be valuable for any future code validation study of glass pour and cooldown phenomena.
- The TEMPEST batch-fill model was sufficiently accurate to be useful for many LFCM applications. However, during periods immediately following a pour, this TEMPEST model overpredicted temperatures by as much as 250°C.
- The underprediction of cooldown at times later than 10 hr after a pour is probably the result of the canister insulation having about a 25% higher effective thermal conductivity than that used by TEMPEST. Further analysis is necessary to confirm this hypothesis.
- The TEMPEST continuous-fill model did a better job of predicting temperatures than did the batch model. Temperatures predicted near the centerline were within 50°C or better over most of the cooldown.

- Experiments using a simulated turntable demonstrated the following:
  - The asymmetrical temperature profile caused by the asymmetrical turntable geometry can be modeled by TEMPEST.
  - TEMPEST produces reasonable predictions of the temperatures within a simulated turntable, despite the code's limitations in computing simultaneous radiation and convective heat transfer, and despite considerable uncertainty in the emissivities of the stainless-steel surfaces.
  - The best agreement between predicted and observed temperatures was found between the overpack to seal liner, the seal liner to thimble, and the thimble to turntable wall. Poorest agreement was observed between the canister wall to the overpack and the turntable wall to the ambient.

## 1.8 REFERENCES


Chick, L. A., et al. 1984. West Valley High-Level Nuclear Waste Glass Development: A Statistically Designed Mixture Study. PNL-4992, Pacific Northwest Laboratory, Richland, Washington.

Farnsworth, R. K., D. W. Faletti, and M. J. Budden. 1988. Application of the TEMPEST Computer Code to Canister-Filling Heat Transfer Problems. PNL-6474, Pacific Northwest Laboratory, Richland, Washington.

Plodinec, M. J., C. M. Jantzen, and G. G. Wicks. 1984. "Thermodynamic Approach to Prediction of the Stability of Proposed Radwaste Glasses." In Nuclear Waste Management. Advances in Ceramics, Vol 8., eds. G. G. Wicks and W. A. Ross, pp. 491-495, American Ceramic Society, Columbus, Ohio.

Wold, H. 1982. In Systems Under Indirect Observation, Part II, eds. K. G. Jareskog and H. Wold, North Holland Publishing Co., Amsterdam, pp. 1-54.

# 2.0 ISOTOPIC HEAT AND RADIATION SOURCE FABRICATION

J. E. Minor and L. K. Holton, Jr., Managers

## 2.1 OBJECTIVE

The objective of this task is to fabricate 30 waste canisters containing prescribed amounts of $^{90}Sr$ and $^{137}Cs$ in a borosilicate glass for the Federal Republic of Germany's (FRG) disposal studies and to fill and test two additional instrumented canisters for heat-transfer model validation.

In addition to operation of the pilot-scale radioactive liquid-fed ceramic melter (RLFCM) in order to fill the canisters with radioactive glass, a necessary component of this task is to provide a facility for welding, testing, characterizing, decontaminating, and storing radioactive canisters. A-Cell is being prepared to provide this facility. The data from this work will provide future users of the technology with a background to aid in the design and operation of liquid-fed ceramic melter (LFCM) systems.

## 2.2 SUMMARY

During FY 1986 Pacific Northwest Laboratory (PNL) received and concentrated the initial cesium ($^{137}Cs$) and strontium ($^{90}Sr$) feed stocks, and filling of the first set of ten canisters began. This first run (RLFCM-7) was terminated by problems with highly volatile feed slurry components. Seven months were then required for modifications to the melter, the off-gas system, and the cell ventilation system to handle the high $^{137}Cs$ concentration in the molten glass.

In October 1986, following the required modifications, filling of the ten canisters planned for RLFCM-7 was completed and RLFCM-8 began. During that run the melter discharge section became plugged. Methods were devised for melting that pluggage, and the run was completed. The ten canisters filled during RLFCM-9 then completed in March 1987 the filling of all 30 canisters intended for FRG repository tests.

While the 30 canisters were filled, preparations for instrumented canister testing were completed. Two canisters were prepared with acoustic

sensors and an array of thermocouples within each canister. Furnace equipment for controlled heating of the canisters was tested and modified. These canisters were filled immediately after the first 30, in March 1987.

Controlled heating and cooling tests were conducted with the radioactive instrumented canisters. Acoustic sensors were used to detect cracking of the annealed glass during cooling, and thermocouples were used to detect the effect of cracking on heat transfer and resultant glass temperatures within the canisters. Fourteen separate tests were conducted between April and July 1987. The resulting data were compiled and provided to the FRG sponsor.

The filled canisters will be provided with a gas tungsten arc (GTA) weld closure to meet the FRG specifications. Canister lids were test-welded to canister flanges and shipped to the FRG for destructive and nondestructive evaluation. A test stand was then fabricated that permitted the testing of remote canister handling and welding. Two nonradioactive canisters were then welded by remote techniques in the presence of FRG observers. Both canisters were successfully leak-tested using a helium-leak test procedure to the required specifications.

A necessary component of the isotopic source fabrication is the capability to decontaminate, characterize, and store the canisters filled with vitrified product in preparation for shipment. Equipment to be installed in A-Cell and the air lock of the 324 Building at Hanford to provide a decontamination, characterization and storage facility includes: 1) helium leak-testing equipment to check for absolute closure of the canister, 2) a system to measure surface radiation dose rate, 3) an electropolishing unit to remove contamination from the outside of the sealed canister not removable by a water/steam spray, 4) a gamma-scanning system for determining glass-fill homogeneity, 5) a gauge for checking maximum diameter and straightness of canisters, 6) equipment to measure surface temperature, 7) a load cell to determine canister weight, 8) a system to determine canister surface contamination, and 9) a water-cooled rack for canister storage. Fabrication of the required A-Cell equipment was completed and functional testing initiated for

most of the equipment. Cleanout and renovation of A-Cell was also completed in preparation for installing the electropolishing system and canister storage rack.

## 2.3 INTRODUCTION

Since 1973 the LFCM process for vitrifying high-level liquid wastes (HLLW) to borosilicate glass has been under development and testing in the United States. Its early success and inherent simplicity led to its adoption as the reference HLLW vitrification process in the U.S., Japan, and the FRG. Currently the LFCM is the Department of Energy's (DOE) reference process for planned defense and commercial nuclear waste solidification facilities, including the West Valley Demonstration Project, the Hanford Waste Vitrification Plant (HWVP), and the Defense Waste Processing Facility (DWPF) at Savannah River.

Because of the LFCM's wide acceptance as the reference waste vitrification process in the U.S., DOE requested that PNL design, construct and operate a prototypical radioactive pilot-scale waste solidification facility employing the LFCM process. Pilot-scale radioactive testing is used to validate the design and operating data that is being applied to the three production-scale projects. The RLFCM will also provide needed documentation of design, data, and operating experience for use by architect-engineers involved with future commercial waste treatment facilities. The RLFCM equipment was installed in FY 1984 (Burkholder and Rusin 1985) and underwent shakedown testing in FY 1985 using higher levels of activity in each test. In FY 1986 preparation of isotopic heat sources for the FRG began. These heat sources use $^{90}Sr$ and $^{137}Cs$ as the active isotopes in borosilicate glass.

Decontamination, characterization and storage of the canisters of waste glass are necessary components of the RLFCM program. This activity requires the use of hot-cell space because the glass contains large quantities of radioactivity. The 324 Building's A-Cell, adjacent to B-Cell where the RLFCM is located, was selected for this work. Cleanout and renovation of A-Cell has been necessary to make space available as the cell contained obsolete equipment used in previous programs. Extensive radionuclide decontamination

of the cell has been necessary to ensure that canisters decontaminated for shipment are not recontaminated during their interim storage period.

2.4 FILLING OF THE FRG ISOTOPIC HEAT AND RADIATION SOURCES - R. D. Dierks, R. W. Goles, J. E. Surma, F. E. Haun, Y. B. Katayama, and N. M. Thomas

The heat and radiation sources being prepared for the FRG contain $^{137}Cs$ and $^{90}Sr$ as the active isotopes. The heat and dose characteristics for the canisters are shown in Table 2.1.

The RLFCM was used to fill the 32 FRG canisters. It is an electrically heated (joule-heated), ceramic-lined melting device designed to vitrify an aqueous radioactive waste/glass-former slurry and to discharge the resultant molten glass into a receiving canister. The melting surface area is 0.5 $m^2$. The melter has been designed for a nominal operating feed rate of 25 L/hr. The melter refractory arrangement has been designed to contain glass at temperatures up to 1300°C and a viscosity of 100 poise.

The first FRG ten-canister campaign (RLFCM-7) began early in December 1985, and the last campaign ended late in March 1987. Figure 2.1 represents the schedule of the RLFCM operation during this period and some of the major activities that prolonged completion of these melter campaigns.

TABLE 2.1. Average Heat and Dose Characteristics for FRG Canisters

| Number of Canisters | Decay Heat, W/Canister | Surface Dose, R/hr |
|---|---|---|
| 10 | 1490 | 272,000 |
| 10 | 1330 | 112,000 |
| 10 | 1860 | 310,000 |
| 2(a) | 1020 | 190,000 |

(a) Instrumented canisters for thermal performance data.

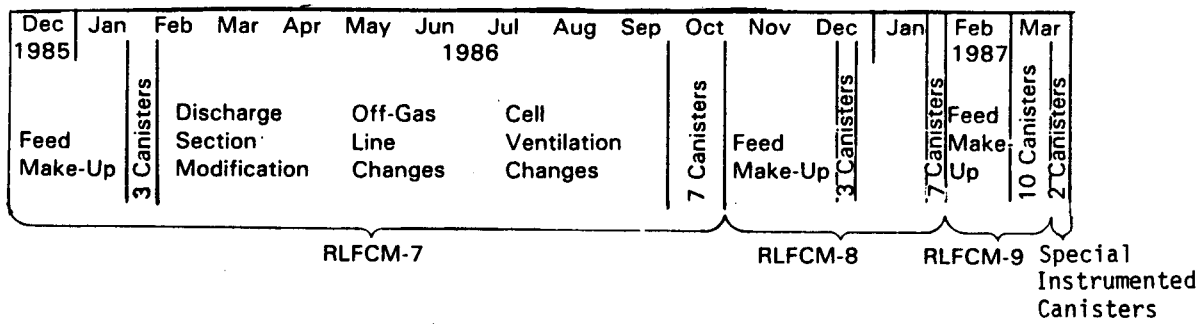


FIGURE 2.1. FRG Heat and Source Canister Production Schedule

### 2.4.1 RLFCM-7

With the first FRG campaign (RLFCM-7), highly volatile feed slurry components created problems not encountered in nonradioactive tests. While Figure 2.1 shows that RLFCM-7 took 11 months, fewer than 25 days of melter operation were required to fill the ten canisters. After a short-lived but encouraging start of RLFCM-7, 7 months were spent modifying the melter, the off-gas system, and the cell ventilation system to handle the high $^{137}Cs$ concentrations in the molten glass.

The composite graphs in Figures 2.2, 2.3, and 2.4 show the operation of the melter for RLFCM-7. It occurred in five active operational periods: 1) January 21 through 25, 2) January 31 through February 5, 3) September 27 through 30, 4) October 6 through 10, and 5) October 19 through 23. To simplify the identification of cause-and-effect relationships among the various operating characteristics, the time-frame format for each figure is identical.

Data were recorded graphically throughout the operation. The graphs, however, do not represent continuous instantaneous data, but discrete data values determined at 1-hr intervals and connected by continuous straight lines. In addition, each 1-hr data value is the average value of 60 instantaneous data values, one obtained every 5 sec over a 5-min period. Thus transient data are not seen on these graphs. Recorded data include feed-tank and melter-tank weight factors, melter-tank pressure, glass temperature (in tank), electrode power values, glass discharge temperature, and melter-tank resistance values.

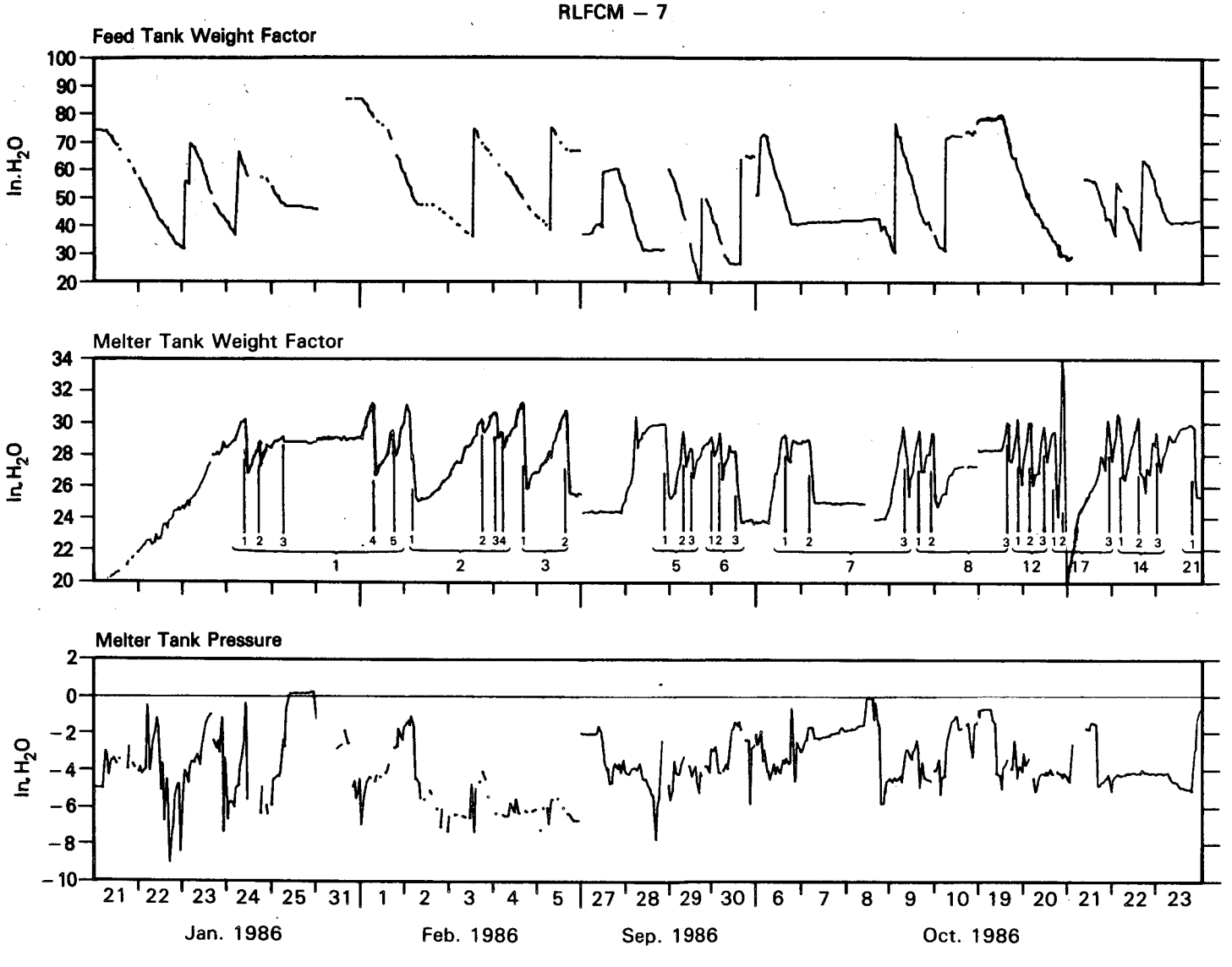


FIGURE 2.2. RLFCM-7 Slurry Feed, Glass Transfer and Melter Vacuum Values

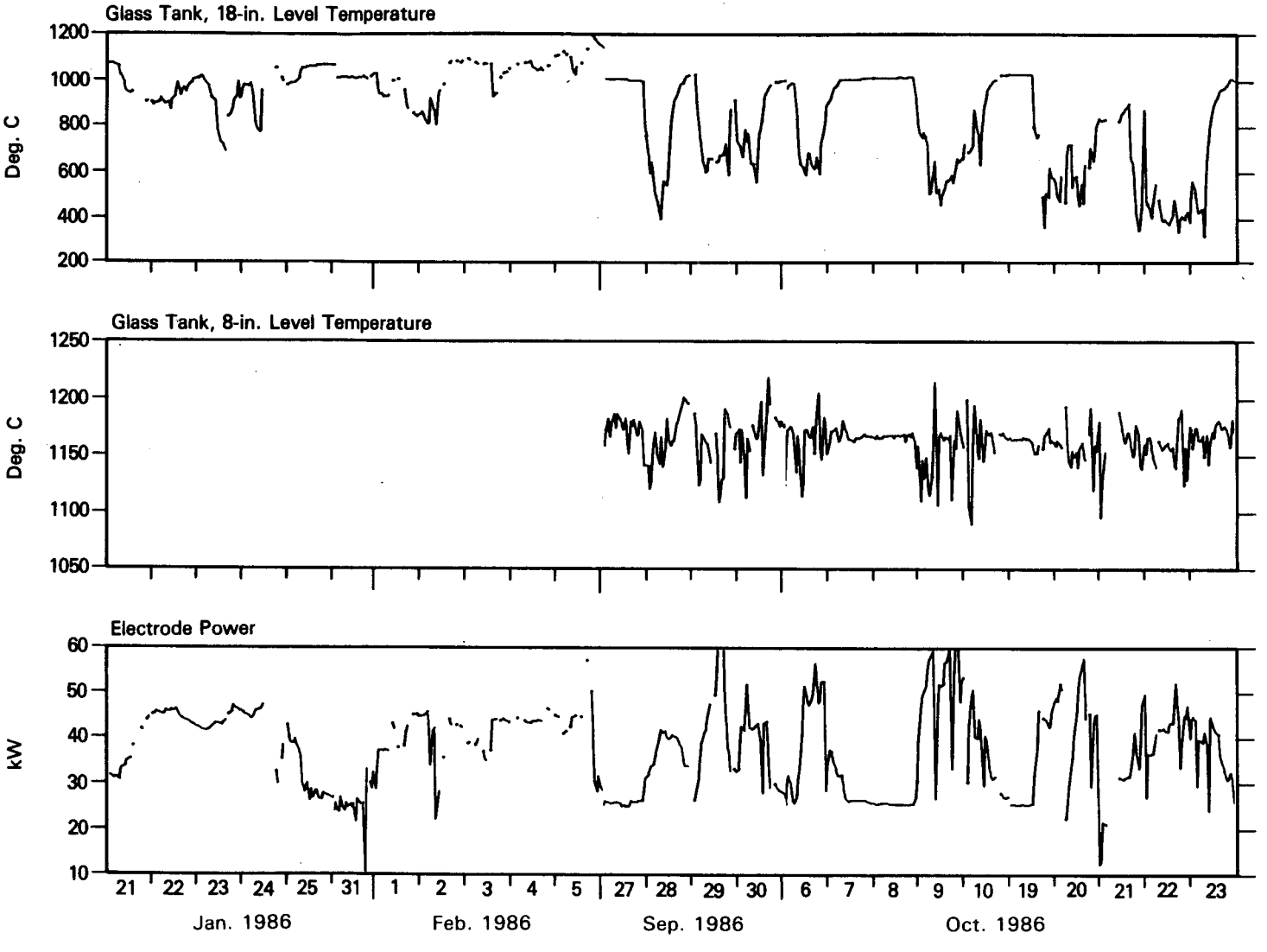


FIGURE 2.3. RLFCM-7 Glass Tank Temperatures and Power Values

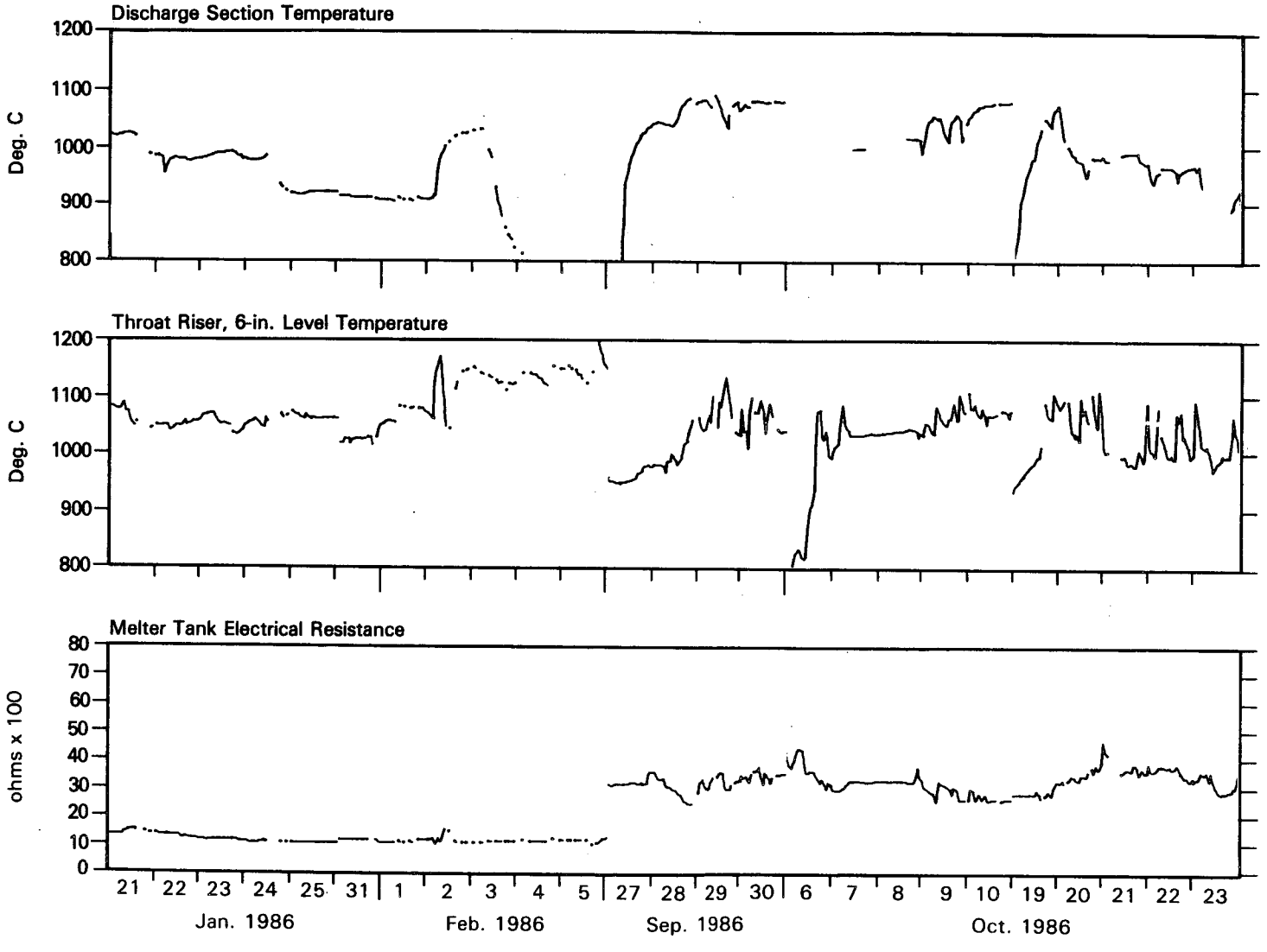


FIGURE 2.4. RLFCM-7 Glass Discharge Temperatures and Melter Tank Resistance Values

Experiment RLFCM-6 had been terminated by reducing the residual glass in the melter tank to a minimum (7-1/4 in.) in preparation for RLFCM-7.

The primary objective of the first portion of RLFCM-7 was to transfer a special feed with a higher than normal concentration of radionuclides to the melter to bring the nonradioactive residual glass from RLFCM-6 up to the glass specifications for the remainder of RLFCM-7. The additions were made in three spike batches, as can be seen on Figure 2.2.

The upper plot in Figure 2.2 shows the feed-tank weight factor indications. These are the product of the depth of slurry feed in the tank and the specific gravity of the slurry. Because the feed tank and its internals are cylindrical, the volume of the tank per inch is constant, and since the specific gravity of the slurry feed is relatively constant, the weight factor indications are directly proportional to the volume of slurry in the tank. Thus slurry feed rates can be inferred from the slope of the weight factor plots.

The vertical lines in these plots result from the feed tank being refilled from the feed makeup tank. These transfers have been labeled with the number of the pour into a receiving canister. Groups of these transfers have been bracketed and given the identification number of the receiving canister. The canister identification numbers do not necessarily correspond with the order in which they were filled.

The lower plot in Figure 2.2 shows the melter tank pressure (vacuum) indications during melter operation. The horizontal line at zero inches of water pressure was added to identify those periods when the melter operated with little or no vacuum in the melter plenum. The difficulty with melter tank vacuum control is clearly seen in these plots.

The middle plot shows the melter-tank weight factor indications during melter operation. The melter tank is symmetrical, making the specific gravity of the molten glass also relatively constant. Thus, as above, the glass-generation rates can be implied from the slope of the melter tank weight factor plots. A reasonable correlation between the slurry feed rates and the glass generation rates is generally apparent; however, when there is a substantial cold cap and the feed is shut off, the glass-level indication

will continue to rise as the cold cap melts. Likewise, if the feed has been shut off after the melter has foamed much, the glass level continues to rise as the glass melts off the walls above the normal glass level and drains into the melter tank.

Figure 2.3 shows the glass tank temperatures of the cold cap (18-in. level) on the top plot and of the glass at the 8-in. level on the middle plot. The power dissipated in the melter tank is shown on the lower plot.

The two horizontal lines have been added to the middle plot to indicate the target range for the glass temperature control. Melter tank glass temperature indications were not available during the melter glass spiking operation. However, with replacement of the thermowell and thermocouple bundle in mid-July, reliable temperature indications were again recorded.

Figure 2.4 shows two other significant temperature indications--that of the discharge section plenum space and that of the discharge throat riser--and indications of the melter tank electrical resistance, which is an inverse function of the glass temperature.

During experiments RLFCM-5 and -6, and before the start of RLFCM-7, it became obvious that the specific gravity and weight factor pneumatic sensing dip tubes were eroding. This proved true when the dip tube assembly was replaced after the "spiking" operation. Both dip tubes had been eroded away by bubbles of purge air breaking away from the bottom of the dip tubes in their normal manner. As a result, no accurate melter tank weight factor or specific gravity data were available during the first half of RLFCM-7. However, based on the dip-stick measurement of the minimum glass level and on the relative weight factor indications before and after the new dip tube assembly was installed, the melter tank weight factor values shown on Figure 2.2 for January 21 through 25 were reconstructed by hand.

Also during experiments RLFCM-5 and -6, it became apparent that most of the thermocouple thermowells had failed (probably dissolved away) and that the fidelity of all the thermocouples except at the 18-in. level had been seriously compromised. The melter tank thermowell and thermocouple bundle were replaced. The new 18-in.-level sensor confirmed the fidelity of the previous 18-in. sensor before its replacement.

The melter is normally operated with the discharge section isolated from the melter plenum and operating at the ambient cell pressure. Thus the pressure above the glass surface in the discharge throat riser tube is at the ambient cell pressure, while the glass surface in the melter tank is at the melter vacuum. Melter tank pressure fluctuations can cause inadvertent glass discharges from the melter.

An inadvertent glass transfer occurred when a temporary obstruction in the off-gas line caused the melter tank's vacuum to decrease to almost zero (Figure 2.2) Simultaneously, a sharp drop in the melter tank weight factor was seen, indicating that about 14 L of glass had been discharged into canister 1. A second obstruction in the off-gas line a few hours later discharged about 11 more liters of glass into the canister. Finally, on completion of the spike feeding, another melter pressurization occurred, this time from a feed pump-flushing operation, discharging another, somewhat smaller, quantity of glass to the receiving canister.

After the spiking, the melter was idled to remove solids accumulations from the off-gas line connecting the melter plenum to the off-gas venturi scrubber and to replace the melter tank weight factor, specific gravity, and tank pressure dip-tube assembly.

Melter operation resumed and was normal for 2 days. Then a sudden melter pressurization, suggestive of the collapse of a cold-cap bridge, discharged an excessive amount of glass from the melter to the receiving canister. During the initial discharge the glass flow rate was very high; some glass missed the hole leading to the receiving canister, and ended up as 7 L of molten glass in a pool 2 in. deep on the bottom of the discharge section floor. This discharge greatly shortened the life of some of the discharge section silicon carbide heaters, which extend to within 1.5 in. of the discharge section floor.

As melter operation continued, the damaged discharge section heaters began to fail. With the drop in discharge section temperature, the viscosity of the discharged glass increased, resulting first in stringing at the completion of glass transfers, and eventually roping during the transfers. This resulted in voids in the glass casting. The dropping melter vacuum, the

pressurized glass transfer, the decreasing discharge temperature, and the increased glass temperature can be seen in Figures 2.2, 2.3, and 2.4. The transfer of feed slurry to the melter was temporarily terminated.

During the next 5 months 1) the discharge section heaters were replaced; 2) the melter off-gas system was cleared of solids accumulations; 3) an in-line reamer was fabricated and was installed in the off-gas line; 4) the melter tank thermowell and thermocouple bundle were replaced; 5) the feed nozzle was replaced; 6) the melter tank weight factor, specific gravity, and tank pressure dip-tube assembly was replaced again; 7) the cell ventilation roughing and A-Frame discharge filters were modified; and 8) the melter was down-loaded in preparation for another melter spike to compensate for the $^{137}Cs$ lost from the melter during the maintenance period.

The melter tank respike was completed in late September 1986, and a normal feed slurry was started to the melter. Problems with the off-gas-line reamer soon suspended melter operations. Continued problems with the reamer and a degradation of the melter vacuum soon forced another shutdown. During this time the off-gas scrubber recirculation pump was replaced, a leak in the off-gas filter housing was repaired, and the off-gas-line reamer was replaced. On October 19, slurry feeding was resumed to the melter and continued without incident until the campaign was completed.

The electrode power indications are of interest. With the new thermocouple bundle installed in July 1986, the temperature was shifted from a constant melter tank electrical resistance system to a constant temperature system, using an averaged melter tank temperature value as feedback to the electrode voltage controller. For the first half of the campaign, under constant resistance control and without glass tank temperature indications, the electrode power variations were relatively minor, with the melter idling at about 25 kW and running with slurry feed at about 40 kW. For the second half of the campaign, under constant temperature control, power variations were considerably more severe.

### 2.4.2 RLFCM-8

Melter operations for RLFCM-7 were completed on October 23, 1986. On the same day glass was transferred into the first RLFCM-8 canister to reduce

the inventory in the melter in preparation for the shift in the RLFCM-8 glass composition. Feed makeup and in-cell housekeeping activities were also started. The silicon-controlled rectifier (SCR) voltage controller that regulates the melter tank electrode voltage was modified from a constant-current device to a constant-power device. This minor change enhanced the operation of the glass tank temperature control system, particularly whenever the controller was switched to manual control.

The composite graphs in Figures 2.5, 2.6, and 2.7 show the operation of the melter for RLFCM-8 during the two active operational periods from December 12 through 24, 1986, and January 23 through February 3, 1987.

Slurry feed transfer to the melter for RLFCM-8 was started on December 13; however, the start was erratic because feed tended to agglomerate and plug the feed line and the feed nozzle. A routine water-flushing procedure was established to minimize the occurrence of slurry feed system plugs. However, excess water from the flushing and high slurry feed rates soon led to unstable melter operation. Erratic melter glass weight factor indications, with stable melter glass specific gravity and melter tank pressure indications, were observed frequently during this period, generally following feed-line flushing operations or during periods of high feed rates.

These observations were interpreted to indicate cold-cap bridging, which extends to the walls of the melter tank and leaves insufficient space for the slurry-evaporation steam and calcination gases to escape. Pressurization under the cold cap increases the weight factor indication but does not affect the specific gravity or pressure indications. Sporadic release of these trapped gases through vent holes or fissures in the cold cap caused the erratic melter weight factor indications observed. When the vent holes are sealed by continued high feed rates, or by excessive feed-line water flushes, the trapped gas pressures are sufficient to cause unwanted glass discharges. During the start of RLFCM-8, several pressurized discharges occurred because of the low power rates, generally causing glass fibers ("hair") to form from the pour stream.

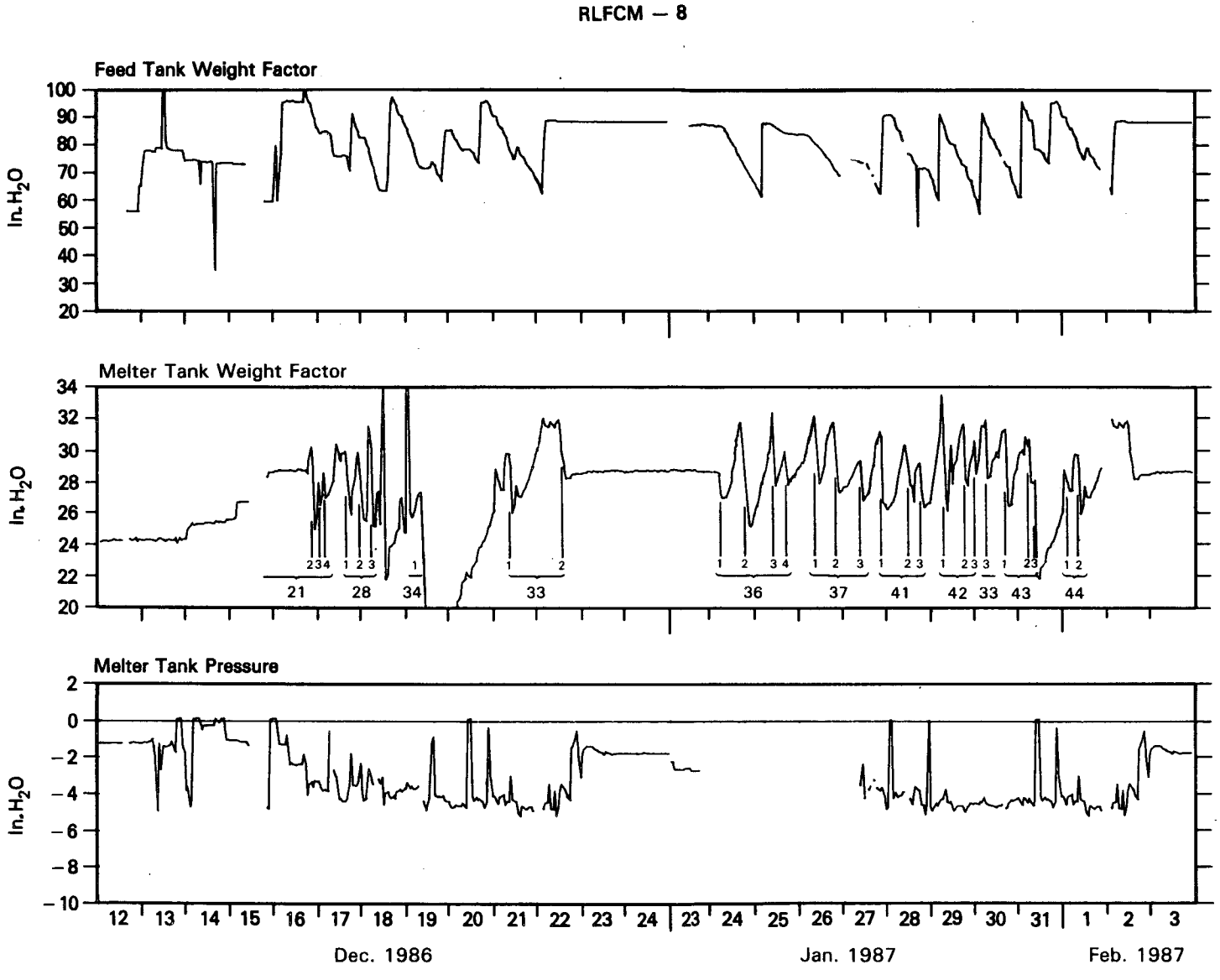


FIGURE 2.5. RLFCM-8 Slurry Feed, Glass Transfer and Melter Vacuum Values

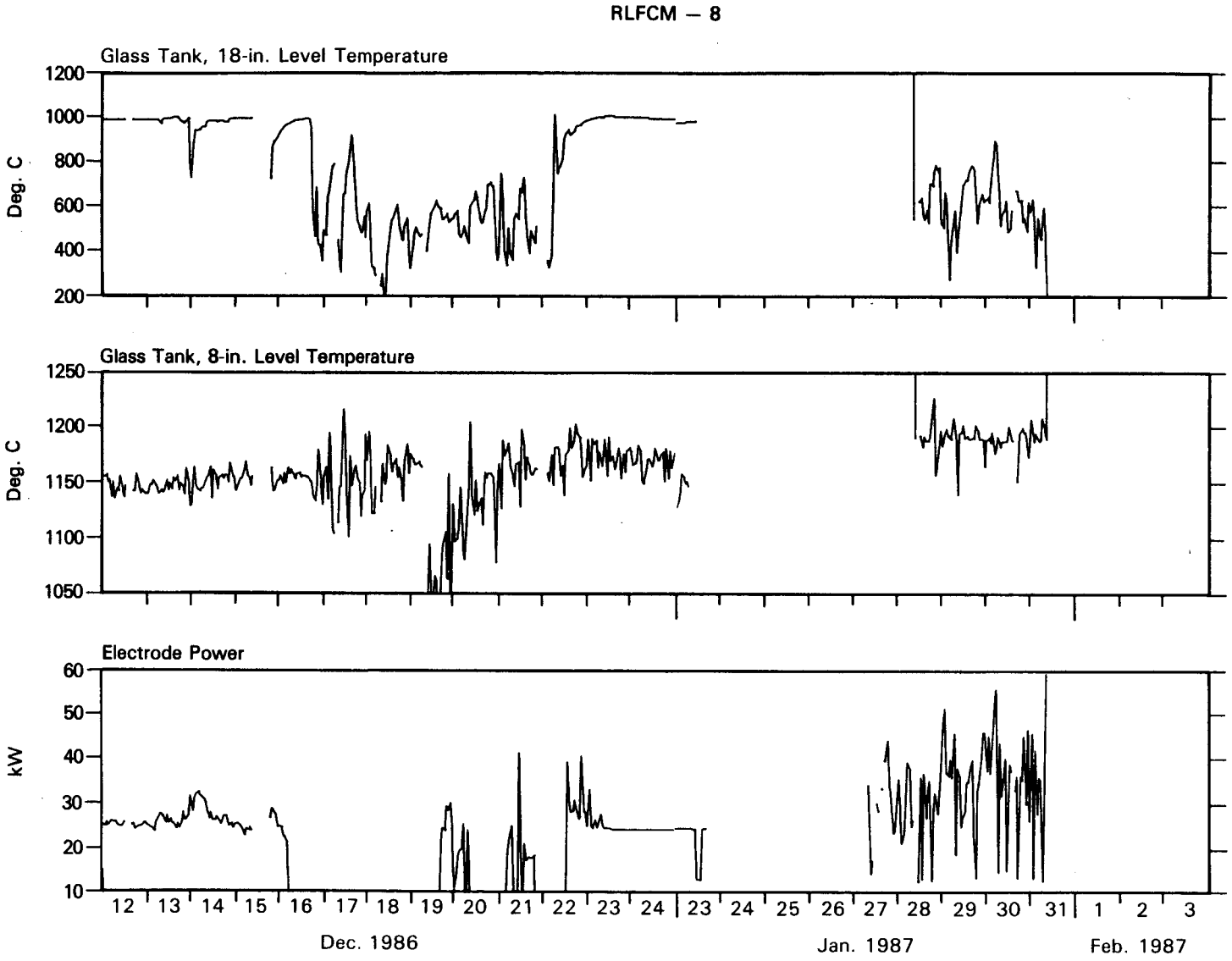


FIGURE 2.6. RLFCM-8 Glass Tank Temperatures and Power Values

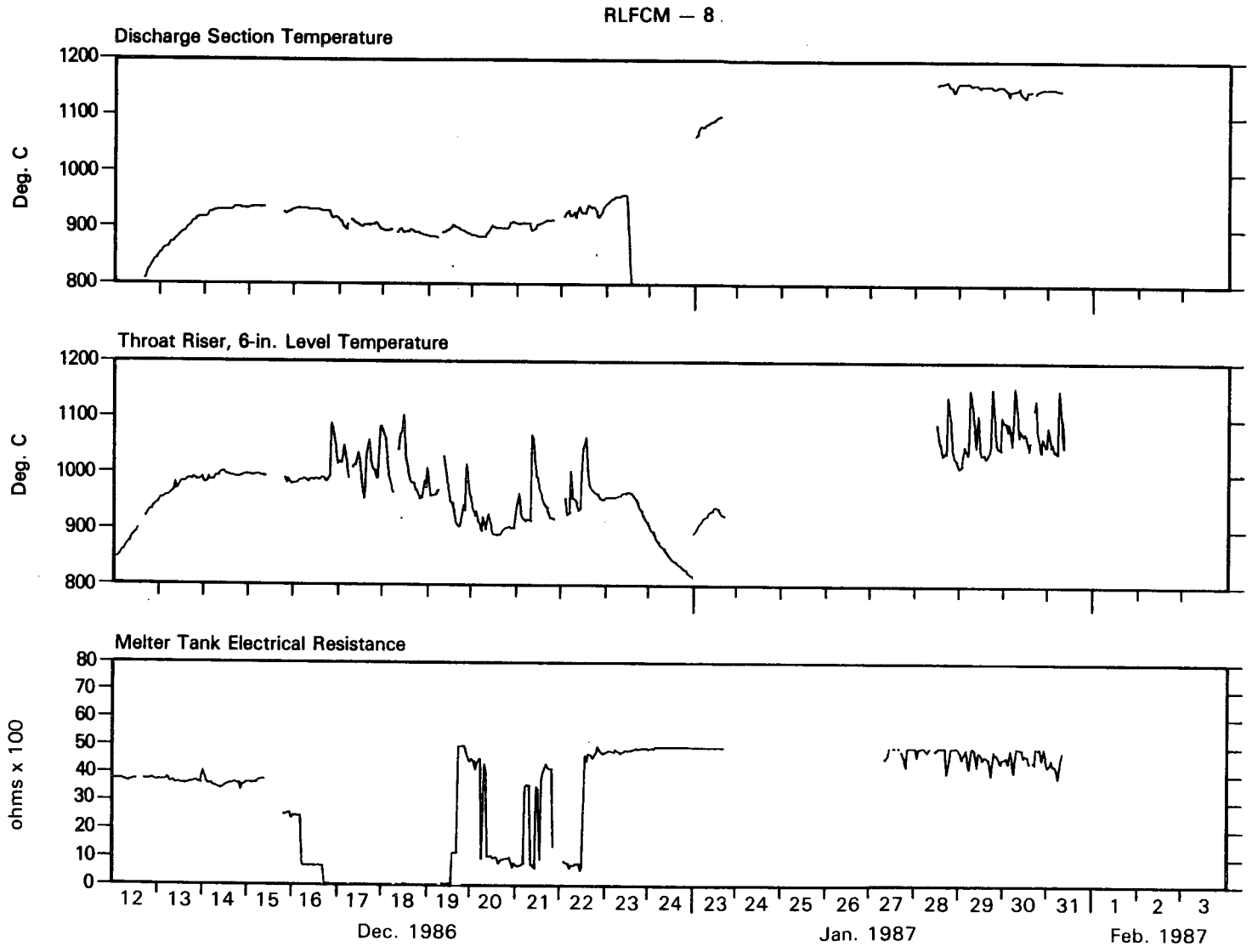


FIGURE 2.7. RLFCM-8 Glass Discharge Temperatures and Melter Tank Resistance Values

Continued indications of cold-cap bridging suggested that the RLFCM feed composition had a very slow melting rate, since the feed rates would not normally be considered excessive. A check of the glass composition revealed the glass to be within compositional bounds. Both sugar and sulfate were added to the feed to improve the calcine melting rate and decrease cold-cap coverage.

Following the first transfer into canister 34 (the third RLFCM-8 canister), unstable melter weight factor indications prompted shutdown and flushing of the air displacement slurry (ADS) pump. Immediately a pressurized discharge from the melter started and exhibited all the indications of a cold-cap bridging. The bridge was broken by lifting the melter tank thermowell slightly, which ended the glass discharge.

Glass transfers to the fourth canister of the campaign went very slowly, generating rather large quantities of glass hair. Higher glass and discharge section temperatures eventually enabled a satisfactory glass transfer rate to be realized. However, the glass-level detection system that monitored the receiving canister did not indicate glass accumulating in the canister. Before long, liquid glass in the inner discharge tube was detected by the operator which confirmed the lack of glass flow into the canister; so the slurry feed to the melter was terminated. Subsequent observation found the inner discharge tube plugged as shown in Figure 2.8.

Several events contributed to the plugging. Heat transfer to the feed slurry was poor, resulting in low glass melting rates, although both sugar and sulfate additions to the feed did improve the melting rate slightly. Feed rates were generally higher than the melter could accommodate, and on occasion too much water was used in flushing the feed line. The occasional high glass discharge rates caused some glass to contact and stick to the inside of the inner discharge tube. Then the frequent low glass discharge rates, which resulted in thin glass streams, generated enough hair so that some began to hang up on the wall of the inner discharge tube. The hair formed a pocket or a "bird's nest" that eventually was able to support a molten stream of glass until the bottom end of the inner discharge tube was completely closed by a pool of molten glass.

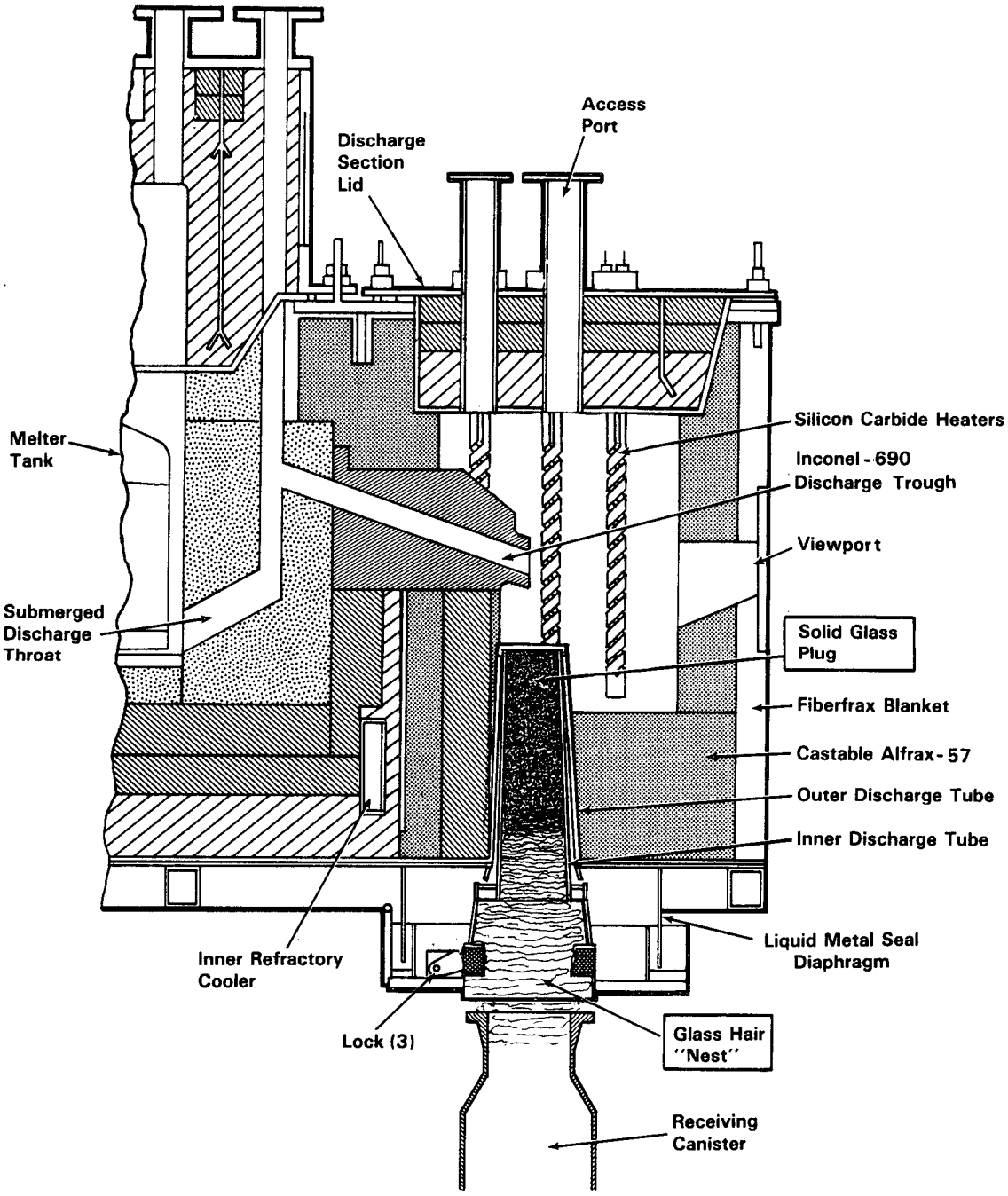


FIGURE 2.8. Plugged Melter Discharge Tube

Melter operations were suspended on December 23 to remove the glass plug from the inner discharge tube. During this maintenance period, the melter tank thermocouple bundle was replaced and a replacement thermocouple bundle was installed in the discharge section thermowell.

On January 23, 1987, RLFCM-8 was resumed and progressed quickly, filling the remaining six canisters in 9 days. Water flushing of the feed line was replaced with a feed-flushing technique to minimize sealing of the cold cap. This technique periodically increased the feed rate by a factor of three for two or three pump cycles. An equipment arrangement that automatically did this once every 30 min was installed and functioned quite well.

Addition of sugar to the cold feed was determined to be ineffective in increasing the calcine melting rate and was discontinued. Sulfate additions appeared to enhance the melting rate of the calcined feed and to minimize the cold cap and subsequent bridging. Thus it continued to be added to the cold feed. However, near the end of RLFCM-8, glass temperatures and melter tank electrical resistance indications suggested there was a molten sulfate layer on the glass surface when the cold cap was allowed to melt away. At this point supplemental sulfate additions to the cold feed were discontinued.

### 2.4.3 RLFCM-9

On February 2 the melter was down-loaded to decrease the glass inventory in preparation for adjusting the glass composition to the specifications for the third FRG canister production campaign (RLFCM-9). Feed makeup operations started on February 3.

During the feed makeup period the melter off-gas-line reamer was replaced as preventive maintenance. The melter discharge section heaters were also replaced with three new units incorporating various techniques to minimize the potential for failure due to condensation of conductive salts. Slurry feed transfer to the melter began on March 2. Increased frequency of off-gas-line plugging, due to the higher cesium concentration in the feed slurry, was a problem early in this campaign. While the rotary chain flail mounted in the melter off-gas nozzle kept this section of the line clear, the jumper between the melter nozzle and the ejector venturi scrubber began to show plugging. A water spray technique, later augmented with a rotating cable flail, was effective in periodically clearing this line section. In general, operation of the melter system was relatively smooth during this last campaign. The composite graphs in Figures 2.9, 2.10, and 2.11 show the operation of the melter between March 2 through 22, 1987, for RLFCM-9.

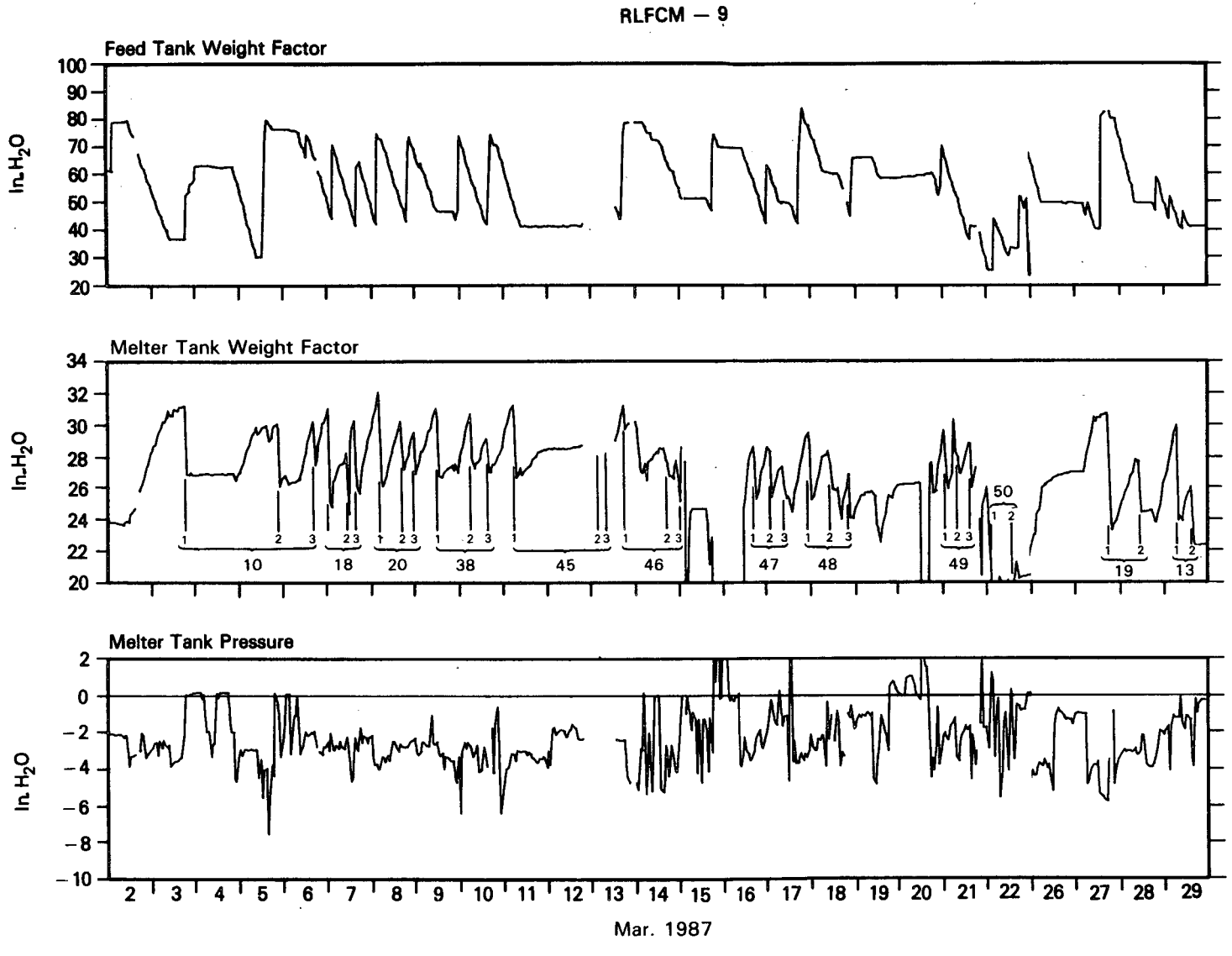


FIGURE 2.9. RLFCM-9 Slurry Feed, Glass Transfer and Melter Vacuum Values

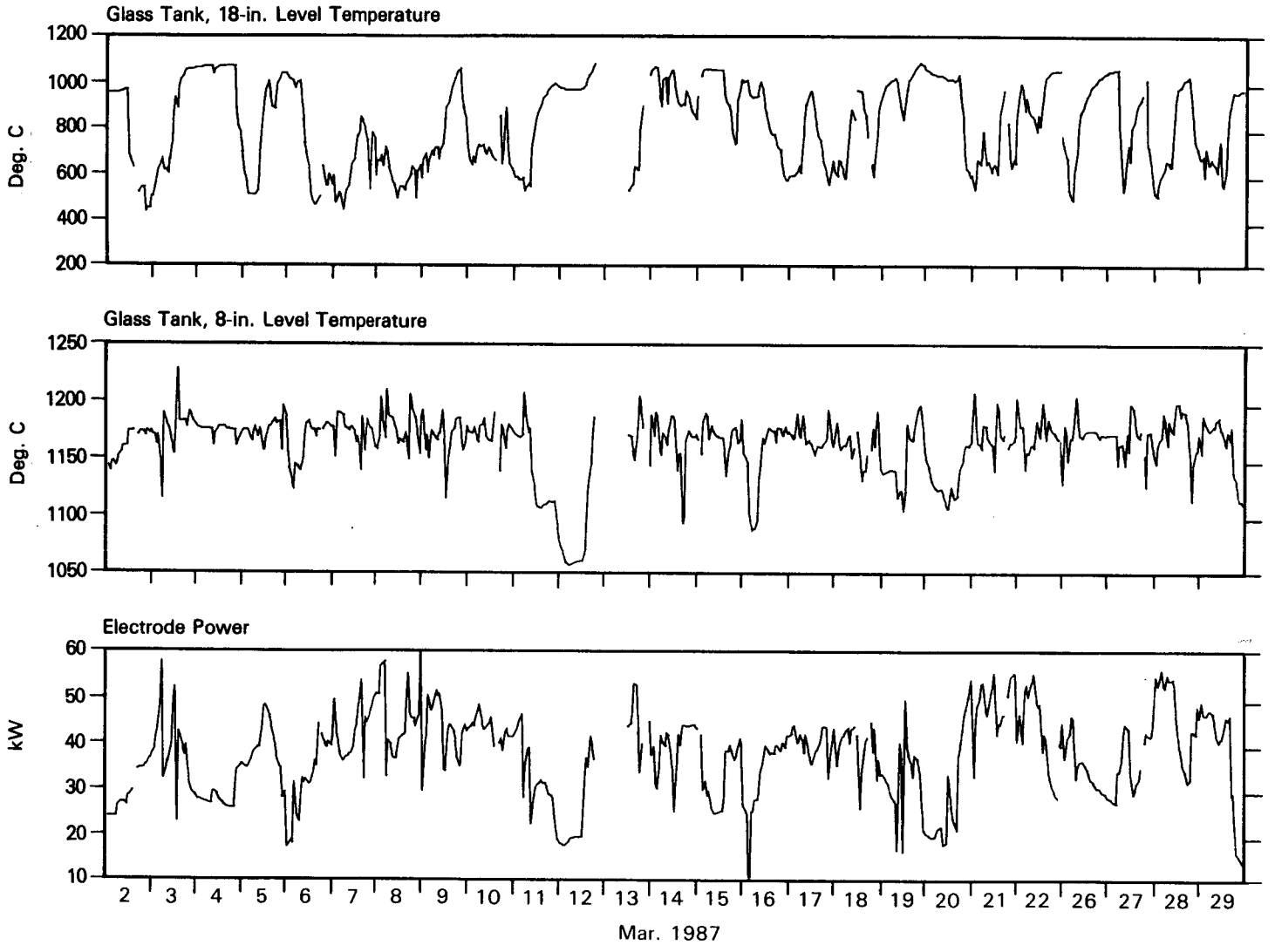


FIGURE 2.10. RLFCM-9 Glass Tank Temperatures and Power Values

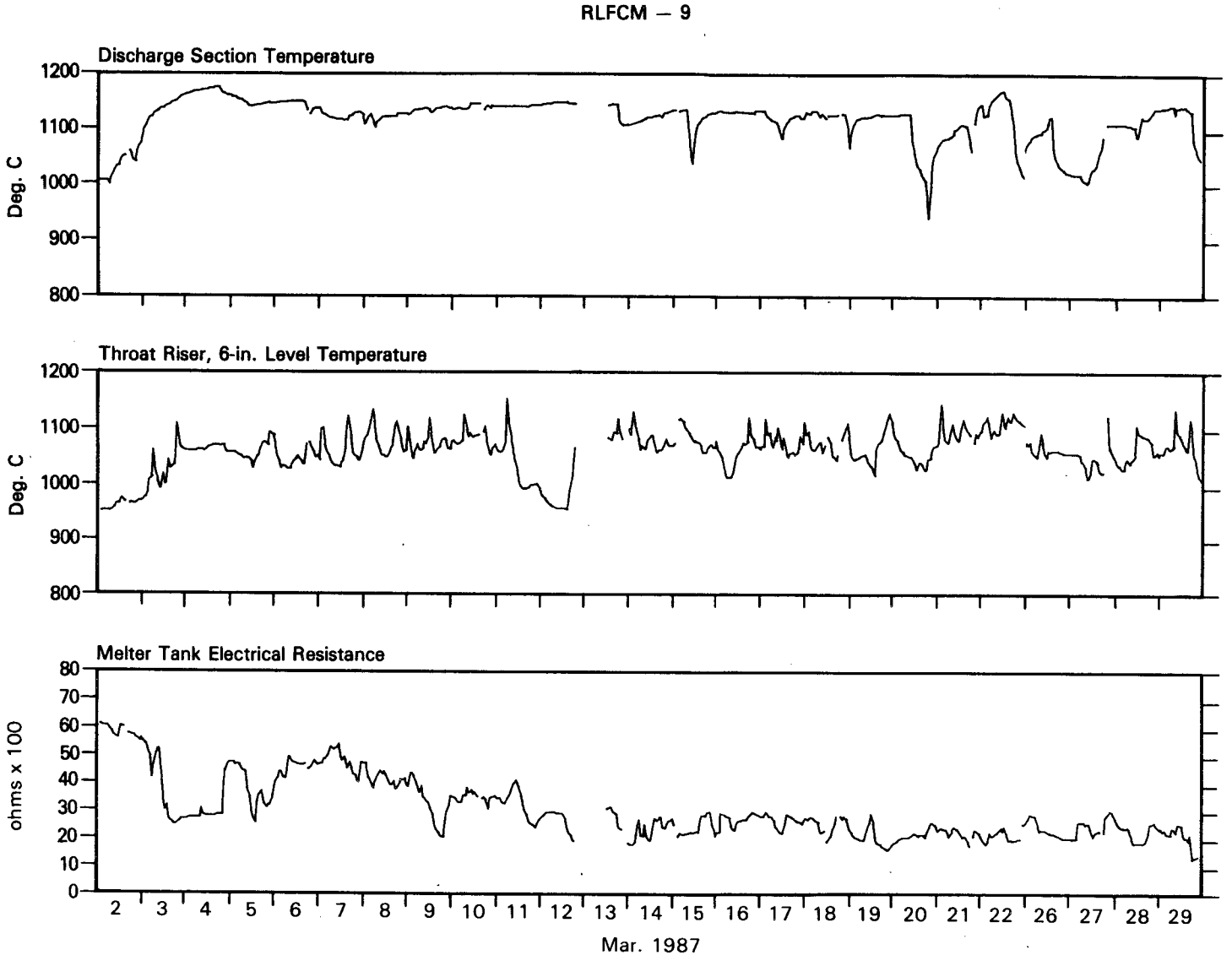


FIGURE 2.11. RLFCM-9 Glass Discharge Temperatures and Melter Tank Resistance Values

Melter operation was suspended from March 22 to March 26 to consolidate the radioactive feed components and to make up feed for filling the two special instrumented canisters for thermal test experiments. These canisters, 13 and 19, were filled during the period March 27 to 29, 1987. Melter operations were terminated March 30, 1987.

## 2.5 TESTING OF INSTRUMENTED CANISTERS - R. D. Dierks, S. D. Halstead, P. H. Hutton, M. A. Friesel, and J. F. Dawson

The two special instrumented canisters prepared during the filling of the isotopic heat and radiation sources each contained a thermocouple array and two acoustic waveguides. The thermocouple array consisted of five thermocouples arranged in a radial pattern at three levels in the canisters (Figure 2.12). One waveguide is a loop waveguide and the other is a single-wire waveguide. The loop waveguide provides the capability to establish the location of cracking by measuring the relative difference in acoustic emission responses from each of the loop ends. Figure 2.13 shows the instrumented canister with the cable that carries temperature and acoustic signals from the glass to the remote connectors. The two instrumented canisters are identical except that one contains ceramic fiber insulation positioned along its inside wall.

After filling with glass, the two instrumented canisters were subjected to a series of controlled heating and cooling tests to study the effect of glass cracking on the heat transfer characteristics of the canisters.

Controlled heating and cooling of the cans was performed in a reheat furnace (Figure 2.14). Functional tests of the reheat furnace were completed prior to installation in the B-Cell facility. These tests indicated that too little heat was distributed to the top and bottom of the furnace to heat the canisters uniformly along the vertical axis. To correct this problem and minimize heat loss from these areas, additional insulation was placed at the top and bottom of the furnace. Also an insulating pad was fabricated upon which to place the reheat furnace, and the lid was redesigned to also include additional insulation.

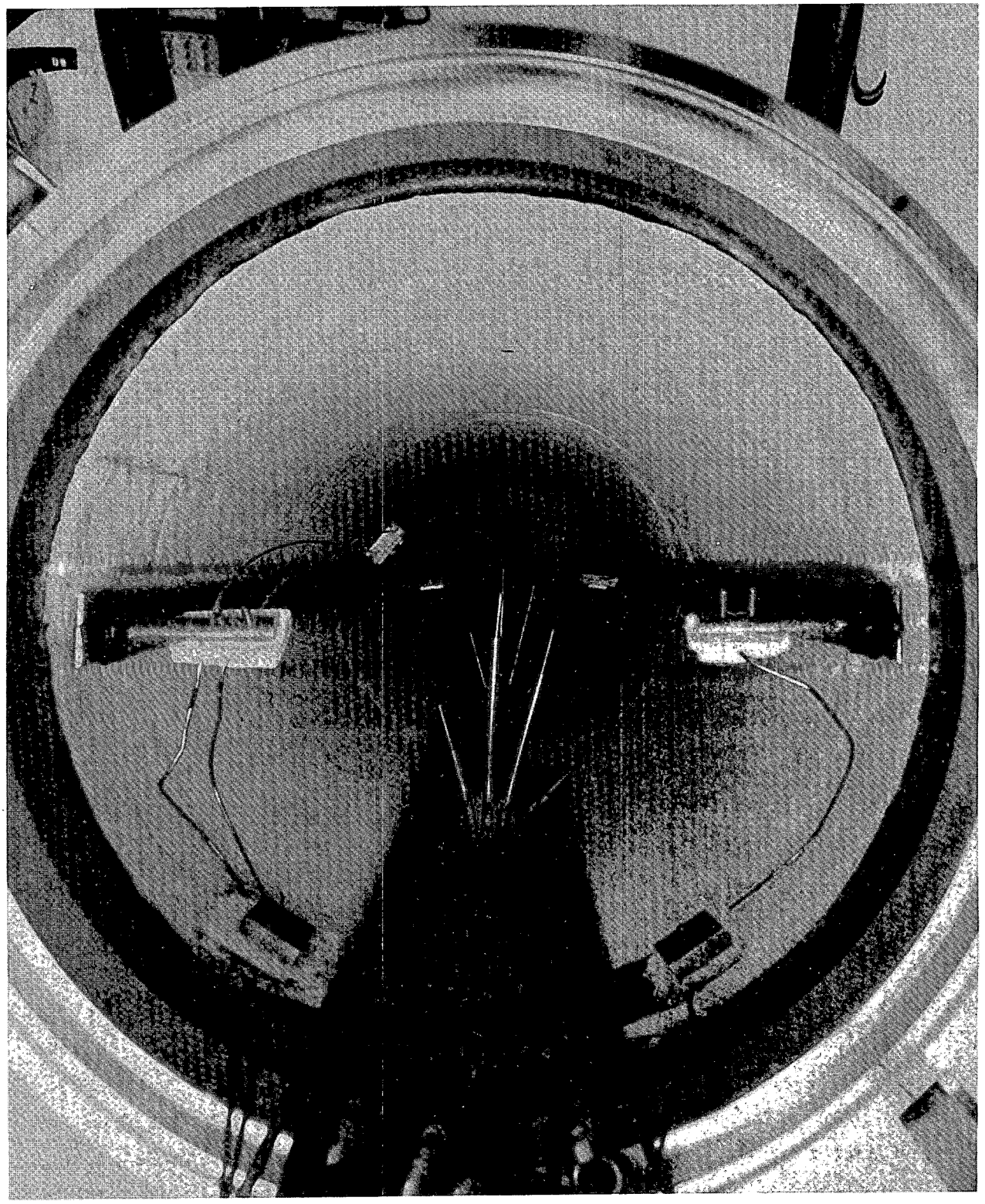

FIGURE 2.12. Instrumented Canister Showing Internal Thermocouples and Acoustic Waveguides

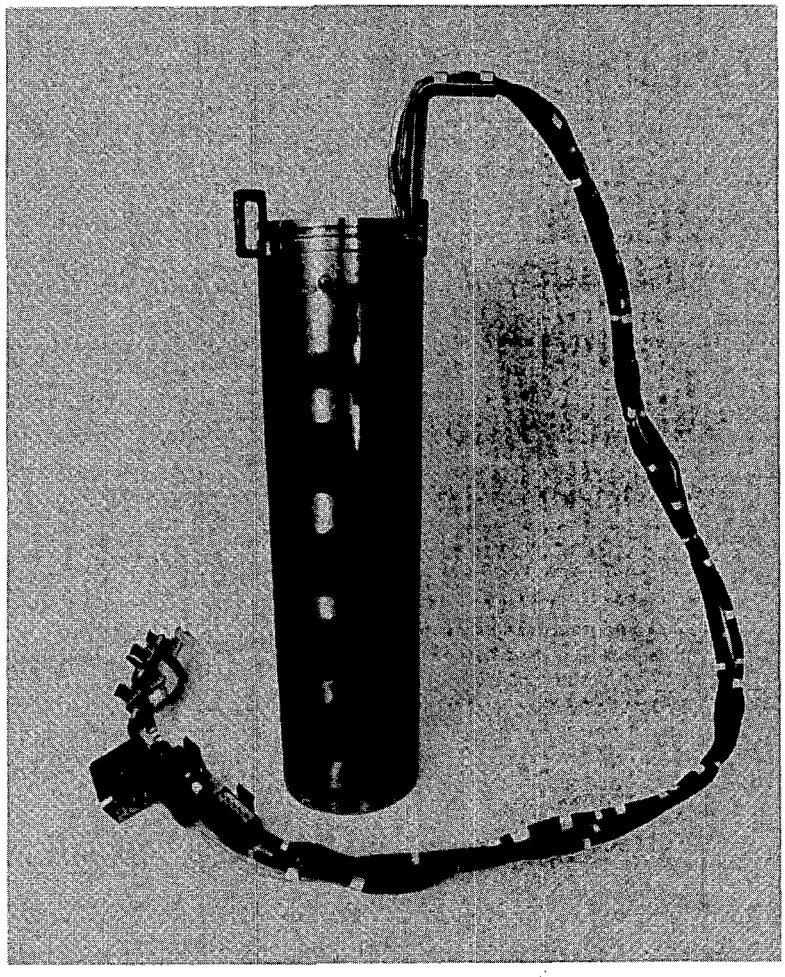

FIGURE 2.13. Instrumented Canister Showing Canister and Instrument Cable

### 2.5.1 Thermal Fracturing Tests

Because of the stresses that build up within the glass as it begins to cool in the waste canister, it is very difficult to produce a canister that contains no glass cracks. The extent of cracking depends mostly on the rate at which the glass cools: the more rapid the cooling rate the more extensive is the cracking.

One reason that glass-cracking in a canister of vitrified waste is detrimental is that cracks decrease its ability to transmit heat. The more extensive the cracking, the more slowly the heat moves through the glass, or the lower is its thermal conductivity. Thus canisters of waste glass, with a significant decay heat level, might have unacceptably high centerline

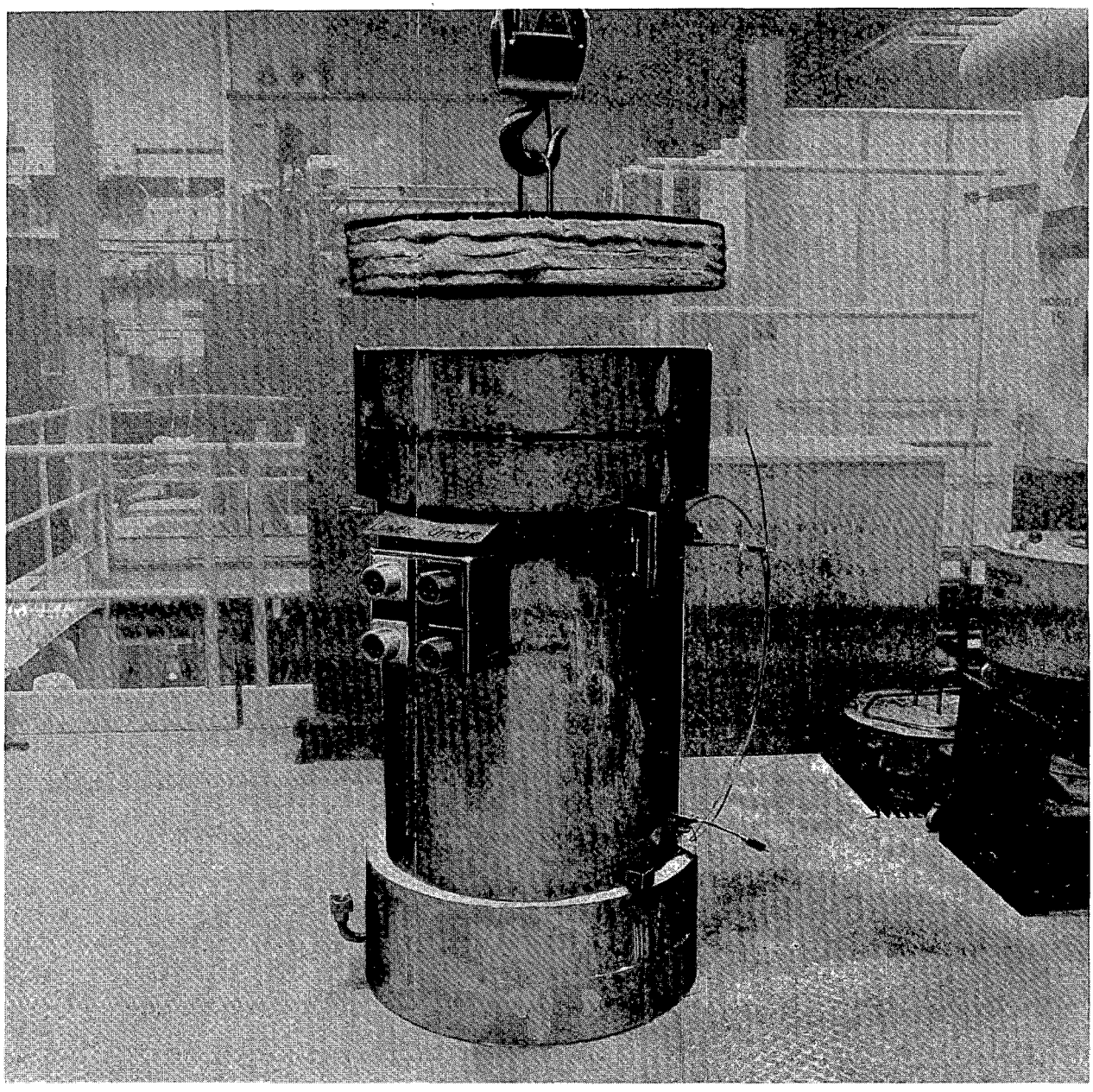

FIGURE 2.14. Instrumented Canister Reheat Furnace

temperatures if their initial cooling has produced extensive fracturing within the glass and decreased its thermal conductivity. With canister centerline temperatures of 500 to 600°C, typical waste glasses begin to soften to the point that molecular devitrification or possibly molecular

enrichment, over very long periods of time, might occur and possibly compromise the waste form's integrity.

The objectives of the thermal fracturing tests are to determine:

1. the effect of self-heating glasses on the steady-state internal temperatures in canisters
2. whether cracking of the glass in the FRG canisters filled recently from the RLFCM was significantly reduced by a two-step process that first brought the glass to steady state in an insulated cooling pod (ICP) and then to steady state in "free air" instead of cooling to steady state in "free air" in a single step
3. whether lining the canister with a thin layer of resilient ceramic fiber insulation significantly reduced mechanical cracking by preventing undue stress on the glass from the compressive force applied by the canister's steel wall.

To realize the objectives, three cooling experiments were requested to be performed on each of two instrumented canisters after they had been filled in the normal manner with radioactive glass from the RLFCM. The two instrumented canisters were identical, except that canister 13 had been lined with a 1/8-in. layer of ceramic fiber insulation and that canister 19 was unlined. Each experiment was duplicated to verify the technique. Before each test, the glass temperatures were raised to 800°C for 4 hr in a remelt furnace to "heal" the glass of all cracks produced in the previous test.

One set of experiments would allow the canisters to cool to steady-state conditions in the ICP that was used to slow the cooling of all 30 FRG production canisters after they had been cast from the RLFCM. A second set of experiments would allow the canisters to cool to steady state in an air cooling frame (ACF) that simulated the "free air" cooling of a stack of FRG waste canisters. The third set of experiments would air-cool the canisters quickly from 800 to 600°C to minimize devitrification-induced cracking, and then control the cooling from 550 to 350°C at 2°C/hr to minimize thermal-stress cracking. Following the controlled cooling to 350°C, the canisters would then be allowed to cool to steady state sequentially, first in the ICP

and then in the ACF, resulting in nearly crack-free glass. A schematic of the thermal fracturing test facility is shown in Figure 2.15.

### 2.5.2 Acoustic Emission Testing

Since the tests involved highly radioactive materials, all were performed remotely inside a hot cell. The approach employed acoustic emission (AE) technology that had been developed under a research program at PNL supported by the U.S. Nuclear Regulatory Commission, Office of Research. The specific plan adopted for the AE monitoring was to install two metal waveguides (one loop waveguide and one single-ended waveguide) inside each of the two test canisters and one metal waveguide in each of the three canister stands such that they would contact the bottom of a canister sitting in the

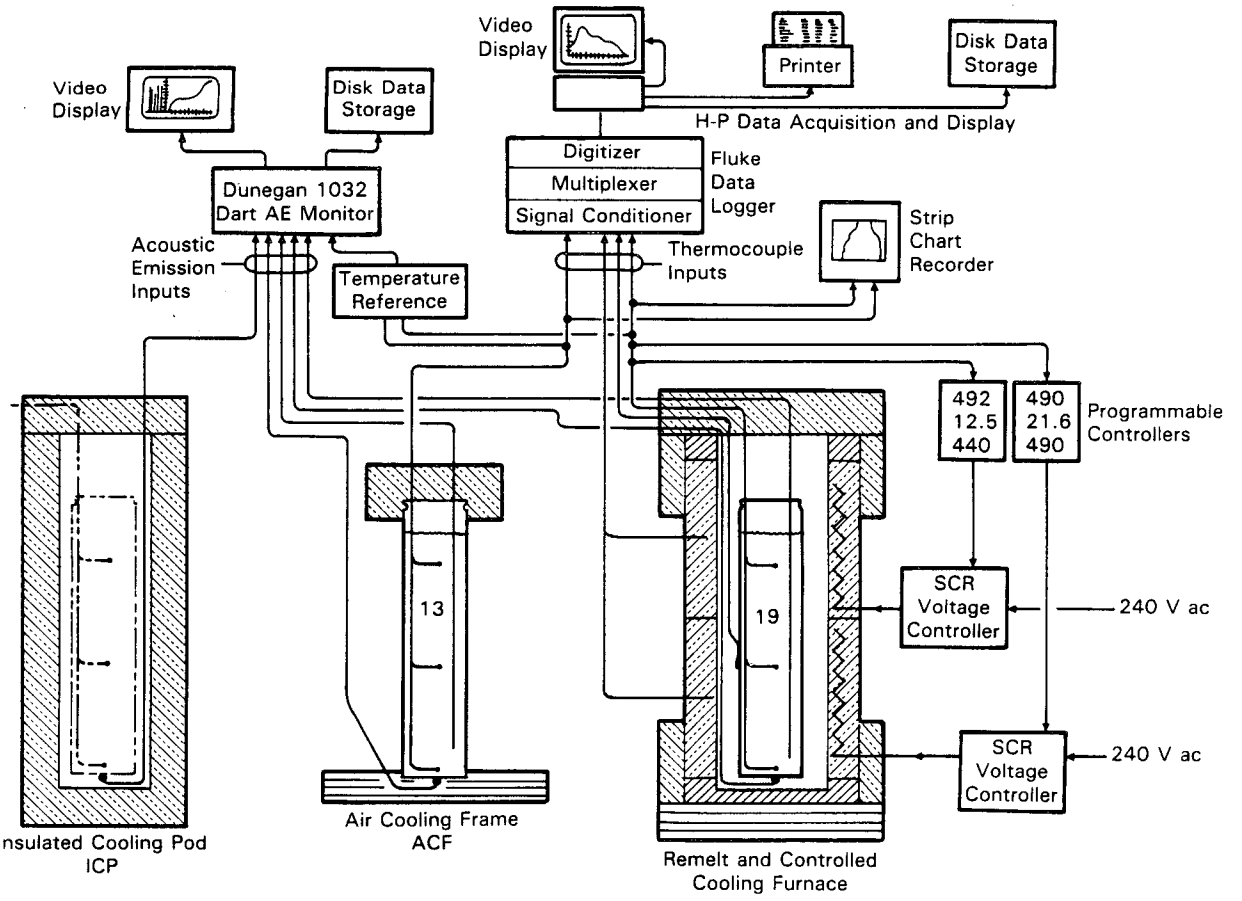


FIGURE 2.15. Schematic of Thermal Fracturing Test Facility

stand. The waveguides inside the canisters were considered to be the primary sensors, with the waveguides in the canister stands as backup. The loop waveguide was intended to serve two special functions: 1) to locate the source of glass-cracking and 2) to minimize the potential for the waveguide to be isolated from cracking signals after an initial crack field formed around it. A piezoelectric crystal was installed on the outer end of each waveguide together with a first-stage preamplifier. The output from these AE sensor assemblies was connected by cables to an AE monitor/recorder system, which also received and recorded temperature data from four thermocouples (two from each canister). Temperature data from the two thermocouples for each canister were to serve only as a correlation link between the AE data and the full array of temperature data. No two thermocouples could be considered as representative of the canister temperature profile.

The sensor concept considered two metal waveguide sensors inside the canister and one waveguide sensor mounted in each fixture that would support the canisters. Waveguide sensors were essential to position the sensing crystal and the preamplifiers away from the canisters, which were heated to 800 to 1000°C at various times during the tests. Several questions required resolution in the design of the waveguides:

1. material that would withstand the temperature and corrosive environment inside the canister
2. sensitivity of the waveguides to acoustic signals striking them on the side rather than the end
3. attenuation in the waveguides since they were required to be at least 4-1/4 m (~14 ft) long
4. resistance of the sensor crystal and the preamplifier electronics to damage by the intense radiation levels (measured to be 26,000 to 48,000 rad/hr of gross gamma).

Stainless steel (SS) type 308 was selected as the AE waveguide material. The waveguides placed inside the canisters were 1.6 mm (0.062 in.) dia. The small diameter was selected to maximize flexibility of the waveguides because they had to trail the canisters into a covered turntable facility when the

canisters were filled at the outset of testing. The small size did not adversely affect sensing ability. Waveguides installed in the three canister support fixtures were 3.3 mm (0.130 in.) dia. The waveguide material was selected based on the results from testing three candidate materials (Zircaloy 2, Inconel 82, and 308 SS) for their acoustic properties versus temperature. The test environment was a tube furnace with an air atmosphere. The test results are shown in Figure 2.16. In addition to poor acoustic properties with increasing temperature, the Zircaloy also showed a very high oxidation rate at the higher temperatures, 800 to 1100°C. The center section of the test waveguide oxidized nearly all the way through in the brief testing time, and the remaining ligament was quite brittle. Both Inconel 82 and 308 SS showed good resistance to oxidation. They were tested for 24 hr at 900°C in the furnace, with no significant oxidation resulting. The 308 SS

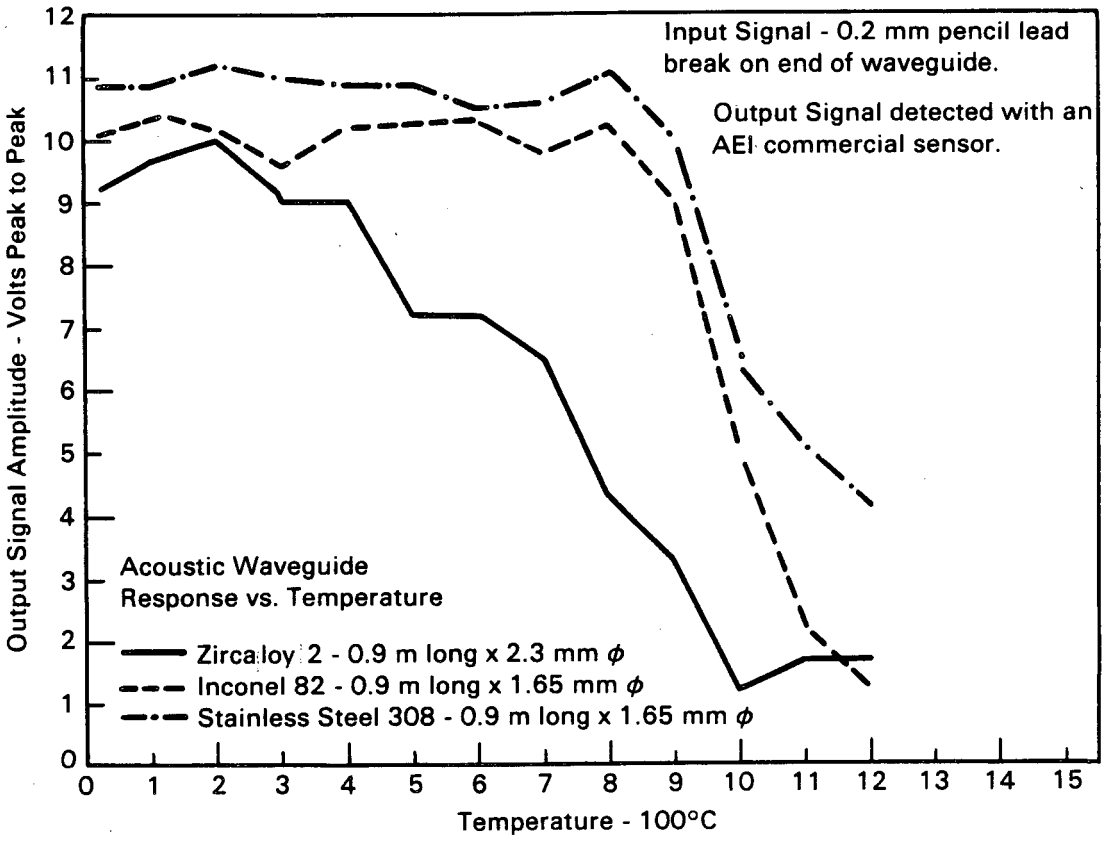


FIGURE 2.16. Acoustic Waveguide Response Versus Material and Temperature

was selected on the basis of better acoustic properties and a melting temperature of 1500°C versus 1400°C for Inconel 82.

The potential corrosion of the waveguides by molten glass inside the canister was also a concern. This was investigated by installing a length of type 308 SS waveguide similar to that being used inside the canisters (16 mm dia) in a ceramic crucible ≈152 mm (6 in.) dia by 203 mm (8 in.) deep. The crucible was then filled with glass and the glass was melted. The waveguide was soaked in the molten glass at 850°C for 60 hr. At the end of that time the waveguide showed no evidence of significant corrosion or embrittlement.

It was questioned whether the waveguide sensors were sufficiently sensitive to acoustic signals striking them from the side rather than the end. This question was investigated several ways. Using pencil lead breaks (an accepted AE method to simulate an AE event) on the side and on the end of a bare waveguide indicated that lateral sensitivity was about 6 decibels (dB) lower than when the signal was injected on the end. The waveguide was subsequently encased in glass and epoxy, and under these conditions there was no difference in lateral and end sensitivity. This may be because the waveguide sees a more diffuse sound field with the homogeneous material surrounding it. The final evaluation point grew out of the test described above in which the waveguide was immersed in molten glass to test corrosion effects. When the glass was subsequently cooled with the waveguide in it, the glass cracked. Acoustic emission from that cracking was clearly detected by the waveguide, which ran completely through the glass (no end exposure). On the basis of these results, it was concluded that lateral sensitivity was not a problem.

A type 308 SS waveguide 1.6 mm (0.062 in.) in dia by 8.75 m (28.75 ft) long, with lead-zirconate-titanate sensing crystals together with a preamplifier mounted on each end, was tested for acoustic signal attenuation and source location accuracy. The length was representative of the longest waveguides used (the loop waveguide inside the vessel). An input signal was generated by breaking a pencil lead against the side of the waveguide. The test was repeated five times to obtain an average of results, summarized in Figure 2.17.

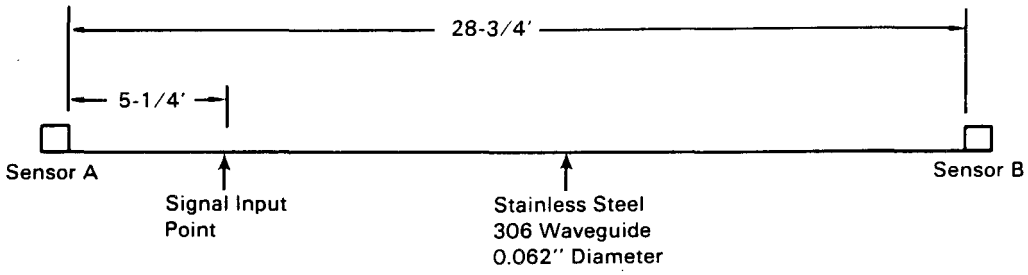


Test Arrangement

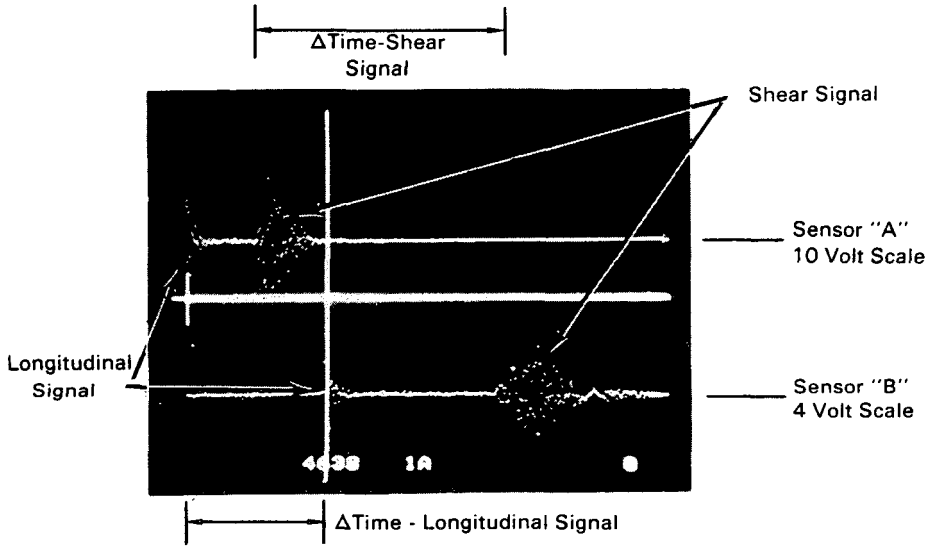


Sensor Response to Signal Input to Waveguide

$$\Delta\text{time - longitudinal} = \frac{4638 \text{ sample points}}{5 \text{ sample points}/\mu\text{sec}} = 928\ \mu\text{sec}$$

$$\Delta\text{time - shear} = \frac{8348 \text{ sample points}}{5 \text{ sample points}/\mu\text{sec}} = 1670\ \mu\text{sec}$$

Velocity (longitudinal) = $2.23 \times 10^5$ in/sec

Velocity (shear) = $1.23 \times 10^5$ in/sec

Indicated Δ distance between sensors and signal input:

Longitudinal: $928 \times 10^{-6}$ sec x $2.23 \times 10^5$ in/sec = 207" or 17-1/4'

Shear: $1670 \times 10^{-6}$ sec x $1.23 \times 10^5$ in/sec = 205" or 17'

Measured Δ distance = (28-3/4' - 5-1/4') - 5-1/4' ≅ 18-1/4'

FIGURE 2.17. Evaluation of Source Location Accuracy and Signal Attenuation in a Loop Waveguide Acoustic Emission Sensor

The digital oscilloscope photo shows the response of the AE sensors to an input signal. Using the difference in time of signal arrival (Δ time) at

the two AE sensors for either the longitudinal or shear propagation mode to calculate the location of the signal input produces a result that is within about 6% of the measured value.

Signal attenuation over a 5.5-m (18 ft) length of waveguide was 8 dB, or 0.44 dB/ft. This value is consistent with other attenuation measurements made on waveguides.

As the gamma radiation level in the hot cell during canister tests would be much greater than that experienced in any previous use of AE sensors, it was considered important to investigate the effect of the radiation on sensor performance. The measured flux level in the hot cell is 26,000 to 48,000 rad/hr of gamma, depending on canister location. A waveguide sensor assembly similar to those to be used in the canister tests was exposed in an irradiation facility to 1.33 MeV gamma radiation at a flux level of $1.23 \times 10^5$ rad/hr for 72 hr. This resulted in a total dose of $8.9 \times 10^6$ rad, but the sensor showed no effects from the exposure. As an added precaution, however, lead shielding boxes 6.6 mm (0.25 in.) thick for the sensor/preamplifier end of the waveguides were fabricated for use on the installed sensors.

Calibration of the AE system began with testing and calibrating of the instrument by the field representative for the AE monitor manufacturer. This was a vital step in view of the expected duration of the canister tests. Results were positive: the instrument operated essentially continuously for 3 months with only one problem. One disk drive failed during testing but was replaced with a spare on hand at a cost of only about 5 hr test-monitoring time.

The other area of concern was the sensitivity of the waveguide AE sensor assemblies. Figures 2.18 and 2.19 show the results of calibration performed on the AE sensors after they were installed in the canisters ready to be moved into the hot cell. In Figure 2.18 the top two photos show the spectral response to a source of white noise (helium jet gas) applied to the surface of the waveguides--first near the waveguide connector box, and then at the top of the canister. The purpose of this test is to show the response of the sensor versus frequency up to 1 MHz. Since this is a relatively low energy

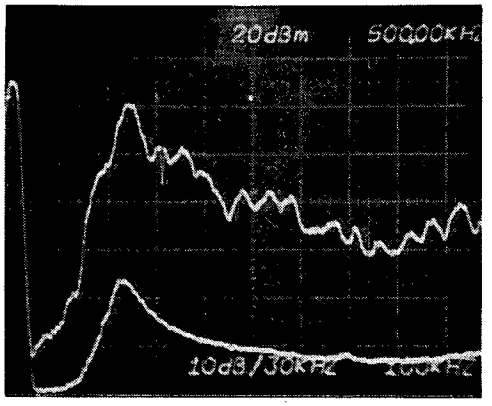


Response to helium jet on waveguide 10 inches from connector box. 0-1.0 MHz, horizontal; +20 to -60 dB, ref. 1 milliwatt into 50 ohms, vertical.

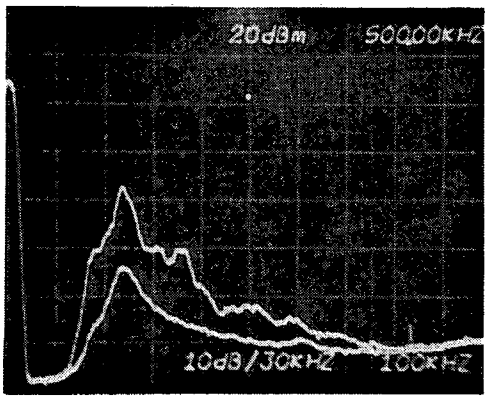


Response to helium jet on waveguide at top of canister. Same scale as above.

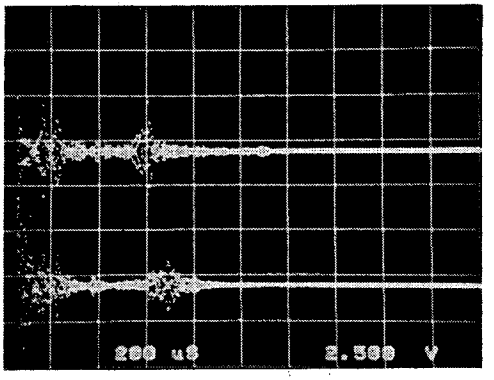


Pencil lead break on loop waveguide at top of canister.

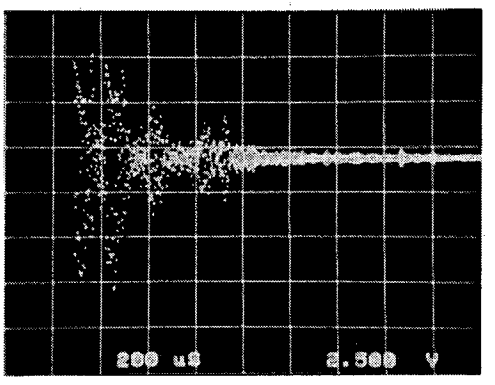


Pencil lead break on single waveguide at top of canister.

FIGURE 2.18. Calibration Results for Waveguides Installed in Canister 19

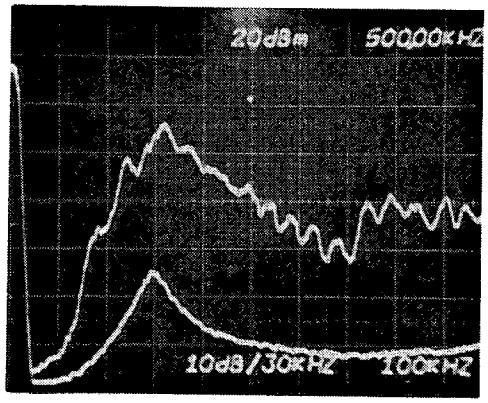


Response to helium jet on waveguide 10 inches from connector box. 0-1.0 MHz, horizontal; +20 to -60 dB ref. 1 milliwatt into 50 ohms, vertical.

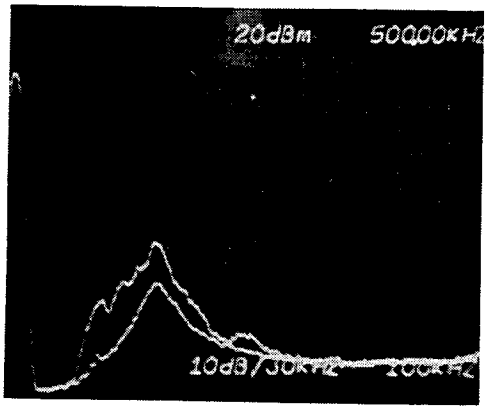


Response to helium jet on wavguide at top of canister. Same scale as above.

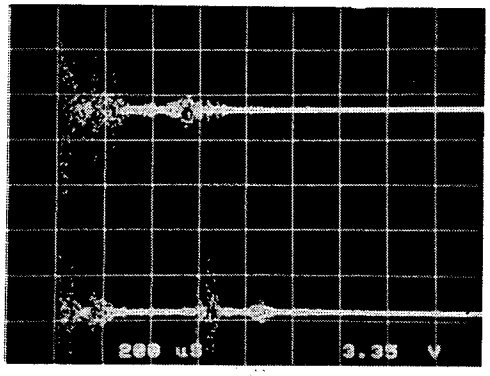


Pencil lead break on loop waveguide at top of the canister.

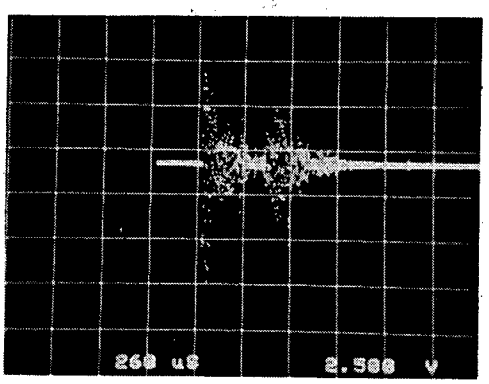


Pencil lead break on single waveguide at top of the canister.

FIGURE 2.19. Calibration Results for Waveguides Installed in Canister 13

signal that produces primarily surface waves in the waveguide, it is not surprising that the signal is attenuated significantly between the canister and the waveguide connector box. The waveguides are taped to the thermocouple leads for protection over that interval. In this calibration we discovered that glass adhesive tape used directly on the waveguides as a spacer was aggravating the signal loss. The tape was removed and a gasket material was placed between the tape and the waveguides. This prevented adhesive from contacting the waveguides but still allowed them to be taped to the thermocouple leads.

The bottom two pictures in Figure 2.18 show sensor response to input on the waveguide surface at the top of the canisters using a pencil-lead break to simulate an AE signal. Response of the system to calibration inputs was considered satisfactory in all cases. The waveguide sensors in the canister support stands were similarly calibrated using pencil-lead breaks with satisfactory results.

A concern was raised that the waveguides might be sensitive to signals or noise originating in the canister wall. Figure 2.20 gives the results of a test addressing this question. A sensor was mounted on the outside canister surface near one of the machine screws holding the waveguide mounting brackets to the canister wall. While this sensor and a waveguide inside the

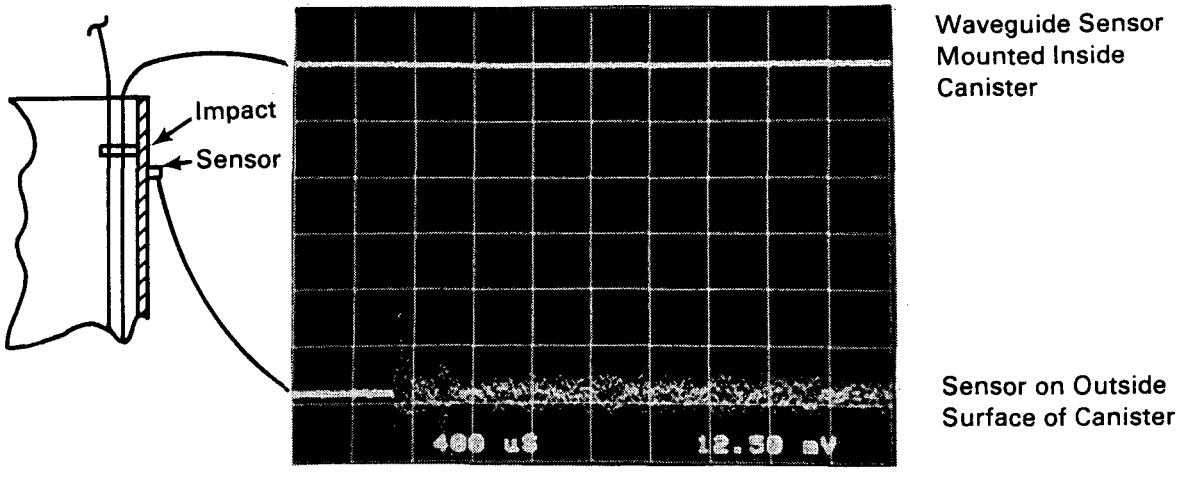


FIGURE 2.20. Results from Test of Waveguide Sensitivity to Noise from the Canister

canister were monitored, the canister was impacted on the backwelded machine screw head. The signal was detected by the surface-mounted sensor, but the waveguide showed no perceptible response.

The final step in calibration considerations was to include a pulser crystal on the side of the waveguides, just below the end where the AE detection crystal was mounted. This pulser could be activated remotely from the AE monitoring station. It was used periodically during testing to assure that the sensors and preamplifiers were functioning properly, and continuity of the loop waveguide could also be checked in this manner. The pulser provided a qualitative calibration of the AE sensing system.

## 2.6 CANISTER LID-WELDING AND HELIUM LEAK-CHECK TESTS - R. F. Klein, R. P. Allen, M. L. Elliott, D. O. Jenkins, D. L. Alexander, and J. L. Duce

A remote mockup demonstration of the FRG canister lid-welding and helium leak-checking process was set up and tests completed using two FRG canisters, previously filled with nonradioactive glass. The canisters were closed by welding on lids with a remotely operated gas tungsten arc welding system (Figures 2.21 and 2.22). Weld integrity was verified by helium leak-checking.

### 2.6.1 Helium Leak-Testing

After filling and welding, the FRG canisters must be leak-tested to ensure freedom from weld defects that could release contamination during subsequent handling, transport, and storage. The helium leak-detection system will be used to verify tightness of the lid closure welds. This will be done by filling a special gas capsule (Figure 2.23) with helium, which will leak through a glass capillary into the canister at a predetermined rate. Before welding the lid on the canister, the helium capsule will be filled, calibrated, and sealed using a helium-filling manifold (Figure 2.24). The capsules will then be placed in the void volume of the canister, the lid

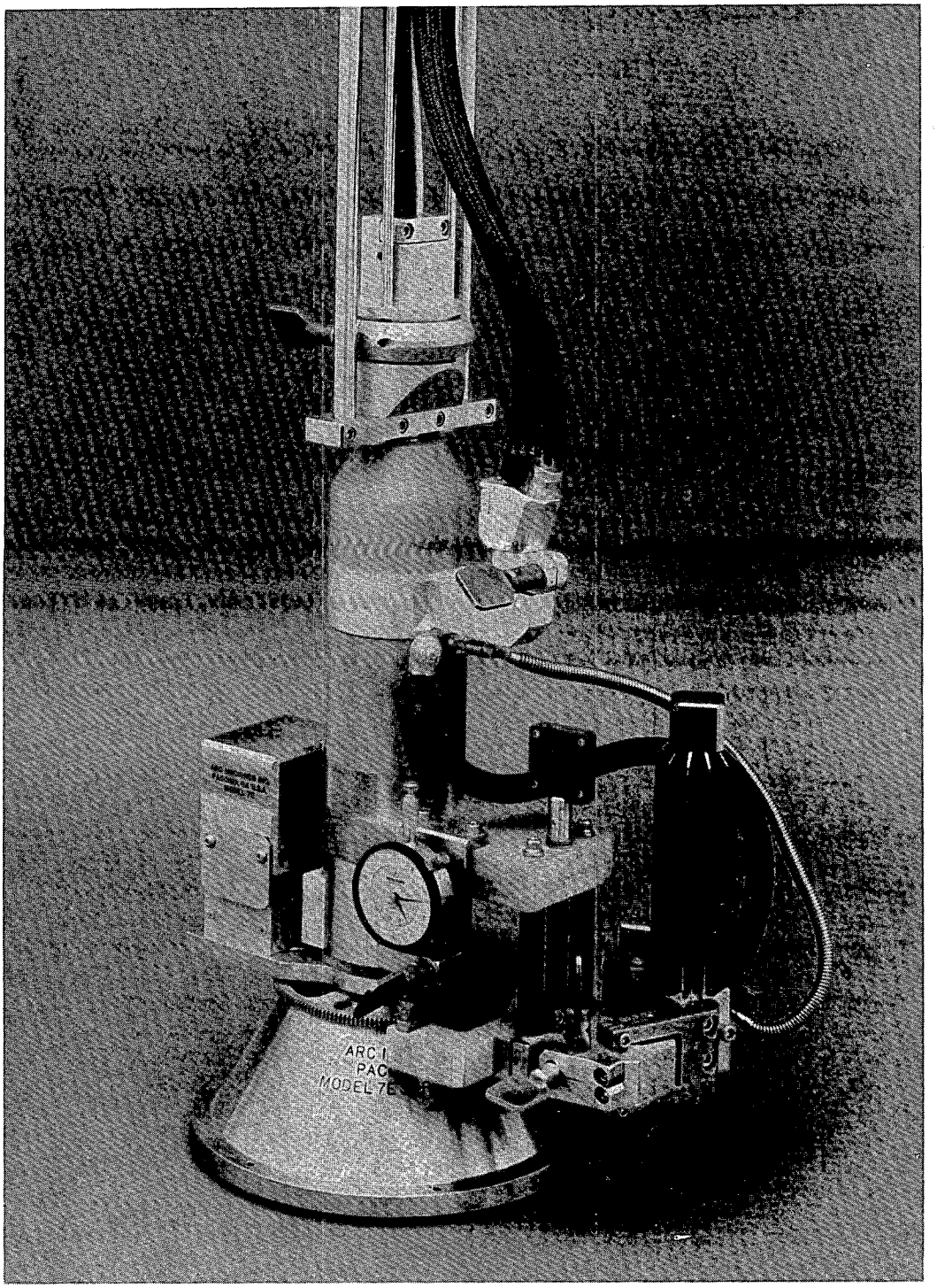


FIGURE 2.21. Remote Canister Lid Welder

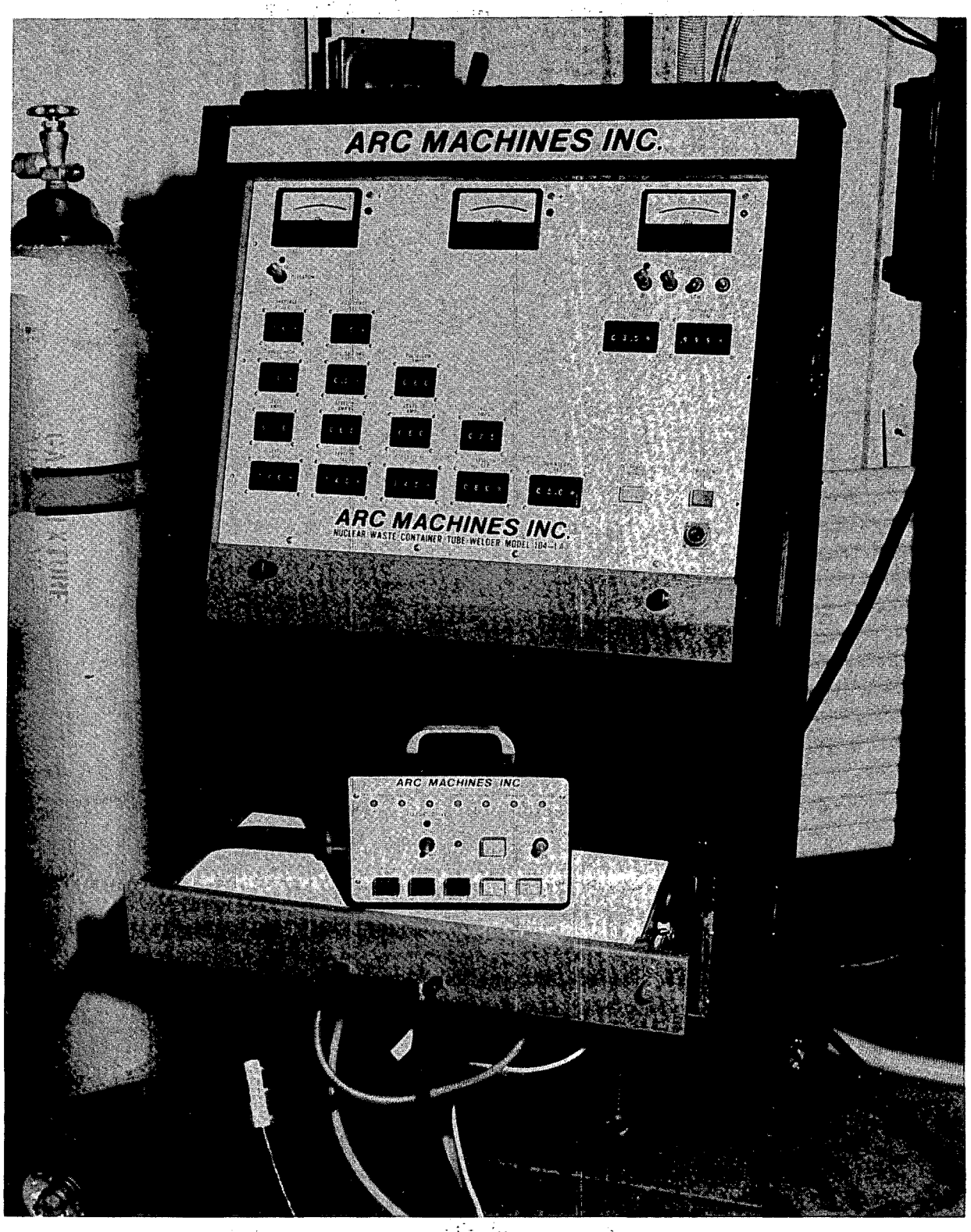


FIGURE 2.22. Welding Power Supply

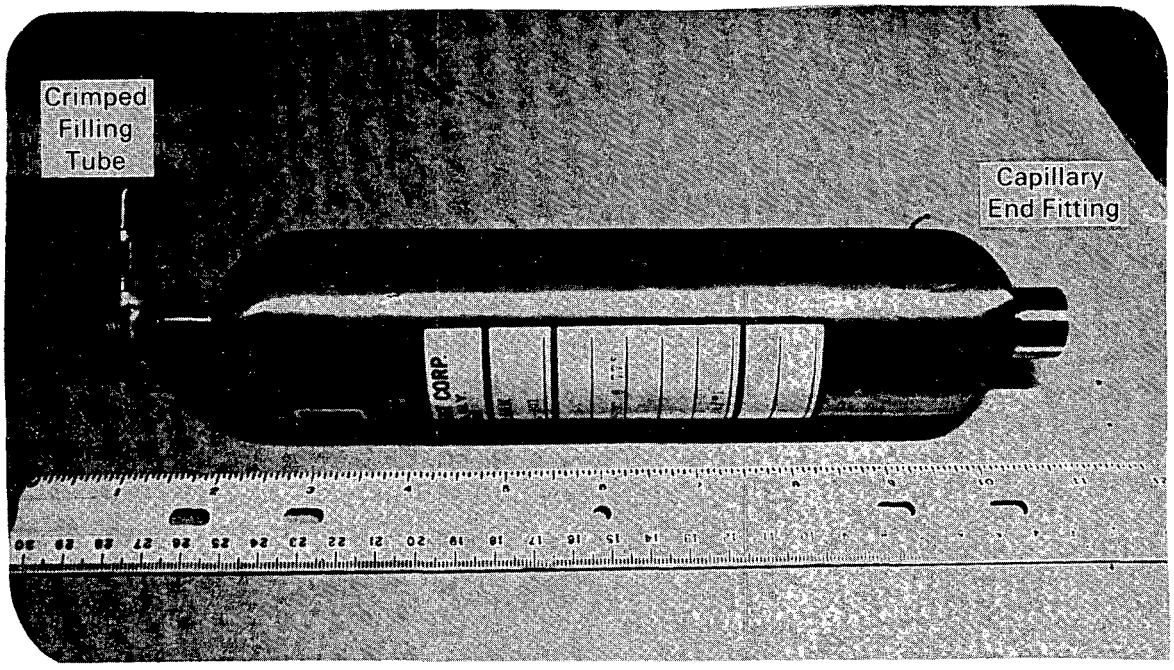


FIGURE 2.23. Helium Leak Capsule

will be welded on, and the weld will be checked for gross leaks of helium. The welded canister will then sit for 8 hr or more while the helium capsule releases enough gas to pressurize the void space. The weld will then be tested using a helium leak-detector and a vacuum vessel (Figure 2.25). The canister will be sealed in the vacuum vessel and the vessel evacuated down to a low pressure (<10 $\mu$ of mercury). The gas from the vessel will be tested for helium using a mass spectrometer leak-detector. The presence of helium would indicate a defective weld, and a contingency plan would be implemented.

In 1987 the helium-filling manifold, the helium test system, and the helium leak-detector were assembled, and nonradioactive testing was completed. The helium-filling manifold (Figure 2.24) is a series of piping, gauges, and valves where the helium capsules can be mounted, filled, calibrated, and sealed before being placed in a canister. The manifold allows for capsules to be filled from a source of compressed helium and for the resulting capillary leak rate to be measured by capturing the escaping gas in a known volume. The manifold was used also to characterize and model the leak rate from the capsules as a function of internal pressure. When a

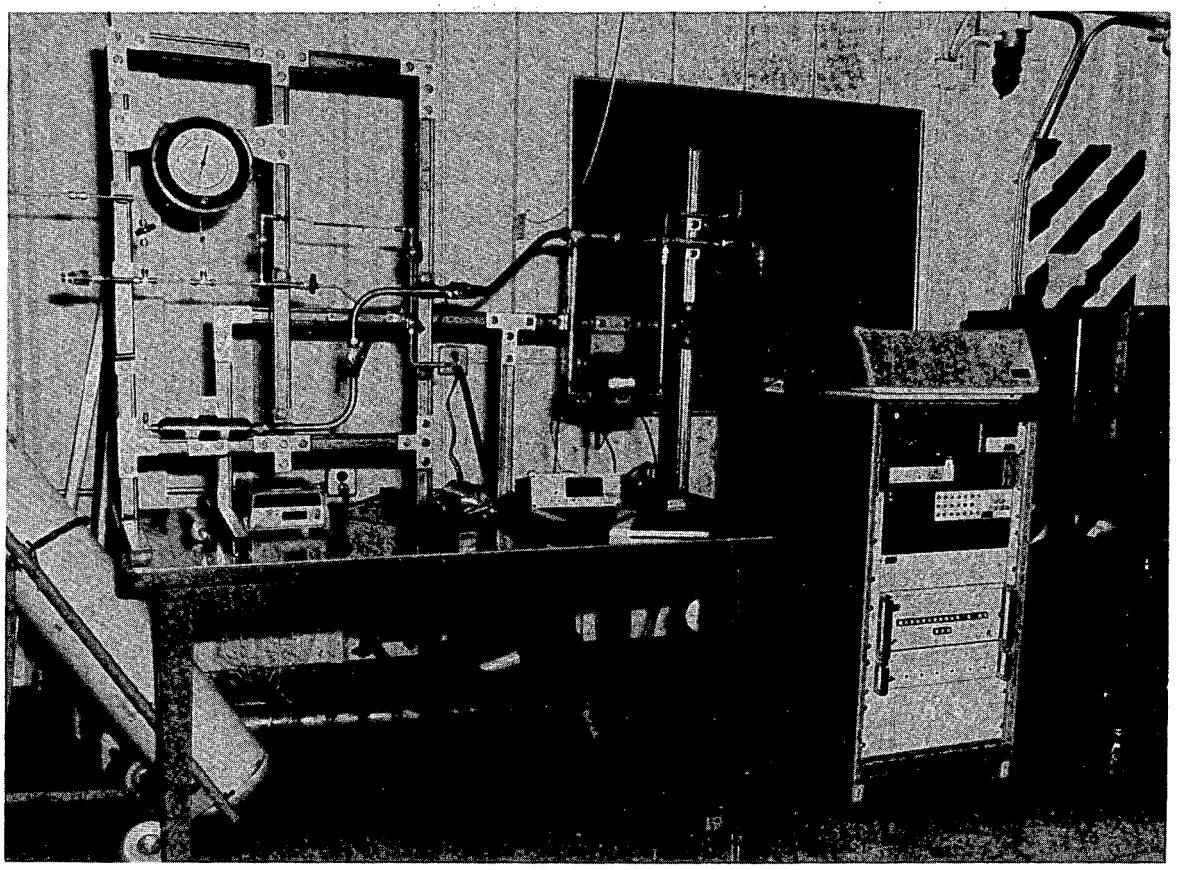

FIGURE 2.24. Helium Capsule-Filling Manifold

capsule was pressurized with helium, the entrance tube to the capsule was sealed by crimping it with a special tool. This eliminates the need for a bulky filling valve on each capsule.

The helium test system consists of a small, resealable vessel surrounded by a clam-shell furnace. The vessel is connected in series with a pressure gauge and vacuum pump to allow pressure increases within the vessel to be measured. This system was used to test the response of the helium leaks in a high-temperature environment similar to that of an FRG canister. The system was used also to characterize the capillary leak rates as a function of temperature as well as to test the durability of the crimping system used to seal the entrance tube of each capsule.

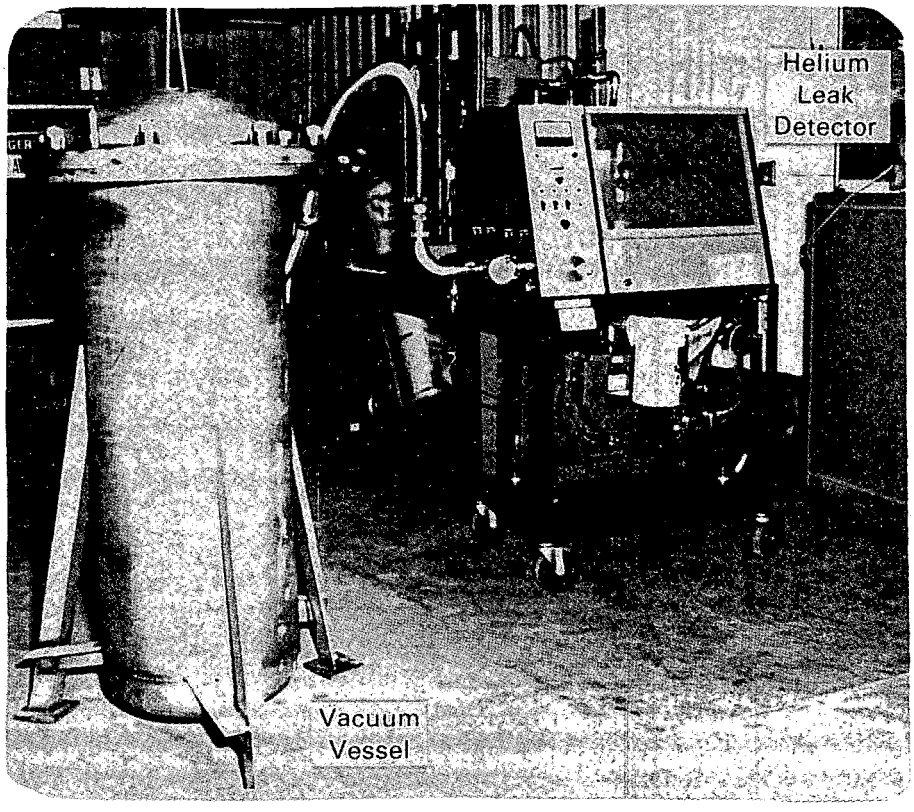


FIGURE 2.25. Helium Leak-Detection System

The helium leak-detection system (Figure 2.25) is a mass spectrometer and a vacuum pump coupled to a 160-L vacuum vessel. The system was tested by placing a recently welded, nonradioactive canister containing a helium capsule in the vacuum vessel. The vessel was evacuated, and the off gas was analyzed for helium. When no leaks were found in the canister, a hole was drilled in the lid to verify that the capsule had built up sufficient helium pressure in the void space. Further testing was conducted to check the response of the system to a simulated leak in a canister. This was accomplished by placing a standard leak in the vessel and observing the response of the leak detector to a known helium leak rate.

### 2.6.2 Canister Lid-Welding Test

The weld and rinse station and a manipulator stand, which duplicates a B-Cell work station, were installed in a test area. These items were used to establish the remote-handling procedures for the canister lid-welding

operation. This operation included placing the canister in the welding station, removing the flange protector and lid, inserting the helium capsule, inspecting the weld area via TV, putting on the canister lid, gross helium leak-testing, positioning and adjusting the weld head and welding torch electrode, and making the seal weld. After these procedures were well established, a series of demonstration welds were made using these remote-handling procedures.

The first canister welded in the demonstration series was filled with sand. A thick ceramic paint was applied over the top of the sand in an attempt to seal the sand from the void above it. A helium capsule was placed in the canister, and the seal weld between the flange and lid was made. The weld had a good, uniform appearance except for one length of ~20 mm. In this area the weld bead skewed toward the center of the canister and thus was not centered in the groove. The entire welded lid can be seen in Figure 2.26, and a close-up of the skewed weld bead is shown in Figure 2.27. There was no obvious cause of the condition.

It was decided to reweld the canister as a test of the procedure for repairing a defective weld and to assess whether a reweld could be made without releasing the internal canister pressure generated by the helium capsule. A reweld 75 mm long was made with the skewed weld bead near the middle of that length. The internal canister pressure did not cause a weld blowout, and the reweld seemed to correct the appearance of the skewed bead. This can be seen in Figure 2.28.

To gain more definitive information, a hole was drilled into the lid and a fitting was installed to allow pressurization to a known value. When the drill broke through to the canister interior, there was a significant release of gas, indicating an internal pressure greater than 1 atm during the initial rewelding. The canister was pressurized to 34 psi. Another 75-mm-long reweld was made, and again no release of internal pressure came through the weld. The canister was then pressurized to 75 psi, which is the approximate maximum internal pressure a canister filled with radioactive material would have. A third 75-mm-long reweld was made, and again there was no release of internal pressure. These rewelded areas can be seen in Figure 2.29.

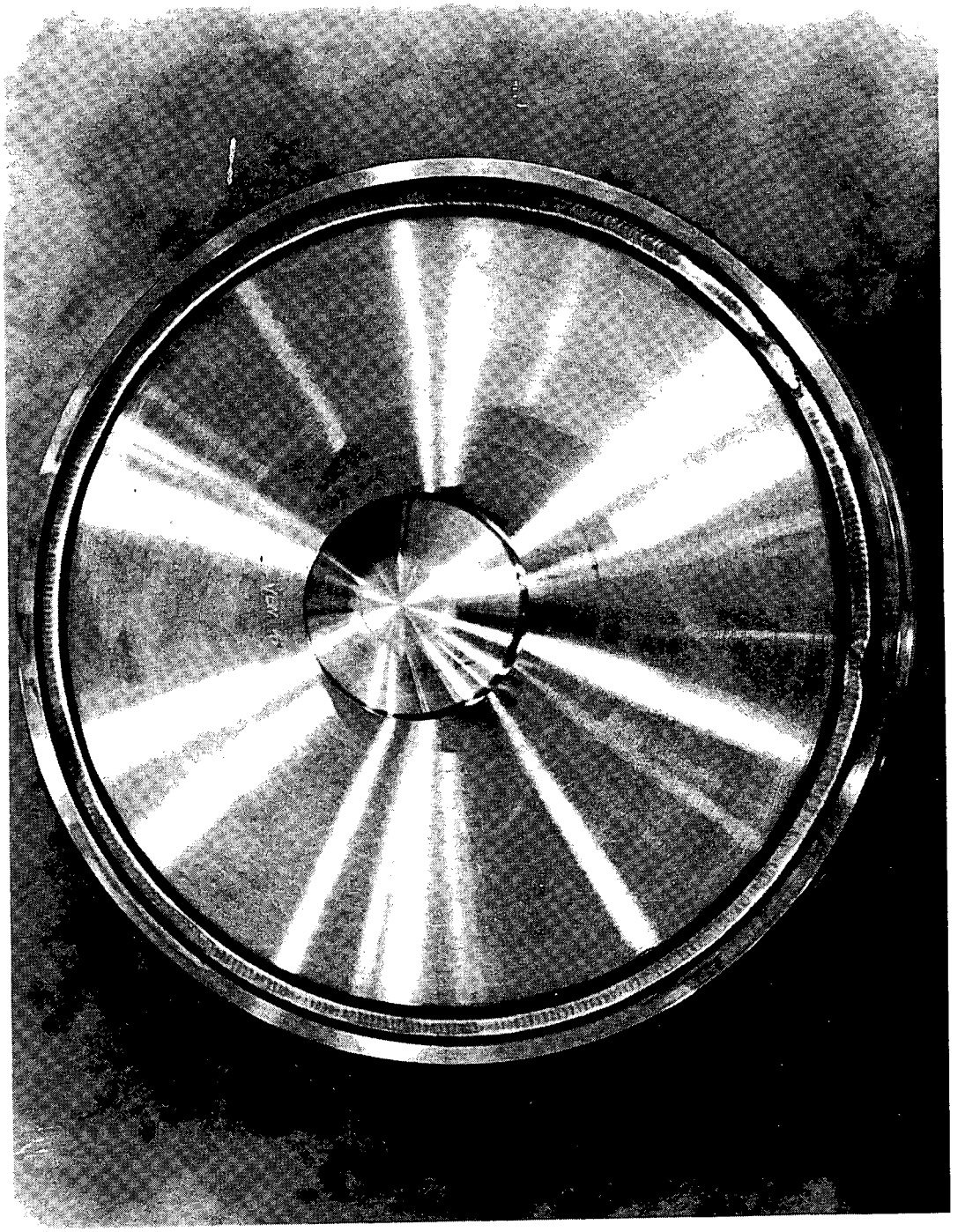

FIGURE 2.26. Canister Lid After Seal Weld

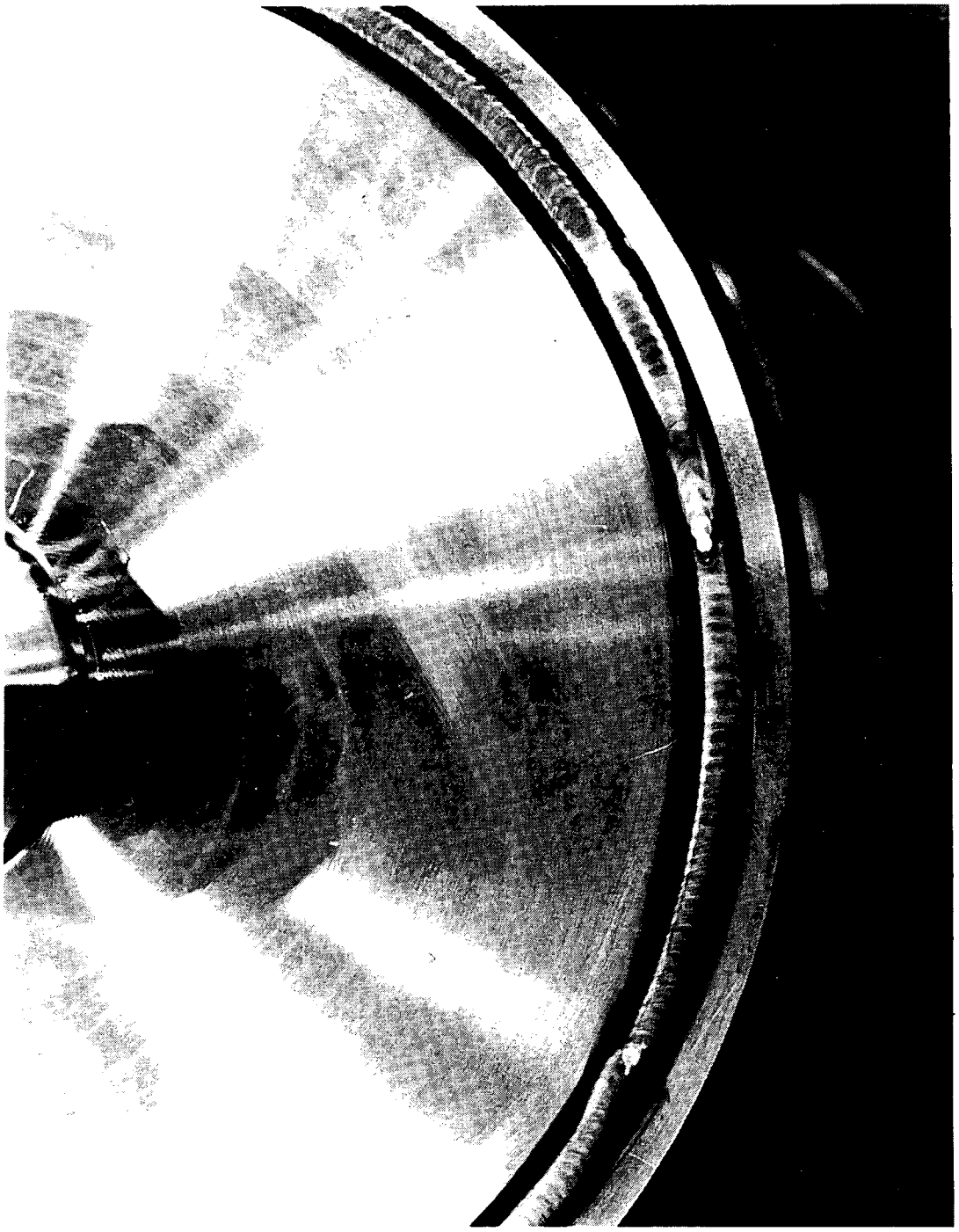

FIGURE 2.27. Close-up of Skewed Weld Area

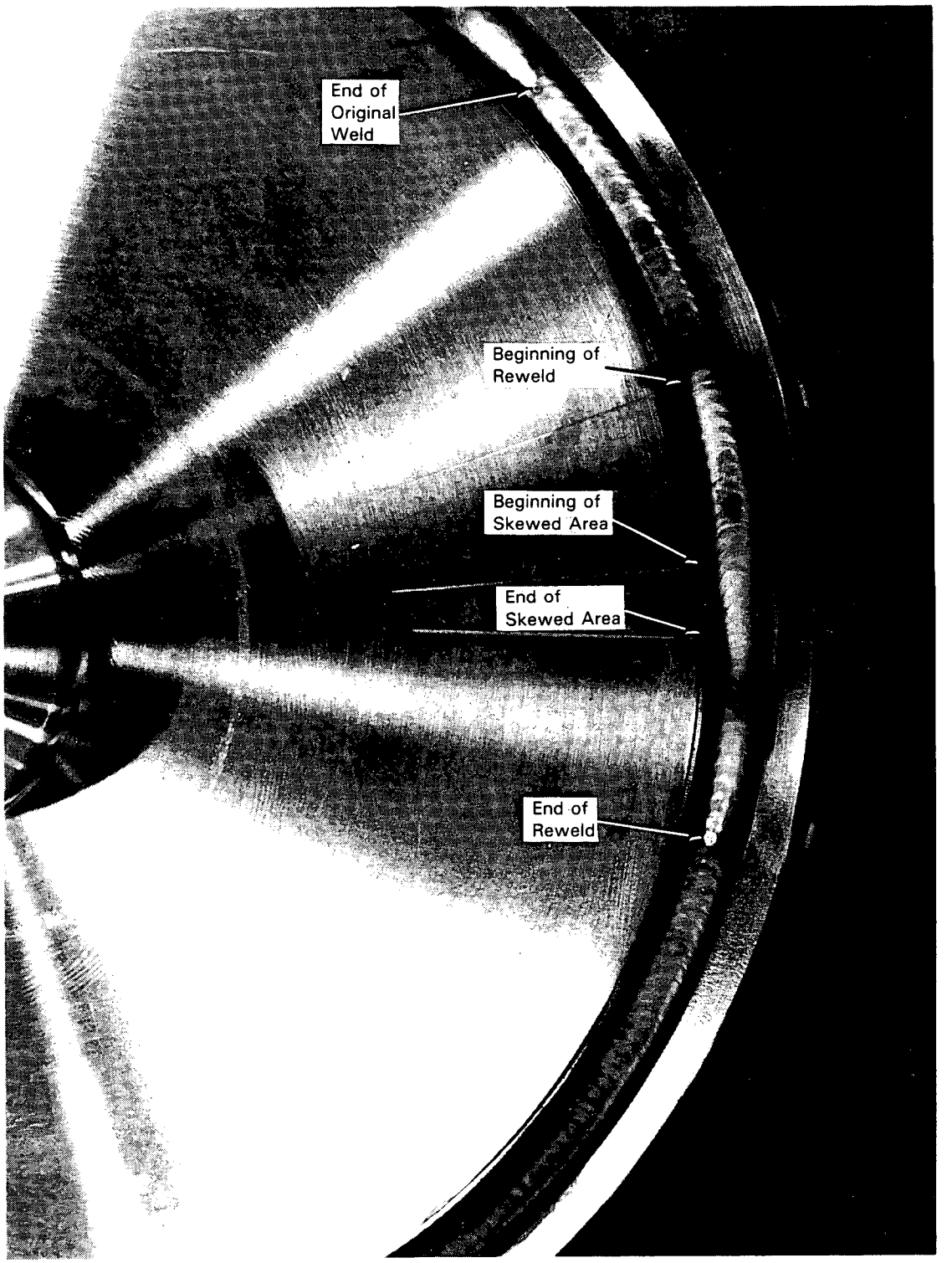


FIGURE 2.28. Canister Lid After First Reweld

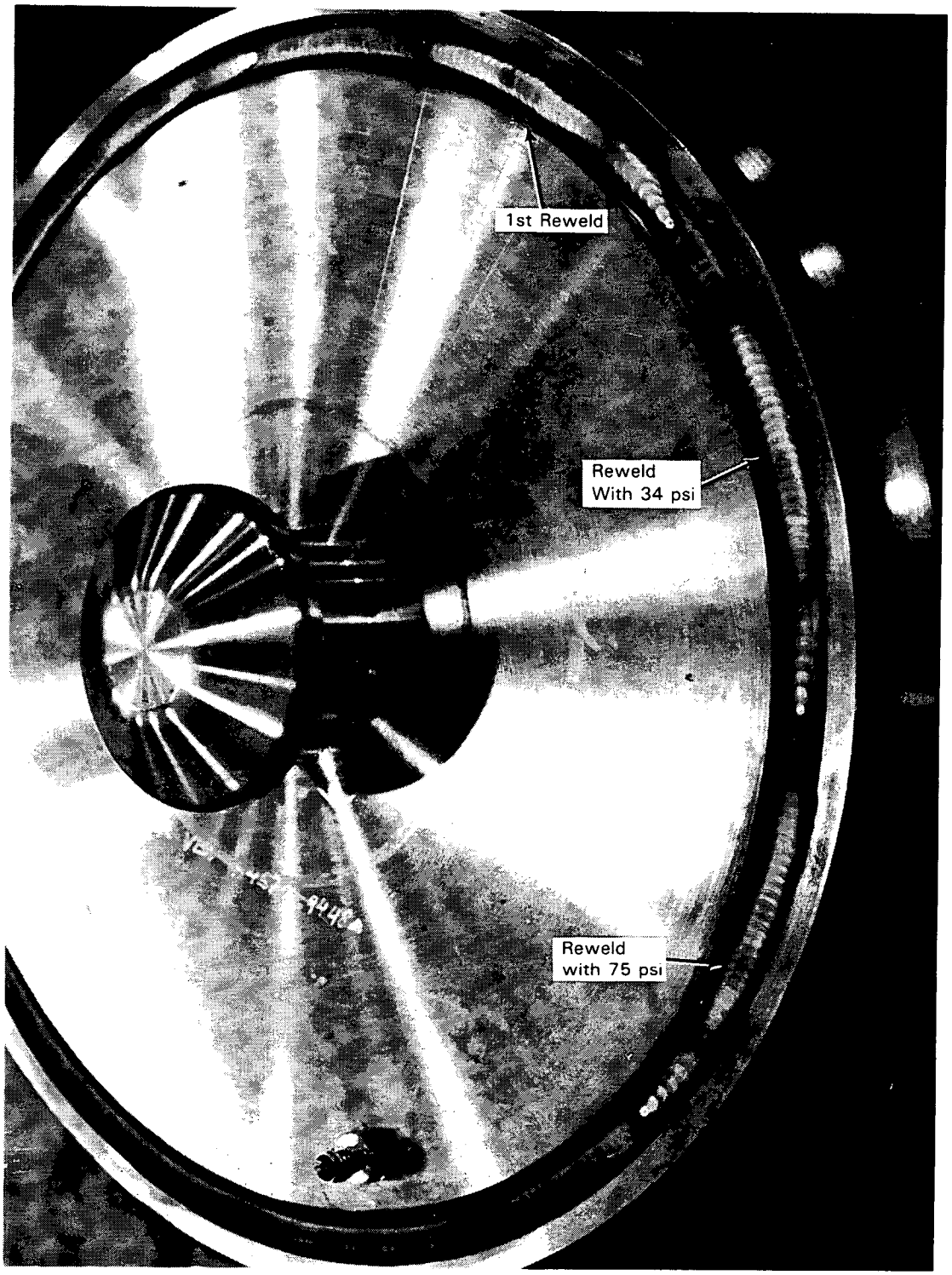


FIGURE 2.29. Canister After Three Rewelds

After the demonstration welds were completed, the power supply that drives the weld-head hoist was changed to improve the operator's control of the hoist speed. The equipment was then prepared for transfer to the hot cell area.

## 2.7 WATER-COOLED CANISTER STORAGE RACK DESIGN - G. H. Bryan

The water-cooled canister storage rack will be used to store the FRG canisters from the time they are electropolished until they are loaded into shipping casks. The storage rack provides cooling to dissipate heat generated within the canisters and also provides an enclosure to prevent contamination from reaching the electropolished canister surfaces.

The water-cooled storage rack consists of an array of ten vertical tubes enclosed in an elliptically shaped tank. These tubes are open at the top, and the canisters will be stacked three high within them. Water will circulate around the array of tubes and pass through a series of baffles to provide uniform cooling for all canisters. The cooling water outlet will drain to the radioactive process sewer. Each storage tube will be covered by a numbered lid, and six of the tubes have thermocouples welded to them to monitor the cooling of the canisters. Using these temperatures, the water flow rate can be adjusted to provide proper cooling. A steam jet is located on the north end of the storage rack to drain the tank to the sewer when cooling is not needed.

## 2.8 ELECTROPOLISHER EQUIPMENT DESCRIPTION AND FUNCTIONAL TESTING - G. H. Bryan, J. E. Surma, R. P. Allen, S. D. Halstead, and S. J. Morris

Functional testing of the canister electropolisher system began in April 1987 and continued through most of the year. During initial canister electropolishing tests, preliminary information was obtained on the operating characteristics of the electropolisher. A summary description of the electropolisher equipment follows.

### 2.8.1 Electropolisher Equipment System

Electropolishing was chosen for decontaminating the FRG canisters because it is proven technology, relatively simple to engineer and operate, and because PNL expertise existed to implement this technology.

The electropolishing tank (EPT), shown in Figure 2.30, contains 85 wt% phosphoric acid at 120°C. During electropolishing, air flow through the tank is maintained by a vessel vent system (VVS) to ensure that the level of

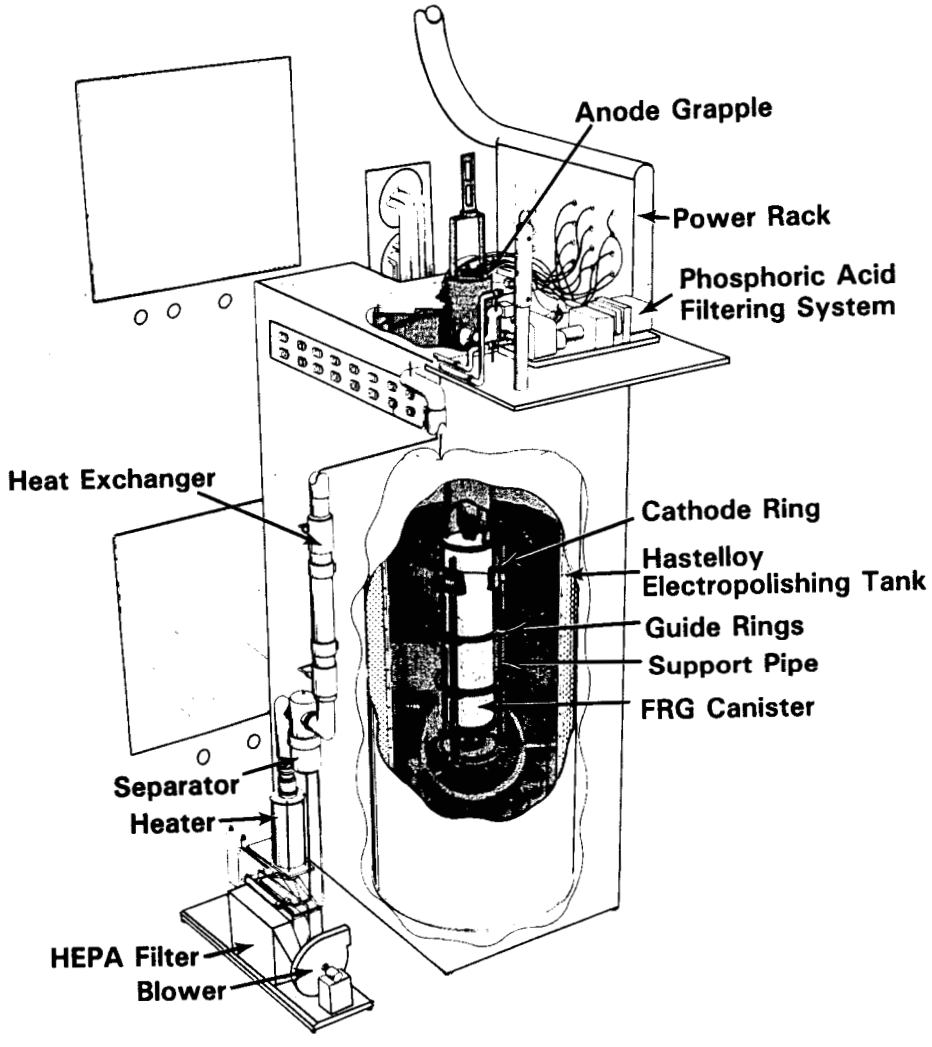


FIGURE 2.30. Cutaway Drawing of the Canister Electropolishing Equipment Rack

hydrogen is noncombustible (±4 vol%). The vacuum relative to the cell is maintained also on the EPT and an adjacent rinse/soak tank (RST) to prevent contamination of the cell by fugitive aerosols. The tank tops are open to the cell to permit canister handling with the cell crane.

The canister is electropolished in segments by passing 500 amp of 12 V dc for 15 min between the canister and an adjacent cathode. The tops of the canister and of the pintle are electropolished first using the cathode ring (Figure 2.30) with the canister sitting on an electrode in the EPT to provide the necessary electrical contact. The canister is then lifted about 6 cm and the bottom of the canister is electropolished using the same electrode in the bottom of the EPT as the cathode. The grapple that supports the canister also provides the electrical contact. A recirculation system pumps electrolyte into the cavity at the canister bottom to displace gas bubbles generated during electropolishing and thereby provide good contact between the solution and the canister. To electropolish the canister walls, the canister is alternately raised 15 cm, and then 500 amp of current at 12 V dc is passed between the canister and the cathode ring, with the anode grapple providing the electrical contact.

Electropolishing conditions and electrolyte temperature (120°C) have been chosen so that about 1 mil of stainless steel (SS) will be removed with minimal thermal shock to the glass. During electropolishing, solution is recirculated via a pump system using two eductors in the tank bottom to increase flow rate and thus enhance the electropolishing process. A filter in the recirculation system removes solids and sediment from the electrolyte.

As the canister is removed from the solution using the anode grapple, it is sprayed with water to remove residual phosphoric acid and is then allowed to air dry above the tank. The dried canister is moved into the RST and released on the tank bottom.

Measuring 4.09 m high and having an outside diameter of 11.38 m, the EPT can hold up to 3800 L of solution (Figure 2.31). The outer wall is constructed of 304L SS; the inner wall and internal piping are constructed of

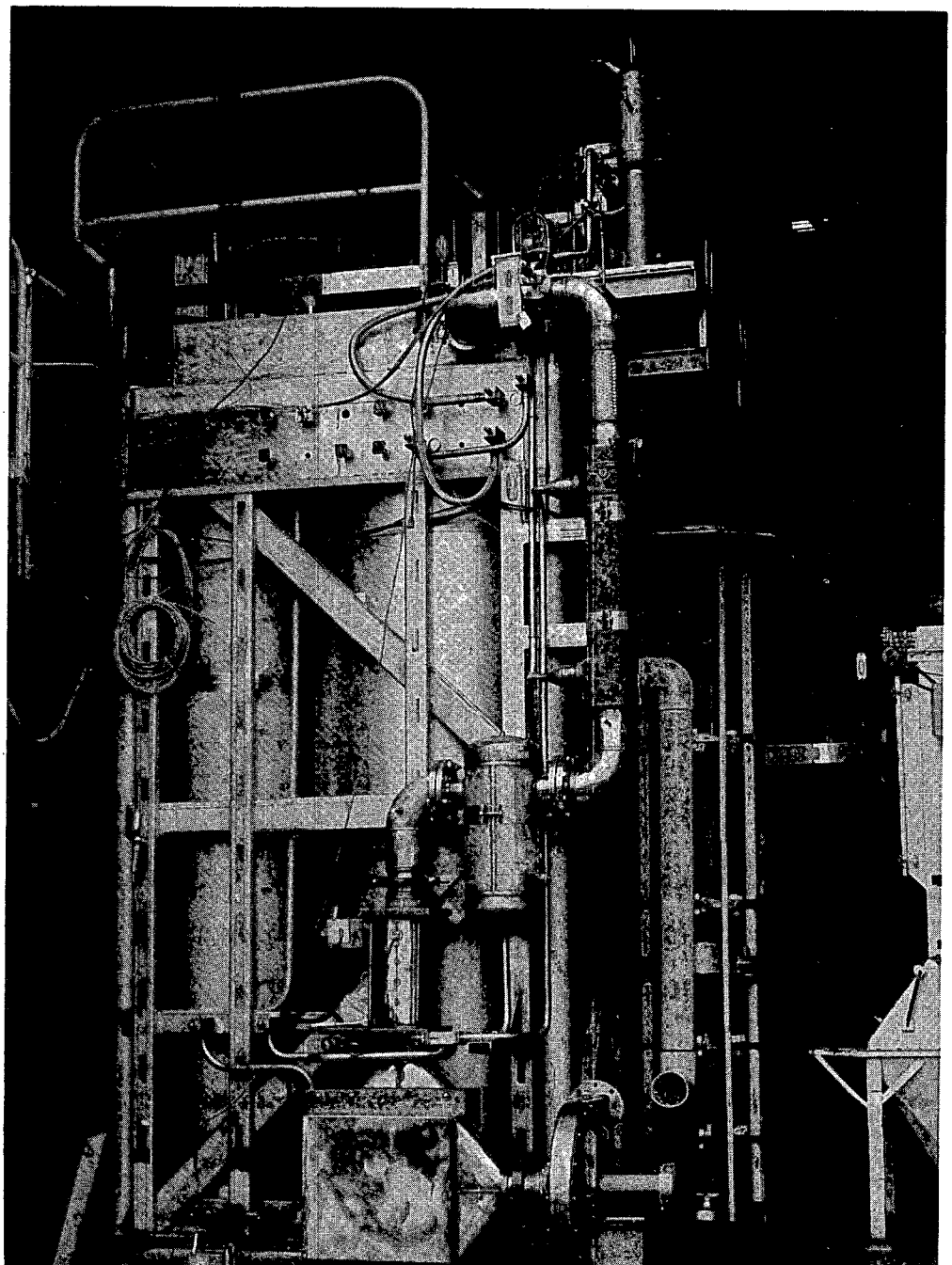

8700589-1cn

FIGURE 2.31. Electropolisher Rack

Hastelloy™ C-276 for resistance to corrosion from hot phosphoric acid. Between the inner and outer walls there is about 10 cm of space containing calcium silicate thermal insulation, a 304L SS cooling coil, and a 304L SS steam jacket for temperature control. The EPT is equipped with three thermowells, located at 3.7, 2.4 and 2.1 m from the top of the EPT, and dip legs for weight factor and specific gravity measurement. The EPT has a spray ring, 1 m in diameter, located 0.5 m from the top flange of the vessel. Two solution circulators (ejectors) on the bottom of the tank agitate the tank contents. The EPT is equipped also with solution sampling equipment, chemical addition services, and solution unloading services.

After electropolishing, a canister is transported to the adjacent RST to rinse off residual phosphoric acid with a water/steam spray. The RST can be used also for immersing canisters. Constructed of 1.3-cm 304L SS plate, the RST is 4.09 m tall, with an outside diameter of 0.6 m, and can hold up to 1000 L of liquid.

The RST has two types of spray systems. One nozzle is located 23 cm from the bottom and rinses the canister bottom. The upper spray system located in the tank top is a ring constructed of 2.5 cm 304L SS pipe with a diameter of 0.21 m and contains 32 holes 0.31 cm in diameter. The canister is rinsed with a water/steam mixture as it is lifted out of the RST. The RST also has a heating/cooling coil for temperature control. Similar to the EPT, the RST is equipped with thermowells, displays for solution level measurement, and lines for sampling and transfer. An air sparge ring in the bottom of the RST, similar in design to the spray ring, promotes solution mixing when the RST is used as an immersion tank.

The VVS provides an air sweep into the EPT and RST to prevent release of contaminated gas or aerosol into the cell. The air also dilutes hydrogen gas produced by water hydrolysis during electropolishing. The VVS consists of a condenser, entrainment separator, and blower. It is supported by a remotely replaceable rack constructed of 304L SS plate and mounted on the EPT rack. The VVS is sized to process 450 scfm of air flow.

---

™ Hastelloy is a trademark of Cabot Corporation, Kokomo, Indiana.

Radioactive particles and sediment, generated during electropolishing, will be removed from the solution by the recirculation system. This system comprises a pump, filter, and flowmeter. The pump is constructed of Hastelloy C-276, is equipped with a 2-hp motor, and has a capacity of 80 L/min. The phosphoric acid flows through a magnetic flowmeter and then through a porous metal filter assembly. Each of the three filter elements is constructed of Hastelloy C-276 and has a pore size of 100 $\mu$. The pressure drop across the filter assembly is measured. When required, the filter is back-flushed to the electropolisher.

The cathode cage (Figure 2.32) functions as a working electrode and as a counter electrode during electropolishing, depending on the electrode polarity. The cathode cage is 3 m high and 0.6 m in diameter. The top of the

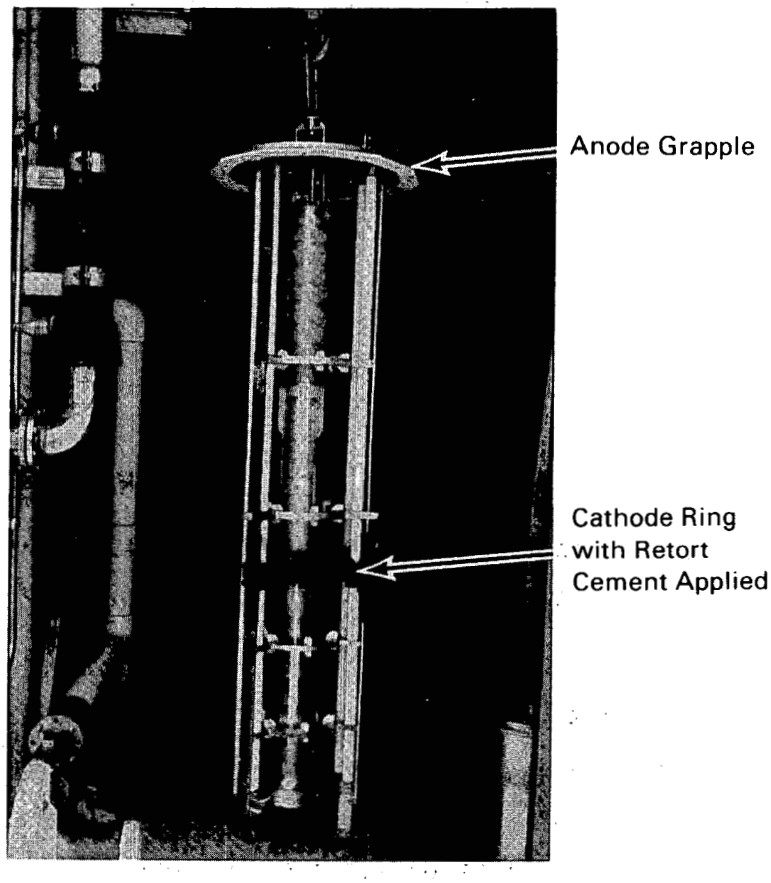


FIGURE 2.32. Cathode Cage for the Electropolisher, Showing Position of the Canister and Anode Grapple During Electropolishing of the Canister Side

cathode supports the cage internals from the tank top. A 2.5-cm ceramic plate is attached to the top of the cathode cage for electrical isolation. Four ceramic guides on the cathode cage keep the canister centered within the cage. Electric current is conducted by two 2.54-cm-dia copper bars, which also provide structural support for the cage. The copper bars have three layers of protective outer coverings: 3.5-cm ceramic tubing as electrical insulator, 3.8-cm Hastelloy C-276 to protect the copper from acid attack, and 6.4-cm ceramic tubing as electrical insulator. One copper bar, 1.8 m long, provides power to the middle electrode. The other, 3.2 m long, provides power to the bottom electrode.

During electropolishing of the canister top, the functions of the middle electrode are reversed when the canister bottom is being electropolished: the bottom electrode then serves as the cathode and the middle electrode is not utilized. In this configuration the anode grapple is used as an anode. During electropolishing of a canister wall, the middle electrode functions as the cathode and the bottom electrode is not utilized. The anode grapple again serves as the anode.

The anode grapple is 2.1 m high with a diameter of about 0.25 m (Figure 2.32). The bottom 1 m of the anode grapple is constructed of Hastelloy C-276; the rest is constructed of 304L SS. Tantalum is used to enhance electrical contact in the two places where the anode grapple contacts the canister. The clamp of the anode grapple is used to latch onto a canister, and this grapple can lift a canister weighing up to 690 kg. Before electropolishing of the canister bottom and side, a torque of 200 ft-lb is applied to the hook-like clamp to close it around the canister lid pintle. As the clamp tightens, the tantalum ring pad makes a positive electrical contact with the canister lid.

### 2.8.2 Electropolisher System Testing

In April 1987 functional testing of the electropolisher system was initiated. A series of canister electropolishing tests were completed to establish the canister electropolishing procedure that produces an acceptable

canister surface characteristic. An acceptable electropolished canister would have 1 to 3 mil of material removed from the surface and have a spectral emissivity of at least 0.4.

Early testing of the electropolisher system revealed that stray currents originating from the back side of the uncoated cathode ring would result in uncontrolled electropolishing of the sides of the canister. Stray currents could also potentially be electropolishing areas on the electropolisher tank. Therefore, electrically nonconductive coatings were tested in the laboratory in a mini-electropolisher to establish their behavior. Based on these tests, a retort cement was selected and applied to the back side of the cathode ring. Laboratory tests on the potential cathode ring coatings revealed that unacceptable coatings failed because hydrogen bubbles formed on the cathode surface. If the coating is found to be even slightly porous, the generation of hydrogen beneath the surface causes the coating to separate from the metal cathode.

Electropolisher testing incorporated the use of thermally oxidized FRG canisters to simulate actual conditions. Tests were conducted to determine the preferred current density for electropolishing the canisters. Testing resulted in a two-stage process for the operation of the electropolisher system. In the first stage the canister is electropolished at a current density of 35 $A/cm^2$ current density, which etches the canister surface. This is desirable for processing of the FRG canisters to enhance the emissivity of the metal surface. The emissivity is required to be greater than 0.4 to adequately transfer heat from the canister surface.

To determine the emissivity of the FRG canister surfaces during the testing of the electropolisher, infrared thermometry was utilized. The infrared thermometer measures the amount of thermal radiation in the range of 8 to 14 $\mu$ reflected from the canister surface. This value, when compared to the amount of thermal energy being emitted from a surface that reflects all incident energy, results in determination of the emissivity of that surface. It was determined that the emissivity of the surface of a canister that had only been electropolished was in the range of 0.2; therefore, the etching

phase of the electropolisher operation was necessary to enhance the emissivity of the surface to at least the minimum level of 0.4. The measured emissivity of the canister surface that had undergone etching was in the range of 0.45.

The final method of operation for the electropolisher system was a double pass of the canister through the cathode, which resulted in an even, highly polished surface, followed by a third pass through the cathode, in which the surface of the canister was etched. The top and bottom of the canister are also polished as separate steps in the operation.

## 2.9 A-CELL FACILITY PREPARATION - G. H. Bryan, Y. B. Katayama, M. L. Elliott, and F. E. Haun

The A-Cell facility, seen in Figure 2.33, will serve as the canister decontamination, characterization and storage area. Activities in fiscal year 1987 were directed toward waste removal and decontamination of the air lock and A-Cell, repair of the A-Cell door hinges, and A-Cell window maintenance, to prepare the facility for installation of the new equipment.

### 2.9.1 A-Cell and Air Lock Decontamination

Decontamination activities in A-Cell were accelerated during the latter part of the year to permit repair of the door hinges, removal and installation of the window, and installation of a crane. This cell needs to be as free of radioactive contamination as possible in order to maintain during storage the very low smearable contamination criterion (<22,000 dpm/100 $cm^2$) mandated by the FRG. Consequently, this criterion necessitated an extensive decontamination effort in the cell.

The decontamination effort went through several stages. A general flush with various decon agents brought the initial readings (dose rate) down to a reasonably low level that allowed longer time periods for manned entry in order to perform hands-on decontamination. A more extensive wipe-down of specific areas was completed to facilitate the removal of the two shielded viewing windows and their refurbishing by an offsite vendor. In addition, a decontamination of the air lock was required in order to facilitate

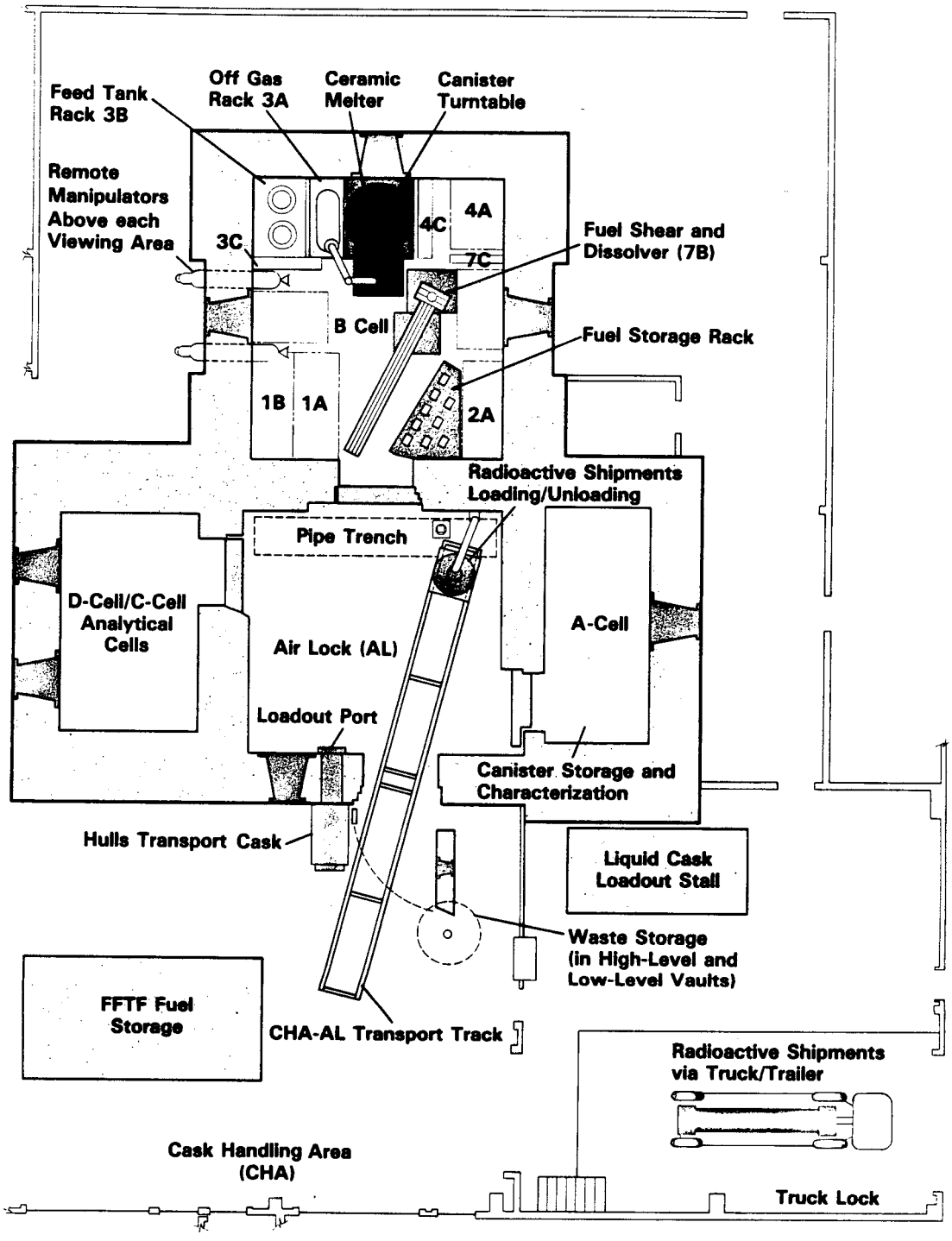


84027-03-1cn

FIGURE 2.33. Plan View of the Radiochemical Engineering Cell Complex

installation of new hinges on the A-Cell shielded doors and to allow installation of a new 5-to-10-ton crane, an exclusive-use crane for A-Cell during completion of this project.

After the hands-on decontamination to acceptable smearable levels, all surfaces within A-Cell were painted; three coats of paint were applied using rollers and brushes, and two coats were applied to the floor. The painting was required to fix contamination trapped in the pores of stainless steel.

### 2.9.2 A-Cell Door Hinge Repair

A concentrated effort was made to decontaminate the air lock and A-Cell to reduce contamination and dose rate levels before replacing the A-Cell door hinges. Reductions in dose rates to less than 100 mrem/hr were achieved in most areas where significant time had to be spent by personnel to replace the door hinges.

The hinges on the upper and lower A-Cell doors had become worn after 20 yr of use and did not allow the doors to open and close without applying significant air pressure (greater than 100 psi) to the door-actuation cylinders. New hinges were fabricated and installed in the A-Cell upper and lower doors. After replacement the upper door was easily opened using only 20 psi air pressure to the actuating cylinder. The lower door could be opened manually without the assistance of the actuating cylinder.

### 2.9.3 A-Cell Window Removal and Renovation

The A-Cell shielding windows had become badly clouded from about 20 years of service and were damaged by an earlier effort to clean the glass in place. Chemical reactions between the in situ cleaning solution and the lead window packing may have caused the packing material to expand, resulting in fractures along the edges of the glass panes. The thermal cycling of the glass during the heating cycle of the in situ cleaning would also have contributed to the fracturing. A contract was awarded to Hot Cell Services, Kent, Washington, to supervise removal, packaging, renovation and reinstallation of the two oil-filled, lead-glass shielding windows located in A-Cell. This renovation was inspected weekly to assess the progress of contractual work, to document the as-found damage to the glass components, and to observe

fabrication steps to repair the damaged glass components in a manner that would not impair in-cell use requirements.

The glass slabs were removed from their band frames without fractured glass breaking away. Examination of the lead packing between the glass slabs and their band frames showed that the packed granulated lead was porous and of sufficient thickness to allow the glass windowpanes to grow during the heating cycle of the in situ cleaning process. Stresses produced by uneven, rapid heating of thick glass slabs are expected to be more severe than any expansion-resisting force by the porous lead packing.

Examination of the removed glass slabs showed that edge-cracking in the glass slabs was limited to the medium-density (3.3 $g/cm^3$) lead glass. The high-density (6.2 $g/cm^3$) leaded glasses were free of edge cracks. They did, however, have a general coating of opaque film, which was described as normal for shielding windows with comparable service lives. In addition to edge cracks, the medium-density leaded glasses were highly etched, apparently in a pattern like those made by typical polishing techniques on large glass slabs. Such patterns may correspond to areas of increased localized stress and may affect siting of the surface etching. Examination of these edge-cracked glass slabs with polarized light showed that the cracked areas were ones of high stress. Some areas among the cracked glass were at the extremely high, red-colored level. Reexamination of the glass slabs, with polarized light after cutting away the cracked edges, showed only areas of low-level, black-colored stress.

In the as-removed condition, the medium-density leaded glass had a visibility-limiting film coating the surface. Some of this film was removed with a commercial-grade window glass cleaner. Most of the deposits of opaque material, however, were in the etched grooves and could not be removed with the glass cleaner. A razor blade was needed to scrape this material from areas where it had accumulated to a depth greater than the etch groove. The crud formation on the leaded-glass pieces was described in a report from an analytical laboratory, contracted by Hot Cell Services, to be a low-form polyethylene with lead as a major constituent. The packing between the glass

slabs and the band frames was found to be very hard. This structure may have allowed the lead to exert thermal expansion forces towards the glass slab edges during heating.

After renovation and assembly at the vendor's facility, the windows were returned to Hanford and successfully reinstalled.

## 2.10 REFERENCE

Burkholder, H. C., and J. M. Rusin, compilers. 1985. Nuclear Waste Treatment Program Annual Report for 1984. PNL-5414, Pacific Northwest Laboratory, Richland, Washington.

# 3.0 WEST VALLEY SUPPORT

J. R. Carrell - Manager

## 3.1 OBJECTIVES

The Western New York Nuclear Services Center (WNYNSC) successfully processed commercial nuclear fuel for 5 years until operations were terminated in 1972. Underground tanks at the site contain high-level waste (HLW) produced, in part, by a commercial fuel reprocessing campaign. The State of New York has assumed responsibility for these wastes. The Department of Energy (DOE) is assisting, through the West Valley Demonstration Project (WVDP), in retrieving and solidifying these wastes. The site contractor for the WVDP is West Valley Nuclear Services Co., Inc. (WVNS).

The overall objective of the West Valley Support Task (WVST) is to provide the technical support required by the WVDP, including the transfer of DOE-developed HLW treatment technology. Specific objectives include 1) designing an acceptable glass-waste form for the West Valley waste and providing characterization data that support its acceptability and 2) assisting WVNS with the technology and equipment required to successfully vitrify the West Valley waste. The following sections summarize the FY 1987 activities of the WVST in support of these objectives.

## 3.2 SUMMARY

The WVST provided significant transfer of technology to the WVDP during FY 1987. Major support focused on the remote technology design, process support, and product qualification.

The remote technology activities provided design criteria and the remote designs for several major components within the West Valley vitrification cell. During the past year components of the tank jumper pits, in-cell feed and sampling system, melter, off-gas system, canister-capping and decontamination systems, and cell maintenance station were prepared. Some of the most significant work included layout of the nozzle locations on the cell walls. The nozzles provide the required services to the process components to support

the vitrification process. Completion of the layout allowed design of the wall modules, by others, to proceed on schedule. These drawings also included the layout of all the major process and process support components in the vitrification cell. During the year a slurry sampler was designed to provide for remote sampling of the feed concentrate slurry prior to transferring it to the melter. The sampling ensures that the correct slurry has been formulated to produce the reference West Valley glass.

Process support activities are associated with equipment performance and process operations in the waste treatment system. The activities address issues related to process chemistry, waste mobilization, feed system, the glass melter, off-gas treatment, and instrumentation and process control. A canister decontamination process was developed that uses the cerium (IV) ion to chemically mill a thin layer from the canister surface. Process streams from the waste tanks to the melter feed tank were simulated on a laboratory scale and were characterized in terms of their chemical and rheological properties. Methods were developed for removing excess sulfate from the melter feed and for determining the metal fines concentration in the sludge wastes. Shear vane tests were conducted to measure the shear strength of the sludge on the bottom of the 8D-2 tank at West Valley, and a sludge simulant with the appropriate rheological properties was developed.

The RECIPE computer code was developed to calculate the quantity of glass-forming chemicals to add to a batch of waste in order to produce a final glass product within a target composition region. The MASBAL computer code was developed 1) to infer the glass composition in the canister based on chemical analyses of the slurry in the feed tank, process measurements, and knowledge of the mixing characteristics of the melter and 2) to establish confidence limits about the inferred glass composition based on uncertainties in the compositions and process measurements. A failure modes and effects analysis of the West Valley vitrification system was completed to evaluate the system's ability to continue vitrification when components fail and to recommend methods to minimize the impacts of these failures on system integrity and performance.

Product qualification activities were focused on waste-form chemical durability and canister impact testing. The effects on chemical durability of glass composition ferrous/ferric ratio (redox state), heat treatments, groundwater source, and chemistry were determined. Impact tests were conducted on several different potential canister designs to determine their resistance to impact and breaching.

## 3.3 REMOTE TECHNOLOGY SUPPORT - J. M. Seay, D. N. Berger, R. E. Thornhill, R. L. Bogart, H. E. Adkins,[(a)] and P. A. Titzler[(a)]

The basic scope of work in this subtask was to provide remote design technology for components integral to West Valley's vitrification process. In general, unless the specific component was developmental or prototypical, the design was limited to defining component size, configuration, interfaces (e.g., nozzles and support attachments) and necessary remote handling attributes through drawings or input into WVNS equipment specifications. Final detailed design responsibility was passed on to the component fabricator. In conjunction, PNL provided technical assistance as deemed necessary by WVNS in reviewing fabricator's detailed designs.

### 3.3.1 Feed Preparation Components

#### 3.3.1.1 Component Test Stand Wall Nozzles - Layout and Location

During FY 1987 the locations for the wall nozzles in the West Valley vitrification cell (Figure 3.1) were finalized. A drawing consisting of 25 sheets detailing the locations of wall nozzles and the component test stand (CTS) components was baselined. It depicts the following: 1) nozzle and jumper layout, 2) key component locations referenced from the PNL datum to the column lines, and 3) nozzle elevations and identification for the east wall, north wall, west wall, south wall, and southeast wall. This drawing will be used in designing all the process jumpers required to connect the vitrification system components to their respective services on the cell walls.

---

(a) Westinghouse Hanford Company

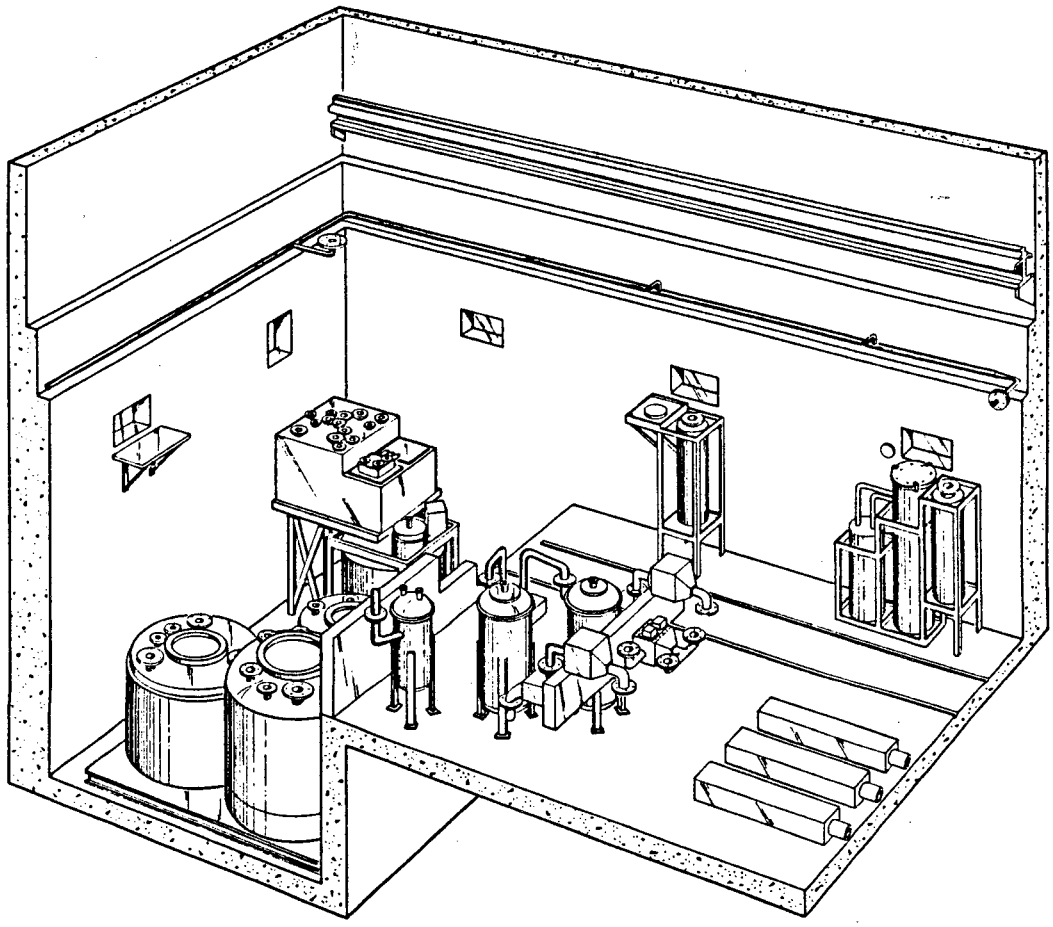

FIGURE 3.1. Vitrification Cell

3.3.1.2 V-011 Mist Eliminator

During FY 1986 the V-001 concentrator feed makeup tank (CFMT) (Figure 3.2) was designed to provide for evaporating water from the West Valley liquid wastes to form the slurry for eventual transfer to the melter. When the concentrator was designed, a mist eliminator was provided atop the tank to demist and condense vented off gases into liquid for return to the tank.

Since the V-011 melter feed makeup tank (MFMT) is essentially an evaporator, a mist eliminator was designed for this tank. Its design is a modification of that previously designed for the V-001 CFMT. The nozzles and

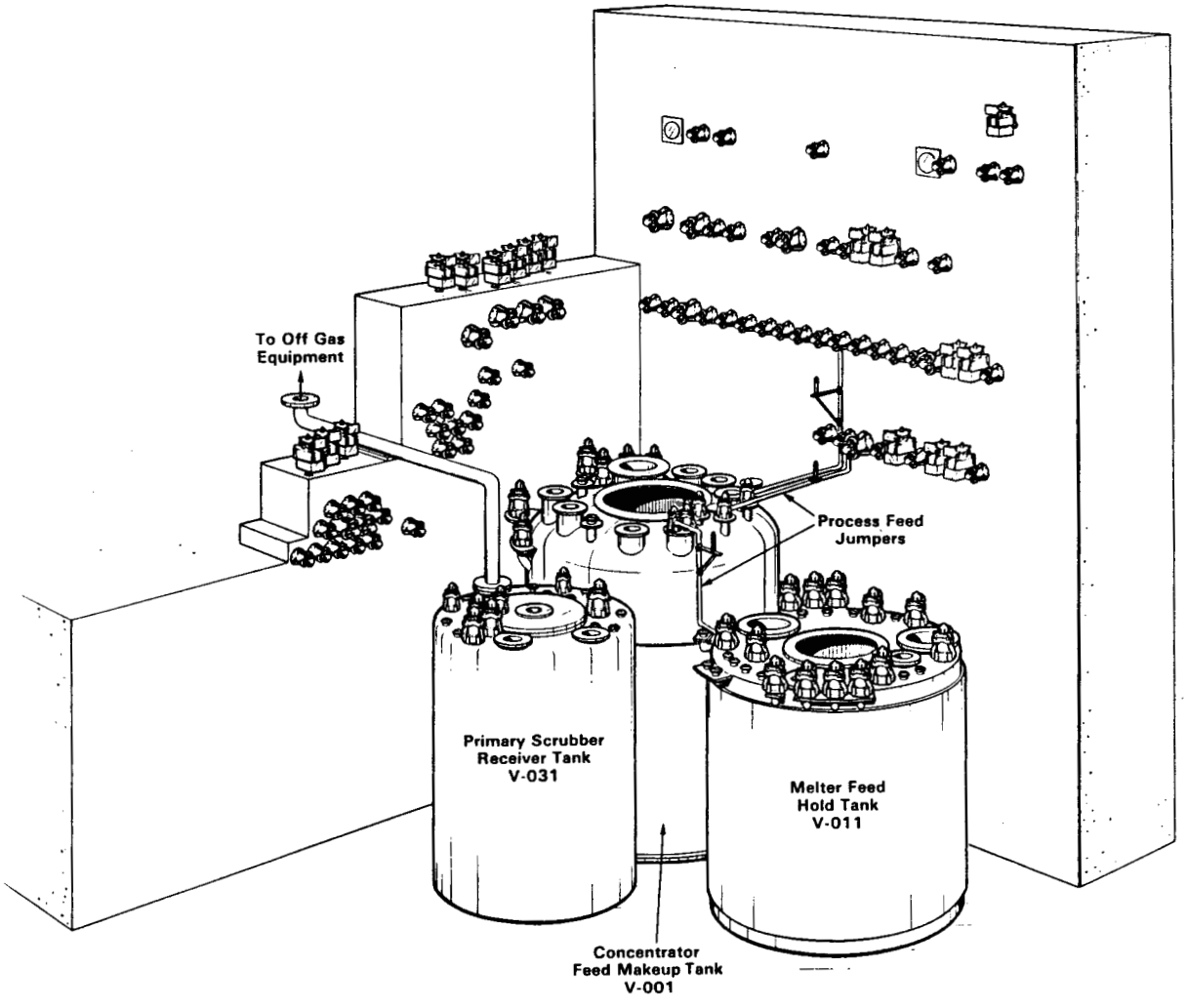


FIGURE 3.2. Concentrator Feed Makeup Tank System

their elevations were changed to interface with the V-011 MFMT. The final drawings were delivered during FY 1987 to WVNS for fabrication of the mist eliminator.

3.3.1.3 V-001 CFMT Seal Pot

The final design for the V-001 CFMT seal pot was delivered to WVNS in May 1987. The seal pot is attached to nozzle H on the V-001 CFMT and provides for fluids in the concentrator to overflow into the CTS waste header in case the tank overfills or pressurizes. It provides a 20-in. water seal between the tank and the waste header. The seal pot has provisions for liquid-level

measurement, via a bubbler, for flushing and jetting the contents into the waste header, and for chemical additions. The design consists of a vessel 6 in. in diameter and 4 ft in height with remote PUREX nozzles connecting it to the V-001 CFMT and waste header. Two PUREX three-way connectors provide connection points for the services to the seal pot. The vessel is remotely installed and removed, and no provisions are made for maintenance as it is considered a disposable component.

3.3.1.4 V-001 CFMT Liquid-Level and Specific Gravity Sensor

The design for the V-001 CFMT liquid level and specific gravity sensor, initiated in FY 1986, was completed in FY 1987. It is adapted from a system already demonstrated in simulated melter feed slurries both at Pacific Northwest Laboratory (PNL) and at Savannah River Laboratory (SRL).

The system is used in the V-001 CFMT to measure both the liquid level in the tank and the specific gravity of the slurry. The level measurement is used during processing to indicate concentrating endpoints, to determine liquid volume for chemical additions, and to provide input into the overall mass balance. During steady-state operation, the system is monitored for increases and decreases in the level which may indicate operating problems. This system will determine the endpoints for concentrating and transferring during non-steady-state operation.

The Holledge P-189 sensors in the design have no elastomers and are available in two standard materials, either 316L stainless steel or Hastelloy C. The bottom of each sensor contains a metal diaphragm 0.010 in. thick. The sensors are actually 1:1 pressure repeaters that balance the supply air pressure with the pressure on the diaphragm exterior. The supply pressure is vented to the vapor space of the tank. A total of three sensors are used to measure both the liquid in the tank and the specific gravity.

Two sensors (#1 and #2) are placed exactly 10 in. apart in an assembly that holds the lower sensor (#1) 1 in. from the bottom of the tank. A third sensor (#3) is placed in the vapor space above the liquid to measure the pressure in the tank. Sensors #1 and #3 are used to determine the liquid level

in the tank, while sensors #1 and #2 are used to determine the specific gravity of the slurry. A schematic of the level measurement system is shown in Figure 3.3.

The outside diameter of the liquid-level measurement system is 4 in. square, allowing it to fit into the 6-in. nozzle (nozzle T) atop the concentrator. The system can be remotely removed and replaced if necessary. Based on experience at PNL and SRL, the sensor is expected to have about 6 months' service life in continuous operation. The instrumentation to support the design consists of three air-flow regulators, two pressure converters, and a signal conditioner and recorder (computer). A precise air-flow regulator is required to ensure proper operation of the system. The signal from the pressure converters is sent to a computer or process control unit. Algorithms must be developed for the West Valley system and included in the data analysis to compensate for known inaccuracies in the system.

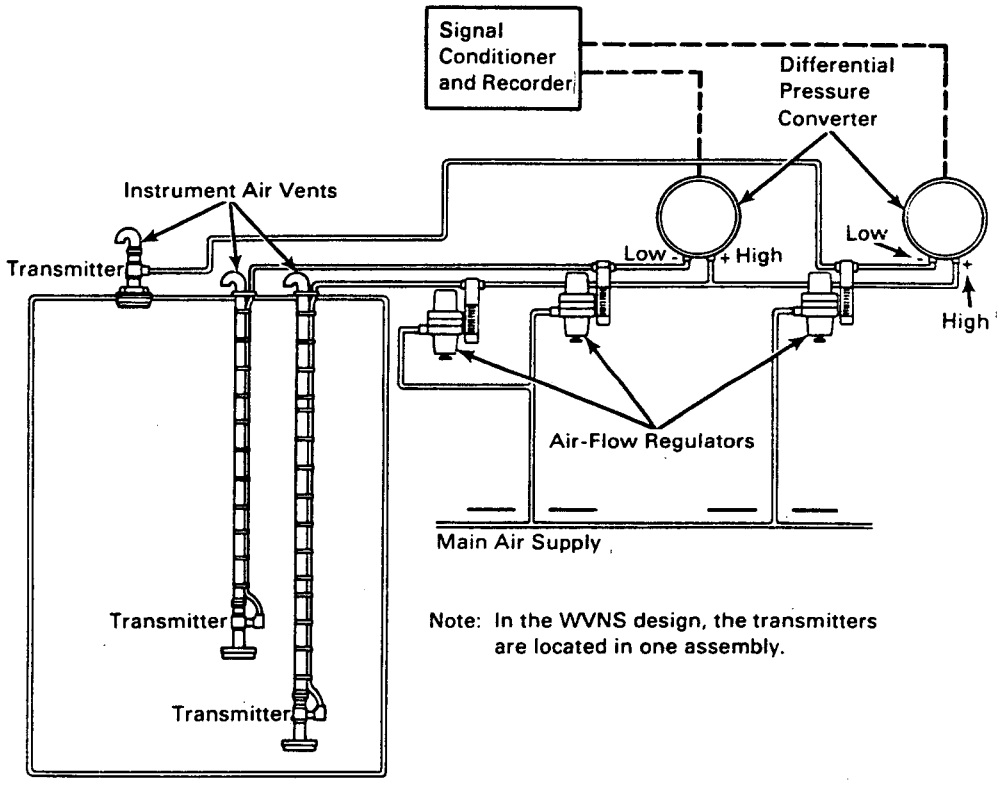


FIGURE 3.3. Instrumentation for Level Measurement System

### 3.3.1.5 V-001 and V-011 Electronic Level Detector

The electronic level detector is used in the V-001 CFMT and the V-011 MFMT as backup to the liquid-level and specific gravity sensor. The detector consists of a Drexelbrook capacitance type continuous level detector modified for remote operations. A dielectric, Kapton, was selected for the sensing element because of its resistance to radiation.

The Drexelbrook level detector consists of a single sensing element that runs the length of the vessel. It contains a level sensor and a second sensor for material composition. Both the level sensor and the additional sensing segment are connected to a transmitter through a single measuring cable.

The slurry surrounding the level-sensing element causes minute currents to flow from the sensor to ground. The admittance is measured by comparing these currents with the supply voltage in a wide-range bridge circuit. The bridge output voltage is applied to a demodulator circuit which produces a direct-current voltage.

The additional composition-sensing segment measures the admittance characteristics (resistive and capacitive currents) of the slurry in the vessel so that the system can "calibrate" itself for the density, temperature, and composition of the material.

Level and the additional composition signals are combined in a circuitry that computes the true level and produces a 4 to 20-mA signal. This signal is then used to operate a remote readout. Drexelbrook's RF Cote-Shield™ technology enables the detector to ignore buildup of coatings that can cause inaccuracy and to give accurate, reliable level measurements over a wide range of vessels, materials, and conditions. Because the system has no moving parts, it can be used for low-level, high-level, and continuous-level control.

### 3.3.1.6 Air-Displacement Slurry Feed and Sample Pumps

The air-displacement slurry pump (ADS) design was modified to 1) increase the flow to 300 L/hr for supplying slurry to the melter and 2) use it to provide circulating flow to the slurry-sampling station. The basic design of the ADS pump is described in a 1986 report Evaluation and Testing of Metering Pumps for High-Level Nuclear Waste Slurries, PNL-5851.

The current pump design in use at WVNS was changed to install two PUREX three-way nozzles on it to provide recirculating flow between the V-001 CFMT and the V-011 CFMT to the sampling station. One pump is installed in each tank for supplying slurry to the sampling station.

For the feed pump, the pump chamber was enlarged from 3 in. to 4 in. in diameter to increase the volume to 2.57 L. Cycle time of the pump was increased about 19%. For a 300 L/hr flow rate, the cycle time of the pump is 31 seconds. The chamber size was the only modification made to the pump. The feed line from the pump to the melter, however, had to be increased from 3/8 in. to 1/2 in. in diameter to achieve the desired flow rate.

### 3.3.2 CTS Off-Gas Components

#### 3.3.2.1 CTS Heat Balance Report

The CTS Heat Balance Report documented the results of the analysis, via the TEMPEST computer code, of the air flows in the CTS vitrification cell. All heat sources and sinks were modeled on the forced-air cooling from the coolers mounted in the cell roof. The model addressed the conditions in the vitrification cell with the crane door open and closed and with the transfer door open and closed.

The cell configuration requires about 160 kW of auxiliary cooling to ensure a temperature of 95°F. Diminishing the cell heat load decreases and simplifies the overall cooling requirements. A desirable approach to reducing the overall cell heat load would be to minimize individual heat sources. Limiting point sources dampens the cell heat load fluctuations and thereby simplifies control of the cell temperature.

Report results formed the basis for determining the adequacy of the coolers and their location. As an alternative to cell cooling, the report addressed the potential for lower forced-air temperature and higher flow rates.

The report presented an alternative that would possibly eliminate the in-cell coolers altogether. This is accomplished by providing an equal amount of cooled forced ventilation air, which would reduce cell temperature. Assuming a design for forced ventilation flow of 4000 scfm, and conditioning the

forced air to 50°F, cooling could be achieved with about 58 kW. The same amount of cooling can also be achieved with a lower chilled air temperature if the forced air flow is increased. The forced-air flow could also be increased if the in-leakage air flow is reduced or the total ventilation flow is increased. The result of increasing the forced-air ventilation would be a more efficient heat-transfer method (due to larger driving force) and provide easier control.

3.3.2.2 Off-Gas Condenser Design

The CTS off-gas condenser receives the vented off gases from the V-001 concentrator and the V-011 melter feed tank during normal operation and from the melter during an upset. It also provides for condensation of vented constituents from the decontamination system, the sample station, and the CTS cell waste header. The condensables from the vessel vent header are returned to the 8D-3 tank. Noncondensable constituents will be returned via a jumper to the submerged bed scrubber.

The condenser is modified for a remote-operation, counter-current, U-tube type of heat exchanger with coolant water within the tubes. There are provisions for adding chemical additives and returning condensate from the vent header. There are also provisions for measuring the $\Delta P$ across the inlet and outlet of the tube sheet and for measuring weight factor.

The tube bundle is remotely replaceable, and provisions are made for remote detection of leaking tubes. Remote plugging of leaking tubes is possible provided that hardware is designed to do the plugging.

The operating and design conditions for the condenser are as follows in Table 3.1.

3.3.2.3 South Stub Wall and Service Wall

The stub wall is a stainless steel frame structure enclosed, where required, with stainless steel plate. The stub wall supports electrical, instrument, steam, and cooling water to connect to standard PUREX jumpers. All nozzle positions are about 12 in. apart, center to center, and accessible

TABLE 3.1. Operating and Design Conditions of Off-Gas Condenser

| Operating Conditions | Shell | Tube |
|---|---|---|
| Pressure | -5 in. water gauge | 60 psig |
| Temperature | 49 to 164°C | 26/32°C |
| Capacity | 935,000 - 1,280,000 Btu | |
| **Design Conditions** | | |
| Pressure | +30 in. water gauge/-120 in. water gauge | 150 psig |
| Temperature | 185°C | 35°C |
| Capacity | 3,000,000 Btu | |

for remote handling of jumper connections. As this wall contains steam lines, a series of vent holes are located atop the north and south sides for convection-venting the wall interior.

This wall extends from the west wall into the vitrification cell 20 ft 3 in., with the north face of the wall on the center line of column 3. The top height of the wall is at an elevation of 109 ft 9 in., and the bottom height is at the elevation 100 ft 0 in. The stub wall services the V-001 concentrator and V-031 submerged bed scrubber in the vitrification cell pit and the process off-gas area to the south with electrical and instrumentation standard 2-in. nozzles and three-way PUREX connections. (See Figure 3.2.)

The stub wall will be welded to the south pit edge at the 100 ft 0 in. level to the stainless steel angle-edge piece. The wall is also bolted to the floor using either the existing holes or newly drilled holes and anchors. The west end of the wall is secured to column 3/D by either welding or anchor bolts.

The wall has been designed with decommissioning in mind. The piping to the stub wall exits the west wall near column 3/D and runs down the face of the west wall and into the southwest end of the stub wall. After the piping to the wall is remote-cut and the connected welds removed, the stub wall can be removed by unbolting it from the cell floor.

The service wall is also a stainless steel frame structure enclosed, where required, with stainless steel and plate. It extends from the west wall at column 3/Z, 17 ft 11-1/2 in. into the cell at a height from 111 ft 1 in. to 114 ft 3 in. The service wall has both electrical and standard PUREX jumper operations, and services the vitrification off-gas components. The design of the nozzle connections is much like that of the stub wall.

The service wall is hard-piped from the penetrations through the west cell wall and provides jumper connections to the process equipment. It is bolted to the floor like the stub wall and can be remotely removed once the process piping has been cut.

The wall is accessed via both direct viewing through the cell windows and closed-circuit television. After installation, no maintenance is anticipated.

3.3.2.4 Filter Gamma Detectors

During FY 1987, PNL prepared a specification for a recommended gamma ionization chamber to monitor the CTS off-gas dry-solid-particulate filter (DSPF) assembly during operation of the CTS vitrification system. It identified the shielding required for the monitor, the recommended connector, and the out-of-cell equipment.

Radiation-hardened ionization probes are routinely used to monitor dose rates under extreme operating conditions. This type of detector is recommended for monitoring the accumulation of aerosol activity on the WVNS in-cell DSPF. The specification describes a particular detector that has been used successfully at PNL in hot-cell applications. It is designed to operate in high radiation fields under moderate temperature conditions and is suitable for the DSPF monitoring task. The gamma detector will be positioned 6 to 12 in. from the DSPF that is to be monitored. The readout of the gamma detector is relative to its distance from the filter.

Maximum activity expected is a level of 2000 Ci of cesium to be collected on a process DSPF before it is to be changed out. A Reuter Stokes RS-C4-0806-112 gamma ionization chamber was selected, which is designed for use in a high gamma flux field and over a wide flux range.

Because of background activity within the CTS Cell, shielding must surround the detector except for a slot that must be pointed away from the majority of the background activity and at the filter to be monitored.

Two methods of installing the detectors were provided to WVNS. One method is to place the gamma detector within the shielding block next to the first DSPF within the filter housing. The gamma detector would terminate with coaxial connections within a special PUREX connector. Coaxial PUREX connectors have been used before at Hanford by du Pont, General Electric, ARHCO, and Rockwell Hanford Company. Reuter Stokes recommends an 18-in. cable-bend radius; this could cause problems regarding actual physical locations of the PUREX connector and the position of the gamma detector next to the DSPF. The shielding block next to the DSPF will require support to prevent stresses on the PUREX connector.

The second concept for installing the gamma detectors would be from the operating gallery. Coaxial cable lengths can be purchased at lengths up to 30 m. This method, less costly, would eliminate the need for the two PUREX connections with special jumpers within the cell. The probe shield would be part of the permanent piping, with the slot pointing upwards.

Either method is acceptable and it will be the decision of WVNS to select the one best suited for their operations.

### 3.3.3 Waste Mobilization Jumper Pits

The waste mobilization jumper pits, transfer piping, and containment trench are part of the sludge mobilization system. The high-level waste (HLW) from storage tanks 8D-1, 8D-2, and 8D-4 will be processed in stages. When the treatment of the supernatant from 8D-2 is completed, tank 8D-1 will contain a cesium-loaded zeolite. The zeolite will be mixed with water to form a solids slurry. The solids will be slurried by the waste mobilization pumps and pumped to tank 8D-2 after sludge washing using the zeolite removal pump installed in the riser of tank 8D-1. Once the zeolite is in tank 8D-2, it will be mixed with the washed PUREX waste sludge remaining in tank 8D-2.

To make these waste transfers at the tank farm, one waste diversion pit (Figure 3.4), pump pits (Figure 3.5) for each tank, transfer piping and its

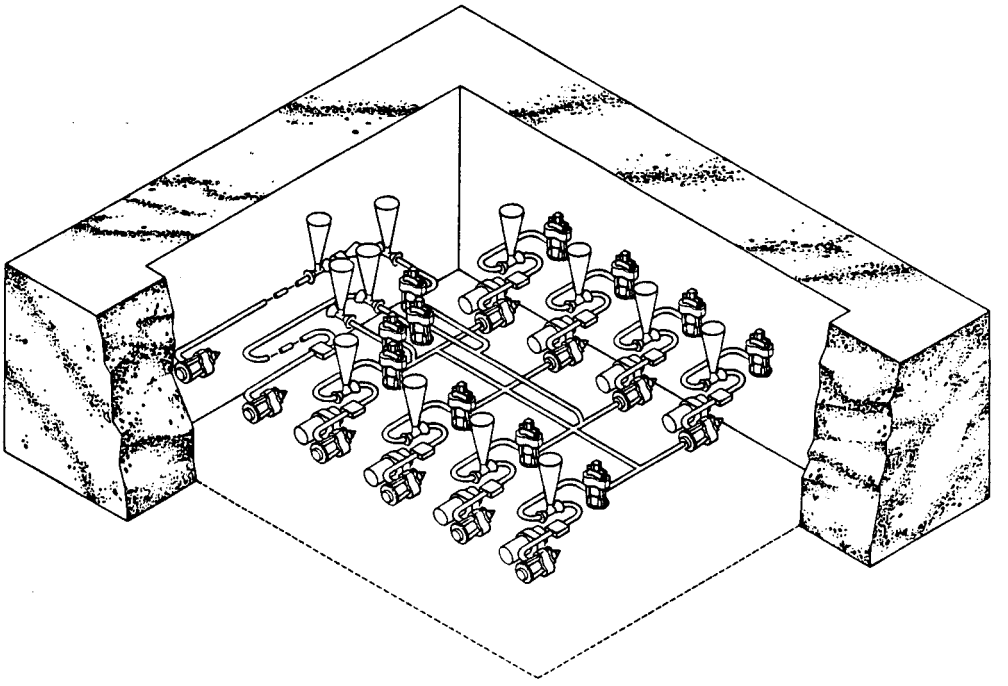

FIGURE 3.4. 8Q-5 Diversion Pit

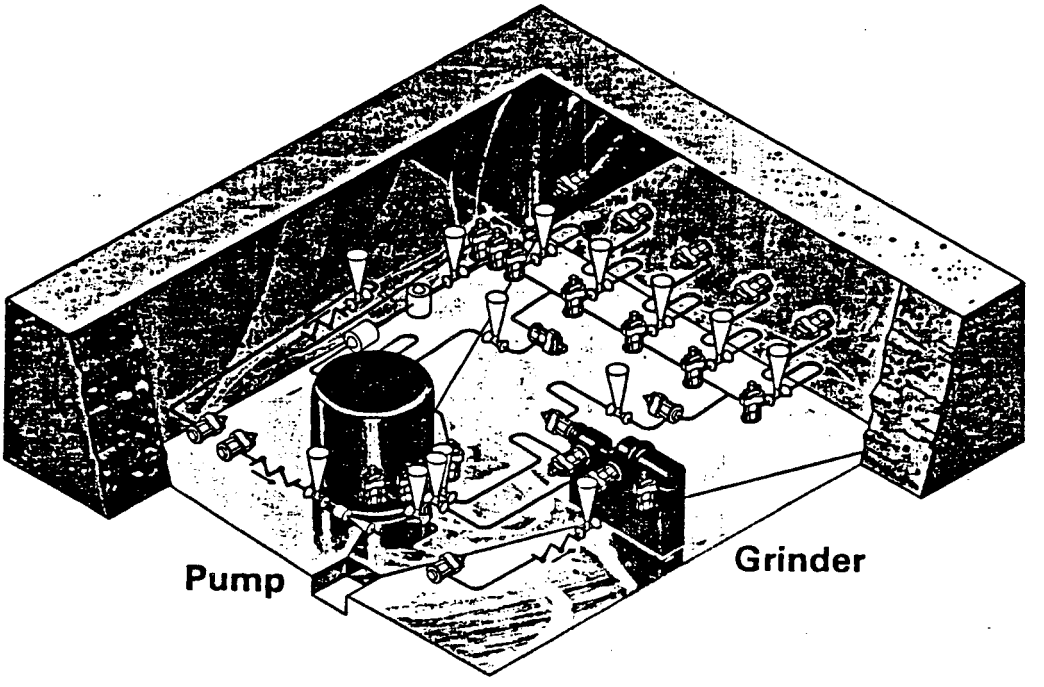


FIGURE 3.5. 8Q-2 Pump Pit

containment trench, and the system utilities are provided. The pits are adequately radiation-shielded to allow for manual valve manipulations and are self-contained and provide for remote maintenance. Services are provided in each pit for line-flushing and washdown and drainage of the pit.

The environment of the pits requires that all equipment be serviced or replaced by remote means. All process and electrical connections are made with remotely coupled "jumpers." These jumpers are connected through piping embedded in the pits' concrete walls. Included in these jumpers are all the instrument and electrical signals required to operate and monitor the transfer system.

The jumper pits are identified as follows:

| Location | Function | Identification Number |
|---|---|---|
| Tank 8D-4 | THOREX removal | 8Q-4 |
| Tank 8D-1 | Zeolite removal | 8Q-1 |
| Tank 8D-2 | PUREX sludge removal | 8Q-2 |
| Tank Farm | Waste diversion | 8Q-5 |

The valving of the pits allows for alternative routing configurations as follows:

- Tank 8D-4 to CFMT V-001
- Tank 8D-4 to tank 8D-2
- Tank 8D-1 to CFMT V-001
- Tank 8D-1 to tank 8D-2
- Tank 8D-2 to CFMT V-001
- Vitrification facility waste header to tank 8D-4
- CFMT V-001 to tank 8D-2
- CFMT V-001 to tank 8D-4
- Vitrification facility vessel vent condenser to tank 8D-3.

The following service utilities are currently provided from the tank farm for use in each pit:

| | |
|---|---|
| Utility air | 90 psig<br>50 cfm |
| Instrument air | 35 psig at the pit wall |
| Process water | supplied by a high-pressure (150 psig) pump from a break tank. |
| Electrical | 480 V, 3-phase |
| Steam | 150 psig<br>500 lb/hr (max) |

A utility manifold of water, steam, and air is permanently piped to the pits. This utility manifold is connected to the HLW transfer piping to allow for the use of each utility separately or together to flush the lines after a waste transfer. Pit washdown is implemented by an external portable spray nozzle that can be inserted through a plug in the pit cover. The nozzle provides a spray pattern that washes down the walls, ceiling and floor of the pit. The floor slopes to a sump or drain for drainage, and washdown solutions are directed back to the respective tank. Diversion pit 8Q-5 washdown solutions are jetted to tank 8D-2 through the basic waste return line. Water for the pit spray nozzles is supplied from an external above-ground header.

All valve operations are manual; handles extend through plugs in the pit covers. Interlocks are provided between some diversion valves to prevent unwanted diversions. Valve funnels are provided for each manual valve so that handles can be installed through the pipe covers.

Instrumentation in each pit, used to monitor the transfer system, is designed for remote removal and replacement. There are no automatic controls; instrument signals, however, will be used to shut down the transfer pumps in case of high-level reading in the V-001 CFMT, pump-bearing failure, loss of tank ventilation, or high vibrations. The design of the instrumentation takes into account that each instrument must be recalibrated yearly.

Pit ventilation is required for preventing the escape of radioactive material. Pump pits 8Q-1, 8Q-2 and 8Q-4 will ventilate into their respective

tanks when covered. Diversion pit 8Q-5 will ventilate to the new supernate treatment system ventilation system. Air flow sweeps across the pits; it comes from outside through a HEPA filter into the valve compartment and leaves the pit through a pipe in the removal pump riser.

To prevent the escape of radioactive material from the pit in case the pit overpressurizes, the pit covers are sealed by gasketing and a HEPA filter on the air intake.

All piping inside the pits and in the pit walls conforms to ANSI B31.3, Category M. All piping contacting the HLW is of 304L stainless steel with full-penetration weld joints where possible. Screwed connections are used for instrumentation. All HLW piping within the pits is single-walled; the pit with its liner provides the required secondary containment. Once out of the pit, i.e., pit wall, the secondary containment is provided by the double-wall waste-transfer piping. Valves in the pits are installed in pipe jumpers for remote replacement.

Each pit has an underliner leak-detection system to identify a leaking liner. Provisions are made for monitoring the primary waste-transfer lines for leaks. Since the low point of discharge lines is at the pit walls, leak-detection equipment and a method to drain the secondary pipe are included in the design.

The major design effort on the diversion pit (8Q-5) and the pump pits (8Q-1, 8Q-2, 8Q-4) was completed during FY 1987. The final drawings will be delivered to WVNS in early FY 1988.

### 3.3.4 Remote Jumpers and Components

#### 3.3.4.1 HEPA Filter System for the Heating, Ventilation and Air-Conditioning

Three banks of high-efficiency particulate air (HEPA) filters containing three 24 x 24 x 12 in. filters are used as the primary exhaust filters for the CTS vitrification cell. The filter housings are designed to use standard nuclear grade super-flow HEPA filters. The housings are located next to the south wall (Figure 3.1) of the CTS cell and are connected to three ducts protruding from the cell wall. Each housing has provisions for remote in-cell

delta operating pressure testing of the filter-to-mounting frame seals as well as $\Delta P$ measurement from the inlet to outlet of the housing. The housings with their filters are designed for an air flow of 3500 cfm.

The housings are constructed of stainless steel and have a remotely removable cover over the filters to protect them from accidental damage by falling objects. The cover and filters are installed and removed by means of the process crane and impact wrench.

The design proposed by PNL is a vendor's information drawing from which final detailed fabrication drawings can be produced. It contains all the key remote features necessary for canyon remote operations. A window on the west wall, between column lines 3/Z and 5, provides direct viewing of the filters for maintenance.

#### 3.3.4.2 SFCM Remote Startup Heaters

The slurry-fed ceramic melter (SFCM) requires that the solidified borosilicate glass be liquefied before the power is turned on to the melter electrodes. Five startup heaters will be individually and remotely inserted into the melter plenum area to heat the glass surface and plenum area before power is restored to the melter electrodes.

The startup heaters are designed to provide about 22 kW each at 127 Vac. The elements of each heater are constructed of Kanthal AF metallic rods with high-temperature ceramic insulators spaced along the length (Figure 3.6). On the end of each heater is a low-temperature meltable ceramic that protects the elements during remote insertion.

The mounting flange, the electrical PUREX connector mounting bracket, and the lifting bail are fabricated of 304L stainless steel. The isolation material is a dielectric with high resistance to current leakage and able to withstand high temperatures (1300°C) without dielectric breakdown. The electrodes, insulating materials, and wiring can withstand a radiation field of about 5000 rad/hr.

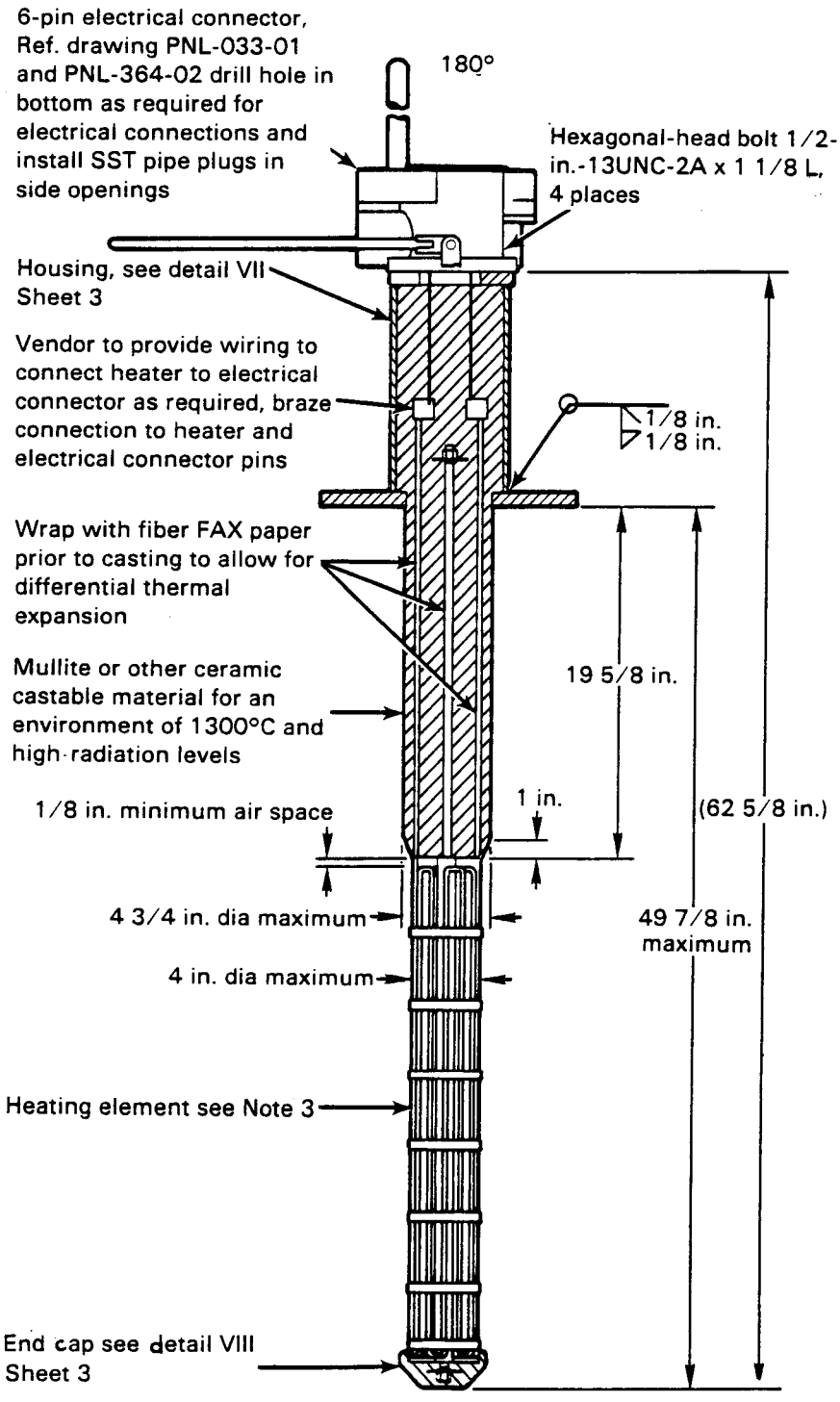


FIGURE 3.6. Heating Element for Slurry-Fed Ceramic Melter Showing High-Temperature Ceramic Insulators

The startup heaters are designed to pass through a 6-in.-dia port in the melter top a distance of 19-1/2 in. before entering the plenum. The heating elements will extend a maximum of 30 in. into the plenum. Mechanical stability is maintained by the insulators for remote handling of each heater.

The heater assemblies are inserted into SFCM ports A, D, E, BB, and FF. Since each port differs in orientation and flange size, only the startup heater designed for the corresponding flange can be inserted into a particular port. Each heater is serviced via electrical jumpers from connectors on the north and east walls near the melter.

All five heater assemblies are designed to be installed and removed remotely by using the process crane and impact wrench. Since they are considered disposable items, no maintenance is required.

### 3.3.5 Miscellaneous Remote Equipment

#### 3.3.5.1 Slurry-Sampling System

The slurry-sampling system (Figure 3.7) is located on the north wall at the window near the V-011 MFMT and consists of a remotely removable work tray, two samplers, and appropriate piping and valving. The system has a source of demineralized flush water, a waste header drain connection, and associated jumpers. A small decontamination station is provided for keeping the fingers on the manipulators clean and performing gross decontamination on the sample vial. A transfer tube permits transfer of the sample vial from the process cell to a transfer cell.

The sampler is a modified Hydragard PL-1 series liquid sampler manufactured by Hinds International, Inc. The CFMT (V-001) will receive high-level liquid waste from several sources. It receives cesium-loaded zeolite slurry from tank 8D-2 and thorium waste from tank 8D-4. Predetermined amounts of the waste solutions are transferred to the concentrator to provide a satisfactory melter feed composition. Nitric acid is added to adjust the pH and to convert the feed to a nitrate form. The slurry is sampled to determine what and how much glass-forming chemicals are required to achieve the proper

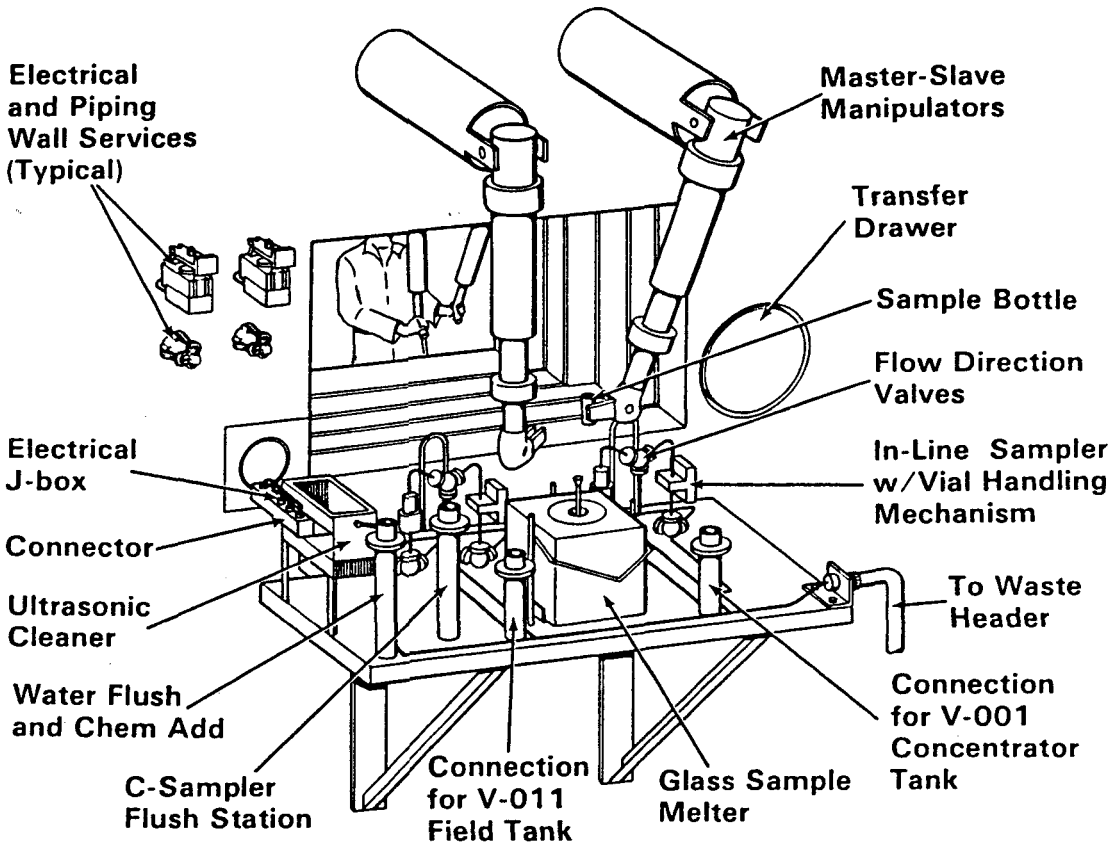


FIGURE 3.7. Slurry Sample Station

chemical and rheological characteristics of the slurry to produce acceptable borosilicate glass in the melter. The slurry is then transferred to the V-011 MFMT.

The slurry in the V-011 MFMT is sampled before sending it to the melter to ensure that the composition has not changed. There are provisions for adding cold chemicals and glass formers to tank V-011, if necessary. To sample the slurry from tanks V-001 and V-011, it is pumped to the sample station via modified ADS pumps and circulated back to the tanks.

The sampling system on the north wall consists of a remotely removable work tray with two samplers, attached to imbeds in the wall. Two separate samplers are provided, one for each tank, with interconnecting valving to permit sampling of both tanks through either station.

A bagged sample vial is placed in the sampler position and raised into position, where the concentric needle of the sampler penetrates the double-septum top.

The sampler valve is mechanically opened by master-slave manipulators. Slurry then flows through the sample vial back to the tank being sampled. After a predetermined number of volume changes have flowed through the sample vial, the sampler valve is closed. The sample vial is removed from the fixture, and the bagging is removed. The vial is then swiped and, if needed, sprayed with a decontamination solution or demineralized water to remove any gross contamination. The sample vial is sent to the transfer cell via a gravity transfer pipe through the wall. In the transfer cell the sample vial is placed in the pneumatic transfer rabbit and sent to the laboratory.

The sampler is then flushed out using a source of demineralized water and a separate sample vial. A three-way ball valve in the supply line to the sampler can be set to connect the sampler to demineralized water. A ball valve in the return line to the tank being sampled is set so that it provides a discharge to the waste header. The flushing would be terminated after four complete system volume changes. A new bagged sample vial is brought into the cell, placed in the sampler position, and raised into position, where the concentric needle of the sampler penetrates the double-septum top. The station is now ready to take the next sample.

The sampling system with its work tray and two sampler positions can be remotely attached to imbeds located in the north wall at the window overlooking the V-011 MFMT. The work tray will carry the dead weight of the two samplers, sample-vial positioning devices, ultrasonic decontamination station and associated jumpers. The work tray also can withstand the dynamic load from a dropped impact wrench.

The valves and actuators associated with the sampling system will be operated remotely with manipulators. No other instrumentation and controls are required for the sampling system.

In situ maintenance of the sampling system is not required. The system provides redundancy in that both tanks can be sampled from either sampler. The whole sampling system can also be replaced if necessary. If individual

components require replacement, however, the system is designed so that the Hydragard sampler, flow-direction ball valves, and piping can be replaced remotely.

3.3.5.2 Ex-Cell to In-Cell Transfer Port

A small pass-through port is provided adjacent to the sampling system for bringing in new sample vials, swipe cloths and various other supplies required for the sampling system. The port has a commercially available transfer drawer that extends into the operating corridor to load supplies on the tray for transfer into the CTS cell. The transfer drawer is then pushed into the cell, and the items are removed for use.

The transfer drawer consists of two stainless steel shielding blocks, 11.825 in. in diameter by 14 in. in length, on rollers with a 20-in. tray mounted between them. The rollers provide support and guide the drawer in the wall penetration of the cell. A handle is attached to the ex-cell shield block to facilitate moving the drawer into the cell. This transfer drawer is commercially made by Central Research Laboratories division of Sargent Industries.

To transfer materials into the cell, the handle is attached and the drawer is pulled into the operating gallery far enough to expose the tray. Materials are placed on the tray, and the drawer is pushed into the cell using the handle until the tray is visible. After the material is removed, the drawer is pulled back into the wall to the point where both shielding blocks are in the wall.

3.3.5.3 Canister Decontamination and Swipe Station

During FY 1987, PNL provided the conceptual design of a canister decontamination and swipe station. This station provides for decontaminating canisters that have been filled with borosilicate glass. During filling, the exterior of the canister will be exposed to volatile fission products, principally $^{137}Cs$, which are expected to condense on the canister exterior. The smearable contamination created by the $^{137}Cs$ is unacceptable since it presents a source of secondary contamination to the interior storage area, as well as the shipping/burial containers.

An oxidation/reaction system Ce(IV)/Ce(III) in a dilute nitric acid carrier solution has been selected as the decontamination process for the WVNS facility.

The station is conceived as able to remove sufficient material from the exterior of the canister to reduce smearable contamination below the level of 220 dpm alpha/100 $cm^2$ and 2200 dpm beta + gamma/100 $cm^2$. Present PNL experimental work indicates this can be accomplished by removal of 0.5 to 5.0 $\mu m$ of material from the surface.

The decontamination and swipe station (Figure 3.8) is envisioned as a single module suitable for removal and replacement using only the vitrification cell bridge cranes, impact wrench, and the transfer cart system. No hands-on operations will be required. All surfaces that may contact Ce(IV) solution will be made of titanium.

After cleansing, the canister will be moved into another part of the module for obtaining swipes of the surface to check for smearable contamination.

Based on this conceptual design, a design drawing will be prepared in FY 1988 from which to develop fabrication drawings.

3.3.5.4 Canister-Capping and Maintenance Station

The function of the canister-capping and maintenance station is to provide filled canisters with a sealed cap before decontamination. Another function of this station is any preparatory work required on the sealing surface of the canister to achieve compatibility with the temporary cap.

The station depicted in Figure 3.9 also includes a small maintenance work table for maintaining small components, replacing light bulbs for cell lighting, replacing gaskets on jumpers, and performing other as yet undefined tasks.

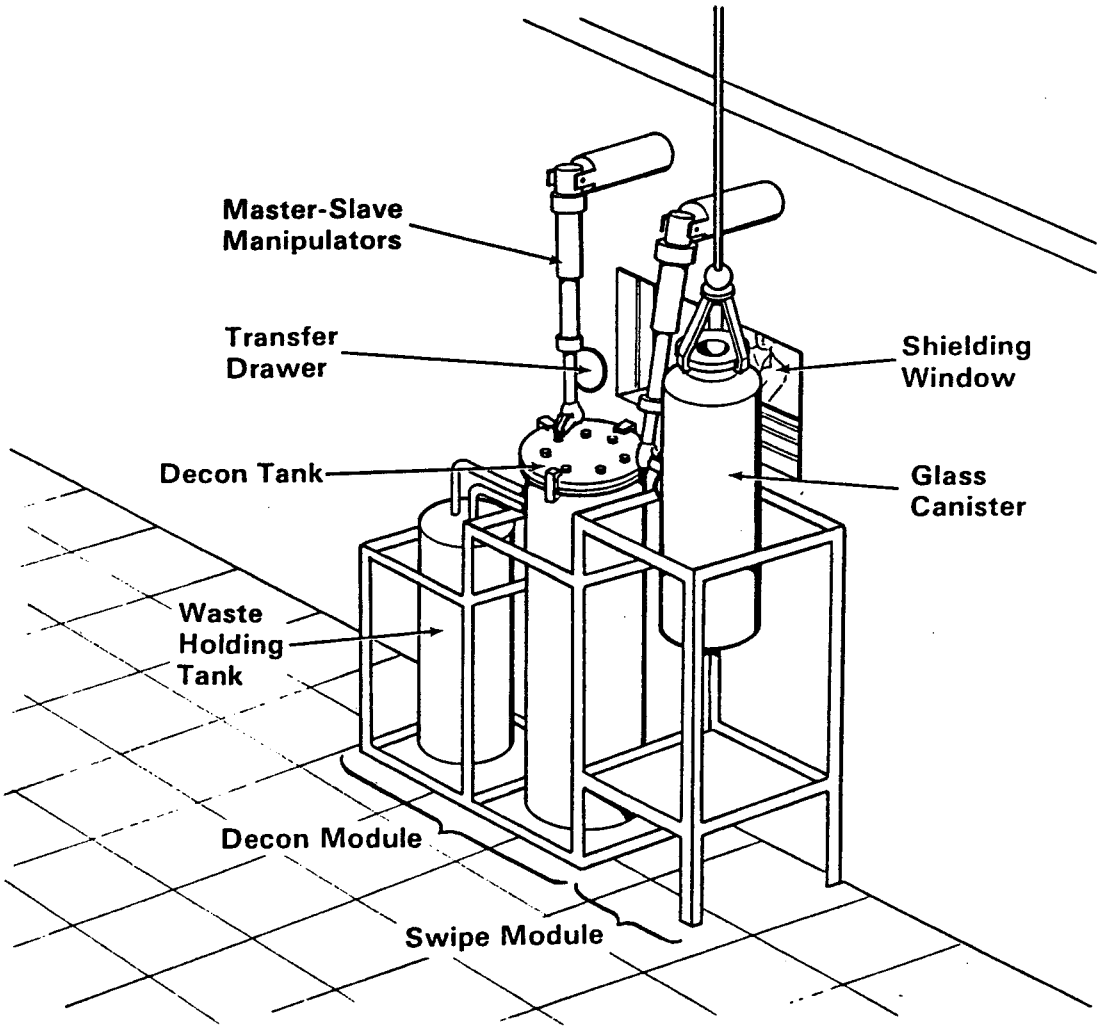


FIGURE 3.8. Decontamination and Swipe Station

The capping station will perform the following functions to prepare a canister for transfer to the chemical process cell:

- Receive a filled canister transferred from the vitrification cooling rack by the cell crane.
- Support the canister without the aid of the crane while it is in the station.
- Inspect the sealing surfaces of the canister.

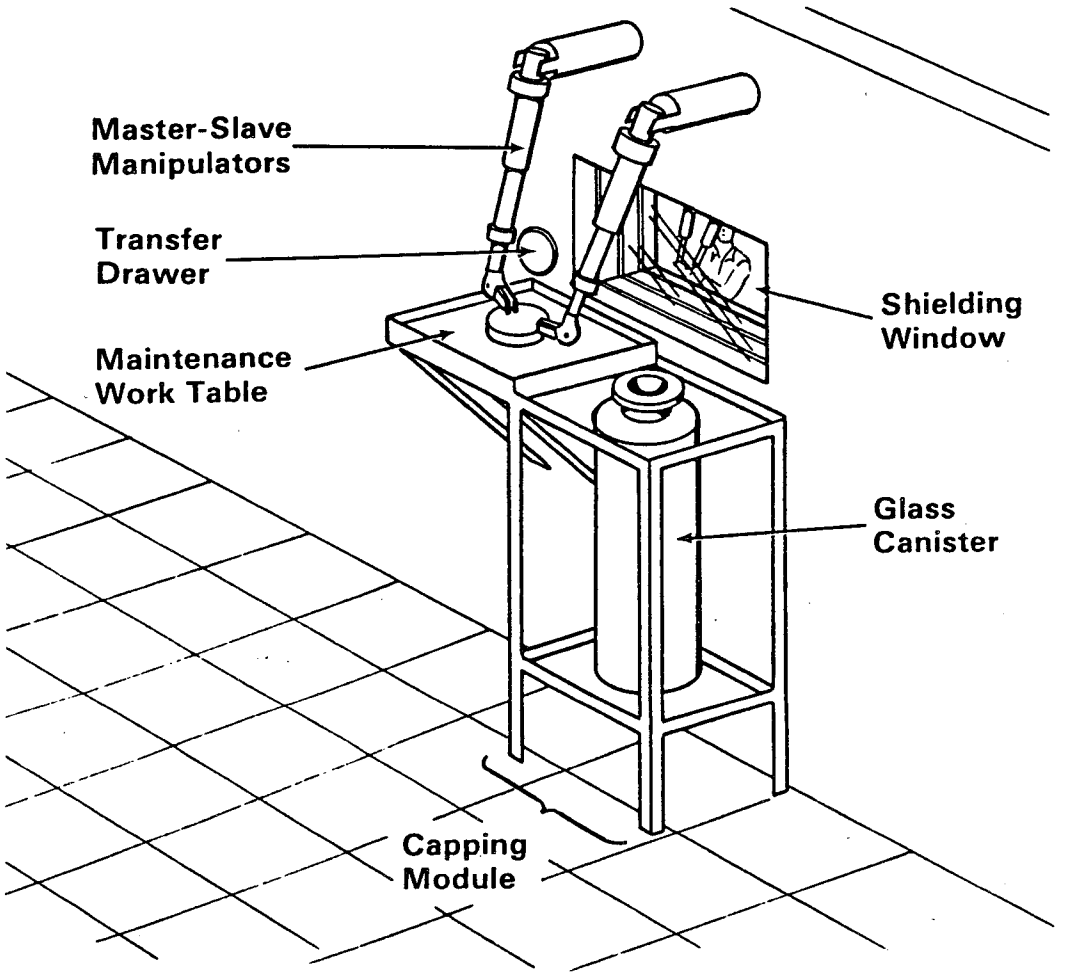


FIGURE 3.9. Maintenance Work and Capping Station

- Clean the sealing surfaces of the canister if needed to accept the cap.
- Apply the canister temporary cap in preparation for transfer to the chemical process cell.
- Keep the sealed canister positioned compatibly with the grapple.

Normal operation of the canister-capping and maintenance station will not require hands-on operation. Master-slave manipulators are available for replacing items such as gaskets or for adjusting any operating equipment.

The capping station will be designed as a self-contained module suitable for removal and replacement using only the vitrification cell bridge cranes,

impact wrench, and the transfer cart system. No hands-on maintenance will be required. (This includes connection/disconnection of mounting provisions.)

Since the method for final sealing of the West Valley canister has not yet been determined, a temporary cap will be placed on the canister for storage in the chemical process cell. This cap is envisioned as only a dust cover to prevent materials from entering the canister during storage and handling. It will be remotely installed and removed at the capping station.

### 3.3.6 Infrared Television Melter Viewing System

A design for an infrared-television melter viewing system has been completed, and the system is currently being fabricated for use in the West Valley melter. It will be used to monitor cold-cap size to aid in melter operations. The system comprises a jumper assembly (drawing #PNL-261, sheets 1-10) and wall plug assembly (drawing #PNL-262, sheets 1-6). As soon as fabricated, the system will be functionally tested and shipped to West Valley for installation.

The jumper will be inserted into melter nozzle B and will interface with the wall plug which is positioned on the north cell wall. A three-element objective lens, located above the melt surface at the bottom of the jumper assembly vertical leg, forms the first of three images of the melt surface. Light from the first image is transmitted by a series of three mirrors to a two-element relay lens located in the horizontal leg of the jumper, thus forming a second image. Light from the second image is collected by two lenses in the wall plug and transmitted by two mirrors to the face of an attached video camera, where the final image is formed.

During October, changes to the design drawings were initiated to incorporate WVNS and PNL design review comments. The wall-plug shielding was analyzed for gamma radiation attenuation, and the optics design calculations were verified.

In November the design of the jumper was modified to optimize the flow of cooling air to the lower optical components. WVNS was requested to relax the minimum lens temperature requirements listed in the viewing system design criteria. These changes were based on the results of system cooling

calculations for the optical components. After incorporation of all changes into the drawings, a design completion report was prepared, the drawing sets were approved, and requests for fabrication proposals were issued for each assembly.

In December the design of a mock-up test stand for remote installation and functional testing of the system began. During design of the test stand, it was learned that the facility architectural engineering drawings showed a service gallery floor located at an elevation that interfered with access to wall-plug penetration. WVNS was advised of this interference, and PNL was instructed to modify the jumper design to account for locating the affected penetration higher.

During January, revisions to the optics calculations and drawings were completed. A technical review of all fabrication offers was conducted, and contracts for fabrication of each assembly were awarded to one local contractor. At that time, based on changes to the jumper drawing, the contractor was requested to prepare a revised cost quote, which was accepted.

The latest issues of the jumper and wall plug assembly drawings were transmitted to West Valley during February.

In May, WVNS directed PNL to procure extra lenses and mirrors because of their long lead times to procure. The intent is to avoid delays in delivery should an optical element become damaged during installation. A cost quote was solicited from the contractor, and additional components were ordered.

In June, PNL was informed by the fabrication contractor that the factory supplying the mirrors had burned down and could not supply these items for at least 6 months. Additionally, the fabricator requested that PNL redesign the lenses, as practical, to match the geometries of the optical machine shop's existing templates. The optics calculations were revised, and a design field change was issued respecifying mirrors. This changed 12 of 14 lens geometries to utilize existing templates. PNL also delivered, to the contractor, a 2-in. three-way horizontal connector and a block of Inconel-690 alloy, to be used for jumper fabrication.

One design field change was issued against each drawing in August. The design field changes were issued based on fabricator recommendations to make construction easier and to correct design errors.

To speed up qualification of the contractors' welder and weld procedures for Inconel-690, PNL supplied Inconel-82 weld filler material and Inconel-690 pipe with certifications. PNL also delivered a 1/8-in. sheet of Inconel-690 plate for use in jumper construction.

## 3.4 PROCESS SUPPORT - J. H. Westsik, Jr., L. A. Bray, W. O. Heath, R. W. Goles, D. W. Faletti, P. W. Reimus, and F. A. Graf, Jr.

The Process Support Subtask comprises those activities associated with the equipment performance and process operations in the waste treatment system. The activities address issues related to the process chemistry, waste mobilization, feed system, melter, off-gas treatment, and instrumentation and process control. Some of the work completed under this subtask directly benefits work performed under the Remote Technology and Waste Form Qualification subtasks.

### 3.4.1 Process Chemistry Studies

PNL has completed several studies to resolve technical issues related to process chemistry. A process was developed that uses the Ce(IV) ion to decontaminate waste glass canisters. Process streams from the waste tanks to the melter feed tank were simulated and characterized in terms of their chemical and rheological properties. Methods were developed for removing excess sulfate from the melter feed and for determining the concentration of metal fines in the sludge wastes. In addition, PNL completed a literature review to identify methods for removing mercury from the vitrification flowsheet and evaluated methods for dissolution of solids in the submerged-bed scrubber.

#### 3.4.1.1 Ce(IV) Canister Decontamination Process

A simple, effective method has been developed for decontaminating HLW canisters. The process employs a reduction/oxidation system {Ce(III)/Ce(IV)} in a nitric acid ($HNO_3$) solution to chemically mill a thin layer from the canister surface. Contaminated canisters are simply immersed for several

hours in the solution at a controlled temperature and Ce(IV) ion concentration. The decontaminated canister is then removed and the spent solution is discarded to the HLW and is ultimately processed into the waste glass. The Ce(IV)/$HNO_3$ solution has been shown to be effective in chemically milling the surface of stainless steel. The process is similar to electropolishing but does not require an applied electric current. This method of chemical decontamination is applicable to a wide variety of contaminated equipment used in the nuclear industry (Bray and Thomas 1987).

WVNS evaluated several methods of canister decontamination, including electropolishing, liquid abrasive blasting, high-pressure water washing, and ultrasonic cleaning, before selecting the Ce(IV)/$HNO_3$ redox process. The initial concept for this decontamination process involved continuous electrochemical regeneration of the ceric {Ce(IV)} ion and would have required extensive in-cell pumping, heat transfer, and electrochemical equipment. As a result of laboratory testing, PNL has simplified the process in the following ways:

- A single-use, throwaway solution is needed.
- An electrochemical cell is not required for producing Ce(IV) for the decontamination facility; Ce(IV) solutions can be easily procured from offsite vendors.
- Contact times of 3 to 6 hr at temperatures greater than 45°C will adequately decontaminate the canisters to below Waste Acceptance Preliminary Specifications (U.S. DOE 1987).
- Approximately 0.06 to 0.13 moles of Ce(IV) will remove a ~1.5-$\mu$m to 3-$\mu$m layer of stainless steel from ~1 $ft^2$ of surface, providing adequate decontamination.
- The stainless steel dissolution rate increases by a factor of 2.5 for every 10°C increase in temperature.

The optimum Ce(IV) concentration in $HNO_3$ was determined for the decontamination of the West Valley stainless steel canisters. Stainless steel removal rates were determined as a function of the initial Ce(IV) concentration [0.0025 to 0.1M Ce(IV)], the temperature (25°C to 78°C), and the time of

contact (1 to 12 hr). The removal rates were determined by weight loss. The stainless steel surface-area-to-solution-volume was maintained at ~53 $ft^2$ (West Valley canister surface area) to 175 gal of decontamination solution. The loss in weight increased with increasing temperature, time, and initial Ce(IV) concentration (see Figure 3.10). The weight loss approaches the value expected from the theoretical Ce(IV)/Fe mole ratio of 3 with increasing contact time. This is based on the following reaction:

$$3\ Ce^{4+} + Fe^{0} \rightarrow 3\ Ce^{3+} + Fe^{3+}$$

Tests were also conducted using contaminated coupons. Stainless steel coupons were installed on the outside of canisters being filled with radioactive glass, within a turntable similar to that to be used by West Valley. The coupons were later analyzed to determine the extent and characteristics of canister contamination that occurred during filling. Some of the contaminated coupons were then used to demonstrate the Ce(IV) decontamination method developed for use at West Valley. Various decontamination schemes were applied, and the coupons were then reanalyzed to determine the decontamination factors (DFs) that resulted from the various methods.

The coupons were analyzed for their initial gamma activity. The activity for the twelve coupons varied from $10^7$ to $10^{10}$ disintegrations per minute per 100 $cm^2$ of surface. Each specimen was then soaked in deionized water at 25°C for 1 min, air-dried, weighed, and recounted. This was followed by a 2-min wash using a minimum volume of 0.5M $HNO_3$ for 2 min at 50°C. DFs for the initial water soak ranged from 3 to 57. The average DF for the minimum treatment of water and nitric acid was 160. When four minimum-treatment coupons were washed twice with a large volume of 0.5M $HNO_3$ for 6 hr at 65°C, the average DF was 8 for the first wash and <2 for the second wash. The average overall DF was ~3140. When four minimum-treatment coupons were washed twice with 0.007M Ce(IV)/100 $cm^2$ of surface, the DF for the coupons averaged ~30 for the first wash and 12 for the second wash. The average overall DF varied from 32,500 to 450,000. When two minimum-treatment coupons were contacted once with 0.014M of Ce(IV)/100 $cm^2$, the average DF was 416, with an average overall DF of ~40,000.

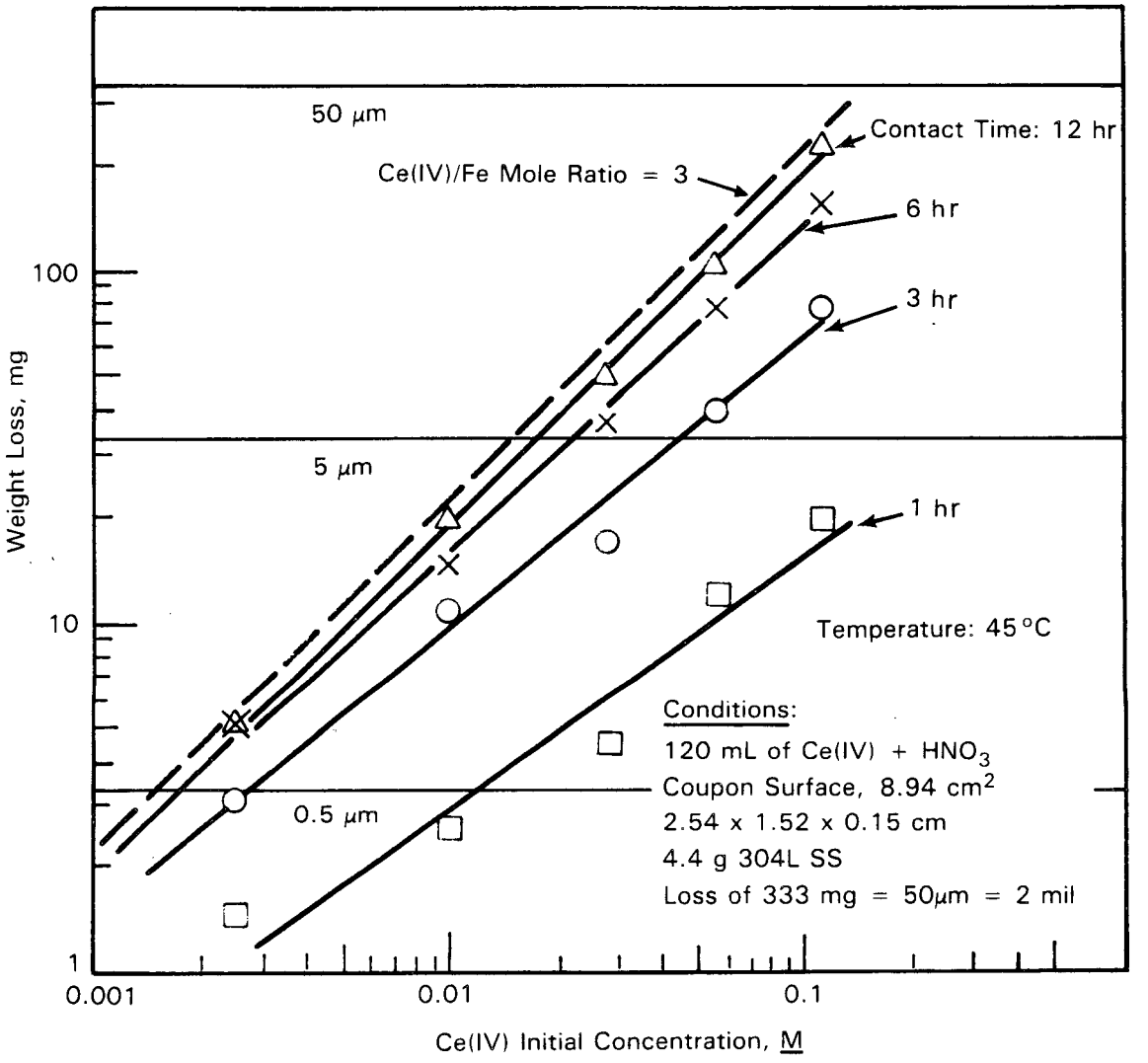


FIGURE 3.10. Effect of Cerium Concentration on the Dissolution of Stainless Steel at 45°C

After the coupons were decontaminated, they were smeared to determine compliance with Waste Acceptance Preliminary Specifications. The results show that minimum treatment and two cycles of 0.5M $HNO_3$ will not meet these specifications. When four coupons were treated with 0.007M Ce(IV)/100 $cm^2$ to remove ~1.5 μm of surface, one coupon met the specifications. When they were treated twice with 0.007M Ce(IV) to remove a total of ~3 μm of surface, all coupons met the specifications. When two coupons were treated once with 0.014M Ce(IV) to remove ~3 μm of surface, both exceeded the specifications.

Milling the stainless steel surface of the canister with Ce(IV) is required to remove the contamination to a nonsmearable level; the use of $HNO_3$ alone will not meet the Waste Acceptance Preliminary Specifications (U.S. DOE 1987).

A scanning electron microscope was used to determine the extent of corrosion and etching of the stainless steel coupons as a function of Ce(IV) dissolution of the surface layer. The photomicrographs show that intergranular attack is not extensive, with a Ce(IV) milling of penetration <6 $\mu$m. Preliminary examination suggests that as much grain and intergranular changes takes place on the surface of the stainless steel during vitrification heating as during the Ce(IV) removal of a 1.5- to 3-$\mu$m layer of oxide film. Complete analysis will require metallurgical cross-sections in order to determine depth and form of attack.

3.4.1.2 Characterization of Process Streams

Prior to vitrification at WVNS, the neutralized PUREX wastes in tank 8D-2, the acid THOREX wastes in tank 8D-4, and the cesium-loaded zeolite from the supernatant treatment system will be treated, combined, and further treated to adjust the slurry pH. A slurry of glass formers will then be added to the wastes, and the blend will be fed to the glass melter. These treatment and processing steps were simulated on a laboratory scale to characterize the chemical and rheological properties of the process solutions at each step. The initial work has been reported (Burkholder and Brouns 1987).

THOREX Waste Dissolution. WVNS analytical data on the composition of tank 8D-4 THOREX acid waste indicated that not all the thorium could be accounted for in the tank liquid. A PNL study showed that large quantities of thorium, iron, and nickel nitrate crystals probably formed in the tank (Burkholder and Brouns 1987). To redissolve the solids, about 4000 gal of condensate water were added to the 9000 gal of THOREX waste. Although the tank could be heated, no mechanical agitation was available; so laboratory simulation was conducted to determine how long it takes to redissolve the solids given these constraints. In the test, 277 mL of water were poured onto 623 mL of THOREX waste containing an unknown volume of crystallized thorium nitrate. The specific gravity of the supernate and crystalline

slurry was measured over time, as shown in Figure 3.11. About 40 days were required to achieve adequate mixing and dissolve the thorium crystals.

Glass-Former Slurry Preparation. Preparation of the glass-former slurry was examined to determine the appropriate order for adding the glass formers and to determine the highest glass-former slurry loading that will provide acceptable rheological properties.

The order-of-addition study indicated that lithium carbonate should be added to a starting mixture of $HNO_3$ and water to avoid severe foaming. (Foam is formed by $CO_2$ that is liberated during the exothermic reaction between lithium carbonate and the nitric acid.) When several glass formers are added

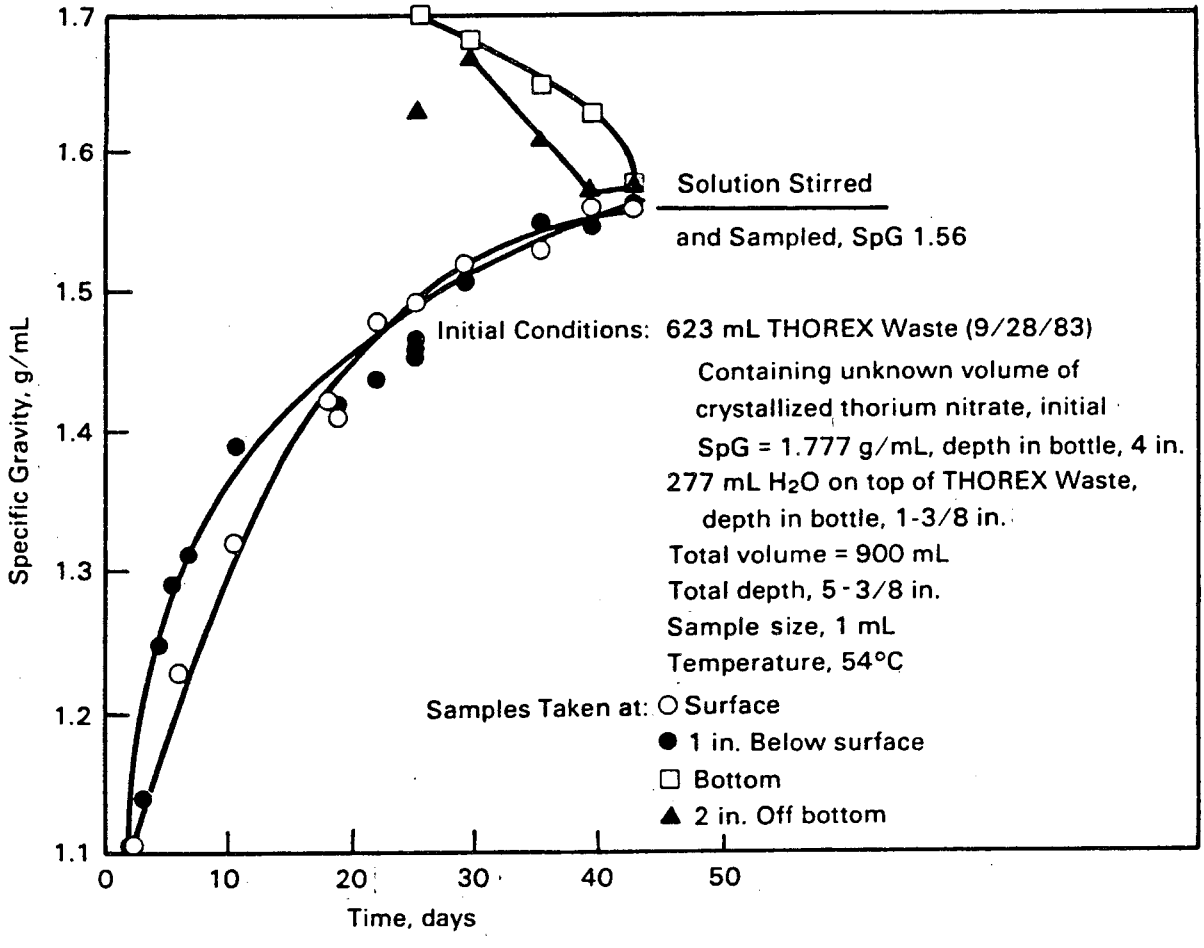


FIGURE 3.11. Specific Gravity in a Simulated THOREX and Water Mixture with Time

with the lithium carbonate, the addition of $HNO_3$ results in a stable foam, which impedes mixing and feed transport. However, this state can be avoided by completing the lithium carbonate metathesis before adding the other glass formers. Sugar should be added last to minimize the possibility of its digestion by residual $HNO_3$ or nitrate derivatives.

The glass-former slurries with 45 to 65 wt% solids were pseudoplastic in the shear range of interest, having yield stresses below 150 dyne/cm$^2$ and specific gravities ranging from 1.40 to 1.69. A 70 wt% slurry formed a solid-like sediment too thick to be tested with the viscometer. Based on these data, 60 to 65 wt% slurries represent the highest advisable range of solids loading that would be easily pumpable, nonclogging, and forming relatively loose gels (4000 dyne/cm$^2$ at 24 hr).

Waste Processing into Melter Feed. Before the neutralized PUREX, acidic THOREX, and cesium-loaded zeolite wastes can be vitrified, four major operations must be performed. First, the PUREX sludge will be washed with water to remove excess sodium sulfate, which adversely affects waste processing. Second, to avoid complication of processing three separate high-level liquid waste (HLLW) streams, the three wastes will be combined and blended in tank 8D-2. Third, the sludge/THOREX/zeolite combined waste will be transferred to a concentrator where excess water will be removed and $HNO_3$ will be added to adjust the waste to a pH of 4. Finally, the nitrate waste will be blended with glass formers. These operations were investigated on a laboratory scale. Synthetic solutions and sludges that closely approximate the known chemical composition of the wastes were prepared and used for the investigations.

Laboratory-scale sludge washing was conducted in a manner similar to that planned for the actual PUREX sludge in tank 8D-2. After four water washes, 97.5% of the sodium and 99% of the sulfates were removed from the sludge, indicating that the sludge-washing method should be effective. Rheological analyses were performed on four samples of the final washed sludge with varying water content. This was done to determine how much water should be decanted from tank 8D-2 (following the fourth wash cycle) to ensure acceptable flow properties in the remaining washed sludge. The most

concentrated sample tested (24 wt% solids) was determined to have acceptable flow and resuspension properties. The most dilute sample (10 wt% solids) was determined unacceptable because its yield stress was too low to maintain large particles (e.g., crushed zeolite) in suspension.

Synthetic versions of THOREX and zeolite/$Cs^+$ wastes were added to the variously concentrated washed sludge samples, and the resultant combined wastes were submitted to rheological analysis. Adding THOREX waste with a neutralizing amount of sodium hydroxide thickened the washed sludge, and adding this waste to the 24 wt% washed sludge resulted in an unacceptably thick mixture. However, subsequent addition of slurried zeolite thinned the combined waste to an acceptable rheology. The final combined tank contents (starting with the 24 wt% sludge) formed a yield-pseudoplastic material that should exhibit good pipe flow, with minimal clogging. The tank-mixing behavior of this slurry is difficult to assess due to the complexity of the mixing phenomena coupled with the slurry's non-Newtonian nature. However, should poor mixing be observed or suspected, the test data indicate that adding small amounts of water will greatly lower the slurry viscosity, yield stress, etc., improving mixing behavior. Based on these findings, the final washed sludge should be decanted to 24 wt% solids and the subsequent waste additions should be conducted as planned.

After the wastes are combined and mixed in tank 8D-2, the resultant waste stream will be transferred in batches to the vitrification facility. The stream will then be acidified to pH 4, concentrated, blended with a glass-former slurry, and fed to the melter. These steps were also investigated in this study.

The effect of acidification was a reduction in yield stress and other rheological properties of the combined waste. This effect is generally observed with most oxide slurries such as waste, glass-former and melter feed slurries. No unusual or noteworthy observations were made during boiling studies. Waste concentration as planned does not appear problematic. A 60 wt% solids glass-former blend was added to variously concentrated, acidified combined waste samples. Further acidification was required to lower the resultant melter feed to pH 4. Rheological data indicate that the melter

feed should be maintained at 40 wt% solids or higher to ensure adequate flow properties and maximum homogeneity. Further testing of the rheology versus concentration of the final melter feed is recommended to establish an acceptable operating range. It would also be prudent to test various rheological additives that have been found to reduce/eliminate line-clogging during radioactive melter runs at PNL, even though the West Valley feed studied here does not appear prone to clogging.

3.4.1.3 Sulfate Removal from Melter Feed

A study was completed to identify chemical and processing methods for removing excess sulfate from the melter feed. The only viable option is to add excess water to the melter feed and then remove a portion of the supernate containing soluble salts. This solution will contain the major fraction of the sulfate in the feed. However, while technically viable, this method is not practical routinely and should be used only as a last resort. Thorough washing of the tank 8D-2 sludge prior to feed makeup is clearly necessary.

3.4.1.4 Analytical Procedure for Metal Fines

An analytical procedure has been developed for determining the concentration of metal fines in the waste slurry in tank 8D-2. The metal fines were produced during the chop leach and solvent extraction processes at West Valley. It is estimated that there are 91 kg of zirconium metal (zircaloy) and 600 to 2000 kg of stainless steel in the waste. Their impact on vitrification is not known.

The analytical procedure requires dissolution of aliquots of the sludge in 4M $HNO_3$, 4M HCl, or 4M HCl + 2.8M HF. Following digestion for 1 hr at 90°C, the resulting solutions are chemically analyzed. When the waste is dissolved in HCl, the difference in the concentrations of iron, chromium, and nickel in solution compared to their concentrations when the waste is dissolved in $HNO_3$ provides the detection for stainless steel fines. Stainless steel can be detected to ~0.5 wt% of the initial dry waste. When the waste is dissolved in HCl/HF, the difference in the aqueous concentration for zirconium and tin as compared to their concentrations in the $HNO_3$ solution

provides the detection for zircaloy fines. Zircaloy can be detected at ~0.05 wt% of the initial dry weight of the waste.

3.4.1.5 Dissolution of Solids in the Submerged-Bed Scrubber

A chemical method was developed to remove deposits from the WVNS submerged-bed scrubber (SBS). Approximately 38 wt% of the SBS solids were soluble in water; no additional solids dissolved when $HNO_3$ was added. All the silica was found in the residue. Greater than 92 wt% of the solids were dissolved using a fused salt dissolution technique. However, the method would require that the SBS be heated to >300°C in order to melt the $KOH/KNO_3$ flux. After this heating, the resulting salt would be dissolved in water to flush out the SBS.

3.4.2 Waste Mobilization Studies

Shear vane tests were conducted in tank 8D-2 to measure the shear strength of the raw sludge layer on the bottom of the tank. Shear strength is a measure of the cohesiveness of the sludge; the higher the shear strength, the more difficult the sludge will be to mobilize and retrieve. The peak values of shear vane torque, $T_{max}$, and the shear strength, $\gamma_s$, as measured at several depths are shown in Table 3.2. These in-tank shear vane measurements can be used to estimate the effectiveness of the planned sludge mobilization equipment.

The shear strength and viscosity of several mixtures of kaolin clay, silica, water, and sodium chloride were measured in support of WVNS efforts to develop a sludge simulant for use in their scale model of tank 8D-2. A mixture of 120 g clay, 4 g NaCl, 80 g water, and 140 mL Ludox™ is recommended as a reference. The shear strength of the mixture is shown in Table 3.3 and its viscosity, when first prepared, is shown in Figure 3.12. The viscosity data are relatively linear, indicating pseudoplastic (shear thinning) behavior.

3.4.3 Evaluation of Off-Gas Treatment

A real-time method of monitoring $NO_x$ concentrations to track the average oxidation state of glasses produced in a liquid-fed ceramic melter was evaluated during a melter test at West Valley. No correlation was observed between the average oxidation states of $NO_x$ effluents and the glass product.

TABLE 3.2. Results of In-Tank Shear Vane Tests

| Depth from Tank Floor, in. | $T_{max}$, in.-$lb_f$ | $\tau_s$, $lb_f/ft^2$ | $\tau_s$, $dyne/cm^2$ |
|---|---|---|---|
| 21 | 5.0 | 13 | 6,344 |
| 14 | 17.5 | 45 | 21,960 |
| 11.5 | 100 | 260 | 126,880 |

TABLE 3.3. Shear Strength of Recommended Sludge Simulant

| Average $\gamma_s$,[a] $dyne/cm^2$ | Elapsed Time After Preparation, hr |
|---|---|
| 94,000 | 24 |
| 130,000 | 48 |
| 84,000[b] | 24 |

(a) Average of shear strength measurements taken at 2 to 3 depths within samples.
(b) Sample stirred for ~45 min before allowing to gel. This sample had the greatest uniformity with respect to shear strength versus depth.

Since a previously observed correlation could not be reproduced, the oxidation state of $NO_x$ may depend strongly upon more than one processing variable. These variables need to be identified and their effects established before $NO_x$ composition can be used as a process control tool.

PNL also completed an assessment of the adequacy of the WVNS off-gas treatment system for controlling the release of aerosols and gaseous effluents and provided a critical review of WVNS off-gas sampling techniques.

### 3.4.4 RECIPE Code Development

The RECIPE computer code was developed to calculate the quantity of glass-forming chemicals to add to a batch of waste in the concentrator feed makeup tank (CFMT) to produce a final glass product of acceptable composition (Faletti et al. 1988). The WVNS operating plan is to make glass such that the concentration of each component lies within some small target region. Because the composition of the wastes is expected to vary somewhat from batch

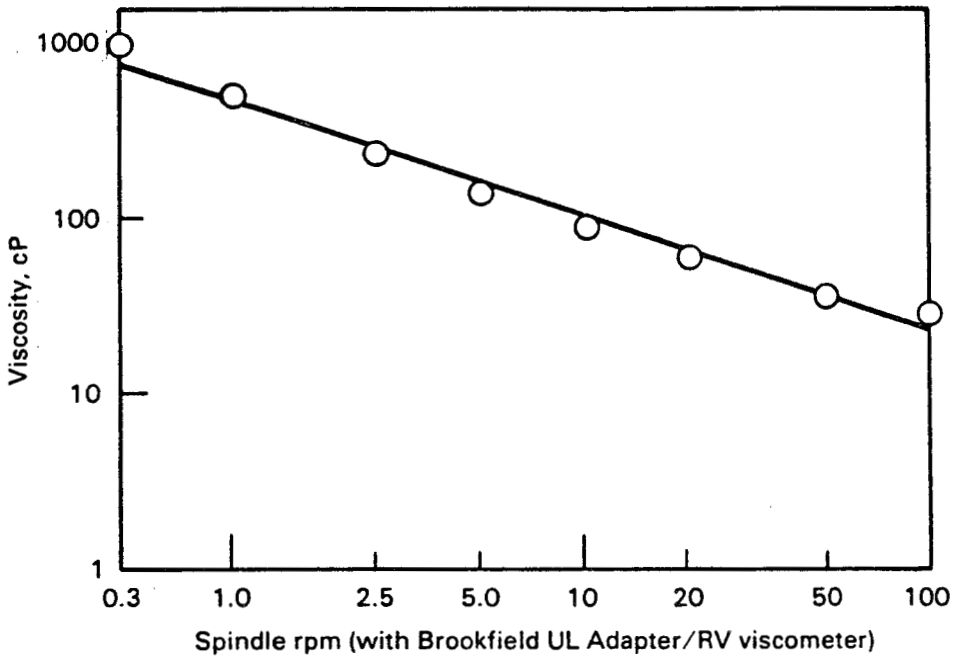


FIGURE 3.12. Viscosity of Freshly Prepared Sludge Simulant

to batch in the CFMT, the quantity of each additive must also vary so that the final glass composition is within the target range. Given the chemical composition of the wastes in the CFMT, the RECIPE code calculates the quantity of chemical additions required to make an acceptable feed for the melter.

RECIPE is written in FORTRAN and uses Linpack software to solve the system of linear equations used to describe the formulation process. The code is designed to run interactively with the operator. Input to the code consists of files containing the chemical composition of the waste in the tank to be adjusted and of the additives and the target composition. Output is the weight of each component to add to the waste so that the slurry will yield the desired glass composition. Table 3.4 shows a simple example for a three-component glass (RECIPE can work with up to 100 components). In addition to the wastes, sources for $B_2O_3$, $Na_2O$, and $SiO_2$ are available to make the final feed slurry. While not shown in this example, each source could consist of as many as five different additives (i.e., NaOH, $Na_2CO_3$). Note, however, that no sodium is

TABLE 3.4. Example of Input and Output to RECIPE Code

| Input | | Concentration in Source, wt%(a) | | | |
|---|---|---|---|---|---|
| Oxide | Concentration in Waste, wt%(a) | $B_2O_3$ Source | $Na_2O$ Source | $SiO_2$ Source | Target Glass Composition, wt% |
| $B_2O_3$ | 0.05 | 71.6 | 4.10 | 0.53 | 20 |
| $Na_2O$ | 6.0 | 0.51 | 71.7 | 1.0 | 12 |
| $SiO_2$ | 5.0 | 0.68 | 3.4 | 72.7 | 68 |

| Output | |
|---|---|
| Oxide | Mass of Source To Add |
| $B_2O_3$ | 37.0 |
| $Na_2O$ | 0.0 |
| $SiO_2$ | 110.0 |

(a) Weight percents will not sum to 100 because of water and decomposition products such as $NO_x$ and $CO_2$.

added in this example; the waste is itself a source for some of the glass components, and RECIPE takes this into account so as to maximize waste loading in the final glass product.

### 3.4.5 MASBAL Code Development

The MASBAL computer program was developed as a tool to aid the waste-form qualification activities for the West Valley Demonstration Project (WVDP). MASBAL has three overall objectives: 1) to predict the composition of nuclear waste glass produced in a slurry-fed ceramic melter based on a knowledge of process conditions, 2) to generate simulated data that can be used to estimate the uncertainty in the predicted glass composition as a function of process uncertainties, and 3) to generate simulated data that can be used to provide a measure of the inherent variability in the glass composition as a function of the inherent variability in the feed composition (Reimus 1987). These three capabilities are important to nuclear waste glass producers because

there are constraints on the range of compositions that can be processed in a ceramic melter and on the range of compositions that will be acceptable for disposal in a geologic repository.

MASBAL was developed specifically to simulate operation of the West Valley component test stand. The program is flexible enough, however, to simulate any slurry-fed ceramic melter system.

MASBAL simulates the flow of material through the system's melter feed tank and the melter. The program can track as many as 100 oxide constituents through the system. Material enters the system by way of the feed tank (slurry transfer from the makeup tank) and leaves the system either by exiting the off-gas system or entering a canister. MASBAL can simulate the addition of glass-forming compounds directly to either the feed tank or the melter. (These actions may be taken if the feed or glass composition deviates significantly from the target composition.) The off-gas system is modeled as a sink for components that have finite melter decontamination factors. The primary outputs of MASBAL are the glass composition exiting the melter as a function of time and the average composition of the glass in each glass pour.

Because the mixing behavior of the West Valley melter is currently unknown, MASBAL provides several options for modeling flow of material through the melter. The melter can be modeled as 1) a single ideally mixed tank, 2) two to five ideally mixed regions in series, or 3) a plug flow region followed by one or two ideally mixed regions in series. The best modeling approach will be decided by the best fit to experimental data. The relative volumes of each region are adjustable for use in calibration/validation activities.

MASBAL operates in three modes. The first mode provides deterministic predictions of the glass composition exiting the melter as a function of time. The key inputs to the program when it is operated in this mode are the values of process measurements (e.g., flow rates) taken at appropriate times during operation of the system (i.e., actual process data).

The second mode generates simulated glass composition data that can be used to estimate the uncertainty in the deterministic predictions provided by the first mode. The process data required as inputs for the first mode are

required also for the second mode. The parameters of statistical distributions that define uncertainties in the process measurements are required also as inputs for the second mode. Each process measurement is treated as the mean or mode of a statistical distribution that is assumed to contain the true value of the variable being measured. Measurement errors are simulated by randomly sampling these distributions; the values returned from the distributions are used in subsequent mass balance calculations as the true values of the measured variables. MASBAL can be run repeatedly in this mode to generate glass composition data that are distributed randomly about the deterministic predictions of mode 1. The absolute differences between the data generated in mode 2 and the predictions of mode 1 provide a measure of the uncertainty in the deterministic predictions.

When MASBAL is run in the third mode, the program generates its own feed composition data by randomly selecting the composition of successive batches of feed from statistical distributions defined by the user. (The concentration of each feed constituent will be taken from a distribution that has a mean or mode of the target concentration.) All process measurements are simulated by randomly sampling statistical distributions that have mean or mode equal to the simulated values of the process variables being measured. The simulated fluctuations in the feed composition and the errors in process measurements cause the calculated glass composition to fluctuate randomly about the target composition. If the process measurements are treated deterministically (i.e., if the standard deviations describing the measurement errors are set to zero), then the absolute differences between the stochastically generated data and the target glass composition will provide a measure of the glass composition's inherent variability as a function of the feed composition's variability. If, however, the composition of successive batches of feed is treated deterministically, then the differences between the stochastically generated composition data and the target glass composition will provide the same information as is provided by MASBAL in mode 2. In mode 3 the program can be run without supplying process data; all that is required are the parameters of distributions that describe feed composition variability and uncertainties in process measurements. This feature gives MASBAL the capability to simulate thousands of hours of operation of the melter

system, thus permitting the collection of enough simulated data to make reasonable estimates of the confidence limits associated with either the predicted or the target glass composition.

MASBAL consists of PNL-developed FORTRAN subroutines that are integrated with the SIMAN simulation language. SIMAN offers 1) a differential equation-solving algorithm for solving the mass balance differential equations that describe the time-dependent concentrations in the system, 2) the capability to model discrete events that interact with or change the values of state variables in the system (e.g., the starting or stopping of the flow of feed to the melter), and 3) the capability to randomly sample statistical distributions. The random sampling of statistical distributions is an essential feature of MASBAL when it is operated in modes 2 or 3.

A user's manual has been prepared for the MASBAL code (Reimus 1987). Validation of the code will require characterizing the mixing behavior of the WVNS melter and estimating the uncertainties of the process measurements that are modeled in the MASBAL code.

### 3.4.6 Failure Modes and Effects Analysis

A failure modes and effects analysis (FMEA) is a systematic, logical process for identifying equipment failure modes for a plant, system, subsystem, or component. It inductively determines the effects of such failures on the desired operational characteristics of the system being analyzed. For example, a desired characteristic of a typical process system is its ability to maintain production. The FMEA includes descriptions of 1) the failure modes and causes of those failures, 2) possible effects of the failures, 3) the probability of the failure, 4) the severity of the failure, and 5) possible corrective actions. The most useful outputs of an FMEA are the assessment of the system's design adequacy to perform its intended function and an increased understanding about the physical and functional interrelationships of its many parts. The FMEA assists the designer in evaluating the inherent strengths and hidden flaws in the design and identifying those potential design improvements that will improve reliability, minimize maintenance requirements, and maximize operational effectiveness.

For the FMEA used in the WVDP, primary emphasis was placed on 1) evaluating the system's ability to continue the vitrification process when components fail and 2) recommending methods to minimize the impacts of these failures from the perspective of system integrity and operational performance. Major equipment components evaluated included the CFMT, the melter feed tank (MFT), the melter, the turntable, and the off-gas treatment system. The components of the off-gas treatment system that were evaluated included the SBS, the off-gas dryer, dual trains of high-efficiency mist eliminators (HEMEs), preheaters, HEPA filters, and a single trench heater. Auxiliary equipment, including instrumentation, pumps, jets, agitators, valves, and services, was also analyzed.

Each system component was carefully examined to determine the consequences of a failure in that component, particularly as related to glass production and/or system integrity. All legitimate modes in which that component could fail were also identified, and for each failure mode the mechanism(s) that could cause such a failure mode were defined. The effects of these failures, at both the subsystem level and at the plant level, were identified. Method(s) were also identified for detecting that a failure had occurred, the action to be taken to recover from the failure (i.e., repair, replace, use redundant path, etc.), and semiquantitative estimates of failure frequency and repair times. In many cases, special consideration had to be given to qualifying conditions such as the impact of multiple simultaneous failures, assumptions, and recommendations.

For the FMEA used in the WVDP, about 115 separate items in the system were examined for their unique failure modes in order to determine their impact on system performance and integrity. About 200 separate failure modes were attributed to these items and, when multiple failure mechanisms that caused specific failure modes were considered, about 300 entries were included in the FMEA.

Nineteen of these items were identified as having a high failure frequency or a medium failure frequency with a high or medium repair time. An additional 30 items were identified whose failures could be mitigated or eliminated by design modifications or by incorporation of additional monitoring

instrumentation. The plant's reliability could be improved by all or a combination of the following: performing periodic preventive maintenance or testing on the item, improving the design of the item itself or of ancillary equipment, or instituting clearly defined operating procedures/philosophy documentation to mitigate the effects of the failed item.

Based on the information generated in this FMEA, the following conclusions regarding the performance characteristics of the WVDP are presented:

- There are no equipment items in the WVNS vitrification system that have both a high failure rate (>2/yr) and high repair time (>1 wk). Nineteen items were identified with a high failure rate or with a medium failure rate (>0.5/yr) and a high or medium (<1 wk) repair time. Thirty additional items were identified whose failures could be mitigated or eliminated by design modifications or additional monitoring.
- The availability analysis indicates that the operating availability of the vitrification system will be near 80% as a result of equipment failures. This analysis is based on the 19 items having a high failure frequency or a medium failure frequency, with medium or long repair times, and uses semiquantitative estimates for the failure frequencies and repair times. Therefore the analysis should not be considered rigorous.
- The largest contributors to system unavailability are the overflow section heaters, which represent about 36% of the unavailability. The second largest contributors are the glass/plenum thermowells, which represent about 14% of the unavailability.

This FMEA was limited in scope to the vitrification system proper within the component test stand at WVNS. Thus some failures and effects that could affect production were not addressed. In particular, the loss of cranes, manipulators, and other handling and transportation equipment should be evaluated. The loss of services (power, instrument air, steam, water, etc.) was examined for each piece of equipment. The system-wide effects of the loss of services should be addressed.

## 3.5 PRODUCT QUALIFICATION SUPPORT - G. B. Mellinger, M. A. Reimus, W. M. Gerry, and M. J. Schweiger

The Product Qualification Subtask provides support for West Valley's waste-form qualification efforts. Testing is being conducted to determine waste-form chemical durability. The effects of composition, ferrous/ferric ratio (redox state), heat treatment, and groundwater were investigated during FY 1987. Impact testing of West Valley HLW canisters was also conducted during the year.

### 3.5.1 Chemical Durability Testing

#### 3.5.1.1 Experimental Methods

The glasses used in this work were prepared primarily with carbonate and oxide sources. Each batch was melted at a temperature at which the glass viscosity was ~100 poise. When oxidation state control was required, a small amount of graphite was added to the batch during the melting process.

Composition. Two sets of glasses with compositional variations were fabricated and leach-tested. The first set of glasses, designated DG-WV1[(a)] through DG-WV8, were based on variations of a glass designated WVCM-47.[(b)] The composition of WVCM-47 is given in Table 3.5. The specific variations of WVCM-47 that were tested are listed below, and their compositions are given in Table 3.6. This table shows both the compositions that were intended to be produced ("target" composition) and those that were actually produced (as "analyzed" compositions).

---

(a) DG: doped glass.
(b) WVCM: West Valley ceramic melter.

TABLE 3.5. Compositions of West Valley Reference Glasses

| Oxides | Weight Percent WVCM-47 | WVCM-50 |
|---|---|---|
| $Al_2O_3$ | 8.05 | 9.86 |
| $B_2O_3$ | 12.08 | 12.27 |
| BaO | 0.05 | 0.19 |
| CaO | 0.60 | 0.82 |
| $CeO_2$ | 0.07 | 0.72 |
| $Cr_2O_3$ | 0.20 | 0.14 |
| $Cs_2O$ | 0.08 | 0.07 |
| CuO | 0.00 | 0.04 |
| $Fe_2O_3$ | 12.20 | 11.93 |
| $K_2O$ | 1.29 | 1.61 |
| $La_2O_3$ | 0.03 | 0.04 |
| $Li_2O$ | 2.03 | 2.22 |
| MgO | 1.33 | 0.79 |
| $MnO_2$ | 1.31 | 1.21 |
| $MoO_3$ | 0.01 | 0.04 |
| $Na_2O$ | 9.27 | 9.79 |
| $Nd_2O_3$ | 0.12 | 0.14 |
| NiO | 0.28 | 0.31 |
| $P_2O_5$ | 2.52 | 2.47 |
| $Pr_6O_{11}$ | 0.03 | 0.04 |
| $SiO_2$ | 42.59 | 39.60 |
| $Sm_2O_3$ | 0.03 | 0.02 |
| $SO_3$ | 0.30 | 0.23 |
| SrO | 0.03 | 0.02 |
| $ThO_2$ | 3.61 | 3.52 |
| $TiO_2$ | 0.99 | 0.84 |
| $UO_2$ | 0.56 | 0.61 |
| $Y_2O_3$ | 0.02 | 0.02 |
| $ZnO_2$ | 0.00 | 0.03 |
| $ZrO_2$ | 0.29 | 0.40 |
| Total | 99.97 | 99.99 |

TABLE 3.6. Compositions of First Set of Compositional Variability Glasses, wt%

| Oxide | DG-WV1 | | DG-WV2 | | DG-WV3 | | DG-WV4 | | DG-WV5 | | DG-WV6 | | DG-WV7 | | DG-WV8 | |
|---|---|---|---|---|---|---|---|---|---|---|---|---|---|---|---|---|
| | Target | Analyzed | Target | Analyzed | Target | Analyzed | Target | Analyzed | Target | Analyzed | Target | Analyzed | Target | Analyzed | Target | Analyzed |
| $Al_2O_3$ | 8.05 | 8.74 | 8.04 | 8.61 | 6.50 | 7.16 | 7.79 | 8.38 | 6.00 | 6.90 | 7.97 | 8.55 | 7.90 | 8.84 | 8.49 | 9.01 |
| $B_2O_3$ | 12.08 | 12.15 | 12.07 | 12.17 | 9.25 | 9.33 | 11.69 | 11.77 | 12.35 | 12.41 | 11.96 | 12.15 | 11.86 | 12.15 | 7.30 | 7.51 |
| BaO | 0.05 | 0.05 | 0.05 | 0.05 | 0.05 | 0.07 | 0.05 | 0.05 | 0.05 | 0.05 | 0.05 | 0.05 | 0.05 | 0.05 | 0.05 | 0.05 |
| CaO | 0.60 | 0.68 | 0.60 | 0.83 | 0.56 | 0.63 | 0.58 | 0.68 | 0.61 | 0.68 | 0.59 | 0.69 | 0.59 | 0.65 | 0.63 | 0.67 |
| $CeO_2$ | 0.07 | 0.07 | 0.07 | 0.07 | 0.07 | 0.10 | 0.07 | 0.07 | 0.07 | 0.09 | 0.07 | 0.05 | 0.07 | 0.07 | 0.07 | 0.10 |
| $Cr_2O_3$ | 0.20 | 0.19 | 0.20 | 0.20 | 0.29 | 0.29 | 0.19 | 0.20 | 0.20 | 0.21 | 0.20 | 0.19 | 0.20 | 0.20 | 0.21 | 0.19 |
| $Cs_2O$ | 0.08 | 0.05 | 0.08 | 0.05 | 0.07 | 0.08 | 0.08 | 0.05 | 0.08 | 0.05 | 0.08 | 0.05 | 0.08 | 0.04 | 0.08 | 0.14 |
| $Fe_2O_3$ | 12.20 | 11.74 | 12.19 | 11.72 | 11.30 | 10.81 | 11.81 | 11.06 | 12.41 | 11.91 | 12.08 | 11.55 | 11.98 | 11.55 | 12.87 | 12.29 |
| $K_2O$ | 1.29 | 1.16 | 1.29 | 0.91 | 3.33 | 1.92 | 1.25 | 1.71 | 1.32 | 1.50 | 1.28 | 0.70 | 1.27 | 1.27 | 1.36 | 1.71 |
| $La_2O_3$ | 0.03 | 0.04 | 0.03 | 0.04 | 0.03 | 0.05 | 0.03 | 0.04 | 0.03 | 0.04 | 0.03 | 0.04 | 0.03 | 0.04 | 0.03 | 0.03 |
| $Li_2O$ | 2.03 | 1.74 | 2.03 | 1.76 | 2.82 | 2.34 | 1.97 | 1.71 | 2.08 | 1.76 | 2.01 | 1.71 | 1.99 | 1.71 | 2.14 | 1.84 |
| MgO | 1.33 | 1.32 | 1.33 | 1.30 | 1.21 | 1.70 | 1.29 | 1.29 | 1.36 | 1.35 | 1.32 | 1.29 | 1.31 | 1.28 | 1.40 | 1.39 |
| $MnO_2$ | 1.31 | 1.30 | 1.31 | 1.32 | 1.22 | 1.76 | 1.27 | 1.30 | 1.34 | 1.36 | 1.30 | 1.30 | 1.29 | 1.29 | 1.38 | 1.37 |
| $MoO_3$ | 0.01 | 0.01 | 0.01 | 0.01 | 0.00 | 0.00 | 0.01 | 0.01 | 0.01 | 0.01 | 0.01 | 0.01 | 0.01 | 0.01 | 0.01 | 0.01 |
| $Na_2O$ | 9.27 | 9.13 | 9.26 | 9.04 | 10.16 | 9.82 | 12.20 | 11.47 | 9.48 | 9.10 | 9.18 | 9.13 | 9.10 | 8.88 | 9.78 | 9.38 |
| $Nd_2O_3$ | 0.12 | 0.12 | 0.12 | 0.11 | 0.17 | 0.16 | 0.12 | 0.14 | 0.12 | 0.12 | 0.12 | 0.11 | 0.12 | 0.09 | 0.13 | 0.13 |
| NiO | 0.28 | 0.31 | 0.28 | 0.27 | 0.32 | 0.36 | 0.27 | 0.27 | 0.29 | 0.30 | 0.28 | 0.28 | 0.28 | 0.28 | 0.30 | 0.30 |
| $P_2O_5$ | 2.52 | 2.58 | 2.52 | 2.60 | 2.33 | 2.41 | 2.44 | 2.54 | 2.58 | 2.63 | 3.50 | 3.56 | 2.48 | 2.51 | 2.66 | 2.68 |
| $PdO_2$ | 0.00 | 0.00 | 0.01 | 0.01 | 0.01 | 0.01 | 0.00 | 0.00 | 0.00 | 0.00 | 0.00 | 0.00 | 0.00 | 0.00 | 0.00 | 0.00 |
| $Pr_6O_{11}$ | 0.03 | 0.03 | 0.03 | 0.03 | 0.00 | 0.00 | 0.03 | 0.03 | 0.03 | 0.03 | 0.03 | 0.03 | 0.03 | 0.03 | 0.03 | 0.03 |
| $RhO_2$ | 0.00 | 0.00 | 0.01 | 0.01 | 0.01 | 0.01 | 0.00 | 0.00 | 0.00 | 0.00 | 0.00 | 0.00 | 0.00 | 0.00 | 0.00 | 0.00 |
| $RuO_2$ | 0.00 | 0.00 | 0.08 | 0.08 | 0.07 | 0.07 | 0.00 | 0.00 | 0.00 | 0.00 | 0.00 | 0.00 | 0.00 | 0.00 | 0.00 | 0.00 |
| $SiO_2$ | 42.59 | 43.25 | 42.55 | 43.60 | 44.87 | 45.46 | 41.22 | 41.94 | 43.54 | 44.43 | 42.16 | 43.42 | 41.80 | 43.03 | 44.91 | 45.83 |
| $Sm_2O_3$ | 0.03 | 0.03 | 0.03 | 0.03 | 0.00 | 0.00 | 0.03 | 0.03 | 0.03 | 0.03 | 0.03 | 0.03 | 0.03 | 0.03 | 0.03 | 0.03 |
| $SO_3$ | 0.30 | 0.30 | 0.30 | 0.30 | 0.27 | 0.27 | 0.29 | 0.29 | 0.31 | 0.31 | 0.30 | 0.30 | 0.29 | 0.29 | 0.32 | 0.32 |
| SrO | 0.03 | 0.03 | 0.03 | 0.03 | 0.03 | 0.04 | 0.03 | 0.03 | 0.03 | 0.03 | 0.03 | 0.03 | 0.03 | 0.03 | 0.03 | 0.03 |
| $ThO_2$ | 3.61 | 2.86 | 3.61 | 2.80 | 3.34 | 2.73 | 3.50 | 2.94 | 3.69 | 3.11 | 3.58 | 2.75 | 5.40 | 3.83 | 3.81 | 2.75 |
| $TiO_2$ | 0.99 | 0.96 | 0.99 | 0.96 | 0.91 | 1.22 | 0.96 | 0.90 | 1.01 | 0.97 | 0.98 | 0.93 | 0.97 | 0.96 | 1.05 | 1.01 |
| $UO_2$ | 0.58 | 0.54 | 0.58 | 0.53 | 0.52 | 0.54 | 0.54 | 0.54 | 0.57 | 0.00 | 0.56 | 0.53 | 0.55 | 0.46 | 0.59 | 0.58 |
| $Y_2O_3$ | 0.02 | 0.02 | 0.02 | 0.02 | 0.02 | 0.03 | 0.02 | 0.02 | 0.02 | 0.02 | 0.02 | 0.02 | 0.02 | 0.02 | 0.02 | 0.02 |
| $ZrO_2$ | 0.29 | 0.59 | 0.29 | 0.56 | 0.27 | 0.64 | 0.28 | 0.54 | 0.30 | 0.60 | 0.29 | 0.56 | 0.28 | 0.62 | 0.31 | 0.57 |
| Total | 99.97 | 100 | 99.99 | 100 | 100 | 100 | 100.01 | 100 | 99.91 | 100 | 100.01 | 100 | 100.01 | 100 | 99.99 | 100 |

| Glass | Description |
|---|---|
| DG-WV1 | WVCM-47 |
| DG-WV2 | WVCM-47 with Ru, Rh, Pd oxides |
| DG-WV3 | ATM-10 (West Valley reference glass) |
| DG-WV4 | WVCM-47 with higher $Na_2O$ (12.20 vs 9.27) |
| DG-WV5 | WVCM-47 with lower $Al_2O_3$ (6.00 vs 8.05) |
| DG-WV6 | WVCM-47 with higher $P_2O_5$ (3.50 vs 2.52) |
| DG-WV7 | WVCM-47 with higher $ThO_2$ (5.40 vs 3.61) |
| DG-WV8 | WVCM-47 with lower $B_2O_3$ (7.30 vs 12.08) |

The second set consisted of 16 glasses, designated DG-WV15 through DG-WV30, based on variations of a glass designated WVCM-50. The composition of WVCM-50 is also given in Table 3.5. One of the test glasses of this set was WVCM-50. The other 15 compositions were chosen from among the vertices of a polyhedronal composition variation region centered around WVCM-50. These 15 compositions were chosen by using computer-aided experimental design techniques which provided optimum information for fitting linear mixture models within an explicitly defined compositional variation region. This compositional variation region is shown in Table 3.7. The specific compositions of the 16 glasses used to characterize this region are shown in Table 3.8.

Glass Redox. Four redox-adjusted glasses, DG-WV11R through DG-WV14R, were fabricated for this study. The target composition of the glass varies slightly from the WVCM-50 composition, with about 1 wt% less $B_2O_3$ and 1 wt% more $K_2O$. The redox state of the glass, as measured by the $Fe^{2+}/Fe^{3+}$ ratio, was varied over a range of 0.07 to 0.42.

Heat Treatment. The purpose of heat-treating was to determine the effects of simulated canister cooling and specified isothermal heat treatments on the chemical durability of WVCM-50 glass. Fifteen samples were treated isothermally. No volatility losses from the specimen glasses or other composition changes due to the heat treatments were observed.

Six samples of the glass were heat-treated using simulated canister cooling rates. These cooling rates were obtained from two instrumented test canisters (TC) produced by West Valley (TC-18 and TC-23). To produce each

TABLE 3.7. Definition of Compositional Variation Region (based on WVCM-50), wt%

| Single-Component Constraints | | |
|---|---|---|
| 9.0 ≤ | $Al_2O_3$ | ≤ 12.0 |
| 10.0 ≤ | $B_2O_3$ | ≤ 14.0 |
| 1.0 ≤ | BaO+CaO+MgO[(a)] | ≤ 3.0 |
| 9.0 ≤ | $Fe_2O_3$ | ≤ 15.0 |
| 11.6 ≤ | $K_2O+Li_2O+Na_2O$[(a)] | ≤ 15.6 |
| 0.5 ≤ | $MnO_2$ | ≤ 2.5 |
| 1.5 ≤ | $P_2O_5$ | ≤ 3.5 |
| 36.0 ≤ | $SiO_2$ | ≤ 44.0 |
| 2.0 ≤ | $ThO_2$ | ≤ 5.25 |
| 0.1 ≤ | $UO_2$ | ≤ 1.0 |
| 1.0 ≤ | Others | ≤ 8.0 |

| Multiple-Component Constraints | | |
|---|---|---|
| 48 ≤ | $SiO_2+Al_2O_3$ | ≤ 54 |
| 23.6 ≤ | Alkalis + $B_2O_3$ | ≤ 27.6 |
| 3.3 ≤ | $(SiO_2+Al_2O_3)$/Alkalis | ≤ 4.1 |
| 3.7 ≤ | $(SiO_2+Al_2O_3)/B_2O_3$ | ≤ 4.7 |

(a) The BaO:CaO:MgO and $K_2O$:$Li_2O$:$Na_2O$ wt% ratios were held constant at their levels in the WVCM-50 glass.

heat-treated glass, crushed glass was placed in a fused silica crucible and melted at 1200°C. When the glass was in a molten state (after about 20 min), it was cooled using a programmable furnace. The furnace controller was "programmed" with a series of linear cooling/heating rates that approximated the thermal history of the site in TC-18 or TC-23 whose thermal history was being simulated.

The isothermal heat-treatment test matrix is given in Table 3.9. The matrix consists of five different treatment temperatures and holding times varying from 6 to 240 hr. A portion of crushed glass was placed in a covered

TABLE 3.8. Compositions of Second Set of Compositional Variability Glasses: DG-WV15 - DG-WV30, wt%

| | DG-WV15 | | DG-WV16 | | DG-WV17 | | DG-WV18 | | DG-WV19 | | DG-WV20 | | DG-WV21 | | DG-WV22 | |
|---|---|---|---|---|---|---|---|---|---|---|---|---|---|---|---|---|
| Oxide | Target | Analyzed | Target | Analyzed | Target | Analyzed | Target | Analyzed | Target | Analyzed | Target | Analyzed | Target | Analyzed | Target | Analyzed |
| $Al_2O_3$ | 9.00 | 9.63 | 9.00 | 9.81 | 9.00 | 9.48 | 9.00 | 9.28 | 12.00 | 12.55 | 12.00 | 12.59 | 12.00 | 12.43 | 12.00 | 13.03 |
| $B_2O_3$ | 12.97 | 12.25 | 12.97 | 12.61 | 10.21 | 9.94 | 10.95 | 10.42 | 10.35 | 9.90 | 11.06 | 10.75 | 10.32 | 9.87 | 11.82 | 11.50 |
| BaO | 0.32 | 0.32 | 0.32 | 0.31 | 0.32 | 0.31 | 0.11 | 0.10 | 0.32 | 0.31 | 0.32 | 0.31 | 0.11 | 0.10 | 1.11 | 0.11 |
| CaO | 1.37 | 1.34 | 1.37 | 1.34 | 1.37 | 1.31 | 0.46 | 0.46 | 1.37 | 1.29 | 1.37 | 1.31 | 0.46 | 0.43 | 0.46 | 0.44 |
| MgO | 1.32 | 1.32 | 1.32 | 1.26 | 1.32 | 1.31 | 0.44 | 0.50 | 1.32 | 1.33 | 1.32 | 1.41 | 0.44 | 0.56 | 0.44 | 0.48 |
| $Fe_2O_3$ | 9.00 | 8.53 | 15.00 | 14.12 | 9.00 | 8.75 | 15.00 | 14.00 | 15.00 | 14.07 | 9.00 | 8.72 | 15.00 | 14.14 | 15.00 | 14.05 |
| $K_2O$ | 1.72 | 2.17 | 1.38 | 1.31 | 1.72 | 1.53 | 1.84 | 2.55 | 1.56 | 1.92 | 1.48 | 1.94 | 1.73 | 2.12 | 1.39 | 1.22 |
| $Li_2O$ | 2.37 | 2.66 | 1.91 | 1.89 | 2.37 | 2.40 | 2.54 | 2.47 | 2.16 | 2.12 | 2.04 | 2.07 | 2.39 | 2.31 | 1.92 | 1.88 |
| $Na_2O$ | 10.46 | 10.86 | 8.42 | 8.60 | 10.46 | 10.62 | 11.22 | 11.65 | 9.53 | 9.94 | 9.02 | 9.14 | 10.56 | 10.71 | 8.47 | 8.44 |
| $MnO_2$ | 2.50 | 2.44 | 2.22 | 2.27 | 2.50 | 2.46 | 0.50 | 0.54 | 0.50 | 0.51 | 0.50 | 0.52 | 2.50 | 2.43 | 2.50 | 2.50 |
| $P_2O_5$ | 1.50 | 1.19 | 3.50 | 2.93 | 1.50 | 1.43 | 1.50 | 1.33 | 1.50 | 1.01 | 3.50 | 3.17 | 3.50 | 3.03 | 1.50 | 1.32 |
| $SiO_2$ | 39.00 | 39.11 | 39.00 | 39.94 | 39.00 | 39.83 | 42.48 | 42.40 | 36.65 | 36.64 | 39.40 | 40.02 | 36.49 | 36.77 | 36.30 | 37.36 |
| $ThO_2$ | 2.00 | 1.87 | 2.00 | 1.53 | 5.14 | 4.66 | 2.37 | 2.06 | 5.25 | 5.22 | 2.00 | 1.59 | 2.00 | 1.70 | 2.00 | 1.74 |
| $UO_2$ | 1.00 | 1.09 | 0.10 | 0.14 | 0.10 | 0.11 | 0.10 | 0.11 | 1.00 | 0.93 | 1.00 | 1.02 | 1.00 | 1.11 | 0.10 | 0.12 |
| Others | 5.47 | 5.23 | 1.49 | 1.93 | 5.99 | 5.86 | 1.49 | 2.12 | 1.49 | 2.18 | 5.99 | 5.44 | 1.50 | 2.28 | 5.99 | 5.78 |
| Total | 100 | 100 | 100 | 100 | 100 | 100 | 100 | 100 | 100 | 100 | 100 | 100 | 100 | 100 | 100 | 100 |

TABLE 3.8. (contd)

| Oxide | DG-WV23 | | DG-WV24 | | DG-WV25 | | DG-WV26 | | DG-WV27 | | DG-WV28 | | DG-WV29 | | DG-WV30 | |
|---|---|---|---|---|---|---|---|---|---|---|---|---|---|---|---|---|
| | Target | Analyzed | Target | Analyzed | Target | Analyzed | Target | Analyzed | Target | Analyzed | Target | Analyzed | Target | Analyzed | Target | Analyzed |
| $Al_2O_3$ | 9.00 | 9.39 | 12.00 | 12.43 | 9.00 | 9.79 | 12.00 | 12.89 | 12.00 | 12.35 | 9.00 | 9.41 | 9.00 | 9.27 | 9.86 | 10.46 |
| $B_2O_3$ | 12.97 | 12.32 | 14.00 | 13.23 | 11.28 | 11.16 | 14.00 | 13.40 | 13.01 | 12.55 | 11.00 | 10.58 | 12.00 | 11.46 | 12.27 | 11.76 |
| BaO | 0.11 | 0.11 | 0.11 | 0.11 | 0.11 | 0.11 | 0.32 | 0.31 | 0.11 | 0.11 | 0.11 | 0.11 | 0.32 | 0.31 | 0.19 | 0.20 |
| CaO | 0.46 | 0.52 | 0.46 | 0.51 | 0.46 | 0.55 | 1.37 | 1.32 | 0.46 | 0.53 | 0.46 | 0.50 | 1.37 | 1.32 | 0.82 | 0.81 |
| MgO | 0.44 | 0.58 | 0.44 | 0.49 | 0.44 | 0.49 | 1.32 | 1.27 | 0.44 | 0.51 | 0.44 | 0.51 | 1.32 | 1.21 | 0.79 | 0.88 |
| $Fe_2O_3$ | 14.57 | 13.91 | 9.00 | 8.82 | 9.00 | 9.06 | 9.00 | 8.84 | 9.00 | 8.79 | 12.72 | 12.11 | 9.00 | 8.77 | 11.93 | 11.46 |
| $K_2O$ | 1.38 | 1.99 | 1.60 | 1.80 | 1.53 | 0.82 | 1.51 | 1.73 | 1.72 | 2.28 | 1.49 | 1.53 | 1.84 | 1.93 | 1.61 | 1.81 |
| $Li_2O$ | 1.91 | 1.51 | 2.22 | 2.13 | 2.11 | 2.05 | 2.08 | 2.09 | 2.38 | 2.33 | 2.05 | 2.08 | 2.54 | 2.62 | 2.22 | 2.15 |
| $Na_2O$ | 8.42 | 9.04 | 9.78 | 9.42 | 9.30 | 9.22 | 9.18 | 9.14 | 10.49 | 10.58 | 9.06 | 9.19 | 11.22 | 10.65 | 9.79 | 9.65 |
| $MnO_2$ | 0.50 | 0.51 | 2.50 | 2.47 | 2.45 | 2.50 | 0.50 | 0.55 | 0.50 | 0.51 | 0.50 | 0.51 | 0.50 | 0.50 | 1.21 | 1.21 |
| $P_2O_5$ | 3.50 | 3.48 | 1.50 | 1.60 | 3.50 | 3.58 | 1.50 | 1.62 | 3.50 | 3.63 | 1.50 | 1.53 | 3.30 | 3.25 | 2.47 | 2.51 |
| $SiO_2$ | 39.00 | 39.06 | 42.00 | 42.01 | 44.00 | 45.46 | 40.38 | 40.51 | 36.14 | 36.73 | 42.68 | 43.15 | 44.00 | 44.53 | 39.60 | 40.02 |
| $ThO_2$ | 5.25 | 4.50 | 2.00 | 2.05 | 5.25 | 3.16 | 5.25 | 4.21 | 4.16 | 2.94 | 2.00 | 1.92 | 2.00 | 1.97 | 3.52 | 2.99 |
| $UO_2$ | 1.00 | 1.01 | 0.90 | 0.89 | 0.10 | 0.11 | 0.10 | 0.10 | 0.10 | 0.09 | 1.00 | 0.90 | 0.10 | 0.11 | 0.61 | 0.65 |
| Others | 1.49 | 2.07 | 1.49 | 2.04 | 1.47 | 1.93 | 1.49 | 2.01 | 5.99 | 6.05 | 5.99 | 5.98 | 1.49 | 2.10 | 3.11 | 3.43 |
| Total | 100 | 100 | 100 | 100 | 100 | 100 | 100 | 100 | 100 | 100 | 100 | 100 | 100 | 100 | 100 | 100 |

TABLE 3.9. Isothermal Heat-Treatment Test Matrix

| Specimen | Temperature, °C | Holding Time, hr |
|---|---|---|
| HT-S-7 - 8 | 500 | 120, 240 |
| HT-S-9 - 11 | 600 | 12, 48, 240 |
| HT-S-12 - 16 | 725 | 6, 12, 48, 120, 240 |
| HT-S-17 - 19 | 800 | 12, 48, 240 |
| HT-S-20 - 21 | 900 | 120, 240 |
| HT-S-22 (test standard) | 500 | 2 |

fused silica crucible and put in the furnace at 1200°C. When the glass was in a molten state (after about 20 min), the crucible was removed and placed in a heat-treatment oven at the specified temperature, where it remained a specified time, and then was removed and annealed for 2 hr at 500°C.

Groundwater. Four leachants representing repository groundwaters were used in this study. Their compositions are given in Tables 3.10 through 3.13. One of these, J-13, is actual groundwater recovered from a well at the Yucca Mountain repository site (Oversby 1985).

The other three leachants are synthetic groundwaters. Permian Basin Brine No. 1 (PBB1) represents the brine that would result from dissolving core samples from a salt horizon considered representative of a bedded-salt-site repository. PBB3 represents an inclusion brine chemistry, i.e., a brine that exists in inclusions in a bedded salt. Grande Ronde-4 (GR-4) water is chemically representative of groundwater found in the Grande Ronde basalt formation underlying the Hanford Site near Richland, Washington (Dill et al. 1985).

Leach Testing. All glasses were tested using the MCC-3 leach test method (MCC 1986). Each test glass was crushed and sieved to obtain a -100 +200 mesh size fraction. The crushed and sieved glass was placed in a Teflon® leach container along with deaerated, deionized water (or a repository groundwater). Tests with groundwater leachants were conducted in air. In tests

® Registered trademark of E. I. du Pont de Nemours and Company, Inc., Delaware, Maryland.

TABLE 3.10. Composition of J-13 Well Water - Tuff Groundwater Used in Groundwater Study

| Species | As Analyzed[a] | As Analyzed[b] | Blank[c] |
|---|---|---|---|
| B | 0.20 | 0.132 | 0.16* |
| Na | 48.20 | 44.70 | 44.90* |
| K | 6.64 | 5.11 | 4.80* |
| Ca | 13.30 | 12.70 | 12.60 |
| Si | 32.60 | 27.10 | 27.60* |
| Mg | 2.17 | 1.92 | 1.33 |
| F | 2.30 | 2.20 | 2.50 |
| Cl | 7.09 | 0.21 | 7.10 |
| $SO_4$ | 17.20 | 18.70 | 17.00 |
| $NO_3$ | 7.64 | 9.60 | 8.50 |
| IC[d] | 24.20 | NA[e] | NA |
| pH | 8.12 | 8.20[f] | 8.26[g] |

(a) Inductively coupled plasma spectroscopy (ICP), ion chromatography (IC), and organic carbon analyses reported by material custodian.
(b) Averages, reported by Oversby (1985).
(c) ICP and IC analyses of test blank sample. Concentrations asterisked were used to correct test results.
(d) Inorganic carbon.
(e) Not available.
(f) Measured immediately preceding test.
(g) Measured at test termination.

with deionized water, the sealed container was placed in an airtight enclosure containing a fresh, unused $CO_2$-sorbent. This enclosure was then placed in a 90°C oven for 7 days. The containers were briefly removed from the enclosure and gently agitated once each day. Three replicates and a blank were run for each glass.

At the end of the leach-test period, aliquots of the leachate were filtered through both 0.45-$\mu$m and 18-Å filters. The leach containers were

TABLE 3.11. Composition of Permian Basin Brine No. 1 Used in Groundwater Study

| Species | Concentration, ppm | |
|---|---|---|
| | Target | As Analyzed[(a)] |
| Na | 124,000.0 | 124,000.0 |
| Ca | 1,600.0 | 1,300.0 |
| Mg | 134.0 | 104.0 |
| K | 39.0 | 87.9 |
| Sr | 35.0 | 13.7 |
| Cl | 192,000.0 | 185,000.0 |
| $SO_4$ | 3,840.0 | 3,500.0 |
| Br | 32.0 | 42.0 |
| $HCO_3$ | 30.5 | 16.2 |

(a) ICP and IC analyses.

TABLE 3.12. Composition of Permian Basin Brine No. 3 Used in Groundwater Study

| Species | Target | As Analyzed[(a)] |
|---|---|---|
| Na | 25,000 ± 5,000 | 22,900 |
| Ca | 18,700 ± 2,000 | 18,500 |
| Mg | 62,500 ± 6,000 | 56,600 |
| K | 11,000 ± 2,000 | 56,600 |
| Cl | 240,000 ± 20,000 | 243,000 |
| $SO_4$ | 250 ± 150 | 209 |
| Br | 3,400 ± 700 | 3,550 |

(a) ICP and IC analyses.

then rinsed with deionized water, and filled with 1% nitric acid solution, and placed in a 90°C oven overnight. The filtered aliquots and the acid-strip solutions were submitted for analysis.

TABLE 3.13. Composition of Grande Ronde-4 - Basalt Groundwater Used in Groundwater Study

| Species | Concentration, ppm | | |
|---|---|---|---|
| | Target | As Analyzed[a] | Blank[b] |
| Na | 334.0 | 364.5 | 349.5* |
| K | 13.8 | 14.15 | 13.8* |
| Ca | 2.2 | 2.22 | 2.2 |
| Si | 45.0 | 43.45 | 36.3* |
| F | 19.9 | 19.9 | 20.0 |
| Cl | 405.0 | 409.85 | 420.0 |
| $SO_4$ | 4.0 | 4.2 | 3.8 |
| IC[c] | 18.1 | 19.25 | NA[d] |
| pH | 9.70 | 10.18[e] | 9.66[f] |

(a) ICP and IC analyses; information supplied by material custodian.
(b) ICP and IC analyses of test blank sample. Concentrations asterisked were used to correct test results.
(c) Inorganic carbon.
(d) Information not available.
(e) Measured immediately preceding test.
(f) Measured at test termination.

In addition to the 7-day MCC-3 testing, limited MCC-1 testing was also conducted. This test was essentially identical to the MCC-3 test except that the test specimen was a small cube of glass instead of a crushed and sieved size fraction. Limited 28-day MCC-3 testing was also performed. However, the results of only the 7-day MCC-3 testing are reported here.

3.5.1.2 Results and Discussion

All glass specimens were analyzed using inductively coupled plasma spectroscopy (ICP) for cations, atomic absorption (AA) for cesium, and laser fluorescence for uranium. The redox state was determined using a spectrophotometric technique. Solution analyses included ICP, laser fluorescence,

and AA. All normalized releases reported were calculated from the elemental concentrations of the 0.45-$\mu$m filtered solutions. Analyses of the 18-Å and acid-strip solutions are not presented here. Analyses of the 18-Å filtered solutions indicated that very few, if any, colloids were formed during the test periods. Analyses of the acid-strip solutions indicated that negligible amounts of dissolution products plated out on the test container walls.

Compositional Variability. The normalized elemental mass releases of Al, B, Cs, Li, Na, Si, Th, and U from the first set of glasses are given in Table 3.14. Each value given represents the average obtained from three replicate tests. Analysis of these releases shows that the chemical durability of WVCM-47 (DG-WV1) and the glass containing noble metal (Rh, Ru, Pd) oxides (DG-WV2) are essentially identical. The "high $P_2O_5$," "high $ThO_2$," and "low $B_2O_3$" glasses (DG-WV6, DG-WV7, and DG-WV8, respectively) appear to be as chemically durable as the reference glass. This indicates that these variations in $P_2O_5$, $ThO_2$ and $B_2O_3$ have little, if any, real effect on the product's chemical durability.

TABLE 3.14. Average Normalized Mass Releases from First Set of Glasses (DG-WV1 through DG-WV8), $g/m^2$

| Element | DG-WV1 | DG-WV2 | DG-WV3 | DG-WV4 | DG-WV5 | DG-WV6 | DG-WV7 | DG-WV8 |
|---|---|---|---|---|---|---|---|---|
| Al | 0.106 | 0.109 | 0.098 | 0.110 | 0.097 | 0.115 | 0.109 | 0.113 |
| B | 0.186 | 0.191 | 0.237 | 0.239 | 0.229 | 0.188 | 0.188 | 0.187 |
| Cs | 0.104 | 0.092 | 0.137 | 0.092 | 0.082 | 0.093 | 0.120 | 0.040 |
| Li | 0.301 | 0.305 | 0.300 | 0.294 | 0.328 | 0.301 | 0.323 | 0.319 |
| Na | 0.158 | 0.163 | 0.218 | 0.239 | 0.204 | 0.155 | 0.170 | 0.176 |
| Si | 0.116 | 0.117 | 0.129 | 0.123 | 0.127 | 0.123 | 0.119 | 0.118 |
| Th | 0.001 | 0.002 | 0.001 | 0.001 | 0.001 | 0.002 | 0.001 | 0.002 |
| U | 0.026 | 0.031 | 0.031 | 0.029 | 0.030 | 0.033 | 0.038 | 0.037 |
| pH | 9.15 | 9.27 | 9.41 | 9.22 | 9.37 | 9.02 | 8.78 | 9.33 |

Table 3.15 lists the normalized elemental mass releases of Al, B, Cs, Li, Na, Si, Th, and U from the second set of glasses. Each value given represents the average obtained from three replicate tests. Roughly half of the glasses tested had greater chemical durability than the nominal WVCM-50 composition. The compositional variation caused maximum boron releases of 34% higher and 29% lower than WVCM-50.

TABLE 3.15. Average Normalized Mass Releases from Second Set of Glasses (DG-WV15 through DG-WV30), $g/m^2$

| Element | DG-WV15 | DG-WV16 | DG-WV17 | DG-WV18 | DG-WV19 | DG-WV20 | DG-WV21 | DG-WV22 |
|---|---|---|---|---|---|---|---|---|
| Al | 0.103 | 0.108 | 0.110 | 0.127 | 0.126 | 0.113 | 0.150 | 0.136 |
| B | 0.264 | 0.181 | 0.273 | 0.210 | 0.207 | 0.148 | 0.205 | 0.185 |
| Cs | 0.097 | 0.089 | 0.097 | 0.061 | 0.085 | 0.112 | 0.099 | 0.091 |
| Li | 0.287 | 0.243 | 0.296 | 0.266 | 0.286 | 0.241 | 0.252 | 0.294 |
| Na | 0.243 | 0.155 | 0.248 | 0.207 | 0.190 | 0.125 | 0.205 | 0.160 |
| Si | 0.115 | 0.111 | 0.117 | 0.126 | 0.112 | 0.105 | 0.136 | 0.128 |
| Th | 0.000 | 0.000 | 0.000 | 0.004 | 0.001 | 0.000 | 0.010 | 0.007 |
| U | 0.023 | 0.022 | 0.019 | 0.042 | 0.036 | 0.006 | 0.044 | 0.036 |
| pH | 7.88 | 8.56 | 9.26 | 9.18 | 9.03 | 8.57 | 8.86 | 8.44 |

| | DG-WV23 | DG-WV24 | DG-WV25 | DG-WV26 | DG-WV27 | DG-WV28 | DG-WV29 | DG-WV30 |
|---|---|---|---|---|---|---|---|---|
| Al | 0.136 | 0.123 | 0.125 | 0.101 | 0.149 | 0.130 | 0.101 | 0.126 |
| B | 0.232 | 0.193 | 0.179 | 0.172 | 0.250 | 0.188 | 0.207 | 0.205 |
| Cs | 0.031 | 0.071 | 0.082 | 0.108 | 0.071 | 0.073 | 0.103 | 0.099 |
| Li | 0.294 | 0.284 | 0.264 | 0.265 | 0.400 | 0.301 | 0.260 | 0.281 |
| Na | 0.172 | 0.156 | 0.153 | 0.144 | 0.208 | 0.156 | 0.194 | 0.206 |
| Si | 0.132 | 0.117 | 0.119 | 0.098 | 0.133 | 0.128 | 0.113 | 0.122 |
| Th | 0.023 | 0.003 | 0.002 | 0.000 | 0.007 | 0.011 | 0.000 | 0.001 |
| U | 0.052 | 0.030 | 0.031 | 0.028 | 0.022 | 0.034 | 0.033 | 0.029 |
| pH | 9.29 | 9.39 | 9.50 | 9.43 | 9.48 | 9.49 | 9.80 | 9.66 |

An empirical linear mixture model was fitted to the normalized boron release data from the second set of glasses (DG-WV15 to DG-WV30). This model has the form shown in Equation (1)

$$\text{Normalized Elemental Release} = \sum_{i=1}^{11} b_i x_i \qquad (1)$$

where $x_1, \ldots, x_{11}$ are the weight fractions of the 11 oxide components listed under Single Component Constraints in Table 3.7 and $b_1, \ldots, b_{11}$ are the model parameters estimated via least squares regression.

The model for the 16-glass data set is given in Equation (2)

$$\begin{aligned} NBR = {} & -1.4572\ Al_2O_3 + 1.0393\ B_2O_3 - 0.3764\ (BaO+CaO+MgO) + \\ & 0.4039\ Fe_2O_3 + 2.3528\ (K_2O+Li_2O+Na_2O) + 0.9566\ MnO_2 + \\ & 0.1607\ P_2O_5 - 0.4841\ SiO_2 + 0.9420\ ThO_2 + 1.8447\ UO_2 + \\ & 0.7892\ \text{Others} \end{aligned} \qquad (2)$$

where NBR is normalized boron release from the 7-day MCC-3 leach test. This model fits its data set well, with an $R^2$ value of 0.94.

Equation (2) was used to predict NBR for the eight glasses of the first set of compositional variability glasses. These results were used to check the model's usefulness as a predictive tool. Table 3.16 listing the measured and predicted values for each glass shows that the predicted NBR values compare well with the observed values. These results are good evidence that the model can be reasonably used for prediction.

To investigate the effects of varying individual oxide components, effects plots (Piepel 1982) are presented in Figures 3.13 and 3.14 for boron and silica releases. In a given effects plot, there is one effect curve for each component. Each curve displays the effect of changing the component over its allowable range as defined by the constraints of Table 3.7. The curves are merely a series of predicted normalized elemental release (NER) values plotted versus weight percent changes from each component's value in a reference glass. The WVCM-50 glass is used as the reference in Figures 3.13

TABLE 3.16. Comparison of Observed Normalized Boron Release Values to Predicted Values

| Glass | Measured Values | Predicted Value |
|---|---|---|
| WV-1 | 0.18, 0.19, 0.19 | 0.19 |
| WV-2 | 0.19, 0.19, 0.19 | 0.18 |
| WV-3 | 0.24, 0.24, 0.24 | 0.22 |
| WV-4 | 0.23, 0.24, 0.24 | 0.26 |
| WV-5 | 0.23, 0.23, 0.23 | 0.26 |
| WV-6 | 0.19, 0.19, 0.19 | 0.18 |
| WV-7 | 0.19, 0.19, 0.19 | 0.18 |
| WV-8 | 0.19, 0.18, 0.19 | 0.15 |

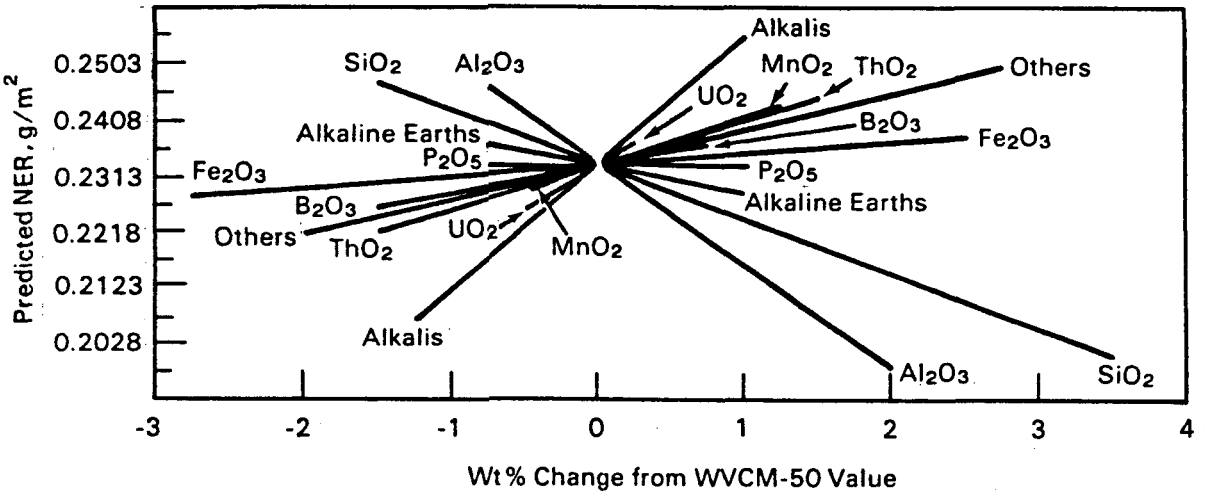


FIGURE 3.13. Effects Plot for Normalized Boron Release (linear mixture model, 24 glasses)

and 3.14. Equation 2 was used to generate Figure 3.13 for boron releases. A similar equation, relating silica release to composition, was used to generate Figure 3.14 for silica releases.

The alkalis ($K_2O$, $Li_2O$, and $Na_2O$), $UO_2$, and $ThO_2$ have the largest positive effects on boron release per unit weight change. Increasing their levels tends to decrease the glass chemical durability. Conversely, the

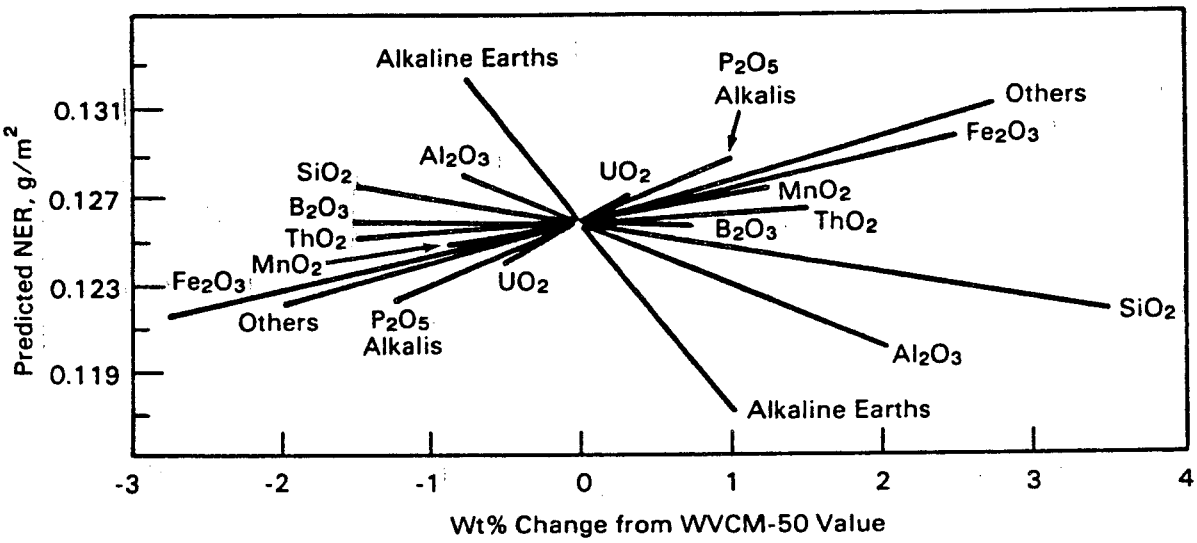


FIGURE 3.14. Effects Plot for Normalized Silica Release (linear mixture model, 24 glasses)

oxides $Al_2O_3$ and $SiO_2$ have the largest negative effects on boron release. Although the per-unit effect of $UO_2$ is relatively large, its total effect is not as large as those of $MnO_2$, "others," and $ThO_2$, which have larger ranges. It may be only the total effects of the components that are of practical interest. Components such as $P_2O_5$, $Fe_2O_3$, $B_2O_3$, and the alkaline earths (BaO, CaO, and MgO) that have nearly horizontal effects curves in Figure 3.13 have no substantial effect on boron release within the region studied.

Glass Redox Effects. The normalized elemental mass releases of Al, B, Cs, Li, Na, Si, Th, and U from the redox-adjusted glasses are given in Table 3.17. Each value given represents the average obtained from triplicate tests. Graphical representations of boron and silica releases are given in Figure 3.15. The error bars represent experimental error of $\pm$ two standard deviations. Figure 3.15 shows that the silica release of each glass tested is identical, within experimental error; this indicates either similar chemical durability or that the silica solubility limit has been reached during the test period. The boron release data, being identical within experimental error, show the durability of each glass to be very similar. Analysis of the release data indicates that for the specific glass that was tested, redox

TABLE 3.17. Average Normalized Elemental Mass Releases, $g/m^2$

| | $Fe^{2+}/Fe^{3+}$ | | | |
|---|---|---|---|---|
| Element | 0.068 | 0.126 | 0.236 | 0.424 |
| Al | 0.119 | 0.113 | 0.114 | 0.121 |
| B | 0.212 | 0.209 | 0.212 | 0.237 |
| Cs | 0.092 | 0.101 | 0.081 | 0.067 |
| Fe | 0.003 | 0.002 | 0.003 | 0.003 |
| K | 0.020 | 0.056 | 0.026 | 0.095 |
| Li | 0.274 | 0.269 | 0.269 | 0.295 |
| Mg | 0.000 | 0.000 | 0.000 | 0.003 |
| Mn | 0.002 | 0.002 | 0.002 | 0.003 |
| Na | 0.209 | 0.203 | 0.215 | 0.249 |
| P | 0.177 | 0.173 | 0.171 | 0.182 |
| Si | 0.116 | 0.112 | 0.112 | 0.121 |
| Th | 0.000 | 0.000 | 0.000 | 0.000 |
| Ti | 0.001 | 0.001 | 0.000 | 0.001 |
| U | 0.024 | 0.023 | 0.021 | 0.025 |
| pH | 9.64 | 9.76 | 9.82 | 9.91 |

state has no large effect on chemical durability. Where an effect is seen, increasing $Fe^{2+}/Fe^{3+}$ ratio (reduction of glass) decreases chemical durability, with the exception of cesium release.

The final pH of the leachate appears to increase with increasing $Fe^{2+}/Fe^{3+}$ of the glass leached. This could be caused by oxidation of $Fe^{2+}$ in the leachate. As $Fe^{2+}$ goes into solution, it is oxidized by dissolved $O_2$ in the following reaction:

$$O_2 + 4H^+ + 4Fe^{2+} \rightarrow 4Fe^{3+} + 2H_2O \qquad (3)$$

This reaction consumes $H^+$ which in turn increases the pH. With greater $Fe^{2+}/Fe^{3+}$ ratios, more $Fe^{2+}$ is available for oxidation. The greater the

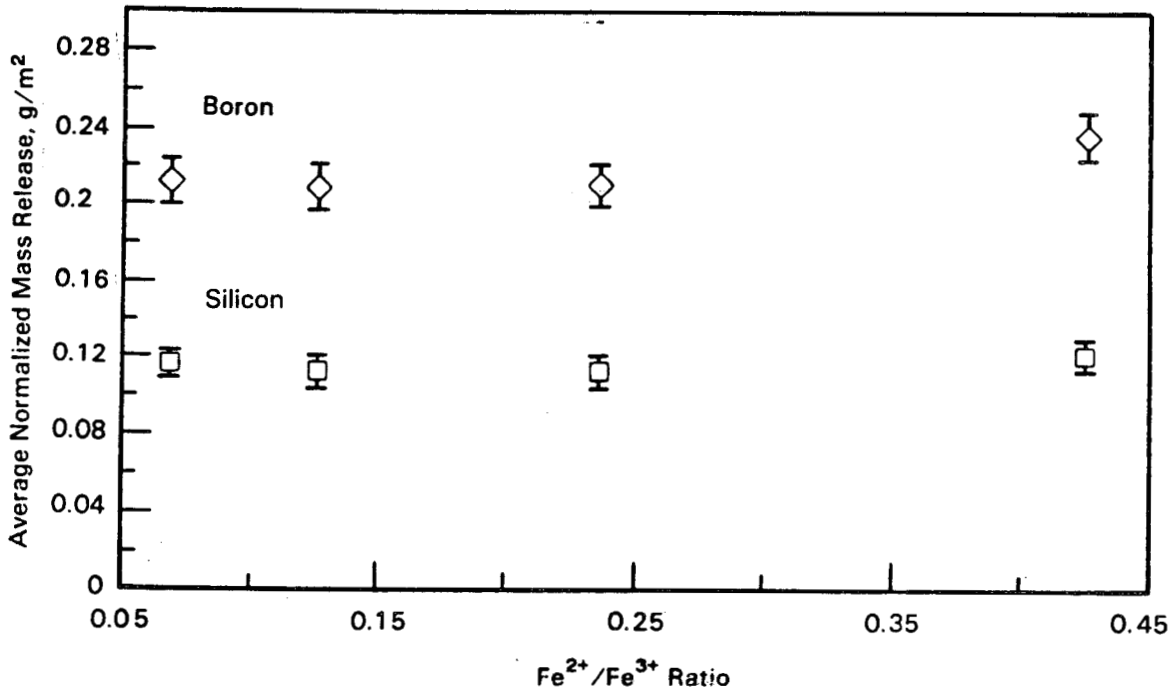


FIGURE 3.15. Comparison of Silicon and Boron Normalized Mass Releases from Redox-Adjusted Glasses (modified MCC-3 test, 90°C, deaerated deionized water, 7-day)

amount of $Fe^{2+}$ oxidized, the greater the increase in solution pH. Calculations comparing available $Fe^{2+}$ concentrations and $H^{+}$ consumption support this theory.

Heat-Treatment Effects. Figure 3.16 shows boron and silicon release data for the glasses that received simulated canister cooldown heat treatments. The error bars represent experimental error of plus or minus two standard deviations based on the results of triplicate tests. The figure demonstrates that the heat treatments have no substantial effect on the chemical durability of this glass. The boron release from the least durable glass, HT-S-1, was only about 15% greater than that from a glass, DG-WV11R, that was not heat-treated. This is about the same decrease in durability observed for the redox-adjusted glasses: (the boron release of DG-WV14R, the most reduced of the redox-adjusted glasses, was 14% greater than the release from DG-WV11R, a glass only slightly reduced).

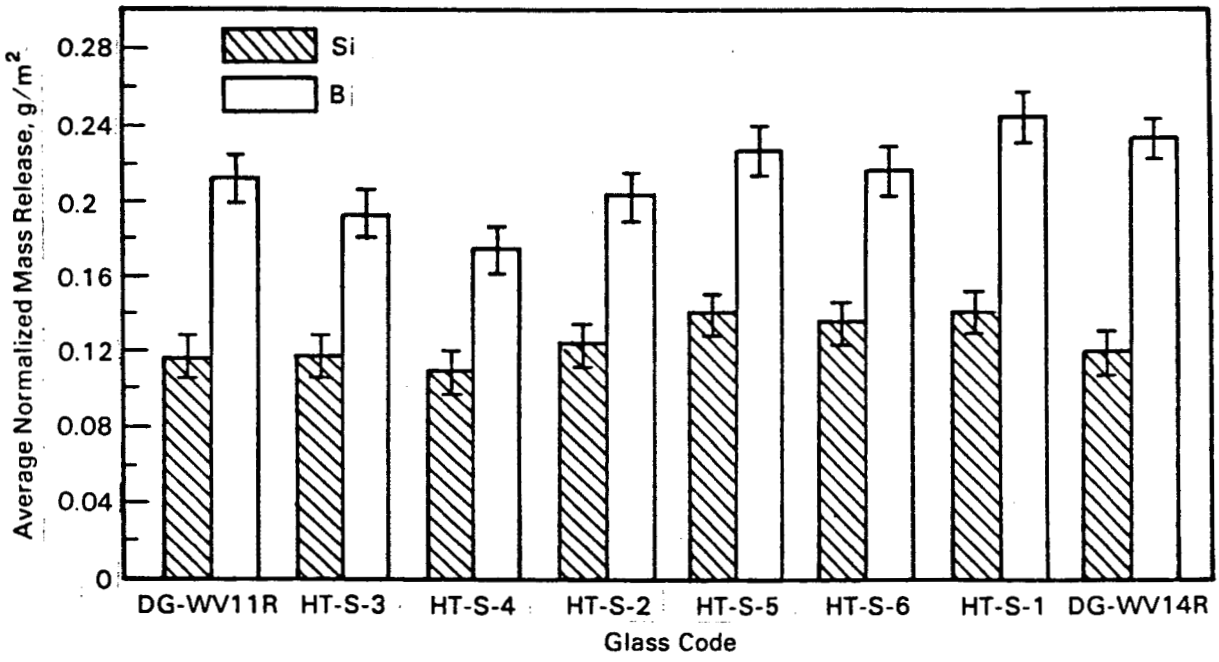


FIGURE 3.16. Comparison of Silicon and Boron Normalized Mass Releases from Slow-Cool Heat-Treated Glasses. Heat-treated glasses are arranged in order from fastest to slowest relative cooling rates (modified MCC-3 test, 90°C, deaerated deionized water, 7-day).

Figure 3.17 shows the boron release data for the isothermally heat-treated glasses plotted as a function of heat-treatment time and treatment temperature on a time-temperature-transformation diagram. The boron release values for each individual sample are shown, as well as the approximate locations of a series of constant-leaching isopleths.

This diagram appears essentially identical to what would be expected if crystallinity were plotted instead of chemical durability. This is not surprising as it is the devitrification (growth of crystallinity) of the glass that is decreasing the durability. A maximum decrease in durability of a factor of two was found for the isothermally heat-treated samples (500°C for 2 hr versus 600°C for 240 hr). Very similar behavior was found for a similar glass, SRL-165 (Jantzen 1983).

Groundwater Effects. Four samples of the reference waste glass used in the heat treatment and redox variation studies were used to evaluate

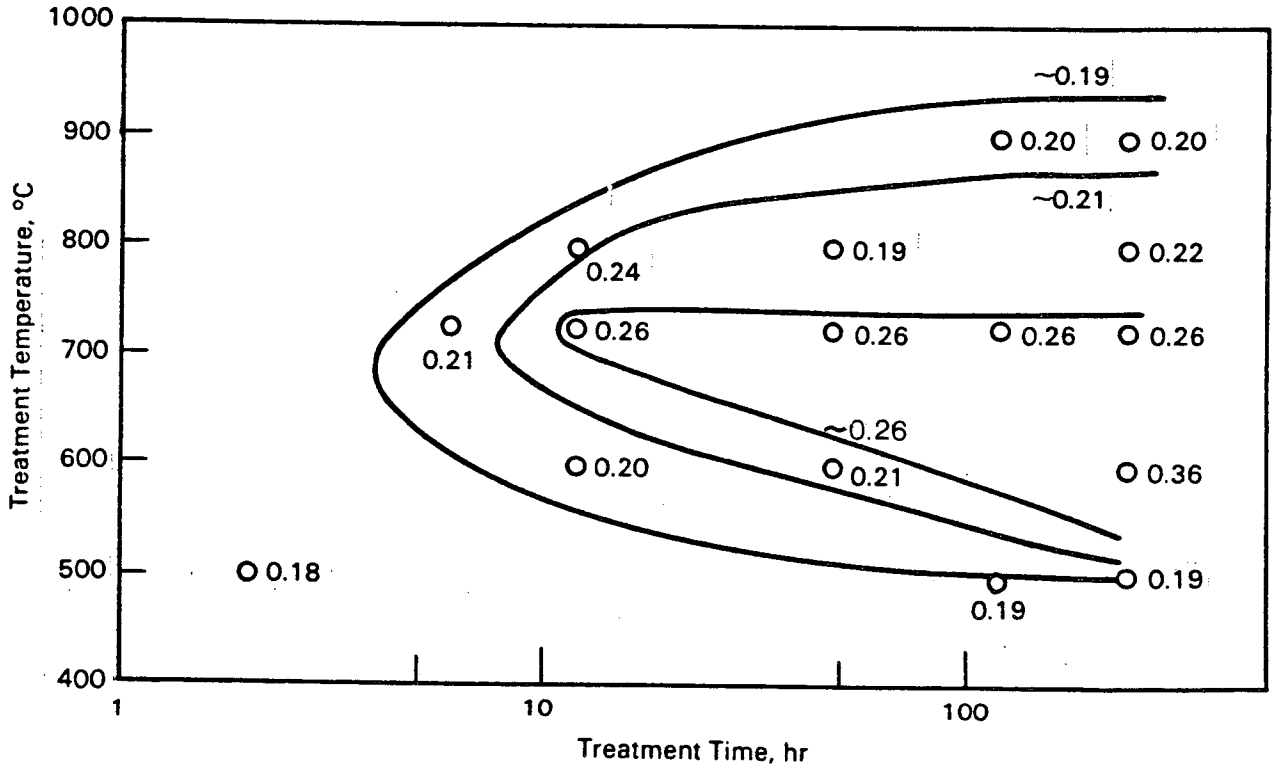


FIGURE 3.17. Boron Releases from Isothermally Heat-Treated WVCM-50 Glass

groundwater effects. Boron and silicon releases are represented graphically in Figure 3.18. The error bars represent experimental error of plus or minus two standard deviations based on the results of triplicate tests. The releases of DG-WV11R are included in the figure to provide comparison between glass chemical durability in deionized water (DIW) versus groundwater. The tests were conducted identically except that DG-WV11R was leached under $CO_2$-free conditions, while the groundwater-leached glasses were leached in an air atmosphere.

Figure 3.18 shows that groundwater type definitely affects the chemical durability of this glass and that the glass is chemically more durable in the groundwaters than in deaerated DIW, under $CO_2$-free conditions. Compared to durability in DIW, the glass is about a factor of five more durable in PBB1 (based on boron release), a factor of four more durable in PBB3, a factor of three more durable in J-13 well water, and a factor of two more durable in GR-4.

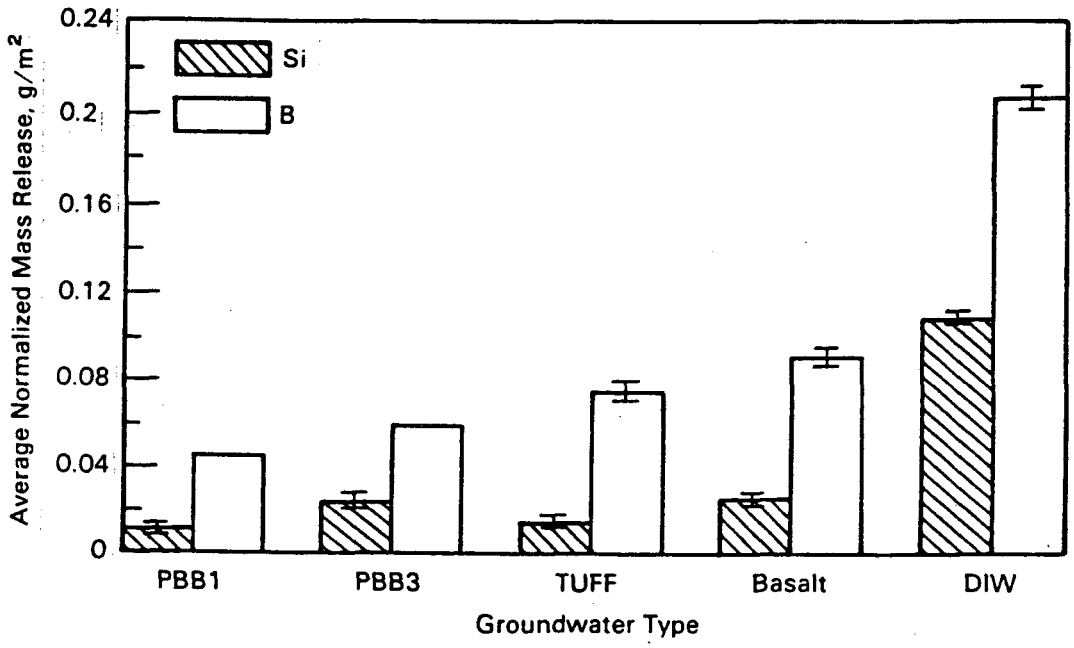


FIGURE 3.18. Comparison of Boron and Silicon Normalized Mass Releases from WVCM-50 Glass in Different Groundwaters (modified MCC-3 Test, 90°C, deionized water (DIW), 7-day)

That the glass was most durable when tested in brines is consistent with the known decreased solubility of $SiO_2$-bearing solids in solutions of high ionic strength. The relative saturation fraction of silicic acid in the leachant also plays an important role in determining the glass reactivity (Strachan, Pederson, and Lokken 1985). This explains why the glass is less durable in DIW than in the basalt and tuff groundwaters. These are silicate groundwaters and become saturated with silicic acid during the glass dissolution more quickly than does DIW.

Figure 3.18 demonstrates also that glass dissolution is greater in PBB3 than in PBB1. The major difference between the brine compositions is the higher magnesium concentration in PBB3. Early leaching studies conducted in brine solutions (Braithwaite 1980) concluded that glass dissolution increases with increasing magnesium content of brine. The researchers attributed this effect to magnesium causing a decrease in pH and to magnesium substituting for divalent oxides like CaO and SrO in the glass matrix. Other brine

leaching studies (McGrail and Reimus 1987) have shown that the kinetics of dissolution of a defense waste glass were not affected, however, by the difference in brine composition.

Glass dissolution was also found to be greater in basalt groundwater than in tuff groundwater. This difference is most probably caused by the higher initial pH of the basalt groundwater (10.18 versus 8.20 for the tuff groundwater), which results in greater attack on the glass network.

### 3.5.2 Canister Impact Testing

Five West Valley canisters were impact-tested during FY 1987. One canister, designated WV-03A, was the reference West Valley design. The other four (WV-024B through WV-027B) were different designs. Each canister's wall was fabricated from 10-gauge material. The top and bottom flanges of the reference canister were fabricated from material 0.1875 in. thick. The top and bottom flanges of the alternative design canisters were fabricated from material 0.375 in. thick. In addition, 0.375-in.-thick sections were added at the top and bottom of each alternative design canister's wall. This thicker material would provide resistance to deformation during impact-testing. Four different lengths of this thicker material were used for the four alternative canister designs. The dimensions for each canister are shown in Figure 3.19.

Prior to impacting of the canisters, strain circles were applied on the external surfaces of all five canisters, emphasizing the areas at and near each canister weld. Strain circles are precise circles permanently inscribed on various surfaces of each canister using an electrochemical process analogous to preparing a contact print from a negative. They were placed on the canisters in regions where large strains from the impact were expected.

The canisters were then sealed by welding a metal plate on the mouth of the canister to prevent any glass from falling out during impact. The plate is not intended to simulate any closure, since the closure for the West Valley canister has not yet been designed.

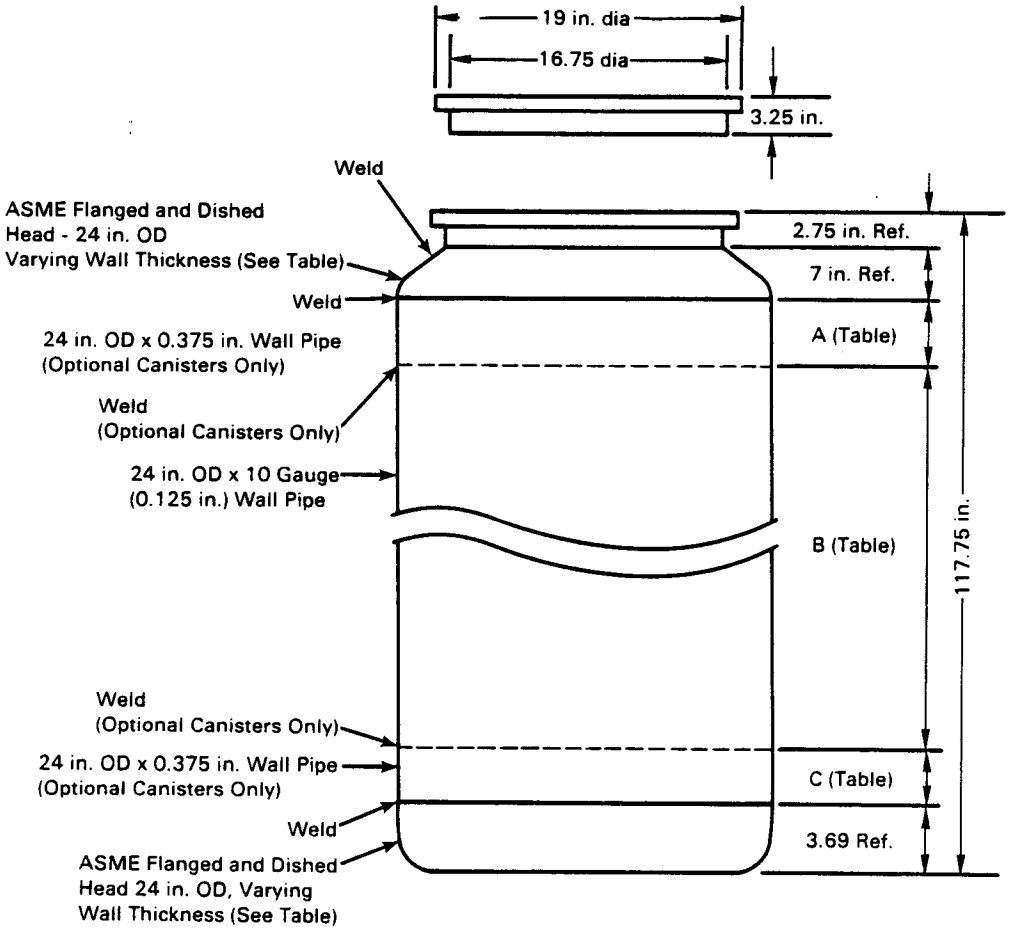


Varying Canister Dimensions

| Canister Number | Head Thickness, in. | Wall Lengths, in. | | |
|---|---|---|---|---|
| | | A | B | C |
| WV-03A | 0.1875 | 0 | 104.31 | 0 |
| WV-24B | 0.375 | 7 | 90 | 8.31 |
| WV-25B | 0.375 | 10 | 89 | 6.31 |
| WV-26B | 0.375 | 12 | 89 | 4.31 |
| WV-27B | 0.375 | 15 | 88 | 2.31 |

FIGURE 3.19. West Valley Canister Designs

Each canister was dropped on its head and bottom from a height of 7 m. The specific orientation of the head and bottom drops depended on the canister's design. For the reference canister the drops were made with the

canister oriented vertically. For the optional designs, the drops were made with the canister's center of gravity oriented over the top and bottom corners.

The impacted canisters were evaluated. All exhibited greater deformation from top impacts than from bottom impacts. This was expected as the glass inside resists deformation in a bottom drop. The top of the canister, however, is empty, and thus all the impact energy for a top drop is dissipated through deformation of the canister material. Also canister walls were significantly dented where the canisters fell on top of shackles used to suspend the canister. Because this denting was more severe than that observed in previous impact tests with other designs, it was recommended to West Valley that impact-testing planned for the final West Valley reference canister include a puncture-bar impact.

The primary deformation of the reference canister as a result of the bottom drop occurred 3 to 7 in. above the 10-gauge-to-3/16-in. bottom weld. This deformation was not large. However, the deformation resulting from the top impact of this canister was large. The canister's head was pressed into the plenum, and two concentric buckles formed in the canister wall. Although hairline cracks were seen at the sites of greatest deformation, they appeared not to have penetrated the canister wall.

For the four optional canister designs, the areas of maximum deformation were in the plenum area between the canister head and wall (top drop) and areas in the 10-gauge wall about 3 to 5 in. above the 10-gauge-to-3/8-in. welds on the wall of each canister (bottom drop). No significant deformation appeared in the 3/8-in.-thick wall area next to the canister impact. Apparently the 3/8-in. thickness presents too much resistance to deformation. As a result, the impact energy moves up the canister wall to the 10-gauge wall. Here the thinner wall resists deformation much less and buckles.

Following this qualitative evaluation of impact deformation, the strain circles on the outside of each canister were analyzed. The strain imparted to the canister material by the impact is determined from the changes in their dimensions. For the bottom drop on the reference canister (WV-03A), the maximum surface strain was less than 3%, which is negligible as far as

failure is concerned. The maximum strain on the top of the reference canister was found on the outside edge of the top wall buckle. The peak axial strain was 44% and the peak hoop strain was about 8%. The peak axial strain compares with a typical failure strain value of 56% for this material. As previously mentioned, hairline cracks were observed on this canister at sites of maximum strain.

No strains measured on the bottom ends of the four optional canister designs exceeded 10%, even those measured near the 10-gauge side wall deformation. Thus the potential for failure from the bottom corner drop is relatively small. Maximum strains in the top ends of the four optional canisters were in the axial direction somewhere between the top-to-side-wall weld and the neck-to-top weld. The maximum measured axial strain for top impacts of the four optional canister designs is about 20%. The magnitude of the hoop strains on the top end were all less than 7%. Failure of the optional canister designs is not very probable.

Helium leak-testing of the five canisters was then completed. Before this testing took place, the lids that had been skip-welded to the canisters prior to impacting were welded to the canisters with full-seal welds. This was done to ensure that any leaks that were detected were the result of a canister breach and not a lid failure. All the canisters were found to leak at rates less than $3 \times 10^{-8}$ atm-cc/sec. Based on a definition of breach as a helium leak in excess of $1 \times 10^{-7}$ atm-cc/sec, none of the canisters breached as a result of either the top or the bottom drop.

## 3.6 REFERENCES


Braithwaite, J. W. 1980. "Brine Chemistry Effects on the Durability of a Simulated Waste Glass." Sci. Basis Nuc. Waste Manag. 2:199, ed. Clyde J. M. Northrup, Plenum Press, New York.

Bray, L. A., and N. M. Thomas. 1987. "Decontamination of Stainless Steel Canisters that Contain High-Level Waste." Trans. Amer. Nuc. Soc. 55:230-231.

Burkholder, H. C., and R. A. Brouns, Compilers. 1987. Nuclear Waste Treatment Program Annual Report for FY 1986. PNL-6325, Pacific Northwest Laboratory, Richland, Washington.

Dill, J. A., et al. 1985. An Evaluation of the Stability of Synthetic Groundwater Formulations GR-3 and GR-4. SD-BWI-TD-013, Rev. 0, Rockwell Hanford Operations, Richland, Washington.

Faletti, D. W., T. A. Erb, H. Harty, and C. A. LoPresti. 1988. User's Guide for West Valley Feed Preparation Code (RECIPE). PNL-6425, Pacific Northwest Laboratory, Richland, Washington.

Jantzen, C. M., et al. 1983. "Time-Temperature-Transformation Kinetics in SRL Waste Glasses." In Advances in Ceramics, Volume 8 : Nuclear Waste Management, eds. G. G. Wicks, W. A. Ross. American Ceramic Society, Columbus, Ohio.

Materials Characterization Center. 1986. Test Methods Submitted for Nuclear Waste Materials Handbook. PNL-3990, Pacific Northwest Laboratory, Richland, Washington.

McGrail, B. P. and M. A. Reimus. 1987. Salt Repository Project - Glass Studies Program: FY 1986 Annual Report. PNL/SRP-6389, Pacific Northwest Laboratory, Richland, Washington.

Oversby, V. M. 1985. The Reaction of Topopah Spring Tuff with J-13 Water at 150°C - Samples from Drill Cores USW G-1, USW GU-3, USW G-4, and UE-25h#1. UCRL-53629, Lawrence Livermore National Laboratory, Livermore, California.

Piepel, G. F. 1982. "Measuring Component Effects in Constrained Mixture Experiments." Technometrics 24:29-39.

Reimus, P. W. 1987. MASBAL: A Computer Program for Predicting the Composition of Nuclear Waste Glass Produced by a Slurry-Fed Ceramic Melter. PNL-6244, Pacific Northwest Laboratory, Richland, Washington.

Strachan, D. M., L. R. Pederson, and R. O. Lokken. 1985. Results from the Long-Term Interaction and Modeling of SRL-131 Glass with Aqueous Solutions. PNL-5654, Pacific Northwest Laboratory, Richland, Washington.

U.S. Department of Energy. 1987. Waste Acceptance Preliminary Specifications for the West Valley Demonstration Project High-Level Waste Form. DOE/RW-0136 (ORG/B-9), U.S. Department of Energy, Washington DC.

# 4.0 LOW-LEVEL WASTE COORDINATION

J. L. Buelt - Manager

## 4.1 OBJECTIVES

The objectives of the Low-Level Waste Coordination Task are to identify and conduct appropriate long-term research and development programs for the Department of Energy (DOE) for low-level radioactive wastes. These programs include both theoretical and experimental studies on many facets of low-level waste (LLW) management. Emphasis is on barrier enhancement, as in the Application of Engineered Sorbent Barriers Program, and on waste-form leaching, as in the Special Waste Form Lysimeters - Arid Program.

## 4.2 SUMMARY

Under the Application of Engineered Sorbent Barriers Program, a comprehensive program plan for development of sorbent barrier technology was prepared. The plan outlines the remaining work necessary to complete the development of the sorbent barrier technology.

Also prepared in FY 1987 was a preliminary economic feasibility study for application of sorbent barriers beneath a shallow-land burial site in a humid climate. This feasibility study included obtaining additional information on barrier performance through the use of flow-through column tests. Results indicate that the clinoptilolite formulation has superior sorption properties and is cost-effective. It is recommended for field testing.

The Special Waste-Form Lysimeters - Arid Program has collected extensive hydrologic and chemical data over the last three years relating to the leaching of commercial waste forms under field conditions. Five different actual LLW forms are being tested at the lysimeter facility, with duplicate samples of each being evaluated. Two radionuclides have been found in lysimeter leachates to date, cobalt-60 and tritium. Chemical inventories, made quarterly, have also revealed migration of other waste constituents: sodium, sulfate, boron, calcium, and magnesium.

To this point, analysis has been largely qualitative. The program's final phase will rely heavily on the iterative process of model simulation and calibration to provide quantitative interpretation. Preliminary analysis, however, indicates that these field data will allow a more definitive analysis of source terms for commercial LLW than is possible with laboratory data alone.

## 4.3 APPLICATION OF ENGINEERED SORBENT BARRIERS - H. D. Freeman

The objective of this study is to develop and evaluate new and cost-effective technology for restricting the migration of radionuclides from low-level wastes by using sorbent materials as engineered barriers. Studies conducted in FY 1987 focused on preparing a comprehensive program plan for development of sorbent barrier technology and on evaluating the incremental cost of placing an engineered sorbent barrier beneath a shallow-land burial site in a humid climate.

### 4.3.1 Comprehensive Program Plan

The comprehensive program plan outlined the remaining work necessary to complete the development of the sorbent barrier technology. The primary tasks presented in this plan are as follows:

- Additional laboratory experiments to investigate the effects of kinetics and pH on the effectiveness of sorbent materials.
- Field testing of sorbent barriers to obtain necessary information on application techniques and on the quality of the barrier as installed by full-scale equipment.
- Development of a design guide to allow any DOE site to design a sorbent barrier for the conditions found at that site.

This comprehensive program plan was completed in March 1987 and submitted to the Low-Level Waste Management Program. This document provides the basis for work to be performed in FY 1988 through FY 1992 and was incorporated into the FY 1990 Field Work Proposal.

### 4.3.2 Economic Feasibility Study

The second task for FY 1987 was the preparation of a preliminary economic feasibility study for application of sorbent barriers at a humid shallow-land burial site. The economic feasibility study consisted of three subtasks: 1) selection of a reference site, including parameters affecting transport of radionuclide through soil, 2) determination of sorbent barrier capacity under flow-through conditions for three barrier formulations and local soil, and 3) estimation of sorbent barrier costs based on the information obtained using a simple radionuclide transport model coupled with information on costs for materials and construction.

This feasibility study included obtaining additional information on barrier performance through the use of flow-through column tests. These tests give more realistic sorption parameters than those obtained with batch contact methods. Data obtained from the flow-through studies were used as part of the economic feasibility study. Results of flow-through column tests designed to determine sorbent barrier capacities (effective Kd) have shown that clinoptilolite is much more effective in sorbing strontium than was found in the FY 1986 effectiveness evaluations. The effectiveness of this barrier for cobalt, however, was not as good as was previously measured.

The estimated costs are preliminary and represent only a rough order of magnitude estimate. Further information obtained from field studies and refined performance models will allow a more precise cost estimate to be prepared at the conclusion of this program. The cost estimation procedures are applicable also to alternative uses of sorbent barrier technology such as redundant barriers around below-grade vaults.

Incremental costs for implementing clinoptilolite sorbent barriers at a humid site with characteristics assumed for the reference site were found to range from \$3.2M to \$76M for a facility designed to accept 560,000 $m^3$ (equivalent to 20 years' waste generation). These costs represent a 0.9% to 21.7% increase over the estimated \$350M required for site construction and operation for the reference site (Cook et al. 1987). The required barrier thickness and cost depend on infiltration rate, site boundary distance, and effectiveness of the natural soils in sorbing radionuclides. Costs for

implementing a barrier utilizing 20 wt% A51 synthetic zeolite are more than an order of magnitude greater due to higher material costs.

#### 4.3.2.1 Site Selection

The thickness and formulation of a sorbent barrier depend on many site-specific parameters such as local rainfall, soil chemistry, radionuclide inventory, depth to the water table, flow rate of aquifer, etc. Hence a reference site was selected to provide a basis for estimating the cost of applying the sorbent barrier technology. Two existing DOE LLW sites--Oak Ridge, Tennessee, and Savannah River, South Carolina--were considered to represent a typical humid site. After reviewing literature about each site, it was decided that the Savannah River Plant site represented more typical conditions for future LLW sites than did Oak Ridge. A number of assumptions were made about the reference LLW site to use in the performance assessment for sorbent barriers. This performance assessment was used to determine the required thickness of a sorbent barrier to meet the proposed EPA drinking water standard, 4 mrem/yr via the drinking water pathway (EPA 1986).

The conceptual design to implement sorbent barriers for new shallow-land burial trenches is illustrated in Figure 4.1. This design assumes that the

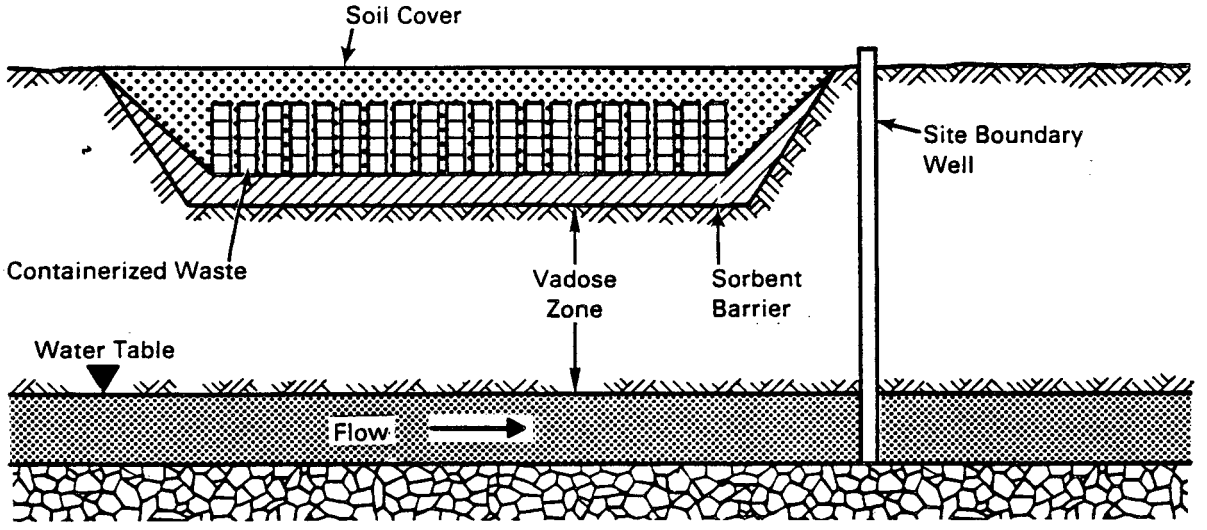


FIGURE 4.1. Conceptual Design for Application of Sorbent Barriers to New Shallow-Land Burial Trenches

sorbent barrier will be placed in the bottom of the trench, directly contacting the underlying soil. The trench will be excavated deeper than normal to compensate for the volume occupied by the barrier. Each trench was designed to accommodate about 28,000 $m^3$ of waste, the expected annual volume generated for disposal at the reference site. A total of 20 trenches will be constructed on the site in two rows of ten trenches each. The width of this site perpendicular to the groundwater flow is assumed to be 375 m. The inventory of cobalt, strontium, and cesium in the trenches is the sum of the projected inventory of the low- and intermediate-level wastes outlined by Cook et al. (1987). This assumption was made to provide a conservative estimate of barrier performance. Table 4.1 gives a complete list of the standard assumptions made for this analysis.

Several flow-through column tests of three barrier formulations and one control soil, as listed in Table 4.2, were conducted to determine the effective distribution coefficient (Kd = ratio of concentration of radionuclide in solid to concentration in contacting liquid) for each barrier. These Kds were used in the performance assessment to determine the required barrier thickness to meet the DOE guidelines. The results of the analysis of the breakthrough curves for cobalt and strontium, in terms of effective Kd, are presented in Table 4.3.

#### 4.3.2.2 Performance Assessment Model

The performance of each sorbent barrier was calculated by using linear deterministic equations (Staley et al. 1979; King et al. 1987) describing radionuclide leaching and transport through porous solids. These equations consider only the retardation of radionuclide movement by interaction with the solid media and do not address transport by dispersion, and thus they describe a one-dimensional model. The additional effort to model dispersion was not warranted for this analysis. These equations calculated the concentration of radionuclides in the aquifer at any point of interest. The concentrations were converted to dose using standard dose conversion factors (ICRP 1987) and assuming the average consumption of contaminated water is 730 L/yr.

TABLE 4.1. Standard Conditions for Reference Shallow-Land Burial Site for Low-Level Waste

| Parameter | Standard Value | Reference |
|---|---|---|
| **General Site Parameters** | | |
| Infiltration, m/yr | 0.4 | Looney et al. 1987 |
| Width of site perpendicular to groundwater flow, m | 375 | Cook et al. 1987 |
| Distance to downstream well, m | 100[(a)] | -- |
| **Waste Properties** | | |
| $^{60}Co$ Inventory, Ci | 180,000 | Cook et al. 1987 |
| $^{90}Sr$ Inventory, Ci | 400 | Cook et al. 1987 |
| $^{137}Cs$ Inventory, Ci | 400 | Cook et al. 1987 |
| Bulk density, $g/cm^3$ | 1.6 | Cook et al. 1987 |
| Porosity | 0.1 | Cook et al. 1987 |
| Leach activity, $yr^{-1}$ | | Looney et al. 1987 |
| $^{60}Co$ | 0.0047 | |
| $^{90}Sr$ | 0.0059 | |
| $^{137}Cs$ | 0.000095 | |
| **Vadose Zone Properties** | | |
| Soil density, $g/cm^3$ | 1.6 | Cook et al. 1987 |
| Porosity | 0.2 | Cook et al. 1987 |
| Distance from bottom of waste to top of aquifer, m | 3.0 | Cook et al. 1987 |
| Vertical velocity, m/yr | 2.2 | Cook et al. 1987 |
| Distribution coefficients, mL/g | | Cook et al. 1987 |
| $^{60}Co$ | 10 | |
| $^{90}Sr$ | 8 | |
| $^{137}Cs$ | 500 | |
| **Aquifer Properties** | | |
| Soil properties | Same as vadose zone | |
| Horizontal velocity, m/yr | 35 | Cook et al. 1987 |
| Mixing depth, m | 10 | Cook et al. 1987 |

(a) A conservative estimate.

TABLE 4.2. Barrier Formulations for Flow-Through Column Tests

| Column | Formulation |
|---|---|
| 1,2 | 20% A51 Zeolite, 6% Activated Carbon, 1% Greensand, 73% Local Soil |
| 3 | 5% A51 Zeolite, 6% Activated Carbon, 1% Greensand, 88% Local Soil |
| 4,5 | 93% Clinoptilolite, 6% Activated Carbon, 1% Greensand |
| 6,7 | Local Soil |

TABLE 4.3. Effective Kds for Materials Tested in Flow-Through Column Tests

| | Effective Kd,[(a)] mL/g | |
|---|---|---|
| Material | Cobalt | Strontium |
| 20% A51 Zeolite | 36 | 440 |
| 5% A51 Zeolite | 41 | 250 |
| 93% Clinoptilolite | 38 | 910[(b)] |
| Local Soil | 27 | 5.9 |

(a) The effective Kd is derived from the 50% break-through point on the curve for pore volume versus breakthrough.
(b) At the time the test was stopped, 50% breakthrough had not occurred. The Kd is based on the number of pore volumes at the end of the test. The actual Kd will be somewhat higher than this.

The model described above was used to calculate the required sorbent barrier thickness to meet the 4 mrem/yr drinking water criterion for a number of different cases. These cases were chosen to represent site conditions ranging from base conditions described in Table 4.1 to worst case, where the bottom of the barrier is at the water table and the site is at the edge of the site boundary (e.g., distance = 1 m). Table 4.4 summarizes the results of these simulations, including estimated dose and cost. The incremental cost of applying the sorbent barrier was calculated from the thickness of barrier and the unit cost of the sorbent material. The actual cost of

TABLE 4.4. Required Barrier Thickness To Meet Proposed EPA Drinking Water Standard

| Case | Barrier Thickness, m | Infiltration, m/yr | Distance to Boundary, m | Depth to Water Table, m | Soil Kd=0 | Drinking Water Dose, mrem/yr | Cost, $M |
|---|---|---|---|---|---|---|---|
| Base Cases for Reference Site. No Sorbent Barrier | | | | | | | |
| 1 | 0.0 | 0.4 | 100 | 12.2 | no | $4.8\times10^{-8}$ | 0 |
| 2 | 0.0 | 0.4 | 100 | 9.4 | no | $6.3\times10^{-2}$ | 0 |
| 3 | 0.0 | 0.4 | 1 | 9.4 | no | $3.7\times10^{-1}$ | 0 |
| 4 | 0.0 | 1.0 | 1 | 9.4 | no | $1.3\times10^{-4}$ | 0 |
| 5 | 0.0 | 0.4 | 1 | 9.4 | yes | $3.6\times10^{6}$ | 0 |
| 6 | 0.0 | 0.4 | 1 | 6.4 | no | $3.9\times10^{6}$ | 0 |
| 7 | 0.0 | 1.0 | 1 | 9.4 | yes | $1.1\times10^{7}$ | 0 |
| 8 | 0.0 | 1.0 | 1 | 12.2 | no | $3.2\times10^{1}$ | 0 |
| 9 | 0.0 | 1.0 | 100 | 12.2 | no | $3.9\times10^{0}$ | 0 |
| 10 | 0.0 | 1.0 | 100 | 6.4 | no | $5.5\times10^{5}$ | 0 |
| Application of A51 Zeolite Formulation to Cases 4,6,7,8 | | | | | | | |
| 11 | 1.40 | 1.0 | 1 | 9.4 | no | 4.0 | 470 |
| 12 | 0.70 | 0.4 | 1 | 9.4 | yes | 3.9 | 230 |
| 13 | 1.86 | 1.0 | 1 | 9.4 | yes | 4.0 | 640 |
| 14 | 0.35 | 1.0 | 1 | 12.2 | no | 3.8 | 110 |
| Application of Clinoptilolite Formulation to Cases 4,6,7,8 | | | | | | | |
| 15 | 1.31 | 1.0 | 1 | 9.4 | no | 4.0 | 44 |
| 16 | 0.67 | 0.4 | 1 | 9.4 | yes | 3.4 | 22 |
| 17 | 1.78 | 1.0 | 1 | 9.4 | yes | 3.8 | 61 |
| 18 | 0.32 | 1.0 | 1 | 12.2 | no | 4.0 | 10 |
| Effect of Infiltration Rate for Clinoptilolite Formulation. No Soil Sorption | | | | | | | |
| 19 | 0.31 | 0.2 | 1 | 9.4 | yes | 4.0 | 10 |
| 20 | 0.49 | 0.3 | 1 | 9.4 | yes | 3.4 | 16 |
| 21 | 0.85 | 0.5 | 1 | 9.4 | yes | 3.6 | 28 |
| 22 | 1.03 | 0.6 | 1 | 9.4 | yes | 3.8 | 35 |

TABLE 4.4. (contd)

| Case | Barrier Thickness, m | Infiltration, m/yr | Distance to Boundary, m | Depth to Water Table, m | Soil Kd=0 | Drinking Water Dose, mrem/yr | Cost, $M |
|---|---|---|---|---|---|---|---|
| Effect of Infiltration Rate for Clinoptilolite Formulation. No Soil Sorption (contd) | | | | | | | |
| 23 | 1.21 | 0.7 | 1 | 9.4 | yes | 3.6 | 41 |
| 24 | 1.40 | 0.8 | 1 | 9.4 | yes | 3.9 | 48 |
| 25 | 1.59 | 0.9 | 1 | 9.4 | yes | 3.9 | 55 |
| 26 | 1.97 | 1.1 | 1 | 9.4 | yes | 3.9 | 69 |
| 27 | 2.16 | 1.2 | 1 | 9.4 | yes | 3.9 | 76 |
| Effect of Distance to Site Boundary. No Soil Sorption | | | | | | | |
| 28 | 0.66 | 0.4 | 10 | 9.4 | yes | 4.0 | 22 |
| 29 | 0.65 | 0.4 | 100 | 9.4 | yes | 4.0 | 22 |
| Effect of Infiltration Rate for Clinoptilolite Formulation. With Soil Sorption | | | | | | | |
| 30 | 0.00 | 0.2 | 1 | 9.4 | no | 4.0 | 0 |
| 31 | 0.32 | 0.6 | 1 | 9.4 | no | 3.7 | 10 |
| 32 | 0.81 | 0.8 | 1 | 9.4 | no | 3.8 | 27 |
| 33 | 1.81 | 1.2 | 1 | 9.4 | no | 3.9 | 63 |
| Effect of Distance to Site Boundary. With Soil Sorption | | | | | | | |
| 34 | 0.45 | 0.8 | 10 | 9.4 | no | 3.8 | 15 |
| 35 | 0.10 | 0.8 | 100 | 9.4 | no | 3.8 | 3.2 |
| Effect of Infiltration, Bottom of Barrier at Water Table | | | | | | | |
| 36 | 0.67 | 0.4 | 1 | 7.1 | yes | 4.0 | 22 |
| 37 | 1.04 | 0.6 | 1 | 7.5 | yes | 3.6 | 35 |
| 38 | 1.41 | 0.8 | 1 | 7.8 | yes | 3.7 | 48 |
| 39 | 1.78 | 1.0 | 1 | 8.2 | yes | 4.0 | 61 |

installing the barrier is expected to be small compared to costs for the material. For the clinoptilolite barrier the material cost is $\$188/m^3$, and for the 20% A51 zeolite barrier it is $\$1904/m^3$.

#### 4.3.2.3 Conclusions

Sorbent barriers are an economically feasible technology for preventing the migration of certain radionuclides, such as $^{90}Sr$, $^{137}Cs$ and $^{60}Co$, over significant distances where they can pose a health risk to the public. Sorbent barriers can retard radionuclides to the point that reliance on sorption by the underlying soil is not required.

The clinoptilolite barrier formulation is recommended for field testing. It was the most cost-effective barrier tested, for the conditions assumed for the reference site, costing $\sim\$190/m^3$; its application would increase overall costs by 0.9% to 21.7% over the estimated $350M required for site construction and operation (Cook et al. 1987). The use of A51 zeolite is not cost-effective since it is more than an order of magnitude more costly than the clinoptilolite yet has inferior sorption properties.

## 4.4 SPECIAL WASTE FORM LYSIMETERS - ARID - T. L. Jones

Regulations governing the disposal of commercial LLW require that all liquid waste be solidified before burial. Most waste must be solidified into a rigid matrix such as cement or plastic to prevent waste consolidation and site slumping after burial. Solidification slows the release of radionuclides and other solutes into the soil. In 1983 the Special Waste Form Lysimeters - Arid Program was initiated at the Pacific Northwest Laboratory to study the release of waste from samples of low-level radioactive waste that had been commercially solidified. The primary method used in this program is to bury sample waste forms in field lysimeters and to monitor leachate composition from the release and transport of solutes.

The lysimeter facility (Figure 4.2) consists of ten lysimeters, each containing one sample of solidified waste. Five different waste forms are being tested, allowing duplicate samples of each one to be evaluated. The

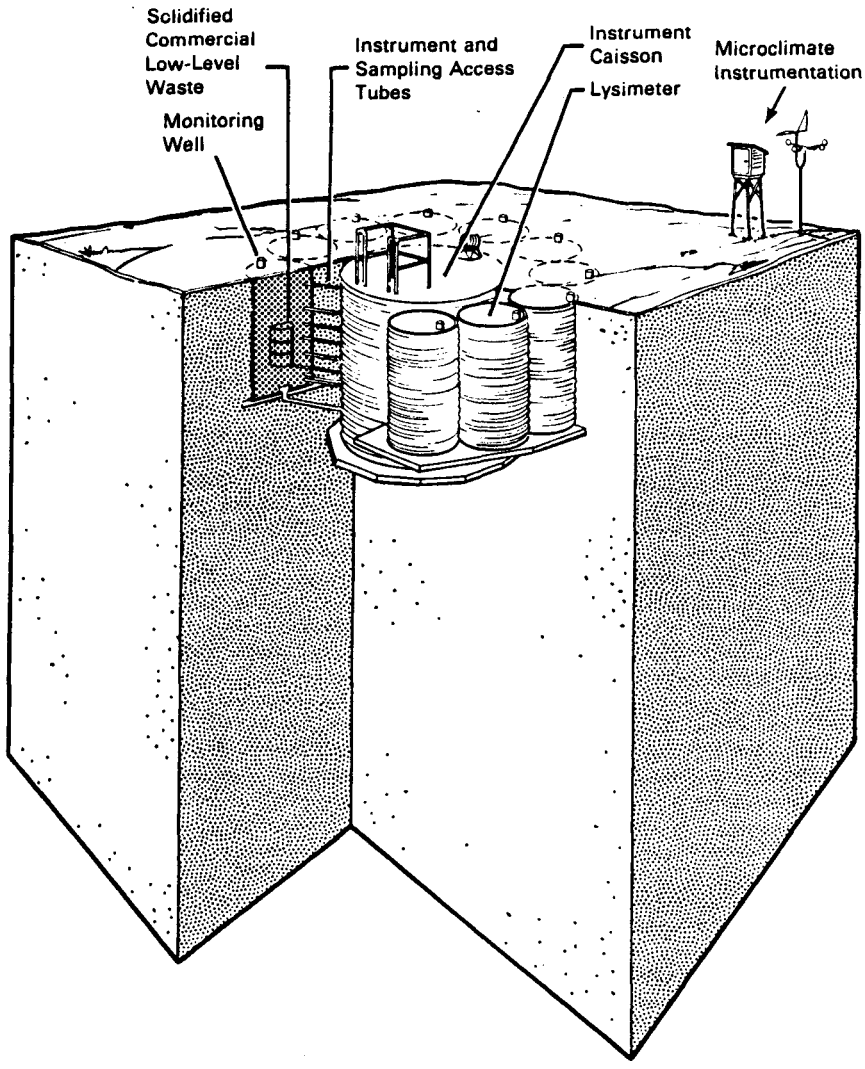


FIGURE 4.2. Schematic of Lysimeter Facility

samples were obtained from operating nuclear power plants and are actual waste forms routinely generated at these facilities and solidified by commercial processes. Sample size is a partially filled 210-L drum. All containers were removed before burial, leaving the bare waste form in contact with the lysimeter soil.

The waste streams represented in the five waste forms are two boric acid evaporator concentrates, one sodium sulfate evaporator concentrate, and one sodium sulfate evaporator concentrate with spent ion exchange resin added. The solidification agents used were masonry cement, Portland III cement, Dow

polymer, and bitumen. The dominant radionuclides contained in the waste are $^{60}Co$ and $^{137}Cs$. Additional radioactive elements include $^{134}Cs$, $^{54}Mn$ and $^{3}H$. The total inventory of radionuclides in each sample is in the millicurie range. According to the waste classification system of 10 CFR part 61, these waste samples would be class A waste.

The hydrologic environment of the lysimeters shows rather large seasonal variations. The volumetric water content at the depth of the waste samples ranges from ~11% in the late winter to a low of about 7% in the late summer. Drainage rates also vary from winter to summer. The resulting pore water velocities reach a peak of about 1 cm/wk in the late winter and decline steadily to less than 0.05 cm/wk in late summer. Total drainage resulting from natural precipitation was 4 cm drainage out of 14 cm precipitation during the 1984-1985 climatic cycle, 12 cm drainage out of 24 cm precipitation during 1985-1986, and 5 cm drainage out of 15 cm precipitation during 1986-1987 (Table 4.5).

Two radionuclides have been found in lysimeter leachates to date. Cobalt-60 has been found in six lysimeters (Figure 4.3). The maximum amount of $^{60}$ Co leached to the bottom of any lysimeter is <0.1% of the total inventory. This amount is small but interesting because laboratory sorption

TABLE 4.5. Average Water Balance Parameters for 1984-1987

| | 9/1/84 to 8/31/85 | | 9/1/85 to 8/31/86 | | 9/1/86 to 8/31/87 | |
|---|---|---|---|---|---|---|
| Total precip, cm | 13.8 | | 21.7 | | 14.5 | |
| Snow, cm | 55.6 | | 86.6 | | 21.3 | |
| Change in storage, cm | 2.1 ± 0.5 | | -0.6 ± 2.2 | | 2.1 ± 1.8 | |
| Drainage, cm | 4.2 ± 0.5 | 30% | 12.3 ± 1.2 | 57% | 5.3 ± 0.7 | 37% |
| Evaporation, cm | 7.5 ± 0.6 | 54% | 10.0 ± 2.8 | 46% | 7.1 ± 1.6 | 49% |
| Change in water content, cm/m soil depth | 6.8 - 11.4 | | 6.9 - 10.7 | | 7.0 - 9.3 | |

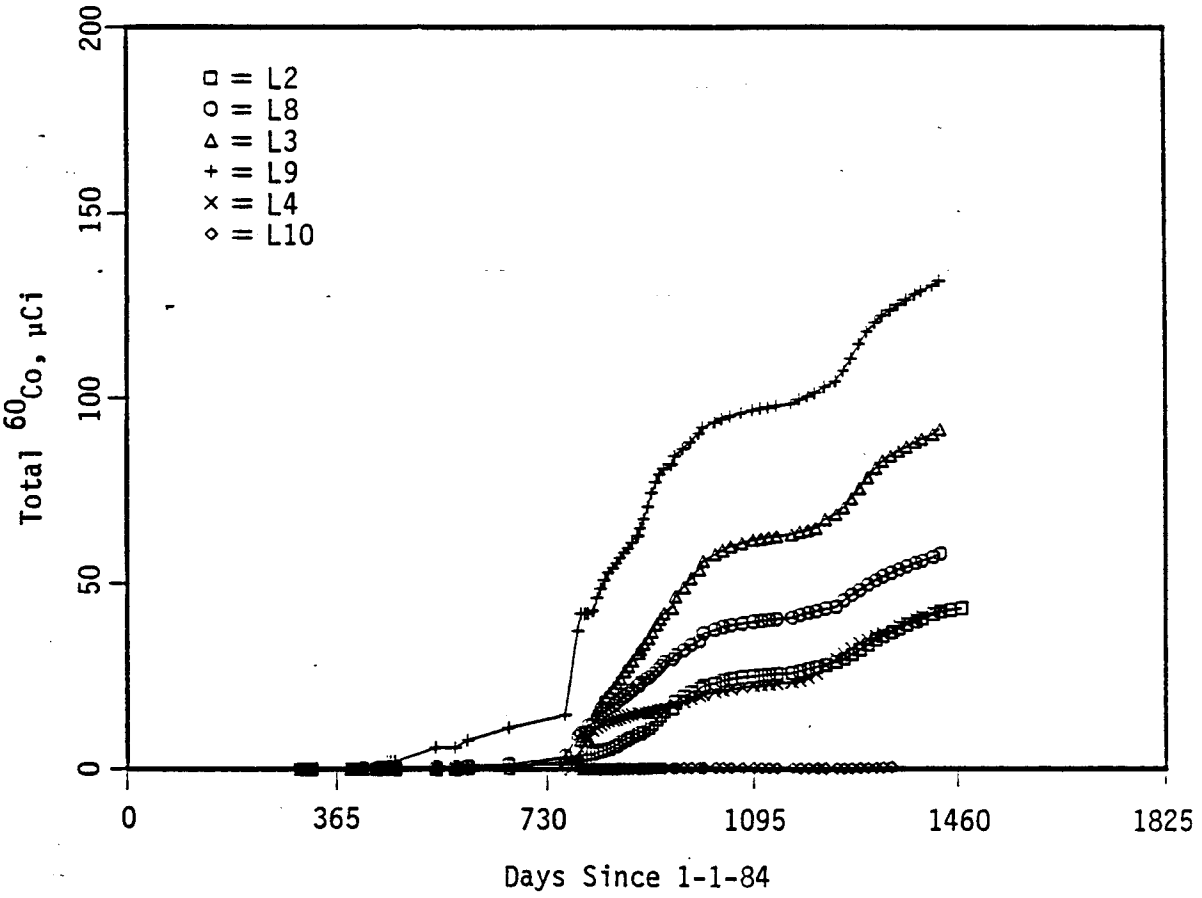


FIGURE 4.3. Cumulative Amount (decay-corrected) of $^{60}Co$ Released from Lysimeters 2, 8, 3, 9, 4, and 10

studies indicate that $^{60}Co$ should be highly sorbed onto soil clays, and therefore no measurable quantities should leach to the lysimeter drain. The presence of this small amount suggests that leaching of a small but highly mobile fraction of $^{60}Co$ has occurred. It is likely that the formation of organic complexes between $^{60}Co$ and organic chelating agents found in the waste is responsible for the $^{60}Co$ mobility. The second radionuclide found in lysimeter leachate is $^{3}H$. Tritium is found in only one of the waste forms being tested, but is found in the leachate from both lysimeters containing samples of this waste form (Figure 4.4). Tritium leached to the lysimeter drain is about 30% of the total tritium inventory.

Analysis of the lysimeter leachates extends beyond identifying radionuclide content. A complete chemical inventory of leachates is made

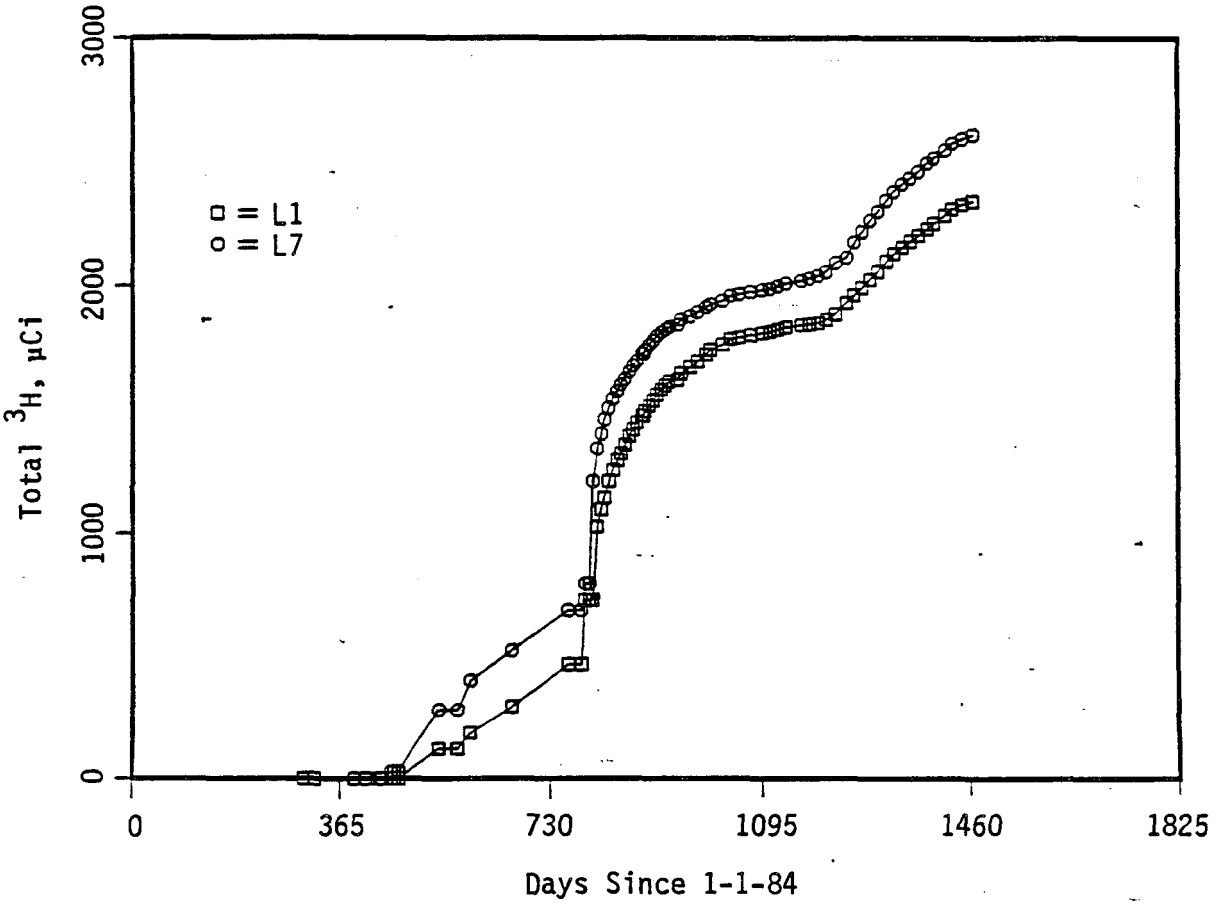


FIGURE 4.4. Cumulative Amount (decay-corrected) of $^{3}H$ Released from Lysimeters 1 and 7

quarterly. Results of these analyses reveal migration of other waste constituents in addition to radionuclides. High amounts of sodium, sulfate, boron, calcium and magnesium are major components found in various waste forms and are all found in the respective leachate samples. A complete quantitative analysis of these leachates will require extensive geochemical and transport modeling; however, some qualitative trends have been identified. It appears that much of the sodium being released from the sodium sulfate wastes is displacing calcium from the soil and then replacing calcium on the soil exchange sites. This results in excess calcium appearing in the leachates and sodium levels being lower than expected. It also appears that the release of boron from the boric acid waste forms is being significantly retarded. In the boric acid/masonry cement waste form, the retardation

mechanism may be a solubility control with boron precipitating with cement solid phases. In the boric acid/bitumen waste form, the mechanism may be physical entrapment of the boron inside the bitumen structure.

The project has collected extensive hydrologic and chemical data over the last 3 yr relating to the leaching of commercial waste forms under field conditions. To this point, analysis has been largely qualitative and speculative. The final phase of the project will rely extensively on the iterative process of model simulation and model calibration to provide quantitative interpretation to the existing data. However, preliminary analysis indicates that these field data will allow a more definitive analysis of source terms associated with commercial LLW than is possible with laboratory data alone.

## 4.5 REFERENCES


Cook, J. R., M. W. Grant, and O. O. Towler. 1987. New Low-Level Radioactive Waste Storage/Disposal Facilities at the Savannah River Plant. DPST-85-862, E. I. du Pont de Nemours and Company, Savannah River Laboratory, Aiken, South Carolina.

International Commission of Radiation Protection. 1977. Radiation Protection. ICRP Publication 26, Pergamon Press.

King, C. M., W. L. Marter, B. B. Looney, and J. P. Pickett. 1987. Methodology and Parameters for Assessing Human Health Effects for Waste Sites at the Savannah River Plant. DPST-86-298, E. I. du Pont de Nemours and Company, Savannah River Laboratory, Aiken, South Carolina.

Looney, B. B., M. W. Grant, and C. M. King. 1987. Estimation of Geochemical Parameters for Assessing Subsurface Transport at the Savannah River Plant. DPST-85-904, E. I. du Pont de Nemours and Company, Savannah River Laboratory, Aiken, South Carolina.

Staley, G. B., G. P. Turi, and D. L. Schreiber. 1979. "Radionuclide Migration from Low-Level Waste: A Generic Overview," Management of Low-Level Radioactive Waste, Vol 2, Pergamon Press.

U.S. Environmental Protection Agency. 1986. "Advance Notice of Proposed Rule-Making for National Primary Drinking Water Standards: Radionuclides," 40 CFR Part 141.

# 5.0 ACRONYMS AND ABBREVIATIONS

AA - atomic absorption
ac - alternating current
ACF - air cooling frame
ADS - air displacement slurry (pump)
AE - acoustic emission
cfm - cubic feet per minute
CFMT - concentrator feed makeup tank
CFR - Code of Federal Regulations
Ci - curies
cm - centimeter
CTS - component test stand
dB - decibels
dc - direct current
DG - doped glass
DF - decontamination factor
DIW - deionized water
DOE - Department of Energy
DSPF - dry-solid-articulate filter
DWPF - Defense Waste Processing Facility
EPA - Environmental Protection Agency
EPT - electropolishing tank
FMEA - failure modes and effects analysis
FRG - Federal Republic of Germany
g - gram
GR - Grande Ronde
HEME - high-efficiency mist eliminator
HEPA - high-efficiency particulate air (filter)
HLLW - high-level liquid waste
HLW - high-level waste
HT - heat treatment
HWVP - Hanford Waste Vitrification Plant
IC - ion chromatography
ICP - insulated cooling pod
ICP - inductively coupled plasma spectroscopy
Kd - distribution coefficient
kg - kilogram
kW - kilowatt
L - liter
LFCM - liquid-fed ceramic melter
LLW - low-level waste
m - meter
MCC - Materials Characterization Center
MFMT - melter feed makeup tank
MFT - melter feed tank
NBR - normalized boron release
NER - normalized elemental release
NWTP - Nuclear Waste Treatment Program
PBB - Permian Basin Brine

PNL - Pacific Northwest Laboratory
psi - pounds per square inch
PUREX - plutonium uranium extraction
rad - radiation absorbed dose
redox - chemical reduction oxidation
RLFCM - radioactive liquid-fed ceramic melter
RPS - radioactive liquid-fed ceramic melter
RST - radioactive process sewer
SBS - submerged-bed scrubber
scfm - standard cubic feet per minute
SCR - silicon controlled rectifier
SFCM - slurry-fed ceramic melter
SRL - Savannah River Laboratory
SS - stainless steel
TC - test canister
THOREX - thorex extraction
V ac - volts alternating current
V dc - volts direct current
VVS - vessel ventilation system
WNYNSC - Western New York Nuclear Services Center
WVCM - West Valley ceramic melter
WVDP - West Valley Demonstration Project
WVNS - West Valley Nuclear Services
WVST - West Valley Support Task

# DISTRIBUTION

No. of Copies

OFFSITE

10 DOE/Office of Scientific and Technical Information

4 DOE Office of Civilian Radioactive Waste Management
Forrestal Building
Washington, DC 20585
ATTN: L. H. Barrett, RW-33
S. H. Kale, RW-20
D. E. Shelor, RW-32
R. Stein, RW-23

3 DOE Office of Defense Waste & Transportation Management
GTN
Washington, DC 20545
ATTN: K. A. Chacey, DP-123
G. H. Daly, DP-124
T. B. Hindman, DP-12

4 DOE Office of Remedial Action & Waste Technology
GTN
Washington, DC 20545
ATTN: J. E. Baublitz, NE-20
J. A. Coleman, NE-24
T. W. McIntosh, NE-24
H. F. Walter, NE-24

A. T. Clark
Division of Fuel Material Safety
Nuclear Regulatory Commission
Washington, DC 20555

V. Stello
Office for the Executive Director for Operations
Mail Station 6209
Nuclear Regulatory Commission
Washington, DC 20555

No. of Copies

Sheldon Meyers
Environmental Protection Agency
Office of Radiation Programs (ANR-458)
401 M Street S.W.
Washington, DC 20460

J. M. McGough
DOE Albuquerque Operations Office
P.O. Box 5400
Albuquerque, NM 87185

P. G. Hagan
Joint Integration Office
Carlmont Executive 1
4308 Carlisle N.E.
Suite 101
Albuquerque, NM 87107

E. Maestas
DOE West Valley Project
P.O. Box 191
West Valley, NY 14171

3 DOE Idaho Operations Office
550 Second Street
Idaho Falls, ID 83401
ATTN: M. W. Shupe
J. P. Hamric
C. R. Enos

F. T. Fong
DOE San Francisco Operations
1333 Broadway
Oakland, CA 94612

M. R. Jugan
DOE Oak Ridge Operations Office
P.O. Box E
Oak Ridge, TN 37830

W. T. Goldston
DOE Savannah River Operations Office
P.O. Box A
Aiken, SC 29801

No. of
Copies

M. J. Steindler
Argonne National Laboratory
9700 South Cass Avenue
Argonne, IL 60439

C. S. Abrams
Argonne National Laboratory
P.O. Box 2528
Idaho Falls, ID 83401

3 Battelle Memorial Institute
Project Management Division
505 King Avenue
Columbus, OH 43201
ATTN: W. A. Carbeiner
R. A. Nathan
Technical Library

L. D. Ramspott
Lawrence Livermore National Laboratory
University of California
P.O. Box 808
Livermore, CA 94550

D. T. Oakley, MS 619
Los Alamos National Laboratory
P.O. Box 1663
Los Alamos, NM 87544

4 Oak Ridge National Laboratory
P.O. Box Y
Oak Ridge, TN 37830
ATTN: W. D. Burch
R. T. Jubin
L. J. Mezga
D. W. Turner

2 Sandia Laboratories
P.O. Box 5800
Albuquerque, NM 87185
ATTN: R. W. Lynch
Technical Library

No. of
Copies

J. R. Berreth
Westinghouse Idaho Nuclear Co., Inc.
P.O. Box 4000
Idaho Falls, ID 83401

5 E. I. du Pont de Nemours Company
Savannah River Laboratory
Aiken, SC 29801
ATTN: M. D. Boersma
J. G. Glasscock
J. R. Knight
M. J. Plodinec
C. T. Randall

R. G. Baxter
E. I. du Pont de Nemours Company
Savannah River Plant
Building 704-S
Aiken, SC 29808

A. D. Rodgers
Mail Stop 2411
EG&G Idaho
P.O. Box 1625
Idaho Falls, ID 83415

R. Shaw
Electric Power Research Institute
3412 Hillview Avenue
P.O. Box 10412
Palo Alto, CA 94303

6 West Valley Nuclear Services Company
P.O. Box 191
West Valley, NY 14171
ATTN: S. M. Barnes
R. R. Borisch
R. A. Humphrey
S. J. Marchette
J. M. Pope
R. A. Thomas

No. of
Copies

J. L. White, Chairman
Energy Research & Development
Authority
Empire State Plaza
Albany, NY 12223

ONSITE

7 DOE Richland Operations Office

R. W. Brown
C. E. Collantes
M. J. Furman
R. E. Gerton
P. E. Lamont
E. C. Norman
D. M. Smith

8 Westinghouse Hanford Company

J. M. Henderson
T. L. Jones
R. E. Lerch
H. E. McGuire
J. L. Scott
D. A. Turner
D. D. Wodrich
B. A. Wolfe

39 Pacific Northwest Laboratory

C. R. Allen
R. P. Allen

No. of
Copies

Pacific Northwest Laboratory
(contd)

W. W. Ballard, Jr.
D. N. Berger
W. F. Bonner
L. A. Bray
R. A. Brouns
G. H. Bryan
J. L. Buelt
H. C. Burkholder
T. T. Claudson
M. R. Elmore
H. D. Freeman
R. W. Goles
W. O. Heath
L. K. Holton, Jr. (5)
M. R. Kreiter
W. L. Kuhn
L. T. Lakey
J. L. McElroy
G. B. Mellinger
M. E. Peterson
J. A. Powell
M. A. Reimus
P. W. Reimus
W. A. Ross
J. M. Seay
S. C. Slate
J. H. Westsik, Jr.
Publishing Coordination
Technical Report Files (5)